The role of mechanical forces in bone formation: Evaluation of long-term responses by osteoblasts to low fluid shear stress in vitro

Claudia Wittkowske

A thesis submitted in partial fulfilment of the requirements for the degree of
Doctor of Philosophy

The University of Sheffield
Faculty of Engineering
Department of Mechanical Engineering
INSIGNEO Institute for in silico medicine

First supervisor: Dr Cecile Perrault
Second supervisor: Prof Damien Lacroix

External examiner: Prof Alicia El Haj
Internal examiner: Dr Vanessa Hearnden

September 2016

Abstract

Bone strength is maintained through the continuous process of bone remodelling within which bone cells work together. Mechanical loading is an important regulator of this process with bone cells being particularly sensitive to fluid shear stress (FSS). The aim of this research was to investigate long-term responses by osteoblasts to low FSS using both monolayer and 3D in vitro models.

The osteoblast cell lines IDG-SW3 and MLO-A5 were cultured for 28 days or 21 days respectively in 6-well plates and were exposed to low FSS generated with a see-saw rocker ($<0.05\,\mathrm{Pa}$) or an orbital shaker ($<0.9\,\mathrm{Pa}$). There were no differences in metabolic activity, cell proliferation, alkaline phosphatase (ALP) activity, mineralisation, collagen deposition and osteocytogenic differentiation between static and dynamic groups.

Despite not reacting to FSS, IDG-SW3 responded to biochemical stimulation. Deposition of collagen and ALP activation were inhibited when ascorbic acid ($50\,\mu\mathrm{g/ml}$) was omitted ($p \leq 0.001$). Mineralisation was positively related to the concentration of β-glycerophosphate (β-GP) which also regulated osteocytogenesis. Treatment with $1\,\mathrm{mM}$ strontium ranelate reduced ALP activity and mineralisation ($p \leq 0.001$), but enhanced expression of the osteocyte marker Dmp1-GFP ($p \leq 0.001$).

To investigate whether IDG-SW3 were more responsive to low FSS in a 3D environment, cells were embedded in collagen ($2\,\mathrm{mg/ml}$). Modification of a transwell insert enabled long-term cell culture under hydrostatic pressure-driven low fluid flow. After 21 days, cells had contracted the collagen by 50% compared to cell-free controls ($p \leq 0.001$). However, no significant differences in gel contraction, cell distribution and mineralisation were detected between static and flow-stimulated groups, further confirming the results from the monolayer experiments.

To improve cell observation in 3D, a bioreactor was designed which combined microfluidics with thin cell-laden collagen layers. Despite successful cell culture under static conditions, dynamic culture failed due to the weak mechanical properties of collagen and technical difficulties such as bubble nucleation.

Acknowledgements

I would like to thank my supervisors Dr Cecile Perrault and Prof Damien Lacroix for providing me with the opportunity to complete my PhD studies at the INSIGNEO Institute for in silico Medicine. I am particularly grateful to Cecile Perrault for providing me with constant encouragement and support over the last three years. I felt very welcome right from the beginning and I hugely appreciate the freedom she gave me in exploring my ideas in and outside the lab. Thanks to Cecile I gained a lot of experience in a wide range of different experimental techniques. She also supported my love for teaching which for me was an important part of my PhD experience. I would like to thank Damien Lacroix for his support as he played an important role in structuring my work and providing me with confidence in my work when I needed it most. Although not formally on my supervisory team, I owe huge gratitude to Dr Gwendolen Reilly who provided invaluable scientific input and contributed great ideas to this project.

My PhD would have not been the same without all the great people around me. I was able to share the exciting moments, but also the frustrating moments when things did not work (again!) or when experiments had to be repeated again and again (and again and again...) with amazing people who always managed to make me believe in myself and - most importantly - make me smile! A big thanks to Liam, Luke and Rob for providing me with great scientific advice and being superb role models on how to keep calm and relaxed when doing (good) science. Thanks to Stefania for providing excellent comments and advice. I also want to thank the rest of the lab team: Aban, Julie, Maryam, Marzia, Marzieh and Raj for always being there for me and for sharing their experiences with me. Ana, Claudia, Iwona and Sofia - thanks for some of my best moments in Sheffield and I am very grateful for having you as my friends. Finally, a huge thanks to all the current and past members of IMSB for being such a great group and making me feel at home in Sheffield!

Contents

List of Figures

List of Tables

Abbreviations

2D . . . . . . Two-dimensional

3D . . . . . . Three-dimensional

α-MEM . . . α-Minimum Essential Medium

AA . . . . . . Ascorbic acid

ALP . . . . . Alkaline phosphatase

ANOVA . . . Analysis of variance

ARS . . . . . Alizarin Red S

ATP . . . . . Adenosine triphosphate

BMP-2 . . . . Bone morphogenetic protein 2

BSP . . . . . Bone sialoprotein

β-GP . . . . . β-glycerophosphate

Ca²⁺ . . . . . Calcium

CaSR . . . . . Calcium-sensing receptor

CiGiM . . . . Cells-in-Gels-in-Mesh

COX-2 . . . . Cyclooxygenase-2

CS . . . . . . Calf serum

Cx43 . . . . . Connexin 43

DAPI . . . . . 4',6-diamidino-2-phenylindole

DPBS . . . . Dulbecco's phosphate buffered saline

DMP-1 . . . . Dentin matrix protein 1

Abbreviations

DMSO . . . . Dimethyol-sulfoxide

DNA . . . . . Desoxyribonucleic acid

ECM . . . . . Extracellular matrix

ER . . . . . . Endoplasmic reticulum

EthD-1 . . . . Ethidium homodimer-1

FGF-23 . . . Fibroblast growth factor 23

FBS . . . . . . Fetal bovine serum

FSS . . . . . . Fluid shear stress

GFP . . . . . Green fluorescent protein

HBSS . . . . Hank's balanced salt solution

hMSC . . . . Human mesenchymal stem cells

hOB . . . . . Human osteoblast-like cell

hFOB . . . . Human fetal osteoblast-like cells

IFN-γ . . . . Interferon-γ

ISF . . . . . . Interstitial fluid

LCS . . . . . . Lacunar-canalicular system

M-CSF . . . . Macrophage colony-stimulating factor

MMP . . . . . Matrix metalloproteinase

MSC . . . . . Mesenchymal stem cell

NADH . . . . Nicotinamide adenine dinucleotide

NO . . . . . . Nitric oxide

OCN . . . . . Osteocalcin

OPG . . . . . Osteoprotegerin

OPN . . . . . Osteopontin

PDMS . . . . Polydimethyl siloxane

PGE$_2$ . . . . . Prostaglandin E$_2$

PIV . . . . . . Particle image velocimetry

PLA . . . . . Polylactic acid

PPFC . . . . Parallel-plate flow chamber

PS . . . . . . Penicillin streptomycin

PSR . . . . . Picrosirius red

RANK . . . . Receptor activator of nuclear factor kappa-B

RANKL . . . Receptor activator of nuclear factor kappa-B ligand

RNA . . . . . Ribonucleic acid

Runx2 . . . . Runt-related transcription factor 2

SD . . . . . . Standard deviation

SHG . . . . . Second harmonic generation

Sr . . . . Strontium

SrR . . . . . . Strontium ranelate

Chapter 1

Introduction

Musculoskeletal conditions, including osteoporosis-related fractures, are one of the disorders which are causing increasing problems in an ageing population (Vos et al., 2015). The discovery of novel, effective treatments to prevent musculoskeletal conditions by enhancing bone formation is challenging (Elvidge, 2016; Mullard, 2016). Only very few compounds succeed as treatment available on the market as they fail during animal and clinical studies (Pammolli et al., 2011). High failure rates can partially be explained by the lack of attention given to the complex mechanisms which guide bone formation during the initial steps of drug discovery. For instance, compound screening in the early stages of the development process often relies solely on monolayer studies performed under static conditions, despite obvious differences to the cells' natural surroundings. Two main reasons prevent the use of more advanced models during drug discovery: (1) an incomplete understanding of the natural cellular interactions and (2) a lack of suitable in vitro bone models combining high-throughput screening technologies and in vivo-like conditions.

This thesis aims to address both of these shortcomings. Specifically, it intends to contribute to a better understanding on how biomechanical forces, fluid shear stress in particular, guide bone formation. Osteoblast behaviour is studied in a controlled environment where both biochemical *and* biomechanical stimuli are incorporated. To study osteoblasts under the impact of fluid shear stress, advanced in vitro bone models are developed which mimic the dynamic and three-dimensional bone environment. In the future, these models have also the potential to be applied as drug discovery platforms for musculoskeletal treatments.

Chapter 2

Background

Sections 2.1 and 2.2 of this chapter have been published as a review article in the research topic "Biomimetic tissue and organ models" in Frontiers in Bioengineering and Biotechnology.

2.1 Bone physiology

Bone is a highly specialised, rigid tissue which provides structural support for the body, allows movement through muscle attachment sites, protects organs, and serves as calcium and growth factor storage (Clarke, 2008). Bone has the power to regenerate and repair constantly throughout the entire life. This process, referred to as bone remodelling, involves different cell types and can be initiated in response to changes in biomechanical loading or to replace old, microdamaged bone with new, mechanically stronger bone (Kini and Nandeesh, 2012).

2.1.1 Bone remodelling

Bone remodelling is an essential process in maintaining bone strength and mineral homeostasis. Remodelling allows the repair of old and damaged bone and adjustment of the bone's architecture to changes in external loading. Specialised cells, namely osteoclasts which remove mineralised matrix and osteoblasts which deposit new bone matrix, work together during this process. Their collaboration is tightly controlled through biochemical pathways (Hadjidakis and Androulakis, 2006). For example, the release receptor activator of nuclear factor kappa-B ligand (RANKL) by osteoblasts induces osteoclast activation through binding to RANK receptors on the surface of osteoclast precursors. This process can be inhibited by osteoprotegerin (OPG) which competitively binds to RANKL (Boyce and Xing, 2008). The

remodelling cycle (Figure 2.1) is composed of four consecutive phases (Clarke, 2008; Markides et al., 2015):

- *Activation:* Hormonal or physical stimuli recruit mononuclear pre-osteoclasts from the circulation to the bone remodelling site. Following attachment to the bone surface, cells fuse to multinucleated osteoclasts.

- *Resorption:* Osteoclasts initiate resorption of organic and mineral bone components which takes between 2 to 4 weeks. Osteoclasts form characteristic Howship's lacunae in trabecular bone and a cutting cone in cortical bone. After these cavities reach a certain size, apoptosis of osteoclasts terminates bone resorption (Sikavitsas et al., 2001).

- *Reversal:* The resorbed surface is smoothed by mononuclear macrophage-like cells and prepared for matrix deposition.

- *Formation:* Osteoblasts lay down new bone by secreting a collagen matrix and controlling its mineralisation. Throughout this process, some osteoblasts become buried within the matrix and differentiate to osteocytes which reside in the fully mineralised lacunar-canalicular system (LCS). After 4 to 6 months this phase is completed and osteoblasts either turn into bone-lining cells or enter apoptosis.

In cortical bone a remodelling rate of 2 to 3% per year is sufficient to maintain bone strength. Trabecular bone presents a higher turnover rate, indicating the importance of bone remodelling for calcium and phosphorus metabolism (Clarke, 2008).

2.1.2 Bone cells

Bone cells work together in a coordinated way during bone remodelling by maintaining a balance between osteoblasts depositing new bone tissue, osteoclasts breaking down bone matrix, and osteocytes orchestrating the activity of osteoblasts and osteoclasts as a response to mechanical loading (Bonewald and Johnson, 2008; Hadjidakis and Androulakis, 2006).

Osteoblasts

Osteoblasts are bone-forming cells which are derived from mesenchymal stem cells (MSC) (Caplan, 1991). MSCs differentiate into osteoblasts under the appropriate stimuli, but they can also turn into cartilage, muscle, tendon and fat cells (Caplan and Bruder, 2001). The osteoblast differentiation and maturation process is governed by both mechanical and biochemical pathways. For example, Runt-related
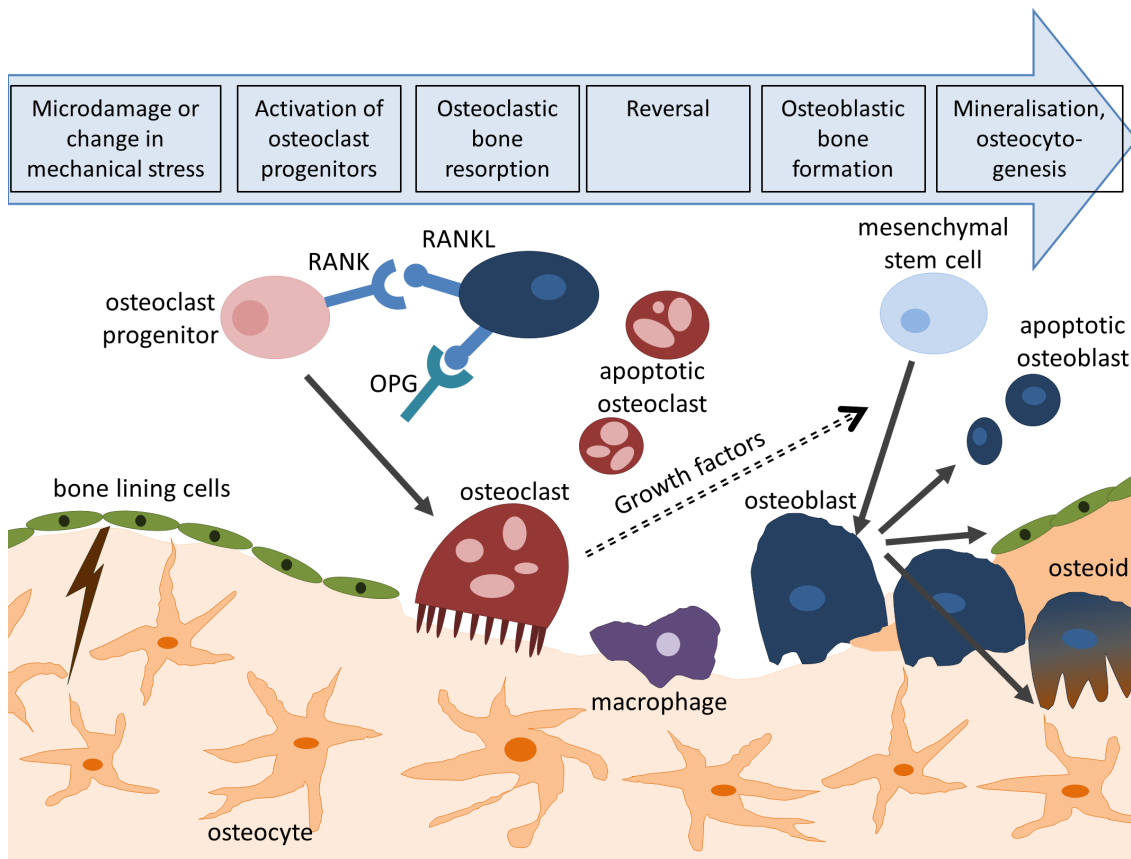
Figure 2.1: Bone remodelling cycle.

Bone remodelling is initiated by microcracks or changes in mechanical loading and consists of four consecutive steps: activation, resorption, reversal and formation. Activation of osteoclasts is controlled through the RANK/RANKL/OPG pathway. Following bone deposition, osteoblasts can differentiate to osteocytes (osteocytogenesis), turn to bone lining cells or enter apoptosis.

transcription factor 2 (Runx2) is essential in pre-osteoblast development where it activates osteoblast-specific genes, including osteopontin, type I collagen, osteocalcin and alkaline phosphatase (ALP) (Ducy et al., 1997; Xu et al., 2015). Mature osteoblast differentiation is controlled by the Wnt signalling pathway, which is activated either by hormones or mechanically (Westendorf et al., 2004).

The morphology of pre-osteoblasts is very similar to fibroblasts, however the latter are not able to produce a mineralised matrix. Mature osteoblasts are typically cuboidal in shape (Franz-Odendaal et al., 2006). Osteoblasts directly regulate bone matrix synthesis and mineralisation by their own secretion mechanism. Bone resorption is indirectly controlled by osteoblasts through paracrine factors acting on osteoclasts. For example, the release of receptor activator of RANKL initiates bone resorption through binding to RANK receptors on the surface of osteoclast precursors (Boyce and Xing, 2008).

The average life-span of osteoblasts ranges from a few days to about 100 days (Rosenberg et al., 2012). At the end of their life, osteoblasts can either (1) become embedded in newly formed bone matrix and differentiate to osteocytes, (2) transform into inactive bone-lining cells which protect inactive bone surfaces or (3) initiate apoptosis (Manolagas, 2000).

Osteocytes

Osteocytes are terminally differentiated osteoblasts which became trapped within newly deposited bone matrix (Franz-Odendaal et al., 2006). Although osteoblast and osteocytes have the same origin, they significantly differ in morphology and function. During osteocytogenesis, i.e. differentiation from osteoblasts to osteocytes, the cell body size decreases and cell processes start to radiate towards the mineralising matrix which may be controlled by E11/gp38, a marker for early-osteocytes (Schulze et al., 1999). After the transition, gene expression of ALP, type I collagen and bone morphogenetic protein 2 (BMP-2) are reduced. Other proteins including osteocalcin, E11/gp38, sclerostin (Sost) and dentin matrix protein 1 (DMP-1) are upregulated or introduced (Mullen et al., 2013).

There is little knowledge about the cues which regulate osteocytogenesis (Dallas et al., 2013). The mechanical properties of the deposited osteoid, which is softer compared to mineralised bone tissue, might guide differentiation (Mullen et al., 2013). In addition, mineralisation of the osteoid and hypoxic conditions might also be a driver for osteocyte formation (Prideaux et al., 2012; Irie et al., 2008).

Research in osteocytes has gained interest in recent years, since they are no longer seen as the 'passive place holder in bone' but as cells with very different functions

(Bonewald, 2011). Osteocytes, which are the most abundant cell type in bone (90-95% of total bone cells), are thought to respond to mechanical loading by releasing signal factors. Through these factors they coordinate bone remodelling by regulating osteoclast and osteoblast activity (Knothe Tate et al., 2004).

Osteoclasts

Osteoclasts are specialised cells which can resorb mineralised bone matrix by secreting acid and lytic enzymes. They are multinucleated cells derived from mononuclear precursor cells which are located in the bone marrow (Boyle et al., 2003). Their differentiation (osteoclastogenesis) is controlled by cytokines such as RANKL and macrophage colony-stimulating factor (M-CSF), which are produced by neighbouring stromal cells and osteoblasts. Differentiation of osteoclasts can be inhibited by OPG which binds RANKL with high affinity and prevents its attachment to the RANK receptor (Suda et al., 1999).

2.1.3 Bone extracellular matrix

The extracellular matrix (ECM) of bone is a composite material consisting of 50% to 70% inorganic mineral, 20% to 40% organic materials, less than 3% lipids, and water (Clarke, 2008). The exact composition depends on factors such as age, bone site, gender or medical conditions including osteoporosis (Boskey, 2013).

The mineral part of bone closely resembles hydroxyapatite and provides the bone with mechanical rigidity and load-bearing strength (Boskey, 2007). This phase can be best described as a crystalline complex of calcium and phosphate which also contains impurities such as sodium, magnesium, citrate and fluoride (Khan et al., 2013). Elasticity and flexibility of the bone is provided by the organic components which include structural proteins such as collagen and fibronectin (Nair et al., 2013). The organic phase is also composed of other non-collageneous matrix proteins which serve important functions controlling matrix organisation and mineral deposition (Boskey, 2013; Young, 2003). For example, mineralisation is likely to be controlled by the small Ca^{2+}-binding protein osteocalcin. Mechanotransduction is facilitated by glycoproteins such as osteopontin and osteonectin which can attach to integrins on cell surfaces. Osteopontin also enables the attachment of osteoclasts to bone surfaces (Gundberg, 2003). The small amount of lipids are crucial for cell signalling and ion flow (Clarke, 2008).

Collagen assembly

The assembly of collagen fibrils is a complex process involving intracellular and extracellular steps. Collagen is first synthesized as precursor molecules (procollagen) in the intracellular space before these molecules are assembled to long fibres outside the cell (Figure 2.2).

Collagen formation is initiated in the nucleus of collagen-producing cells such as osteoblasts but also fibroblasts. In the nucleus a particular segment of desoxyribonucleic acid (DNA) is transcribed into messenger ribonucleic acid (mRNA). After the mRNA has moved out of the nucleus into the cytoplasm it is translated into polypeptide chains, known as pre-pro-collagen. Each chain is about 300 nm in length and 1.5 nm in diameter. They are characterized by a strict pattern consisting of multiple triplet sequences of Gly-Y-Z. Glycine residues (Gly) have to be present in every third position to allow proper folding of these chains later on. Although Y and Z can be any amino acid, they are commonly proline and hydroxyproline (Rest and Garrone, 1991). Each chain is terminated by a few characteristic amino propeptides and carboxy propeptides on either side. These terminal propeptides are essential in preventing self-assembly of long collagen fibres within the cell.

Proline and lysine residues are then hydroxylated in the endoplasmatic reticulum (ER) which will aid cross-linking of peptide chains later. This enzymatic step requires ascorbic acid (vitamin C) as a cofactor. A lack of ascorbic acid would either result in the formation of looser collagen triple helices or prevent collagen synthesis altogether resulting in diseases such as scurvy (Canty and Kadler, 2005). Three modified peptide chains will form a triple helix which is further stabilised by disulphide bonds. In the case of type I collagen, two α1 chains and one α2 chain assemble to form a triple helix, referred to as procollagen.

After the proteins have achieved their helical conformation, they move from the ER to the Golgi apparatus where they are packed into secretory vesicles. These carriers vary in size and morphology and have been either described as vacuoles around 500 nm in length (Leblond, 1989), or as larger tubular-saccular structures (Polishchuk et al., 2000). The vesicles move along the microtubules towards the plasma membrane where they release the procollagen in the extracellular space.

Once procollagen has been released from the cell, collagen fibres start to form directly on the cell membrane. This proximity potentially allows the cell to directly control fibrogenesis and possibly even the formation of long-range assemblies, e.g. parallel bundles in tendon and ligament or interlocking weaves in bone (Kadler et al., 2008). Fibronectin and specific cell-surface integrins, such as the collagen-binding $\alpha 2 \beta 1$ integrin, have been found to be essential in the organization and deposition

of fibrillar collagen (McDonald et al., 1982; Li et al., 2003). Wenstrup et al. (2004) also found that small amounts of type V collagens are necessary for the induction of fibrillogenesis of collagen I fibres in vivo.

Collagen fibres can only form after specific enzymes remove the terminal propeptides from the procollagen which are then called tropocollagen (Prockop et al., 1998). Tropocollagen units assemble spontaneously into collagen fibres. Several hundred tropocollagen molecules line up in a characteristic "quarter staggered" array, so that the composite fibre appears as a striated pattern by electron microscopy. The striated pattern results from the longitudinal staggering of the molecules which leaves a "hole" roughly the size of one quarter of the length of tropocollagen (67 nm) between the end of one molecule and the beginning of the next (Scott, 1995). The fibres are further supported through the formation of covalent bonds. The enzyme lysyl oxidase catalyses the formation of bonds by converting hydroxyl groups on lysines and hydroxyl lysines into aldehyde groups (Kagan and Li, 2003). Consequently, the fibres increase up to tenfold in diameter and dramatically in length following lateral and end-to-end fusion (Birk et al., 1995).

Collagen orientation

Two types of bone can be distinguished based on the orientation of collagen fibres within the bone matrix: (1) woven bone which consists of randomly oriented collagen fibrils, and (2) lamellar bone which is characterised by highly orientated collagen fibres (Kini and Nandeesh, 2012). Collagen fibres in lamellar bone are arranged in arrays of parallel fibres which successively change orientation to form a 'twisted plywood-like' structure (Weiner et al., 1997). The alternating orientation of collagen arrays results in significantly higher strength of lamellar bone compared to woven bone (Clarke, 2008). This plywood structure can be found in the cylindrical osteons which are the primary building blocks of compact bone. Osteons are made up of several concentric lamellae which are arranged in different orientations around the Haversian channel containing the blood and nerve supply (Figure 2.3). The long axis of an osteon is usually parallel to the long axis of the bone and the dominant collagen fibre orientation commonly follows the direction of load (Heřt et al., 1994; Martin and Boardman, 1993; Seto et al., 2008). Furthermore, longitudinal collagen fibres are primarily present in regions supporting tensile loads while regions under compressive loading are composed of transverse fibres (Martin et al., 1996; Riggs et al., 1993).

Besides the spatial orientation of collagen fibres, mechanical properties of bone are also determined by several other factors, which include total bone mass and material properties of bone mineral (Viguet-Carrin et al., 2006). While the latter is more
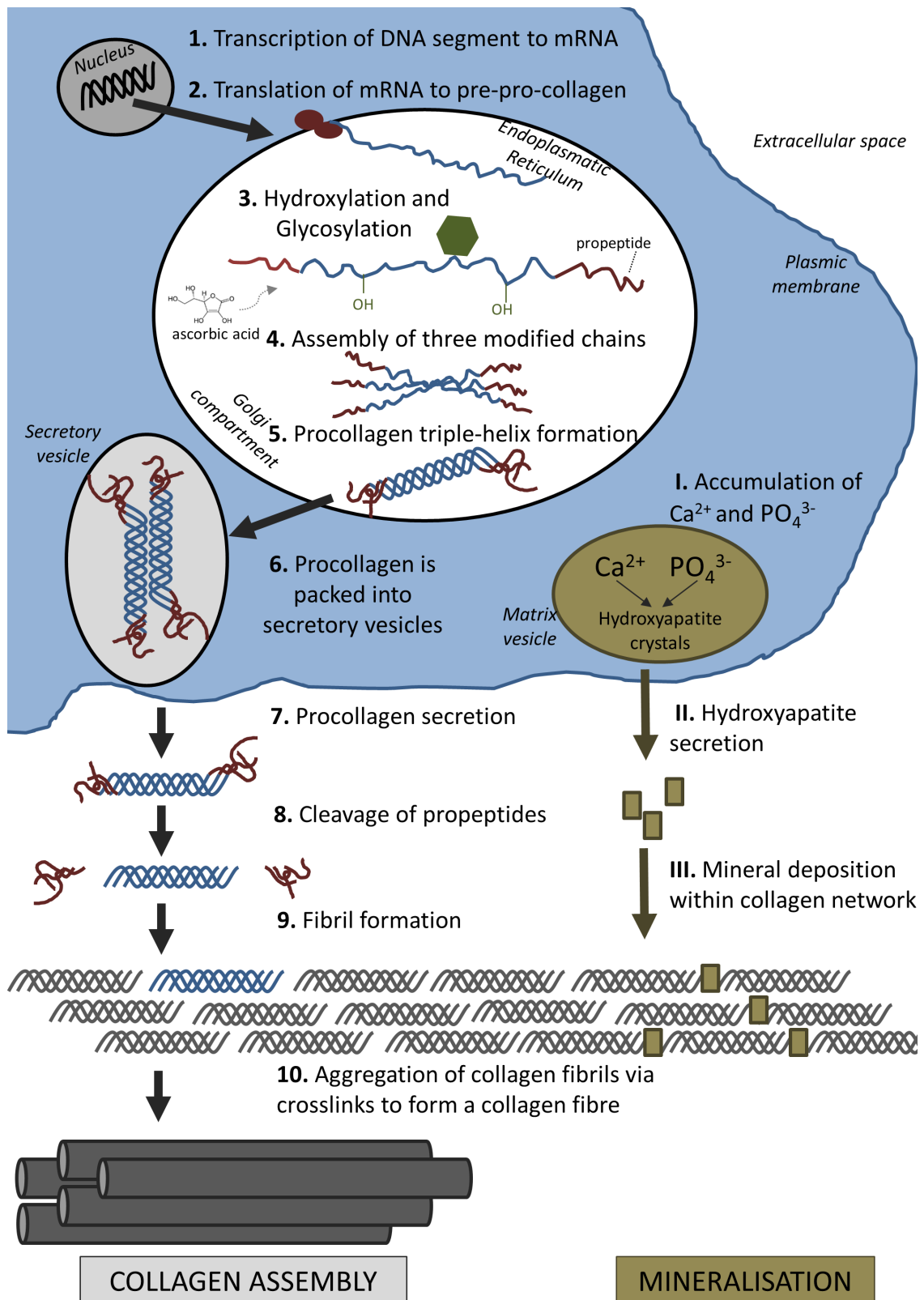
Figure 2.2: Formation of extracellular matrix: collagen assembly and mineralisation.

important with respect to bone stiffness and yield strength, the collagen network appears to have a greater impact on post-yield properties including ultimate strength and toughness of bone (Garnero, 2015). Even though the dependence of fibre orientation on bone strength is well accepted, it remains difficult to estimate exactly the effect collagen orientation has on mechanical properties of bone (Viguet-Carrin et al., 2006).

The mechanisms which guide the spatial arrangement of collagen fibres have been a matter of research for more than 40 years. In 1975, Jones et al. (1975) observed that collagen fibres were oriented in the same direction as osteoblasts producing the collagen, but they could not determine whether the cells controlled the orientation of the collagen fibres or vice versa. The central question since then has been revolving around whether the 3D organisation of collagen fibrils is a result of self-assembly (Giraud-Guille et al., 2008) or cell activity (Matsugaki et al., 2015b). It is generally accepted that collagen fibre formation on the nanometre length scale is driven by self-assembly (Kadler et al., 2008), while on a macro scale there is clear evidence of collagen fibre orientation following external loading patterns as described above (Martin et al., 1996; Puustjärvi et al., 1999). As a result, research focusses on determining the mechanisms which regulate collagen fibril assembly on intermediate length scales and whether cells influence this process (Kerschnitzki et al., 2011).

Mechanically weaker woven bone is produced in situations where no bone matrix is present, i.e. during bone formation in the foetus and newborn or in early phases of bone repair following fractures and osteotomies. Under such conditions, mesenchymal osteoblasts secret collagen fibres rapidly and randomly in all directions (Shapiro, 2008; Shapiro, 1988). However, most bone in a healthy adult which is formed as a result of the remodelling process described above is composed of highly orientated, lamellar bone (Figure 2.3). It is thought that the production of parallel collagen fibres requires collective, organised action of bone-producing cells (Kerschnitzki et al., 2011).

Weakly organised woven bone or pre-existing old bone matrix is believed to act as trigger for cells enabling lamellar bone formation. In particular, the nanofibrillar topography of bone appears to be a powerful substrate specific cue for cell and collagen alignment. In vitro studies have shown that osteoblasts align uniformly along the direction of grooves in the micrometre (Wang et al., 2000; Wang et al., 2003) and nanometre range (Zhu et al., 2005; Lamers et al., 2010; Yang et al., 2009). Highly oriented natural and artificial collagen fibre matrices can also act as scaffold inducing alignment of osteoblasts (Matsugaki et al., 2015b; Delaine-Smith, 2013). These studies further show that newly secreted collagen fibres and apatite crystals follow

the cell direction. In contrast, Matsugaki et al. (2015a) recently cultured osteoblasts on nanogrooved biomedical alloys. However, they observed a mismatch between cell orientation following the direction of the grooves and collagen matrix and apatite crystals orientation which aligned perpendicular to the cell direction. The authors explained this 'abnormal' orientation with a yet to define impact of pattern spacing and the potential existence of a threshold for parallel or perpendicular organisation of bone matrix produced by osteoblasts.

Mechanical stimulation might be another trigger coordinating 3D matrix arrangement. For example, osteoblasts collectively change orientation under cyclic stretching probably to minimise strain applied to them and secrete better organised collagen bundles (Matsugaki et al., 2013). The influence of mechanical forces on collagen fibre alignment has been extensively researched in soft tissues where fibroblast deposit an unmineralised collagen matrix. For example, interstitial fluid flow might act as mechanical stimuli for fibroblast-mediated collagen alignment. Ng et al. (2005) observed perpendicular cell and collagen fibre alignment relative to the direction of fluid flow in a 3D collagen model. They explained the perpendicular fibre alignment with a reduction in shear and drag forces affecting the fibroblasts (Pedersen et al., 2010).

Most of the hierarchical fibre assembly is believed to take place extracellularly. However, some suggest a fibre pre-orientation already inside the transport vesicles before the procollagen is released from the cell (Leblond, 1989). In addition, cell surface "fibropositor" structures have been described in embryonic tendons indicating that there might be mechanisms in place which determine fibre orientation before the extracellular release of procollagens (Holmes et al., 1998; Canty and Kadler, 2005). Importantly, to date this feature appears to be specific to tendon development only and has not been found in bone-producing osteoblasts.

In bone, the mechanisms involved in the alignment of collagen fibres by osteoblasts are not well understood yet (Matsugaki et al., 2013). In soft tissues, traction forces exerted by fibroblasts are thought to be the main driver in remodelling ECM (Harris et al., 1981; Feng et al., 2014). For example, contraction of myofibroblasts and the transmission of these forces to the collagen network is considered a crucial step in wound healing (Tomasek et al., 2002). Traction forces applied by osteoblasts might be able to orient fibres in a similar way as observed with fibroblasts (Curtze et al., 2004). Using traction force microscopy, Poellmann et al. (2015) demonstrated that differentiated, collagen-producing osteoblasts exert higher traction forces compared to pre-osteoblasts found in the marrow which are not yet involved in collagen secretion. In addition, time-lapse images suggest that traction forces combined with

cell motility enables osteoblasts to actively reorganise the ECM by moving 'packets' of fibriliar material around (Dallas, 2006). Traction forces induced by osteoblasts might also create strains within the osteoid layer which initiate collagen fibre alignment through degradation of unstrained collagen fibres (Flynn et al., 2010; Heck et al., 2015). Furthermore, interaction between fibronectin, integrins and other collagens such as collagen V may also play a role in the collagen fibre orientation process in vivo (Kadler et al., 2008).

Mineralisation

The organic collagen matrix in bone is strengthened by a mineral phase. Similar to the deposition of the organic collagen matrix, mineralisation is also a cell-controlled process. For example, osteoblasts initiate calcification at selected, non-random sites and they regulate the ion flux into the ECM (Boskey, 2007).

Mineralisation occurs in two steps (Figure 2.2). First, hydroxyapatite crystals are formed within matrix vesicles inside the osteoblast. In the second step of mineralisation, hydroxyapatite is secreted through the membrane into the ECM and deposited within the collagen fibrils (Anderson, 1995).

During the first phase, calcium ions and phosphates are accumulated in matrix vesicles. This step is controlled by calcium binding molecules and enzymes including ALP (Anderson, 2003). ALP is a plasma membrane bound enzyme which is thought to promote mineralisation by increasing the local concentration of phosphate and by breaking down extracellular mineralisation inhibitors such as pyrophosphates (Golub and Boesze-Battaglia, 2007). Once the concentration of calcium ions and phosphates exceed their solubility point, hydroxyapatite is formed within the matrix vesicles (Orimo, 2010).

During the second phase of mineralisation, matrix vesicle walls are broken down and hydroxyapatite crystals are secreted into the extracellular space. The organic collagen network acts as scaffold for mineral deposition and together with non-collageneous proteins defines the size and distribution of apatite crystals in the bone (Wang et al., 2012). The small crystals are first deposited at the gap zones within the quarter-staggered collagen fibrils (Katz et al., 1989). Initially, apatite crystals align their c-axes parallel to collagen fibres, but ultimately all available intra-fibrillar space is filled with mineral (Golub, 2009). Fluid shear stress (FSS) might also influence formation of bone apatite, since better organised apatite crystals were formed under low FSS environment ($\leq 1\,\mathrm{Pa}$) compared to higher FSS (Niu et al., 2016).
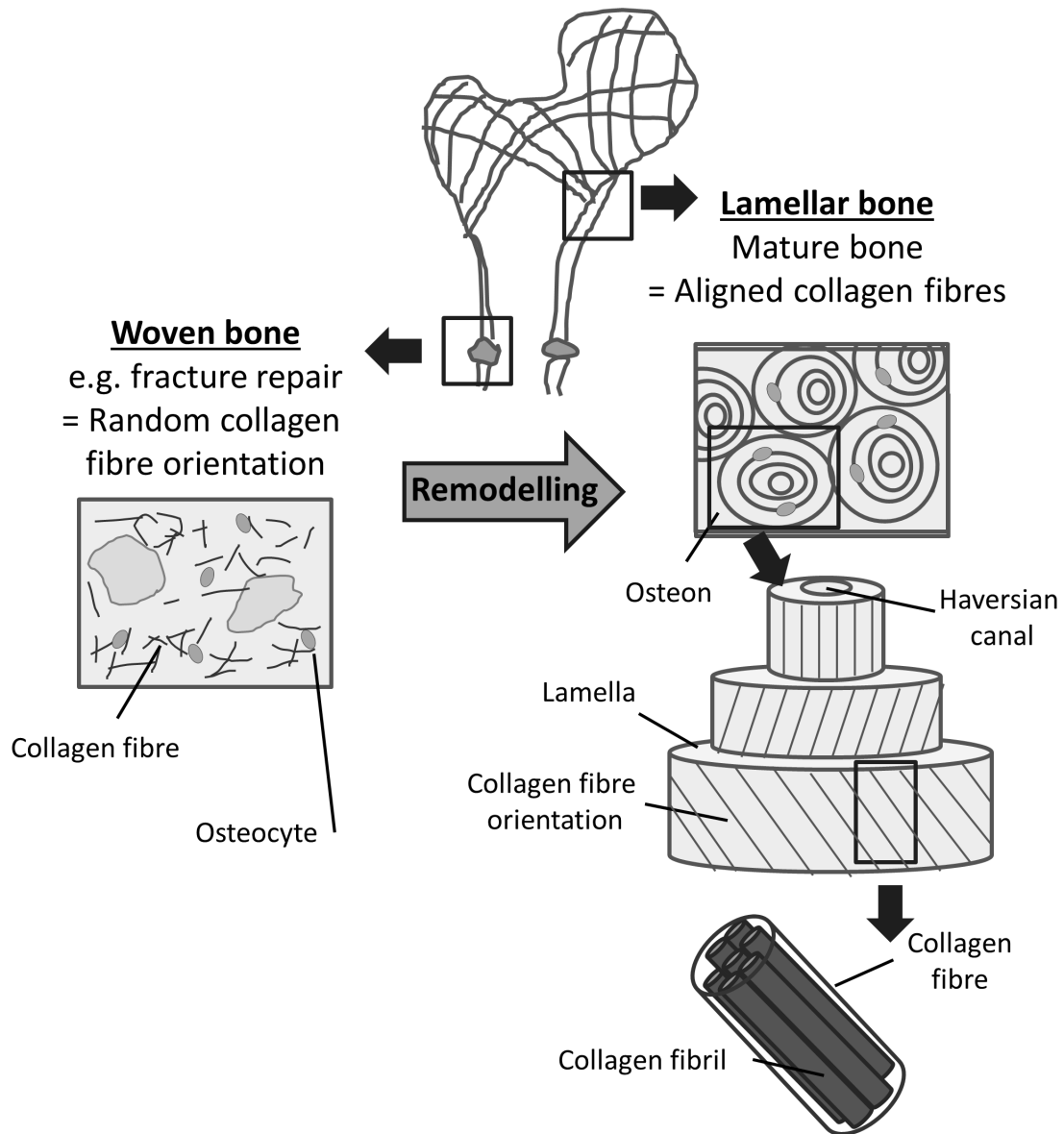
Figure 2.3: Woven and lamellar bone.

Two types of bone can be distinguished based on the orientation of collagen fibres within the bone matrix. Woven bone (left) consists of randomly oriented collagen fibrils and exists during fetal development and fracture repair. Following bone remodelling, most mature bone can be characterised as lamellar bone (right). Lamellar bone is characterised by highly orientated collagen fibres arranged in lamellae and osteons. The alternating orientation of the collagen lamellae results in significantly higher strength of lamellar bone compared to woven bone.

2.2 Bone mechanotransduction

The mechanism through which cells convert mechanical stimuli into biochemical responses is called mechanotransduction (Ingber, 2006). It is widely accepted that mechanical forces influence cell behaviour and play a central role both in normal tissue physiology and diseases. Endothelial cells for example experience one of the greatest forces within mammalian tissues (2 Pa to 4 Pa) as a result of blood shear and pressure. These cells have been shown to alter their cell morphology and orientation and determine vascular physiology and pathology as a result of fluid shear stress (Davies, 1995). Other examples include the auditory system and lungs. It has been shown that mechanotransduction is fundamental for the ability to hear. Changes in sound pressure bend hair cells in the inner ear and initiate a cascade of biochemicals signals, e.g. release of Ca^{2+} (Vollrath et al., 2007; Gillespie and Müller, 2009). Lung function is also controlled by mechanical forces which include tissue strain, fluid shear stress and compression (Schumacker, 2002).

Similarly, mechanical loading has been identified as one of the main drivers on the mass and structural adaptation of bone. In the 19th century, Julius Wolff (1892) postulated in 'Wolff's law of bone transformation' the idea that bone architecture is a result of mechanical stress and related it to a mathematical law. Although more recent research has shown that some of Wolff's assumptions were incorrect, the general idea that mechanical forces are closely linked to bone adaptation remains (Lee and Taylor, 1999).

Several in vivo studies demonstrated that gravitational forces and mechanical loads generated by muscle contractions are essential for stimulating bone remodelling and maintaining optimal mechanical performance. For example, reduction in mechanical stimulation due to extended periods of bed rest (Leblanc et al., 1990), microgravity in space (Vico et al., 2000) or limb paralysis (Weinreb et al., 1989), are associated with reduced bone formation and increased bone resorption.

2.2.1 Mediators of mechanotransduction in bone

Mechanical forces can be sensed and tranduced by various means at the cellular level in bone (Figure 2.4) (Freund et al., 2012). The matrix-integrin-cytoskeleton pathway is thought to play an important role in bone mechanotransduction, since integrins directly connect bone cells with their ECM. Integrins are membrane-bound glycoproteins which allow rapid transmission of physical stimuli from the ECM via the cytoskeleton to the nucleus, where they could initiate changes in gene expression (Duncan and Turner, 1995). The cytoskeleton itself, which is composed of actin,

microtubules and intermediate filaments, not only connects all components of the mechanosensing system, but actin fibres in cell processes have also been shown to be crucial for osteocyte mechanosensing (Klein-Nulend et al., 2012). The primary cilium, which is a microtubule-based antenna-like extension, has been identified as another mechanosensor in bone cells (Malone et al., 2007; Delaine-Smith et al., 2014). The glycocalyx, which is a cellular coating rich in hyaluronic acid, might also contribute to bone cell mechanotransduction via force transmission to the cytoskeleton and integrins (Burra et al., 2011; Reilly et al., 2003). Moreover, membrane bound proteins such as connexins allow exchange of molecules between adjacent cells and are therefore thought to be essential in osteocyte communication (Rubin et al., 2006). In addition, channels which are sensitive to fluid flow or membrane stretch can respond rapidly to mechanical stimulation by admitting or releasing ions, such as Ca^{2+} (Walker et al., 2000).

2.2.2 Mechanical forces in bone

Gravitational forces and muscle contractions result in small deformations of bone which generate matrix strain and interstitial fluid flow within the porous bone.

Matrix strain

Small deformations of mineralised bone induce tissue strain which - to some extent - may be directly sensed by bone cells. In 1987, Frost related macrostructural bone deformations to bone remodelling in his 'mechanostat theory', where he postulated that physiological strains range between 0.03% and 0.15%. Below this range bone absorption is initiated and between 0.15% and 0.3% bone mass is increased through bone remodelling (Frost, 1987). These thresholds have been confirmed experimentally in vivo (Frost, 2003; Al Nazer et al., 2012). In vitro however cells require much larger strains (1%-10%) to induce osteogenic responses (Klein-Nulend et al., 1995b; You et al., 2000); strains of this magnitude would cause bone fracture in vivo. Therefore, cells might not directly sense bone strains as described by Frost, but rather microstructural strains near lacunae and microcracks within the bone. These strains are thought to be several times greater and might be able to stimulate osteoblasts directly (Bonivtch et al., 2007).

Fluid shear stress

Interstitial fluid (ISF) is a main component of body mass (up to 20%) and is distributed throughout the ECM. It provides cells with nutrients and waste removal and can also be found in cortical and cancellous bone where it fills the porosities within the tissue. The three levels of porosities in bone are: (1) the vascular
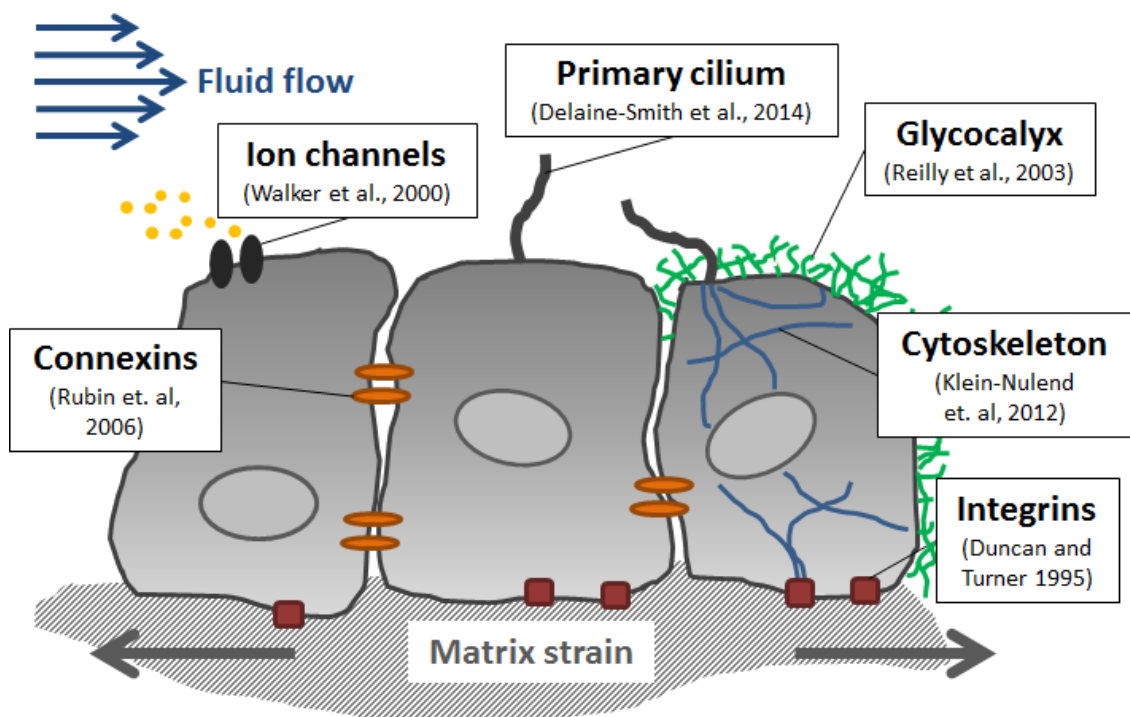
Figure 2.4: Mediators of mechanotransduction in bone.

Several cellular structures have been identified in bone cells which contribute to sensing mechanical stimuli including fluid flow induced shear stress and matrix strain.

porosity within the Volkmann canal and the Haversian canals (20 μm radius), (2) the lacunar-canalicular system (LCS) which are the channel structures within the mineralised bone tissue surrounding osteocytes and their processes (0.1 μm radius), and (3) tiny spaces between crystallites of the mineral hydroxapatite and collagen fibres (0.01 μm radius) (Cowin and Cardoso, 2015).

ISF flow is generally linked with lymphatic drainage, where plasma that has leaked out of the capillaries is being returned to the blood circulation (Swartz and Fleury, 2007). The hydrostatic and osmotic pressure differences between blood, interstitium and lymphatics are considered the driving forces for the slow but constant ISF present in most soft tissues and they also affect flow in the vascular porosity and the small channels of the LCS, in particular during rest periods without physical activity (Xing et al., 2014).

In contrast to ISF flow in most soft tissues, substantially greater flow rates can be generated in bone tissue by muscle contractions inducing blood pressure changes, and mechanical loading (Figure 2.5A) (Burger and Klein-Nulend, 1999; Knothe Tate et al., 2000). Mechanical loading results in bending of bones and matrix deformation. Compressive stress is generated on one side of the bone and tensile stress on the other (Figure 2.5B). The resulting pressure gradient in the ISF is thought to drive the fluid from regions of compression to tension (Duncan and Turner, 1995). ISF fluid has to squeeze through the narrow channels, canaliculi, which connect osteocytes residing in small spaces, lacunae, within the mineralised bone matrix. Due to the small dimensions of the channels, high wall shear stress comparable to vascular wall shear stress is generated. A numerical model by Weinbaum et al. (1994) estimated the mechanical-loading induced FSS sensed by osteocytic processes within their proteoglycan filled canaliculi to range between 0.8 Pa and 3 Pa.

More recently, Weinbaum and colleagues put forward an alternative hypothesis which advocates fluid-shear induced strain instead of FSS as dominant mechanical stimuli in osteocytes. The group developed mathematical models, which predict strong mechanical stimulation due to fluid drag forces on actin filament bundles of the cell processes and tethering fibres. Tethering fibres anchor osteocyte cell processes to the canalicular walls and centre them within the canaliculi. Fluid drag forces generate a 'circumferential hoop strain' which can be compared to the force applied by pulling a ring off a finger. These forces are thought to be 1-2 magnitudes larger than whole tissue strains and several times larger than fluid shear forces on the cell surface (You et al., 2001b; You et al., 2004; Han et al., 2004). Interestingly, this hypothesis yet again puts strain (although this time it is fluid shear-induced strain) at the focus of attention.

Defining the mechanical environment of osteoblasts is even more challenging than of osteocytes. It is unlikely that the model by Weinbaum et al. (1994) can also be applied for matrix-depositing osteoblasts. Unlike osteocytes, osteoblasts are not located within tiny channels and surrounded by a stiff, calcified bone matrix. Osteoblasts can be found on the surface of soft osteoid and newly-formed bone mineral at remodelling sites, i.e. in regions with bigger porosities and hence reduced fluid flow and FSS (Liegibel et al., 2004). Estimation of FSS values is further complicated due to the constant remodelling of the channel geometries which surround osteoblasts and a lack of knowledge regarding the mechanical properties of the soft osteoid. Based on experimental and computational studies, McGarry et al. (2005) hypothesized that the in vivo mechanical environment of osteoblasts is distinctively different to osteocytes. Bonewald and Johnson (2008) further stress that osteoblasts are unlikely to be subjected to great FSS in vivo and that the form and magnitude of FSS are very different from what osteocytes sense in the LCS. Therefore, even though medium to high FSS (>0.8 Pa) might be the dominant stimulus for osteocytes within the LCS and under mechanical loading during physical activity, osteoblasts might regularly encounter lower, interstitial-like FSS (Figure 2.5C).

Matrix strain or fluid shear stress?

Matrix strain and fluid shear stress both cause cell deformation. However, the nature of the deformation is not the same. While strain is applied directly through the cell attachments, fluid flow is sensed through the cell membrane first (Mullender et al., 2004). Consequently, it appears that both mechanisms excite different signalling pathways (McGarry et al., 2005). There are only few in vitro studies which directly compare effects of fluid flow and mechanical strain on bone cells and although cells often react to both stimuli, greater responses can be seen under fluid flow (Owan et al., 1997; You et al., 2000). Therefore, this review focuses on studies that investigate the direct impact of fluid shear stress on bone cell behaviour.

2.2.3 In vitro models for fluid shear stress mechanotransduction

Our understanding of mechanotransduction in bone cells has been greatly enhanced by in vitro models (Delaine-Smith et al., 2015). In vitro models aim to recreate the fluid shear forces found within the bone in a controlled cell culture environment. Since the magnitude of fluid shear forces in bone is still debated, in vitro models prove useful for studying the impact of tightly defined types of flow, for example by comparing unidirectional to oscillatory flow or varying the magnitudes of fluid flow.
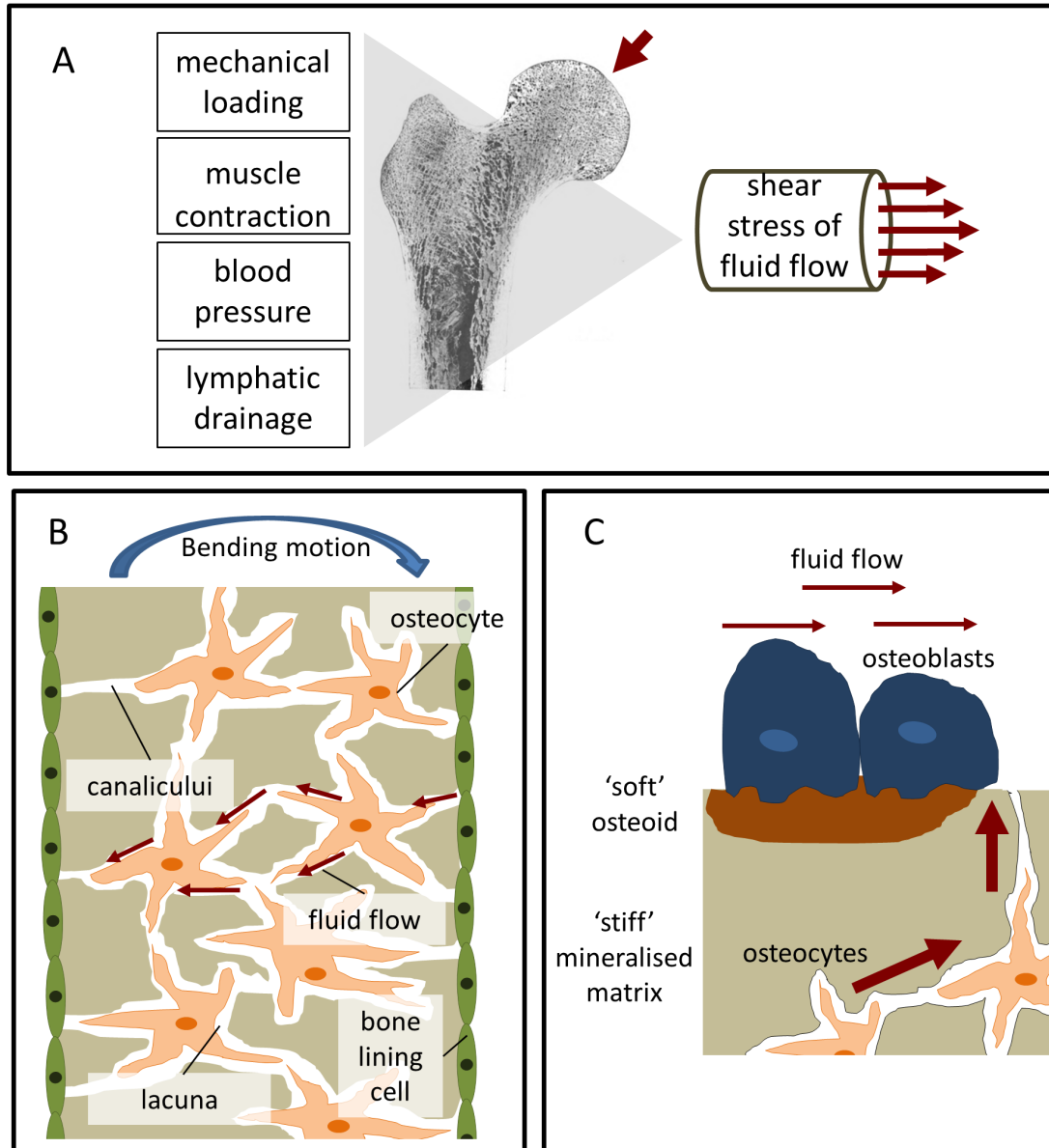
Figure 2.5: Fluid shear stress in bone.

A: Fluid flow in bone can be generated through mechanical loading, muscle contraction, blood pressure and lymphatic drainage. B: Bending of bone generates tension and compression forces which initiates interstitial fluid flow (adapted from Duncan and Turner (1995)). C: The biomechanical environment experienced by osteoblasts and osteocytes differs regarding flow velocities and matrix stiffness.

Parallel-plate flow chamber

Fluid shear stress is commonly applied to monolayer cell cultures in a parallel-plate flow chamber (PPFC, Figure 2.6). Most designs of PPFC are modifications of the original set-up by Frangos et al. (1985), where cells were grown on a glass slide encased by a polycarbonate chamber, sealed with a rubber gasket and the fluid flow was controlled via hydrostatic pressure. Fluid flow can also be controlled by pumps generating unidirectional (Reich et al., 1990; Genetos et al., 2004), pulsatile (Hillsley and Frangos, 1997; Klein-Nulend et al., 1997; Bacabac et al., 2004; Reich et al., 1990) and oscillatory (Lu et al., 2012a; Jacobs et al., 1998) flow profiles. Physiologically relevant wall shear stresses in the range of 0.001 Pa to 3 Pa can be generated with PPFC (Yu et al., 2014). In particular, the application of very high shear rates is an advantage of PPFC compared to other systems.

Except near the inlet, flow in PPFC can be considered laminar since Reynolds numbers are generally very small. Laminar flow generates a simple flow profile resulting in a high degree of control over the flow pattern and generated shear stresses. Shear stress τ acting on the cells inside the channel can be calculated using the following equation:

$$\tau = \frac{6Q\mu}{bh^2} \qquad (2.1)$$

where Q is the flow rate, μ is the viscosity of the flow media, h is the height of the channel, and b is the width of the channel. In most chambers more than 85% of the cells are exposed to a homogeneous wall shear stress for $b/h > 20$ (Bacabac et al., 2005). However, to ensure this uniformity, flow profiles should be verified for each channel design with numerical simulations or experimental methods such as particle image velocimetry (PIV) (Anderson et al., 2006).

Pump-driven flow often generates high pressure at the chamber inlet which easily causes leakages (Anderson et al., 2006). Such systems subject cells not only to fluid shear but also to substantial pressures, therefore cellular responses are not just the result of FSS but of a mixed stimulus. A closed loop system where fluid is simultaneously pushed and pulled can provide an alternative method and significantly reduce pressure build-up within the device (Huesa et al., 2010).

In order to perform experiments more efficiently and to test different shear rates at the same time, the basic concept of PPFC has been extended to multi-shear devices. For example, Yu et al. (2014) designed a complex microfluidic network consisting of relatively large cell culture chambers. They were able to generate different FSS on the same chip by using different widths and lengths of the inlet channels.
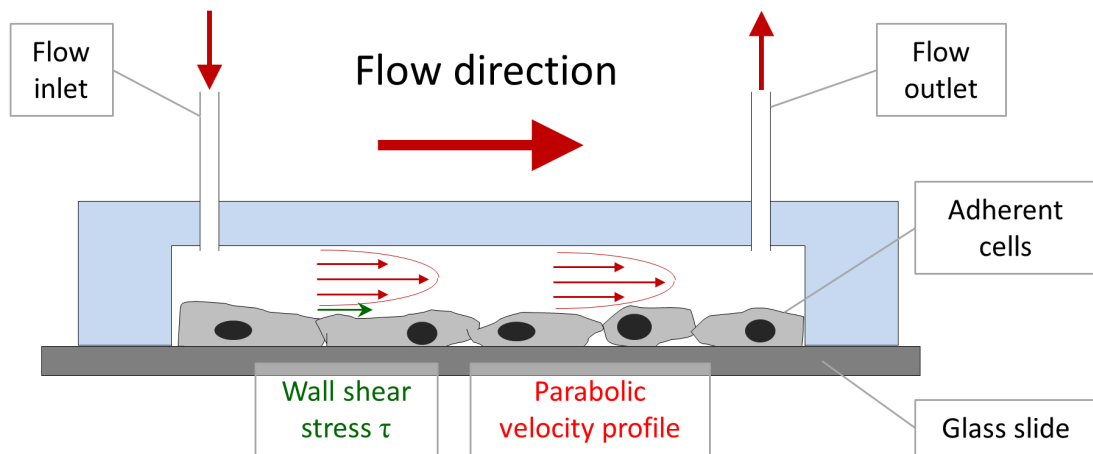
Figure 2.6: Parallel-plate flow chamber.

Parallel-plate flow chambers are common devices used to perform in vitro studies to examine the influence of well-defined flow and thus shear stress on adherent cells.

PPFC can also be combined with micro-patterned systems which enable cell organisation. For example, Lu et al. (2012a) applied micro-contact printing and self-assembled monolayer surface chemistry technologies to establish an osteocyte network on a chip.

One drawback of PPFC is the difficulty of applying flow for more than 24 hours, limiting their use for long-term experiments. Commonly associated problems of PPFC include the formation of air bubbles within the channels over time which can completely alter the biochemical and biomechanical environment of cells (Anderson et al., 2006). Higher flow channels (Scaglione et al., 2008), intermittent fluid flow (Morris et al., 2010), and disassembly of PPFC following flow application (Kreke et al., 2005), are some of the alterations which have been made in the past to circumvent this issue enabling the use of PPFC for long-term experiments. However, these changes result in lower shear stress rates, constraints in experimental designs as well as complicated sample handling increasing the chances of contamination, respectively. In the future, PPFC could be designed with this in mind focussing on methods which allow straightforward assembly and disassembly of the chamber, for instance.

Multi-well plates on rocking platforms

Alternative methods for long-term culture of cells under fluid stimulation include culturing cells in multi-well plates. FSS can be applied to cell monolayers in these plates via rocking or orbital shaking platforms. Both systems have the advantage of allowing a high-throughput of samples. However, both systems are only able to generate low magnitude FSS with non-uniform patterns. The magnitude of shear stress sensed by the cells depends on several factors, most importantly their location within the well, the frequency of movement and the amount of liquid in the well.

Rocking 'see-saw' systems generate oscillatory FSS in the range of 0.001 Pa to 0.25 Pa. The characteristic shear stress τ at the bottom of the plate can be estimated using an analytical model described by Zhou et al. (2010):

$$\tau = \frac{\pi \mu \theta_{max}}{2\delta^2 T} \tag{2.2}$$

where μ is the fluid viscosity, θ_{max} the maximal flip angle, δ the ratio of fluid depth to well length and T the time for one cycle.

The 'sea-saw' rocker system has also been characterised with a computational finite element model and validated with PIV measurements. For a rocking frequency of 0.5 Hz, a maximum shear stress of 0.22 Pa was detected near the well edge but

the time-averaged shear stress along the majority of the plate centre line was much lower with 0.033 Pa (Tucker et al., 2014). The analytical characteristic shear stress of 0.027 Pa which was calculated for the same rocking frequency and the same maximum tilt angle of 7°, was slightly lower compared to the time-averaged shear stress estimated with the finite element model.

In vitro, fluid flow generated by 'see-saw' rockers has been shown to increase ALP activity and deposition of mineralised matrix in MSCs (Delaine-Smith et al., 2012) and to increase collagen secretion in tenocytes (Tucker et al., 2014). In another experiment, conditioned media from 'rocked' osteocytes has upregulated osteogenic genes in MSCs (Hoey et al., 2011).

Oscillatory flow profiles can also be generated by orbital shakers which are described in more detail in Salek et al. (2012). Orbital shakers have been applied in bone mechanotransduction research for example when investigating osteoblast attachment (Aryaei and Jayasuriya, 2015), focal adhesion kinease functions (Young et al., 2011), and osteoblastic differentiation of mesenchymal stem cells (Lim et al., 2014).

3D perfusion bioreactors

Different scaffold materials have been used for 3D bone cell culture aiming to provide a more natural cell environment compared to flat plastic or glass surfaces. Scaffolds have been manufactured using a wide range of different materials such as metals, ceramics, synthetic and natural polymers and composites which are combinations of these materials. Scaffold composition and architecture intend to mimic the natural properties of bone including its porosity and stiffness. These properties are not only determined by the scaffold material itself but also by its fabrication process. Some of the most common methods to generate porous scaffolds are solvent casting, gas foaming, phase separation, freeze-drying, rapid-prototyping and sintering (Karageorgiou and Kaplan, 2005; Stevens et al., 2008). Examples of scaffolds for bone cell applications include titanium fibre meshes (Bancroft et al., 2002), chitosan scaffolds (Su et al., 2014), polymerised high internal phase emulsions (PolyHIPEs) (Owen et al., 2016) and non-fibrillar hydrogels such as poly(ethylene glycol) (PEG) (Chatterjee et al., 2010). Furthermore, collagen, which is a natural hydrogel, has been applied extensively in models mimicking the fibrillar, collageneous osteoid matrix (Prideaux et al., 2014; Parreno et al., 2008). Properties of bone scaffold materials have been reviewed in more detail for instance by Hutmacher (2000), Stevens et al. (2008) and Bose et al. (2012).

Several bioreactor types have been developed to combine fluid flow with 3D culture including spinner flasks, rotating wall bioreactors and perfusion systems (McCoy

and O'Brien, 2010). The latter being most advantageous because a homogeneous microenvironment is generated within the porous scaffold by forcing fluid through the entire construct (Bancroft et al., 2002). Shear stress magnitudes within the scaffold can be approximated using the cylindrical pore model which takes into consideration the geometry of the scaffold and its porosity. The mean velocity through the pores V_m can be calculated using the following equation:

$$V_m = \frac{Q}{\phi\pi(D/2)^2} \tag{2.3}$$

where Q is the perfusion rate, ϕ is the porosity, and D is the diameter of the scaffold. Assuming a parabolic flow profile and cylindrical pores, the resulting shear stress at the scaffold wall τ, can be calculated:

$$\tau = \frac{8\mu V_m}{d} \tag{2.4}$$

where μ is the media viscosity and d is the diameter of the cylindrical pores in the scaffold (Goldstein, 2001).

In scaffolds, FSS is most likely not only caused by direct flow perfusion, but it might also be an indirect product of scaffold strain (Sumanasinghe et al., 2006) and compression (Vazquez et al., 2014; Sittichockechaiwut et al., 2009). This behaviour has been observed in natural bone where FSS is primarily a result of bone matrix deformation (Weinbaum et al., 1994). However, estimating FSS resulting from matrix strain and compression is not straight-forward. Moreover, a direct comparison of estimated shear stress magnitudes between monolayer and 3D experiments is often not relevant as the mechanical environment in 3D is more complex. For example, shear stress in 3D can also be transmitted to ECM fibres leading to ECM strain and thus cytoskeletal strain transmitted via integrins which can further increase the stress sensed by cells in 3D (Ng and Swartz, 2003).

2.2.4   Bone cell models for in vitro mechanotransduction research

Advancement in bone mechanotransduction research depends on the availability of suitable cell model systems which can sense and respond to mechanical stimuli similar to cells in vivo. Bone cells can be sourced from different origins including

- pluripotent stem cells which are differentiating to osteoblasts (Jaiswal et al., 1997),

- primary osteoblasts and osteocytes from different species (Jonsson et al., 2009; Prideaux et al., 2016), and

- immortalised and osteosarcoma cell lines (Kato et al., 2001; Woo et al., 2011).

Each cell model has its own advantages and disadvantages, hence the appropriate cell model has to be selected depending on the aim of the research (Czekanska et al., 2012).

Osteoblast cell models

Primary osteoblasts have been successfully isolated and cultured from human bones (Jonsson et al., 2009). Human-derived cells are a good candidate for clinical research since outcomes are not influenced by interspecies differences. However, primary human osteoblasts are a heterogeneous population and their behaviour depends on several factors, including isolation method (Voegele et al., 2000), cell location within the skeleton and donor age (Martínez et al., 1999). All of these factors can be better controlled by isolating primary cells from animals, including rats (Orriss et al., 2012) and mice (Bakker and Klein-Nulend, 2012). In addition, animal derived primary cells are more easily accessible and available in greater quantities (Czekanska et al., 2012).

Compared to primary cells, cell lines can provide even more homogeneous cell populations. They are either generated from immortalised primary cells, e.g. MC3T3-E1, human osteoblast-like cells (hOB) and human fetal osteoblast-like cells (hFOB), or they are derived from osteosarcomas, e.g. MG-63 and SaOS2 (Kartsogiannis and Ng, 2004).

A commonly used cell line in bone mechanotransduction research is MC3T3-E1 (Owan et al., 1997; You et al., 2001a; Genetos et al., 2004). This cell line was originally derived from primary cells collected from newborn mouse calvaria. MC3T3-E1 represent a pre-osteoblastic cell type capable of differentiating into osteoblasts, and deposit collagen and mineral nodules in vitro (Sudo et al., 1983; Franceschi and Iyer, 1992). However, variations in culture condition might have resulted in the formation of multiple sublines of this cell line. Studies comparing cells obtained from different sources found great differences in cell behaviour, for example regarding mineralisation (Wang et al., 1999) and PGE_2 production (Leis et al., 1997). These alterations in cell behaviour should be considered when comparing results of different studies which are potentially not using the same MC3T3-E1 subclones but subclones in different differentiation stages.

The MLO-A5 cell line also originates from primary mice cells and has been used

primarily in long-term studies investigating the mineralised matrix deposition (Delaine-Smith et al., 2012). In contrast to MC3T3-E1, MLO-A5 represent a post-osteoblast/pre-osteocyte cell type which more rapidly mineralises (Kato et al., 2001). MLO-A5 express typical late-osteoblast markers such as high ALP, bone sialoprotein (BSP), and osteocalcin (OCN) (Stern et al., 2012).

Osteosarcoma cells have also been used as a cell model when researching bone mechanotransduction (Myers et al., 2007). The cell line MG-63 for example, was originally derived from an osteogenic sarcoma of a 14-year old male (Heremans et al., 1978). Osteosarcoma cell lines can be a valuable tool for investigating specific aspects of bone cell function such as cell adhesion. However, in certain aspects they behave very different to normal bone cells, specifically their growth characteristics and ALP activities differ considerably from primary osteoblasts (Clover and Gowen, 1994).

Moreover, mesenchymal stem cells (MSCs) can also be used as osteoblast cell models. Since MSCs are pre-osteoblasts, they are a good model for gaining a better understanding of the mechanisms guiding MSC differentiation. To induce osteogenic behaviour in MSCs in vitro, they are commonly cultured in dexamethasone-supplemented culture medium (Kreke and Goldstein, 2004; Scaglione et al., 2008).

Osteocyte cell models

Although osteocytes are the most abundant cell type in bone, their isolation and culture is very challenging due to their location deep within the bone matrix. Primary osteocytes were first successfully isolated from chicken calvariae. The cell isolation process involved digestion of chick bones with collagenase and EDTA, followed by purification of the heterogeneous cell population with an osteocyte specific antibody (Plas and Nijweide, 1992). Similar procedures were applied for the isolation of primary osteocytes from mice (Stern et al., 2012), rats (Gu et al., 2006) and most recently humans (Prideaux et al., 2016). However, primary osteocyte culture still faces many obstacles. For example, the yield of osteocytes after isolation is normally low and since they are terminally differentiated cells they also lack the capability to proliferate in culture (Stern et al., 2012).

The first osteocyte cell line was developed by Kato et al. (1997). They isolated the cell line MLO-Y4 from the long bones of transgenic mice. This cell line can be considered as the most common osteocyte cell model and it has been widely applied in mechanotransduction studies (Li et al., 2012a; Ponik et al., 2007; Zhang et al., 2006). MLO-Y4 cells represent an early osteocyte cell type. Unlike osteoblasts, MLO-Y4 cells produce large amounts of osteocalcin but low levels of ALP and

collagen. In addition, MLO-Y4 cells are characterised by extensive dendrites and increased expression of connexin 43 as expected in osteocytes (Kato et al., 1997). In contrast, MLO-Y4 do not express the genes dentin matrix protein 1 (DMP-1) and Sclerostin (Sost) which are normally found in osteocytes (Stern et al., 2012).

This short-coming has been overcome by the development of the osteoblast-to-late-osteocyte cell line IDG-SW3. In the beginning of culture, IDG-SW3 show characteristics of osteoblasts, e.g. expression of ALP, deposition of collagen type I and mineral. Over time, IDG-SW3 cells differentiate towards early osteocytes (expression of E11/gp38, DMP-1, Phex) and subsequently towards late osteocytes which possess a characteristic dendritic morphology and express SOST/sclerostin and FGF23 (Woo et al., 2011). IDG-SW were isolated from long bones of transgenic mice in which the Dmp1 promoter drives the expression of the green fluorescent protein (GFP), which allows observation of osteocytogenesis by fluorescence microscopy. The more recently developed osteocyte cell line Ocy454 was isolated from the same transgenic mouse model as IDG-SW3. In contrast to IDG-SW3, Ocy454 demonstrated osteocytic characteristics within a considerably shorter period of time and did not require specific differentiation medium containing ascorbic acid or β-GP (Spatz et al., 2015).

2.2.5   Responses of osteoblasts to fluid shear stress

Osteoblasts respond to a wide range of different shear stimuli in vitro (Reich et al., 1990; Owan et al., 1997; Bakker et al., 2001; Yu et al., 2014).

Responses to high fluid shear stress

Relatively high FSS ranging between 0.5 Pa to 2 Pa have been widely reported to impact osteoblasts in vitro, including changes in biochemical factors and gene expression (Table 2.1). For example, flow shear rapidly increases intracellular calcium (Hung et al., 1995; You et al., 2001a), inositol trisphosphate (Reich et al., 1990), nitric oxide (NO) (Johnson et al., 1996; Owan et al., 1997), prostaglandin E$_2$ (PGE$_2$) (Reich et al., 1990; Klein-Nulend et al., 1997; Bakker et al., 2001), and adenosine triphosphate (ATP) (Genetos et al., 2004) levels in osteoblast cultures. PGE$_2$, NO and ATP have all been shown to depend on calcium signalling. Fluid flow has also been shown to regulate expression of osteoblast genes for osteopontin (OPN) (Owan et al., 1997; You et al., 2001a), cyclooxygenase-2 (COX-2), and c-FOS (Pavalko et al., 1998) but also genes related to matrix metabolism such as collagen I (Myers et al., 2007).

Most experiments have been performed in PPFC, but the short flow durations indicate the previously discussed challenges of culturing cells in channels for more

than a couple of hours (Zheng et al., 2010). In addition, osteoblast proliferation and matrix deposition will change the channel geometry over time and thus alter the shear stress (Nauman et al., 2001).

Responses to low fluid shear stress

As discussed previously, osteoblasts unlike osteocytes might be more commonly subjected to low FSS (Figure 2.5C). Osteoblast responses to low FSS below 0.5 Pa have also been shown in vitro (Liegibel et al., 2004; Yu et al., 2014; Aisha et al., 2015). Responses of osteoblasts, which were cultured on planar surfaces as monolayer, to low FSS were comparable to high FSS responses (Table 2.2). It should be noted however, that fewer studies investigated the lower stress range. Low FSS resulted in an increased production of PGE_2 (Liegibel et al., 2004), ALP (Xing et al., 2014; Aisha et al., 2015) and collagen (Xing et al., 2014). Furthermore, osteoblasts tended to proliferate more under low flow (Liegibel et al., 2004; Xing et al., 2014; Aisha et al., 2015). mRNA expression of osteogenic genes Runx2, ALP, Col I and osteocalcin was also increased under low FSS (Yu et al., 2014). Similar to high FSS experiments, PPFC were often used to provide the required stimuli in low FSS applications (Kou et al., 2011; Xing et al., 2014). In addition, rockers and orbital shakers were also used to generate FSS in this range (Liegibel et al., 2004; Aisha et al., 2015).

Long-term responses by cell monolayers

Osteoblasts respond within hours to fluid flow by releasing signalling factors including NO and prostaglandins (Bakker et al., 2001). However, it takes days to weeks for osteoblasts to begin laying down a collagen matrix which later mineralises. For example, MLO-A5 or MC3T3-E1 require at least 3 days (Kato et al., 2001) or even 2 weeks (Fratzl-Zelman et al., 1998) respectively before they begin to mineralise. Evaluation of such late responses - in addition to early responses - is important for a better understanding of bone remodelling and improved tissue engineering strategies. Bone strength for example is directly influenced by long-term responses such as mineral content and collagen fibre distribution but only indirectly linked to signalling factors such as NO (Bouxsein and Seeman, 2009).

Due to the previously discussed difficulties in culturing cells for days and weeks under controlled flow conditions, only a small number of studies is looking into downstream responses of osteoblasts (Table 2.3). Morris et al. (2010) cultured MLO-A5 osteoblasts in commercially available PPFC for 10 days while applying fairly high intermittent unidirectional fluid flow (0.8 Pa). By applying fluid flow intermittently for 1 h on only 2 days of culture, they were able to avoid any of the previously

Table 2.1: Osteoblastic responses to medium and high fluid shear stress.

Cell type	Shear stress	Flow type	Flow time	Culture system	mRNA	Other factors	Reference
Rat	0.6 Pa	s	12 h	PPFC		NO ↑	Johnson et al., 1996
Rat	0.1-2.4 Pa	s, p	30 min	PPFC		PGE_2 ↑	Reich et al., 1990
Mouse	0.7 Pa	p	1 h	PPFC		PGE_2 ↑	Klein-Nulend et al., 1997
MC3T3	-	-	72 h	Bending device	OPN ↑		Owan et al., 1997
Mouse	0.4-1.2 Pa	p	15 min	PPFC		NO ↑, PGE_2 ↑	Bakker et al., 2001
MC3T3	2 Pa	o	2 h	PPFC	OPN ↑	Ca^{2+} ↑	You et al., 2001a
MC3T3	1.2 Pa	s	1 h	PPFC	COX-2 ↑, c-FOS ↑		Pavalko et al., 1998
MC3T3	1.2 Pa	s	5 min	PPFC		PGE_2 ↑, ATP ↑	Genetos et al., 2004
MG-63	1 Pa	p	12 h	PPFC*	Col I ↑		Myers et al., 2007

Cell types refer to primary cells unless a specific cell line is stated. In case of oscillatory or pulsatile fluid flow the value given refers to the peak shear stress. * A Streamer[TM] unit was used. ATP - adenosine triphosphate, Ca^{2+} - calcium ions, Col I - collagen type I, mRNA - messenger ribonucleic acid, o - oscillatory, OPN - osteopontin, p - pulsatile, PGE_2 - prostaglandin E_2, PPFC - parallel-plate flow chamber, NO - nitric oxide, s - steady.

Table 2.2: Osteoblastic responses to low fluid shear stress.

Cell type	Shear stress	Flow type	Flow time	Culture system	mRNA	Other responses	Reference
hOB	1-63μPa	o	10-96 h	Orbital shaker	ALP ↑	FN ↑, PGE$_2$ ↑, TGF-β ↑, CP ↑	Liegibel et al., 2004
Rat	0.03-0.3Pa	s	2 min	PPFC		Ca^{2+} ↑	Kou et al., 2011
Rat	0.5 Pa	s	24 h	PPFC	Col I ↑	FN ↑, ALP ↓, coll. ↑, CP ↑	Xing et al., 2014
MC3T3	1.5-412μPa	s	24 h	PPFC	ALP ↑, OCN ↑, Col I ↑, Runx2 ↑, OSX ↔	CP ↑	Yu et al., 2014
NHOst	-	o	72 h	Orbital shaker		CP ↑, ALP ↑, OCN ↔	Aisha et al., 2015

Cell types refer to primary cells unless a specific cell line is stated. In case of oscillatory fluid flow the value given refers to the peak shear stress. ALP - alkaline phosphatase, Ca^{2+} - calcium ions, coll. - collagen, Col I - collagen type I, CP - cell proliferation, FN - fibronectin, hOB - human osteoblast, mRNA - messenger ribonucleic acid, NHOst - normal human osteoblast, NO - nitric oxide, o - oscillatory, OCN - osteocalcin, OSX - osterix, PGE$_2$ - prostaglandin E$_2$, PPFC - parallel-plate flow chamber, Runx2 - runt-related transcription factor 2, s - steady, TGF-β - transforming growth factor beta.

reported technical difficulties associated with long-term culture in PPFC. Scaglione et al. (2008) were also able to culture cells continuously over 10 days in a PPFC, but their system consisted of higher channels (2 mm vs 0.4 mm) which facilitated long-term cell culture without obstructing the channels. However, high channels meant that only low FSS in the millipascal range could be generated with this system. Other studies apply flow only for a couple of minutes to a maximum of several hours before disassembling the chambers and continuing cell culture outside of the flow chambers (Kreke et al., 2005; Kreke et al., 2008). Less defined and very low flow was also successfully applied by Delaine-Smith et al. (2012), who generated fluid flow in six-well plates with a see-saw rocker over 21 days.

The few long-term monolayer studies available report conflicting results whether fluid shear stress can indeed increase collagen deposition and mineralisation. Nauman et al. (2001) reported no change in mineralisation under pulsatile fluid flow. Other studies show a significant increase in collagen and calcium deposition as a result of fluid flow (Scaglione et al., 2008; Delaine-Smith et al., 2012; Morris et al., 2010). Scaglione et al. (2008) reported in the same study a lower mRNA expression of OCN under fluid stimulation. OCN is a late phenotypic marker of osteoblastic differentiation and associated with mineralisation. In contrast, Kreke and Goldstein (2004) report higher levels of OCN protein in the culture media when cells were exposed to high, intermittent shear stress. However, increased levels of OCN proteins did not translate directly to higher mineralisation. Instead, the number of cell aggregates, where mineralisation would initiate, decreased under fluid flow in the same study (Kreke and Goldstein, 2004).

Long-term responses by cells in 3D

In contrast to the few long-term flow studies available on flat surfaces, osteoblast behaviour on scaffolds in 3D has been studied extensively (Table 2.4). In vitro experiments have demonstrated that perfusion increases osteogenic differentiation and production of calcified extracellular matrix in 3D (Bancroft et al., 2002; Sikavitsas et al., 2005). Perfusion bioreactor studies however were normally not able to distinguish between effects caused by an increased nutrient transport or the stimulatory effects of FSS on the cultured osteoblasts (Ban et al., 2011; Sikavitsas et al., 2005). It is possible to separate the effects of FSS and mass transport by changing the culture media's viscosity (Sikavitsas et al., 2003; Li et al., 2009). For example, Sikavitsas et al. (2003) added dextran to the culture medium and demonstrated that enhanced osteogenic differentiation was indeed a result of increased FSS and not only greater mass transport.

FSS in perfusion bioreactors is commonly several magnitudes lower than shear stress

Table 2.3: Long-term effects or fluid flow on osteoblasts.

Cell type	Shear stress	Flow type	Culture time	Culture system	mRNA	Other responses	Reference
Rat MSC	0.06-0.6Pa	p	24 d	PPFC		MS $\leftrightarrow$, PGE$_2$ $\uparrow$	Nauman et al., 2001
Rat MSC	0.036-0.27Pa	s	21 d	RFC		CP $\leftrightarrow$, OCN $\uparrow$, PGE$_2$ $\uparrow$, no MS	Kreke and Goldstein, 2004
Rat MSC	0.16 Pa	s	20 d	PPFC	OPN $\uparrow$, BSP $\uparrow$	CP $\leftrightarrow$, ALP $\leftrightarrow$, OCN $\uparrow$	Kreke et al., 2005
Rat MSC	0.23 Pa	s	14 d	PPFC	OCN $\uparrow$, OPN $\uparrow$, Col I $\uparrow$, COX-2 $\uparrow$, BSP $\uparrow$		Kreke et al., 2008
Human MSC	1.2 mPa	s	10 d	PPFC	ALP $\downarrow$, OCN $\downarrow$, OPN $\leftrightarrow$, COL I $\uparrow$, OSX $\uparrow$, cbfa-1 $\uparrow$, BSP $\leftrightarrow$	CP $\downarrow$, coll. $\uparrow$, MS $\uparrow$	Scaglione et al., 2008
MLO-A5	0.051 Pa	o	21 d	Rocker		CP $\leftrightarrow$, coll. $\uparrow$, MS $\uparrow$, ALP $\leftrightarrow$	Delaine-Smith et al., 2012
MC3T3	1.2 Pa	s	12 d	PPFC	ALP $\uparrow$, Runx2 $\uparrow$, COX-2 $\uparrow$, BMP-2 $\uparrow$	coll. $\uparrow$, MS $\uparrow$, ALP $\uparrow$	Mai et al., 2013b; Mai et al., 2013a
MLO-A5	0.051 Pa	o	12 d	Rocker		CP $\leftrightarrow$, MS $\uparrow$	Delaine-Smith et al., 2014

Cell types refer to primary cells unless a specific cell line is stated. In case of oscillatory or pulsatile fluid flow the value given refers to the peak shear stress. ALP - alkaline phosphatase, BMP-2 - bone morphogenetic protein 2, BSP - bone sialoprotein, CP - cell proliferation, Col I - collagen type I, coll. - collagen, o - oscillatory, OCN - osteocalcin, OPN - osteopontin, OSX - osterix, MS - mineralisation, MSC - mesenchymal stem cell, mRNA - messenger ribonucleic acid, p - pulsatile, PGE$_2$ - prostaglandin E$_2$, PPFC - parallel-plate flow chamber, RFC - radial flow chamber, s - steady.

generated with PPFC (Goldstein, 2001). However, exact estimation of FSS is difficult since shear stress profiles are often inhomogeneous depending on the porosity of the (irregular and often anisotropic) scaffolds. Furthermore, matrix deposition will alter the porosity and therefore change the magnitude of FSS over time.

2.2.6 Responses of osteocytes to fluid shear stress

Osteocytes comprise between 90% to 95% of bone cells and are embedded deeply within the mineralised bone matrix. Osteocytes were found to be extremely sensitive to mechanical loading and to respond by releasing soluble factors enabling them to control bone remodelling directly or via paracrine signalling (Bonewald, 2011).

Direct responses to fluid shear stress

Osteocytes subjected to FSS have been shown to release several physiological relevant messengers in vitro (Table 2.5), including Ca^{2+} (Lu et al., 2012a; Jing et al., 2013), ATP (Genetos et al., 2007), NO (Klein-Nulend et al., 1995a), and PGE_2 (Klein-Nulend et al., 1997; Kamel et al., 2010).

FSS also regulates the release of RANKL and OPG. The relative abundance of RANKL compared to OPG is indicative of the amount of bone resorption. Downregulation of RANKL combined with upregulation of OPG as result of steady or oscillatory flow have been demonstrated in flow chamber experiments (Li et al., 2012a; Li et al., 2013). In addition, the mRNA expression of SOST/sclerostin, which functions as an inhibitor of bone formation, was reduced in short-term fluid flow studies (Spatz et al., 2015).

Osteocytes possess long dendritic processes which they use to form networks with neighbouring osteocytes or cells on the bone surface (Kamioka et al., 2001). As a response to FSS, osteocytes are able to modify and enlarge this network. For example, Zhang et al. (2006) demonstrated that FSS increased dendricity and elongation of osteocyte dendrites because of a greater expression of E11 mRNA. The dendritic protein E11 is one of the earliest osteocyte markers appearing on the elongating dendritic processes. E11 is absent on primary osteoblasts and increases with time following differentiation into an osteocyte-like cell type.

Osteocytes communicate with each other and osteoblasts and osteoclasts on the bone surface primarily through gap junction channels also referred to as connexins. Connexin 43 (Cx43) is the most abundant gap junction channel on bone cells which can be found both on cell bodies and on their dendritic processes (Yellowley et al., 2000). Connexins allow small molecules, including Ca^{2+} and PGE_2 to pass through

Table 2.4: Osteoblastic responses to fluid flow in 3D.

Cell type	Shear stress	Culture time	Scaffold	mRNA	Other responses	Reference
Rat MSC	<0.1 Pa	16 d	titanium fibre mesh		MS ↑, OCN ↑, NO ↑	Bancroft et al., 2002
Rat MSC	<0.03 Pa	16 d	titanium fibre mesh		ALP ↑	Sikavitsas et al., 2003
MC3T3	n.i.	7 d	bone	ALP ↑, OCN ↑, Runx2 ↑	CP ↑	Cartmell et al., 2003
Rat MSC	0.005 Pa	16 d	PLLA		MS ↑, CP↑	Sikavitsas et al., 2005
MC3T3	0.3 Pa	4 h	porous collagen	Col I ↑		Tanaka et al., 2005
Rat MSC	n.i.	16 d	bone and titanium fibres		MS ↑	Datta et al., 2006
MC3T3	0.07-0.6Pa	13 d	PDMS		ALP ↑, CP ↓	Leclerc et al., 2006
MC3T3	n.i.	49 h	collagen-GAG	OPN ↑, Col I ↑, COX-2 ↑	PGE$_2$ ↑, CP ↓	Jaasma and O'Brien, 2008
Human MSC	0.005-0.015Pa	28 d	β-TCP		MS ↑, ALP ↑, OCN ↑	Li et al., 2009
Rat	0.1 Pa	12 d	bone	ALP ↑, OCN ↑	MS ↑	Ban et al., 2011
MG-63	n.i.	21 d	chitosan	OCN ↑, Col I ↑	ALP ↑	Su et al., 2014

Cell types refer to primary cells unless a specific cell line is stated. ALP - alkaline phosphatase, Col I - collagen type I, CP - cell proliferation, GAG - glycosaminoglycan, mRNA - messenger ribonucleic acid, MS - mineralisation, MSC - mesenchymal stem cell, n.i. - not identified, OCN - osteocalcin, OPN - osteopontin, PDMS - polydimethyl siloxane, PGE$_2$ - prostaglandin E$_2$, PLLA - polylactic acid, NO - nitric oxide, Runx2 - runt-related transcription factor 2, TCP - tricalcium phosphate

and enable a coordinated response to external stimuli by osteocytes. Physiological FSS of 1.6 Pa enhanced osteogenesis through upregulation of Cx43, indicating the involvement of gap junctions in mechanical loading induced signalling (Li et al., 2013).

Paracrine signalling between osteocytes and osteoblasts

Paracrine signalling enables osteocytes to control bone remodelling even though they cannot actively deposit or resorb bone matrix (Klein-Nulend et al., 2013). The release of signalling factors as a result of FSS (as summarised above) allows osteocytes to orchestrate osteoblast and osteoclast activity, which can be studied in co-culture experiments (Table 2.6). Experimental set-ups include the culture of osteoblasts either (1) with conditioned media, i.e. culture media of previously mechanically stimulated osteocytes (Hoey et al., 2011; Vezeridis et al., 2006; Bakker et al., 2013) or (2) in transwell inserts allowing only indirect contact between cell types (Taylor et al., 2007).

Co-culture experiments demonstrated that osteocytes subjected to FSS regulate osteoblast proliferation (Vezeridis et al., 2006) and differentiation for example through the RANK ligand pathway (Bakker et al., 2013; Hoey et al., 2011). Osteocytes cultured both statically (Heino et al., 2004) and with fluid flow (Taylor et al., 2007; Vezeridis et al., 2006) induced enhanced ALP expression in osteoblasts.

In addition to the effect of FSS on paracrine signalling, Vazquez et al. (2014) demonstrated the impact of compression in a 3D co-culture model. In their model, osteocytes were embedded in type I collagen gels with osteoblasts cultured on top of the hydrogel. Osteocytes formed networks within the 3D collagen gels and osteoblasts responded to mechanical loading with increased collagen production. The effects of dynamic compression were also investigated in a trabecular bone explant model by Chan et al. (2009). They observed increased PGE_2 release by bone cells when osteoblasts were co-cultured with osteocytes during a four week culture period.

Table 2.5: Osteocytic responses to fluid flow.

Cell type	Shear stress	Flow type	Flow time	mRNA	Other responses	Reference
Chicken	0.5 Pa	p	45 min		NO ↑, PGE$_2$ ↑	Klein-Nulend et al., 1995a
Mouse	0.7 Pa	p	1 h		PGE$_2$ ↑	Klein-Nulend et al., 1997
Chicken	0.7 Pa	p	10 min		PGE$_2$ ↑	Ajubi et al., 1999
MLO-Y4*	0.4-1.62Pa	s	2 h	E11 ↑		Zhang et al., 2006
MLO-Y4	0.8Pa, 1.1Pa	s, o	24 h		OPN ↑, COX-2	Ponik et al., 2007
MLO-Y4*	2 Pa	o	15 min		Ca^{2+} ↑, PGE$_2$ ↑, ATP ↑	Genetos et al., 2007
MLO-Y4	0.2-3.2Pa	p	2 h		PGE$_2$ ↑	Kamel et al., 2010
MLO-Y4	0.5-5Pa	o	4 h	COX-2 ↑, RANKL/ OPG ↓		Li et al., 2012a
MLO-Y4	2 Pa	s, o			Ca^{2+} ↑	Lu et al., 2012a
MLO-Y4	1.6-3.2Pa	s	24 h	Cx43 ↑, RANKL ↓, OPG ↑, SOST ↓	viability ↓	Li et al., 2013
MLO-Y4*	0.5-4Pa	s	10 min		Ca^{2+} ↑	Jing et al., 2013
Ocy454*	0.05-0.8Pa	s	2 h (3 d)	SOST ↓ RANKL ↓, 0.8Pa: RANKL ↑ + DMP-1 ↑		Spatz et al., 2015

Cell types refer to primary cells unless a specific cell line is stated. In case of oscillatory or pulsatile fluid flow the value given refers to the peak shear stress. * Studies which compare osteocytic responses to osteoblastic responses. ATP - adenosine triphosphate, Ca^{2+} - calcium ions, Cx43 - connexin 43, DMP-1 - dentin matrix protein 1, o - oscillatory, OPG - osteoprotegerin, OPN - osteopontin, p - pulsatile, PGE$_2$ - prostaglandin E$_2$, mRNA - messenger ribonucleic acid, NO - nitric oxide, RANKL - receptor activator of nuclear factor kappa-B ligand, s - steady.

Table 2.6: Osteoblastic responses to paracrine signalling from osteocytes.

Osteo-blast	Osteo-cyte	Shear stress	Flow type	Flow time	Culture system	mRNA	Other re-sponses	Reference
hFOB, MC3T3	MLO-Y4	0.44 Pa	-	1 h	Insert with rotating disk		ALP ↑	Taylor et al., 2007
MC3T3, C3H10T1/2	MLO-Y4	0.05 Pa	o	2 h	Rocker	MC3T3: no changes; C3H10T1/2: COX-2 ↑, Runx2 ↔		Hoey et al., 2011
Chicken	Chicken	0.7 Pa	p	1 h	PPFC		CP ↓, ALP ↑	Vezeridis et al., 2006
MC3T3	MLO-Y4	0.7 Pa	p	1 h	PPFC	Runx2 ↓, OCN ↓, Ki67 ↑, DMP-1 ↔		Bakker et al., 2013

Cell types refer to primary cells unless a specific cell line is stated. In case of oscillatory or pulsatile fluid flow the value given refers to the peak shear stress. ALP - alkaline phosphatase, CP - cell proliferation, DMP-1 - dentin matrix protein 1, hFOB - human fetal osteoblast-like cells, mRNA - messenger ribonucleic acid, o - oscillatory, OCN - osteocalcin, p - pulsatile, PPFC - parallel-plate flow chamber, Runx2 - runt-related transcription factor 2.

2.3   In vitro bone models in drug discovery

In vitro bone models are not only required for a better understanding of the cellular mechanisms controlling bone remodelling, but they are also an essential tool in drug discovery for bone-related diseases. The development of novel drugs for treating musculoskeletal conditions is a long, complex and expensive process. In particular, the development of therapeutic agents which stimulate osteoblasts to enhance bone formation and thereby improve treatment of osteoporosis-related fractures has been difficult (Mullard, 2016). Most existing drugs for osteoporosis are anti-resorptive, which means they can prevent further bone loss but are unable to increase bone formation (Brommage, 2015). Currently, there is only one agent available, teriparatide, which stimulates new bone formation by activating osteoblasts. Another agent, romosozumab, has just completed Phase 3 clinical trials and is another promising candidate which might be able to promote bone formation in the future (Elvidge, 2016). Overall, output in terms of new approved drugs has decreased over the last years, even though investment in pharmaceutical research and development has increased (Pammolli et al., 2011). High failure rates during the drug development process might be partially attributed to current in vitro models which are unable to mimic the natural cell environment and therefore cannot reliably predict the effectiveness of drugs at an early stage of drug development (Hulsart-Billström et al., 2016).

Cells grown as monolayer (2D models) were – and most often still are – the standard approach for early-stage in vitro drug development studies (McGuigan et al., 2008). Bone cells are routinely cultured in flat vessels made from polystyrene or glass (Prideaux et al., 2012). Advantages of monolayer culture over other techniques include the availability of standardised culture vessels and protocols, straight-forward cell observation and easy analysis of a wide range of parameters. 2D models are routinely used for evaluating the effectiveness and safety of a library of molecules before advancing to animal studies and human clinical trials (Breslin and O'Driscoll, 2013). However, relying solely on results from monolayer culture bears significant risks. Most importantly, cells lose their histological, natural organisation and polarisation in two-dimensional conditions leading to changes in their cellular functions including receptor expression, transcriptional expression, cellular migration, and apoptosis (Haycock, 2011).

To avoid mistakes in the initial, but crucial 'stop/go' decision in the beginning of drug development, the use of three-dimensional (3D) models may provide an opportunity to improve the current drug development process. 3D models mimic more closely the bone cells' natural environment. For example, osteoblasts have

been found be more sensitive to compounds including transforming growth factor-β (TGF-β) and platelet-derived growth factor (PDGF) in 3D compared to 2D (Matthews et al., 2014). Different materials have been used as scaffolds for in vitro bone models including metal and polymer meshes, as well as natural and synthetic hydrogels (Bancroft et al., 2002; Su et al., 2014; Li et al., 2012b). An increasing number of studies has used type I collagen gel as scaffold for bone models as collagen hydrogel closely resembles the fibrillar osteoid matrix deposited by osteoblasts (Woo et al., 2011; Prideaux et al., 2014; Matthews et al., 2014; Vazquez et al., 2014). Unfortunately, these 3D systems are not yet routinely used during the initial stages of drug development. Disadvantages include the need for specialised equipment, a lack of standardised protocols and techniques, difficulties in retrieving cells from scaffolds following 3D culture, problems in analysing 3D culture results, and higher initial costs (Breslin and O'Driscoll, 2013).

The biomechanical, dynamic environment is another aspect which is often not considered during the initial stages of drug screening. Biomechanical forces and fluid shear stress in particular, are essential stimuli controlling bone cell behaviour (Reich et al., 1990; Klein-Nulend et al., 1997). Microfluidic devices are most commonly used to control the dynamic conditions and to apply defined shear stress on bone cell monolayers (Owan et al., 1997; You et al., 2001a). More difficult is the combination of 3D culture and fluid flow, in particular when using collagen as scaffold. Only few systems have been able to maintain the collagen's mechanical integrity under fluid perfusion, none of them using bone cells (Ng et al., 2005; Trietsch et al., 2013; Polacheck et al., 2011).

Miniaturisation is another aspect which is critical for the successful application of in vitro bone models in drug development. Organs-on-chips are thought to be "at the frontiers of drug discovery" (Esch et al., 2015) as they try to resemble most closely the natural cell environment (e.g. mechanical forces, extra-cellular matrix interactions, cell-cell communication, biochemical gradients) - all of it in a very small space. Consequently, organs-on-chips require less volume of expensive compounds and also have shorter transport distances of molecules which results in faster reaction times compared to traditional methods. A wide range of organ-on-chips have been developed which mimic critical functions of organs such as the lung, gut and heart (Huh et al., 2010; Kim et al., 2012; Agarwal et al., 2013). Only few systems, however, tried to resemble the bone microenvironment (Bersini et al., 2014; Torisawa et al., 2014), but none of them mimic the critical process of bone formation.

The development of in vitro bone models which mimic the dynamic, three-dimensional and multi-cellular environment within which osteoblasts reside is crucial for finding

novel treatment methods for musculoskeletal conditions. Advanced models could provide important improvements in preclinical drug discovery such as target identification and validation and target-based screening (Esch et al., 2015).

2.4 Summary

Osteoblasts and osteocytes respond to fluid shear stress over a wide range of magnitudes as demonstrated extensively in vitro (Figure 2.7). These responses indicate that FSS controls factors known to be important in bone formation. Different experimental set-ups and bone cell models have been applied over the last decades to investigate how fluid flow affects bone formation. These experiments have created a better understanding of how bone cells respond to different flow patterns and magnitudes of shear forces. For example, osteocytes respond to high fluid shear stress by releasing signalling factors which can also influence osteoblast behaviour via paracrine signalling. The biomechanical environment of osteoblasts is less defined, hence magnitudes of FSS ranging from only a few millipascals to more than 1 Pa have been investigated. Although early responses of bone cells are fairly well understood, more research is required into the long-term effects of FSS. A better understanding of collagen deposition and mineralisation may aid the development of more reliable bone disease models and improved bone tissue engineering constructs which try to control the cell and collagen fibre orientation. Potentially, this requires the development of more sophisticated in vitro bone models which overcome the limitations of conventional two-dimensional parallel-plate flow chambers. Organs-on-chips are thought to have great potential as platforms for improved drug discovery as they mimic the natural cellular environment in a small space.
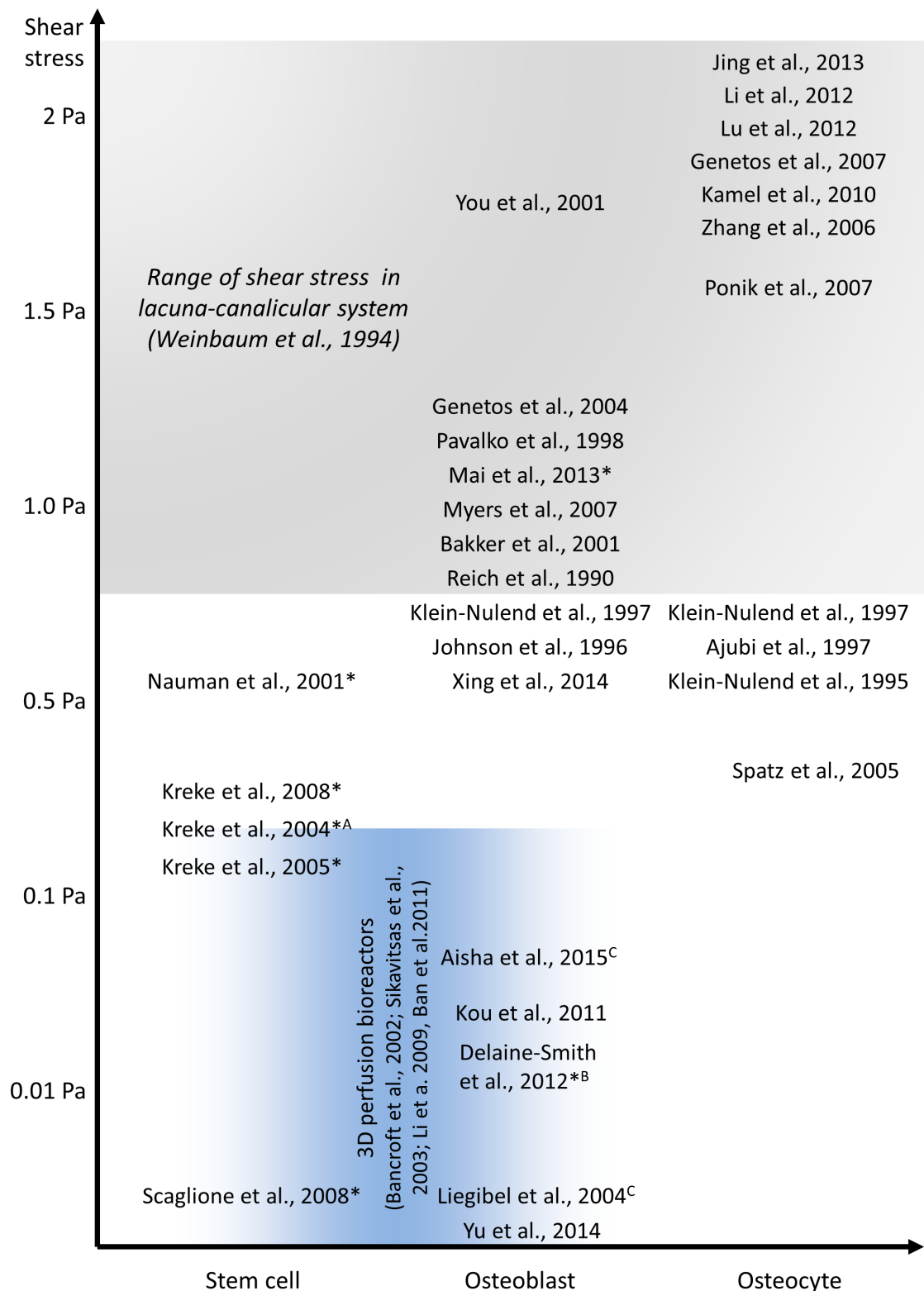
Figure 2.7: In vitro studies investigating the effect of fluid shear stress on osteoblast and osteocyte behaviour.

All experiments were performed using PPFC, exceptions: [A] radial flow chamber, [B] rocking platform, [C] orbital shaker and 3D perfusion bioreactor experiments in blue area. Long-term experiments are indicated with *.

Chapter 3

Materials and Methods

3.1 Materials

All reagents were purchased from Sigma-Aldrich (UK) unless otherwise stated. Tissue culture plastics and flasks were obtained from Thermo Fisher Scientific (UK).

3.2 Methods

3.2.1 Cell lines

Cell line IDG-SW3

The mouse early-osteoblast cell line IDG-SW3 was purchased from Kerafast (USA) and used between passages 18 to 36. IDG-SW3 cells were grown in 0.1% gelatin-coated $75\,cm^2$ or $175\,cm^2$ tissue culture flasks in α-Minimum Essential Medium (α-MEM) Eagle supplemented with nucleosides and $2\,mM$ UltraGlutamine I. Proliferation medium (Table 3.1) was further supplemented with 10% heat inactivated fetal bovine serum (FBS), 50 units/ml interferon (IFN)-γ, and a solution of 100 units/ml penicillin and $100\,\mu g/ml$ streptomycin (= penicillin streptomycin, PS). To ensure cells maintained an undifferentiated, proliferative state, IDG-SW3 were cultured at $33\,°C$ in a humidified incubator with 5% CO_2 (Woo et al., 2011). To induce osteogenic differentiation, cells were transferred to $37\,°C$ and culture medium was supplemented with $5\,mM$ β-glycerophosphate (β-GP) and $50\,\mu g/ml$ L-ascorbic acid 2-phosphate sequimagnes (ascorbic acid). In Chapter 6 differentiation medium was further supplemented with HEPES (4-(2-hydroxyethyl)-1-piperazineethanesulfonic acid) buffer. The same batch of FBS was used throughout this project. Culture medium was changed every two to three days. Cells were passaged when they reached confluence.

Table 3.1: IDG-SW3 cell culture medium composition.

Medium type	Composition	Manufacturer
Proliferation medium, 33 °C	α-MEM Eagle with nucleosides and 2 mM glutamine	Lonza, UK (LZBE02-002F)
	10% FBS	Labtech, UK (FCS-SA, Lot No. 31003H)
	100 units/ml penicillin and 100 µg/ml streptomycin	Sigma, UK
	50 units/ml IFN-γ	Sigma, UK
Differentiation medium, 37 °C	α-MEM Eagle with nucleosides and 2 mM glutamine	Lonza, UK (LZBE02-002F)
	10% FBS	Labtech, UK (FCS-SA, Lot No. 31003H)
	100 units/ml penicillin and 100 µg/ml streptomycin	Sigma, UK
	5 mM β-GP	Sigma, UK
	50 µg/ml ascorbic acid	Sigma, UK
	25 mM HEPES buffer - *only used in Chapter 6*	Sigma, UK

Cell line MLO-A5

The osteoblast cell line MLO-A5 was kindly donated by Prof Lynda Bonewald (University of Missouri, USA) and was used between passages 55 to 65. These cells were grown in 0.1% gelatin-coated $75\,cm^2$ tissue culture flasks in α-MEM supplemented with 10% heat inactivated FBS, $2\,mM$ glutamine, 100 units/ml penicillin and $100\,\mu g/ml$ streptomycin (Table 3.2). MLO-A5 cells were maintained at $37\,°C$ in a humidified incubator with 5% CO_2. To induce osteogenic differentiation, culture medium was supplemented with $5\,mM$ β-GP and $50\,\mu g/ml$ L-ascorbic acid 2-phosphate sequimagnes (ascorbic acid). Culture medium was changed every two to three days. Cells were passaged when they reached confluence.

Table 3.2: MLO-A5 cell culture medium composition.

Medium type	Composition	Manufacturer
Proliferation medium, $37\,°C$	α-MEM	Lonza, UK (LZBE12-169F)
	10% FBS	Labtech, UK (FCS-SA, Lot No. 31003H)
	100 units/ml penicillin, $100\,\mu g/ml$ streptomycin and $2\,mM$ L-glutamine	Sigma, UK
Differentiation medium, $37\,°C$	α-MEM	Lonza, UK (LZBE12-169F)
	10% FBS	Labtech, UK (FCS-SA, Lot No. 31003H)
	100 units/ml penicillin, $100\,\mu g/ml$ streptomycin and $2\,mM$ L-glutamine	Sigma, UK
	$5\,mM$ β-GP	Sigma, UK
	$50\,\mu g/ml$ ascorbic acid	Sigma, UK

Cell line MLO-Y4

The osteocyte cell line MLO-Y4 was kindly donated by Prof Lynda Bonewald (University of Missouri, USA) and used between passages 36 to 40. These cells were grown in $75\,cm^2$ tissue culture flasks coated with $0.15\,mg/ml$ rat tail tendon type I collagen (Thermo Fisher Scientific, UK) in $20\,mM$ acetic acid. Cells were cultured in α-MEM supplemented with 5% heat inactivated FBS, $2\,mM$ glutamine, 100 units/ml penicillin and $100\,\mu g/ml$ streptomycin (Table 3.3). The same batch of FBS was used throughout this project. These cells were maintained at $37\,°C$ in a humidified in-

cubator with 5% CO_2. Culture medium was changed every two to three days. Cells were passaged when reaching 70% confluence.

Table 3.3: MLO-Y4 cell culture medium composition.

Medium type	Composition	Manufacturer
Proliferation medium, 37 °C	α-MEM	Lonza, UK (LZBE12-169F)
	5% FBS	Labtech, UK (FCS-SA, Lot No. 31003H)
	100 units/ml penicillin, 100 µg/ml streptomycin and 2 mM L-glutamine	Sigma, UK

3.2.2 General cell culture

Cells were cultured following common aseptic techniques for mammalian cell culture (Freshney, 2010).

Passaging of cells

Culture medium was removed and cells were washed with Dulbecco's phosphate buffered saline (DPBS) before adding 1 ml of trypsin-EDTA solution per 25 cm² flask area. Flasks with trypsin-EDTA solution were incubated for 5 min at 37 °C to initiate detachment of the cells from the culture vessel. After checking that all the cells had detached from the bottom of the flaks, the same amount of warm culture medium was added to the trypsin-EDTA cell suspension to deactivate the trypsin. The cell suspension was centrifuged (Eppendorf centrifuge 5702, Germany) at 1000 rpm for 5 min to form a cell pellet. The supernatant was discarded and the cell pellet was re-suspended in culture medium. Cells were counted with a hemocytometer. Suspended cells could then be used in an experiment or split 1:10 and seeded in new flasks.

Long-term storage of cells

Cells were stored long-term in liquid nitrogen at −196 °C. After the cells had been detached from the bottom of the flask, the cell pellet was re-suspended at a concentration of 1×10^6 cells/ml in a 10% dimethyl sulfoxide (DMSO) solution in fetal bovine serum (FBS). The cells were placed in an isopropoanol container and stored at −80 °C for 24 h before moving the cells to liquid nitrogen for long-term storage.

Thawed cells were immediately placed in 10 ml of fresh, warm medium and centrifuged at 1000 rpm for 5 min before re-suspending in cell culture medium and seeding into a culture flask.

3.2.3   Cell digestion

Cellular DNA had to be released from the cells prior to DNA and ALP quantification. Cell membranes were broken down using detergent-based cell lysis in combination with freeze-thaw cycles and mechanical agitation. Cell culture medium was removed and cells were washed with DPBS. A known volume of cell digestion buffer solution was added to each well (1 ml to 6-well plates, 0.5 ml to 24-well plates). Cell digestion buffer was prepared fresh on the day by diluting 10%vol of cell assay buffer in deionised water and adding 1%vol Triton-X. The cell assay buffer contained TRIS-hydrochloride buffer (1.5 M, pH 8.8) with 1 mM $ZnCl_2$ and 1 mM $MgCl_2$. The cell assay buffer could be stored for several weeks in a fridge. Well plates with cell digestion buffer solution were kept in the fridge overnight or for 2 h at room temperature. Cells were scraped off the culture vessels with a pipette tip and transferred to a microcentrifuge tube. To further break down the cell membrane, cell lysates were briefly vortexed and subjected to a freeze-thaw cycle for three times (10 min at $-80\,°C$, 15 min at $37\,°C$). Finally, the lysates were centrifuged at 10,000 rpm for 5 min and could be analysed or stored at $-80\,°C$.

3.2.4   Cell fixation

Cell culture medium was removed and samples were washed with DPBS. Samples were then fixed in 10% formalin solution or 3.7% formaldehyde solution for 20 min at room temperature. The fixing solution was removed and samples were washed three times with DPBS. Alternatively, samples were washed with distilled water if they were used for collagen or calcium staining.

3.2.5   Determination of total DNA amount

The amount of DNA was determined with the Quant-it PicoGreen dsDNA assay kit (Life Technologies, UK). The principle of this assay was based on green fluorophores becoming fluorescent upon binding to double-stranded DNA (dsDNA). The amount of DNA was determined with a plate reader since the fluorescence intensity is directly proportional to the amount of DNA available. 2.5 µl to 10 µl of cell lysates (see Chapter 3.2.3) were added to Tris-buffered EDTA solution containing the QuantiT PicoGreen reagent (diluted 1:200). In total, a volume of 90 µl of solution was added to each well of a black 96-well plate. Adequate mixing and binding of sample and

reagent was ensured by shaking the well plate for $10\,\text{s}$ in the microplate reader and waiting for $10\,\text{min}$ before taking the fluorescence readings. Fluorescence intensity was recorded with an Infinite 200 PRO microplate reader (Tecan, Switzerland) using $485\,\text{nm}$ excitation, $520\,\text{nm}$ emission and 30% gain. A standard curve (Figure 3.1) was used to derive Equation 3.1 which calculated the amount of DNA per sample:

$$DNA = Dilution \times ((0.0309 \times Fluorescence) - 1.2993) \qquad (3.1)$$
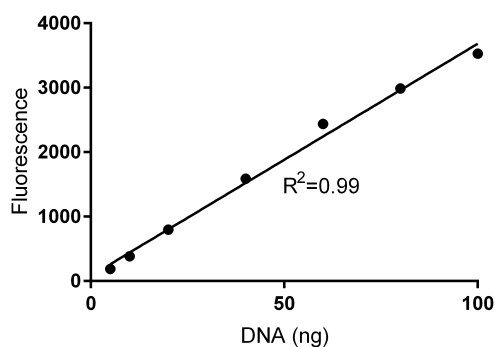
Figure 3.1: DNA standard curve.

A standard curve (Figure 3.2) linked the detected amount of DNA to the number of cells per well.
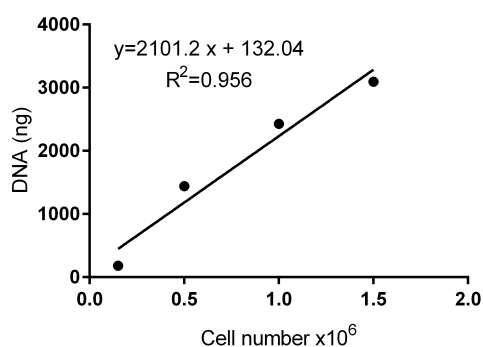
Figure 3.2: DNA standard curve to estimate cell numbers.

3.2.6 Assessment of metabolic activity

Cell viability was assessed by measuring the metabolic activity of cells with resazurin-based assays. In contrast to the DNA assay described above, resazurin-based assays allow monitoring of live cells which can be further cultured since resazurin is not toxic to cells if applied only for short periods of time. Resazurin-based assays rely

on the reduction of resazurin by redox enzymes such as nicotinamide adenine dinucleotide (NADH) which are active only in live cells. NADH, for example, plays an integral part in cellular metabolism as electron carrier in redox reactions. Metabolic active cells are able to reduce the non-fluorescent blue dye resazurin to the pink, intensely fluorescent dye resorufin (579 nm excitation, 584 nm emission).

Resazurin-reduction assay

Resazurin sodium salt was dissolved in deionised water to create a 1 mM stock solution. The stock solution was further diluted in proliferation medium (10%vol) on the day of experiment creating a deep blue coloured solution. Culture medium was removed from samples and replaced with 500 µl of warm resazurin solution per well of a 24-well plate. After 4 h of incubation inside a humidified incubator, 150 µl of reduced resazurin solution was transferred in triplicate from each well to a black 96-well plate. Fluorescence intensity was measured with a microplate reader (540 nm excitation, 590 nm emission). The measurements were corrected for background fluorescence by including control wells containing only resazurin solution without any cells. If cells were further cultured, excess resazurin solution was removed from the wells and washed twice with DPBS before adding fresh culture medium.

PrestoBlue assay

The commercially available PrestoBlue assay (Invitrogen, UK) is based on the above described resazurin reduction reaction. Compared to the traditional resazurin-reduction assay, it has the advantage that it requires a shorter incubation time and has a higher sensitivity. The PrestoBlue stock solution was diluted in proliferation medium (10%vol) on the day of experiment to create a working solution. Culture medium was removed from samples and replaced with 750 µl of warm PrestoBlue solution per well in a 6-well plate. After 1 h of incubation inside a humidified incubator, 180 µl reduced PrestoBlue solution was transferred in triplicate from each well to a black 96-well plate. Fluorescence intensity was measured with a microplate reader (540 nm excitation, 590 nm emission). If cell culture was continued, excess PrestoBlue solution was removed from the wells and cells were washed twice with DPBS before adding fresh culture medium.

3.2.7 Calcium measurement

Calcium signalling happens within seconds of mechanical stimulation. Therefore, a culture system was required which allowed simultaneous fluid flow application and fluorescence microscopy. Since dynamic cell culture in well plates in combination

with see-saw rocking platforms and orbital shakers (see Chapter 3.2.14) did not fulfil this requirement, cells were instead cultured in ibidi flow channels. 250,000 cells were seeded per 0.1% gelatin-coated ibidi μ-slide (ibidi, Germany) and left to adhere for 4 h or overnight in a humidified incubator at 37 °C. Intracellular calcium release was detected with the fluorogenic calcium-sensitive dye Cal-520 (492 nm excitation, 514 nm emission, Abcam, UK). Fluorescence of the dye Cal-520, which is able to cross cell membranes, was greatly enhanced once intracellular calcium was released and bound to the dye. The dye was diluted in proliferation medium to a final concentration of 4.5 μM and mixed with 0.02% Pluronic F-127, which facilitated dye dissolution in cell culture medium. Following cell attachment in the ibidi μ-slides, cells were pre-loaded with this solution and incubated for 75 min at 37 °C in the dark. After incubation, cells were carefully washed with sodium buffered saline (1.5 mM Ca^{2+}) to remove unbound dye. The slides were attached to a microscope stage and connected to an ibidi pump system (ibidi, Germany). Fluid flow was applied for 3 min. One of four different flow settings was used per slide, i.e. unidirectional flow generating a shear stress of 0.3 Pa or 1.5 Pa or oscillating flow (1 Hz) also generating a shear stress of either 0.3 Pa or 1.5 Pa. Fluorescence images were acquired every second with 10 reference images prior to flow initiation and another 10 images after stopping the flow. Image stacks were post-processed with the open-source software ImageJ (available at http://rsb.info.nih.gov/ij). 50 cells were randomly selected per image. The average intensity of each of the cells for the first 10 s under static conditions was calculated. In addition, the maximum intensity of each cell during flow and the corresponding time were retrieved. The relative increase in intensity was calculated by subtracting the cell's intensity under static conditions from the maximum intensity value to account for differences in the initial brightness of cells. Fluorescence peaks caused by small floating particles were excluded from analysis. Different flow conditions were compared by calculating the median intensity values of 50 cells and counting the number of responsive cells, i.e. where the intensity change caused by fluid flow was positive.

3.2.8 Prostaglandin E_2 measurement

Prostaglandin E_2 (PGE_2) is one of the first factors released by cells into the surrounding culture medium in response to mechanical stimulation. The amount of PGE_2 in cell culture supernatants was quantified with a commercially available assay kit (R&D systems, UK) following the manufacturer's instructions. The assay is based on two incubation steps. First, PGE_2 contained in the samples binds to a mouse monoclonal antibody. In a second incubation step, PGE_2 labelled with horseradish peroxidase (HRP) binds to the remaining antibody sites which results

in a colour change of the mixture after adding a substrate solution. To measure PGE_2 release in this project, culture medium in the well plates was removed directly after mechanical stimulation via rocking or shaking (see Chapter 3.2.14) and 1 ml of fresh proliferation medium was added to each well. After 1 h of incubation at 37 °C under static conditions, cell culture supernatants were collected and samples could be stored at −80 °C. All samples were diluted three-fold in calibrator diluent which was provided by the manufacturer. The optical density of each well was determined using a microplate reader set to 450 nm. In addition, subtract readings at 570 nm were also taken to correct for optical imperfections in the plate. The corrected absorbance at 450 nm was inversely proportional to the concentration of PGE_2 in the sample. To determine the exact amount of PGE_2, a four parameter logistic curved was fitted to a standard curve (Figure 3.3) using the statistic software GraphPad Prism (Graphpad Software, USA). The curve could be described by Equation 3.2 below:

$$Y = 0.09305 + \frac{0.50325}{1 + 10^{(2.726-X) \times (-1.327)}} \tag{3.2}$$
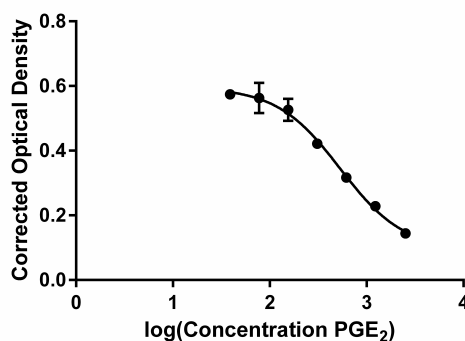
Figure 3.3: PGE_2 standard curve.

3.2.9 Nitric oxide measurement

Nitric oxide (NO), which is an important signalling molecule, could not be detected directly. Instead, nitrite (NO_2^-) which is one of the stable breakdown products of NO was measured using a commercially available Griess reagent kit (Promega, UK). Culture medium samples were taken from the cells after 10 min, 30 min and 1 h of mechanical stimulation. Alternatively, cell culture medium was replaced prior to rocking with DPBS to increase sensitivity of the assay. 50 µl sulfanilamide solution was added to each 50 µl sample and incubated for 10 min before adding 50 µl of the N-1-napthylethylenediamine dihydrochloride (NED) solution. Samples were incubated at room temperature for a further 10 min. Absorbance at 540 nm was measured with

a microplate reader. Measurements were compared to a standard curve (Figure 3.4) which was prepared using either cell culture medium or DPBS.
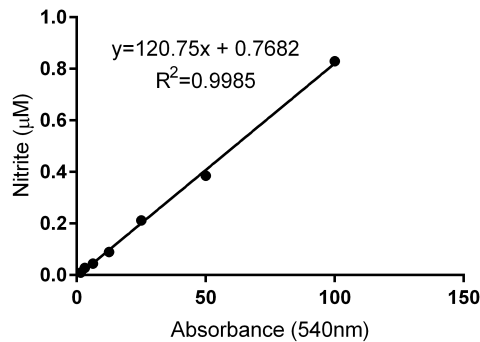
Figure 3.4: Nitrite standard curve prepared with DPBS.

3.2.10   Collagen deposition

Collagen deposition was assessed with picrosirius red (PSR) staining and second harmonic generation imaging (SHG).

Picrosirius red staining

PSR is a collagen stain which is not specific to a particular type of collagen (Lattouf et al., 2014). Stained collagen fibres appear bright red when observed under a bright-field or fluorescence microscope (Vogel et al., 2015). PSR solution was produced by dissolving direct red 80 in saturated picric acid (1%w/v). The solution was filtered to ensure that no particles remained. A defined volume of PSR solution was added to each sample and left for 1 h on an orbital shaker (IKA, Germany) at 100 rpm. The staining solution was removed and the samples were washed four times with deionised water and gentle orbital shaking. Four washes were sufficient for water in a well without any cells to remain clear which indicated that all loose dye had been removed. The stained collagen fibres were observed under a fluorescent microscope (Nikon, Japan). Stain distribution within the well was documented by taking photos with a digital camera (Canon, Japan). To quantify the amount of dye attached to collagen, samples were de-stained with a defined volume of 0.2 M sodium hydroxide and methanol in a 1:1 ratio for 15 min on an orbital shaker at 100 rpm. 150 µl of de-stain solution was transferred in triplicate from each well to a transparent 96-well plate. Absorption was measured with a microplate reader. The absorption values were converted to the amount of PSR dye attached to collagen fibres per sampled using Equation 3.3 which has been derived from a standard curve (Figure 3.5).

$$PSR = Dilution \times ((42.693 \times Absorbance) + 0.71) \tag{3.3}$$
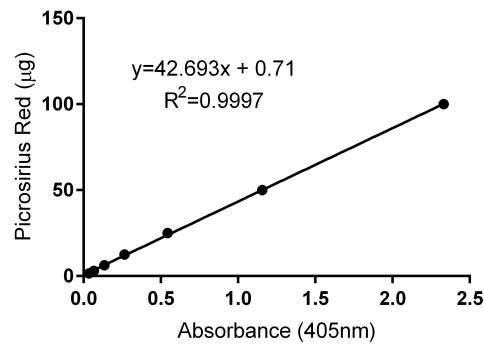
Figure 3.5: Picrosirius red standard curve.

Second Harmonic Generation Imaging

Second Harmonic Generation (SHG) imaging has emerged as a powerful tool for imaging fibrillar collagen. Collagen molecules have no centre of symmetry and a highly crystalline triple helical structure which makes them strong emitters of SHG (Chen et al., 2012). SHG is generated by multi-photon lasers, such as a femtosecond laser, which produces short near-infrared pulses. If two near-infrared photons emitted by the laser hit a molecule which is not symmetric, then these photons scatter and anisotropy creates an oscillating field at twice the frequency (half the wavelength), which is referred to as the second harmonic. These newly generated photons can be detected at half the wavelength of the photons that excited the sample (Cox and Kable, 2006).

SHG images were obtained using a LSM 510 Meta upright confocal microscope (Zeiss, Germany) equipped with a tuneable (700 nm to 1060 nm) Chameleon Ti: sapphire multi-photon laser. Images were taken using an excitation wavelength of 800 nm. SHG emissions were collected in the backward scattering direction filtered through a 10 nm bandpass filter centred around 400 nm. The pinhole was set to maximum and the same excitation power, detector gain and scan speed were used for all samples. A 40x water immersion objective was used in all experiments. Fixed and live cells were imaged.

3.2.11   Mineral deposition

Calcium phosphate crystals are deposited by osteoblasts in a process referred to as mineralisation. Mineralisation can be quantified by measuring the amount of calcium within the sample. Alizarin red S (ARS) stain, for example, forms a complex with calcium in a chelation reaction which can be semi-quantified by subsequent destaining (Gregory et al., 2004). Moreover, stained calcium minerals also turn bright red and can easily be visualised by bright-field microscopy. Samples were fixed and

washed three times with distilled water to remove any calcium ions which were not part of the deposited minerals. ARS was added to distilled water (1%w/v) on the day of analysis and filtered through a 0.45 µm filter to remove any undissolved particles. A known volume of ARS was added to each sample and incubated for 1 h on an orbital shaker (IKA, Germany) at 100 rpm at room temperature. Excess dye was removed and the samples were washed four times with distilled water. Four washes were sufficient to ensure that water remained clear in a control well without any cells. Images of mineral deposits were acquired using bright-field microscopy (Nikon, Japan) and a digital camera (Canon, Japan). The amount of ARS in a stained monolayer of cells was quantified by de-staining the samples with a defined volume of 5% perchloric acid for 15 min on an orbital shaker at 100 rpm. Absorption of each sample was measured in triplicate at 405 nm using a clear 96-well plate in a microplate reader. The amount of stain was quantified using the Equation 3.4 which had been derived from a standard curve (Figure 3.6).

$$ARS(mg) = Dilution \times 0.3473 \times Absorbance(405nm) - 0.0215 \qquad (3.4)$$
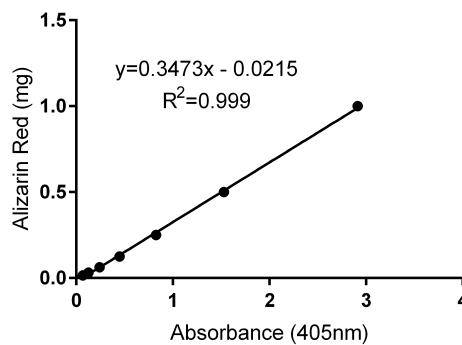
Figure 3.6: Alizarin Red S standard curve.

3.2.12 Alkaline phosphatase activity

The enzyme alkaline phosphatase (ALP) is a widely used osteogenic marker. The activity of ALP was assessed with a commercially available p-Nitrophenyl Phosphate (pNPP) phosphatase activity assay (Thermo Fisher Scientific, UK). This assay determined the rate of hydrolysis from p-nitrophenyl phosphate to p-nitrophenol by the enzyme ALP. P-nitrophenol is a chromogenic substance with an absorbance at 405 nm. Therefore, the change in absorbance over time is an indicator for the ALP activity of the sample. Depending on the cell number, 5 µl to 20 µl of cell lysates (see Chapter 3.2.3) were added to 180 µl of p-nitrophenol phosphate solution. The following conversion to p-nitrophenol, i.e. the colour change from transparent to

yellow, was measured by recording the absorbance value once per minute for up to 30 min in transparent 96-well plates. ALP activity was calculated using Equation 3.5 below:

$$ALP = Dilution \times \Delta_{\text{Absorbance}} \times K \tag{3.5}$$

where ALP is the ALP activity in nmol pNPP converted per minute and $\Delta_{\text{Absorbance}}$ is the change of absorbance per minute. K is a constant which equals the change of one absorbance value per minute and was determined as 19.75 nmol of p-nitrophenol with a standard curve. ALP activity was normalised to the total DNA content per sample.

3.2.13   Assessment of osteocytogenesis

Dmp1-GFP is a marker for osteocytic differentiation in IDG-SW3 (Kalajzic et al., 2004). Microplate reader measurements and analysis of fluorescence images were used to assess Dmp1-GFP expression.

Fluorescence top reading with microplate reader

GFP fluorescence was quantified in live cells with a microplate reader. Culture medium was replaced by 1 ml Hank's Balanced Salt Solution (HBSS) prior to measurements to avoid background fluorescence caused by phenol red, vitamins and other components in the culture medium (Waters, 2009). In addition, blank measurements of wells containing only HBSS were subtracted from each reading. All measurements were performed in fluorescence top reading mode (excitation 485 nm, emission 535 nm, 50% gain) with the cover of the well plate removed. A total of 36 measurements were taken per well. In 6-well plates, a 3 mm border area was excluded from the measurements to reduce the impact of the polystyrene on the measurements. Exceptionally high or low readings were excluded from further analysis when caused by cell layer detachment.

Fluorescence imaging and image analysis

Fluorescence images were obtained with a Ti-E Nikon inverted microscope (Nikon, Japan). Only live cells were imaged since Dmp1-GFP expression was found to be negatively affected by cell fixing. Fluorescence signal was detected using a filter system with 470 nm excitation, 525 nm emission and a 2 s exposure time. In order to compare images taken at different time points, all settings had to remain unchanged over the course of the experiment. Image analysis was performed using ImageJ, where the brightness in all images was set between 50 and 20,000 intensity units. The mean intensity value of five randomly selected locations per well was recorded.

The five locations per well were selected only based on phase-contrast images to avoid operator bias.

3.2.14 Generation of fluid shear stress in well plates

A see-saw rocker and an orbital shaker were used to generate FSS in 6-well plates.

See-saw rocker

Oscillatory FSS was generated in 6-well plates with a see-saw rocker (Stuart, UK; Figure 3.7). This method has been previously applied by Delaine-Smith et al. (2012). Fluid shear stress was applied once a day for either 1 h or 5 h. An analytical model developed by Zhou et al. (2010) was used for estimating the magnitude of FSS generated on the bottom of a 6-well plate. This model makes a couple of assumptions including that the fluid movement is primarily driven by gravity and that the surface of the fluid stays horizontal. The model also ignores centrifugal forces which act on the fluid because of its low angular acceleration and velocity. The following equation was used for calculating the characteristic shear stress τ at the centre of a well when the plate was in a horizontal position:

$$|\tau| = \frac{\pi \mu \theta_{max}}{2\delta^2 T} \tag{3.6}$$

where μ is the fluid viscosity (10^{-3} Pa s), θ_{max} is the maximum tilt angle (in rad), δ is the ratio of the fluid depth in the well to the well diameter, and T is the time for one cycle (in seconds). Each well was filled with 2 mL of cell culture medium resulting in a fluid depth of 2.08 mm. Hence, in circular 6-well plates with a diameter of 35 mm the ratio δ was 0.06. The maximum tilt angle was set to approximately 7°. Three different rocking frequencies were tested: 0.7 Hz (= 42 cycles/min), 0.75 Hz (= 45 cycles/min) and 1 Hz (= 60 cycles/min) which generated maximum shear forces of 0.038 Pa, 0.041 Pa and 0.054 Pa, respectively.

Orbital shaker

Fluid shear stress was also generated in 6-well plates using an orbital shaker (IKA, Germany; Figure 3.8). Orbital motion of a 6-well plate generated a complex three-dimensional flow pattern within each well which varied both in time and space. Each well of a 6-well plate was filled with 2 ml of culture medium and the rotation frequency of the orbital shaker was set to 200 rpm. Salek et al. (2012) had previously simulated flow under the same conditions using Computational Fluid Dynamics (CFD). Their results showed that the wall shear stress τ_w was only approximately
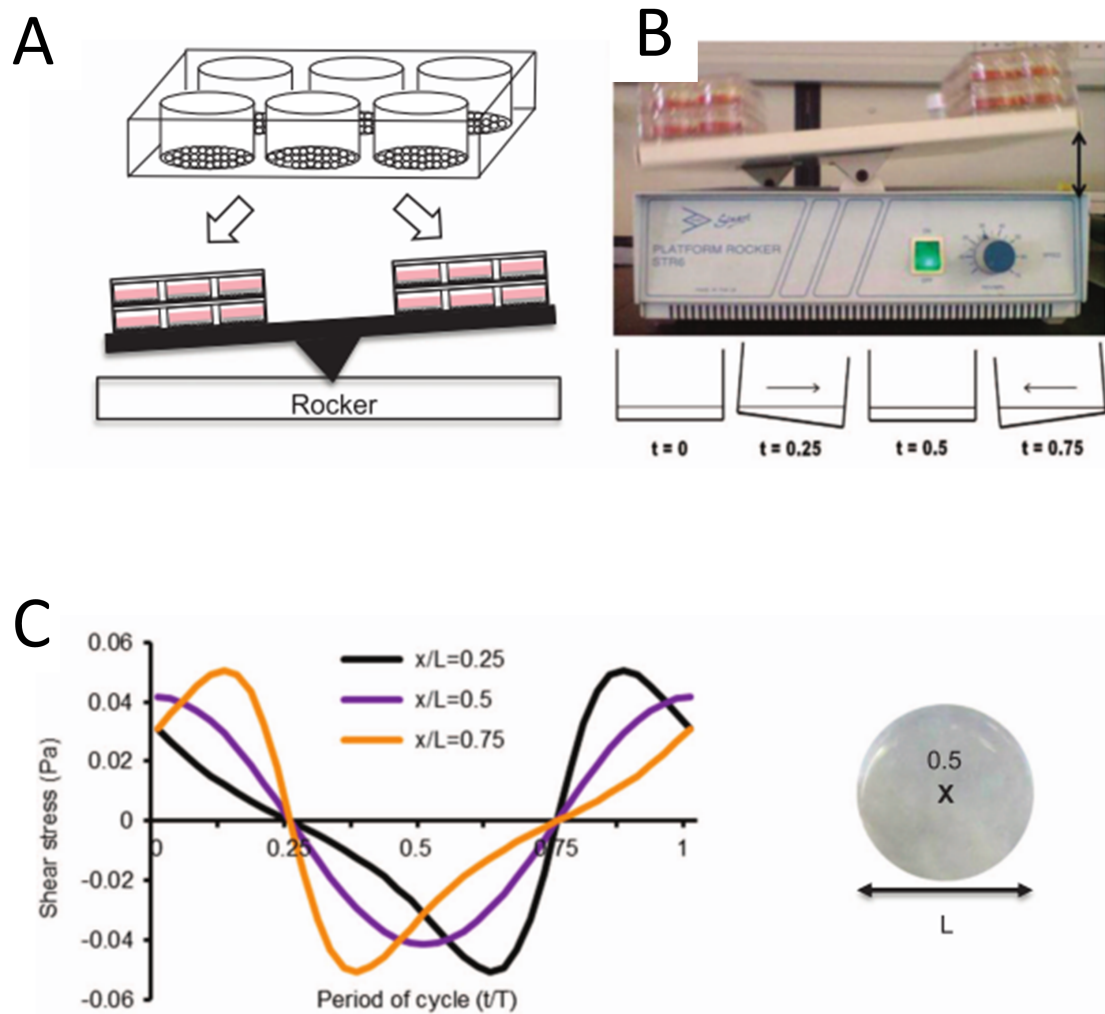
Figure 3.7: Generation of fluid shear stress with a see-saw rocker.

A: Several 6-well plates can be placed on a see-saw rocker at the same time. B: Rocking frequency and tilt angle (black arrow) influence the magnitude of fluid shear stress on the bottom of the well plate. C: Oscillatory fluid flow is produced across the well bottom. x/L is a point along the well bottom. The centre of the well is located where x/L=0.5. Calculated shear stress values are based on a tilt angle of 6° and a time of 1.33 s for one cycle. Images taken from Delaine-Smith et al. (2015).

constant near the centre of the well, where the value was close to 0.83 Pa. The average shear stress magnitude over the whole bottom of the well at 200 rpm was 0.87 Pa, which was more than a magnitude higher compared to the maximum shear stress generated with the see-saw rocker.

3.2.15 Statistical analysis

Statistical tests were performed using GraphPad Prism 7.01 software (Graphpad Statistical, USA). All data were tested for normality (D'Agostino-Pearson omnibus test) and outliers (ROUT method) in order to fulfill the assumptions of the two way analysis of variance (ANOVA) test. Significance ($p<0.05$) was determined by two way ANOVA, followed by Tukey's post hoc test.

To provide more statistical power, each cell culture experiment was repeated independent of each other at separate times. The number of times each cell culture experiment was repeated, i.e. the number of independent replicate experiments n, is specified in the respective methods sections and figure legends. In addition, each independent experiment consisted of three technical replicates in which cells were cultured using the same culture medium, in the same incubator at the same time but in separate culture dishes. Although these replicates cannot capture biological variation, they can limit the impact of random noise associated with protocols or equipment. Biological replicates were not conducted as the use of cell lines prevented the parallel measurements of biologically distinct samples.
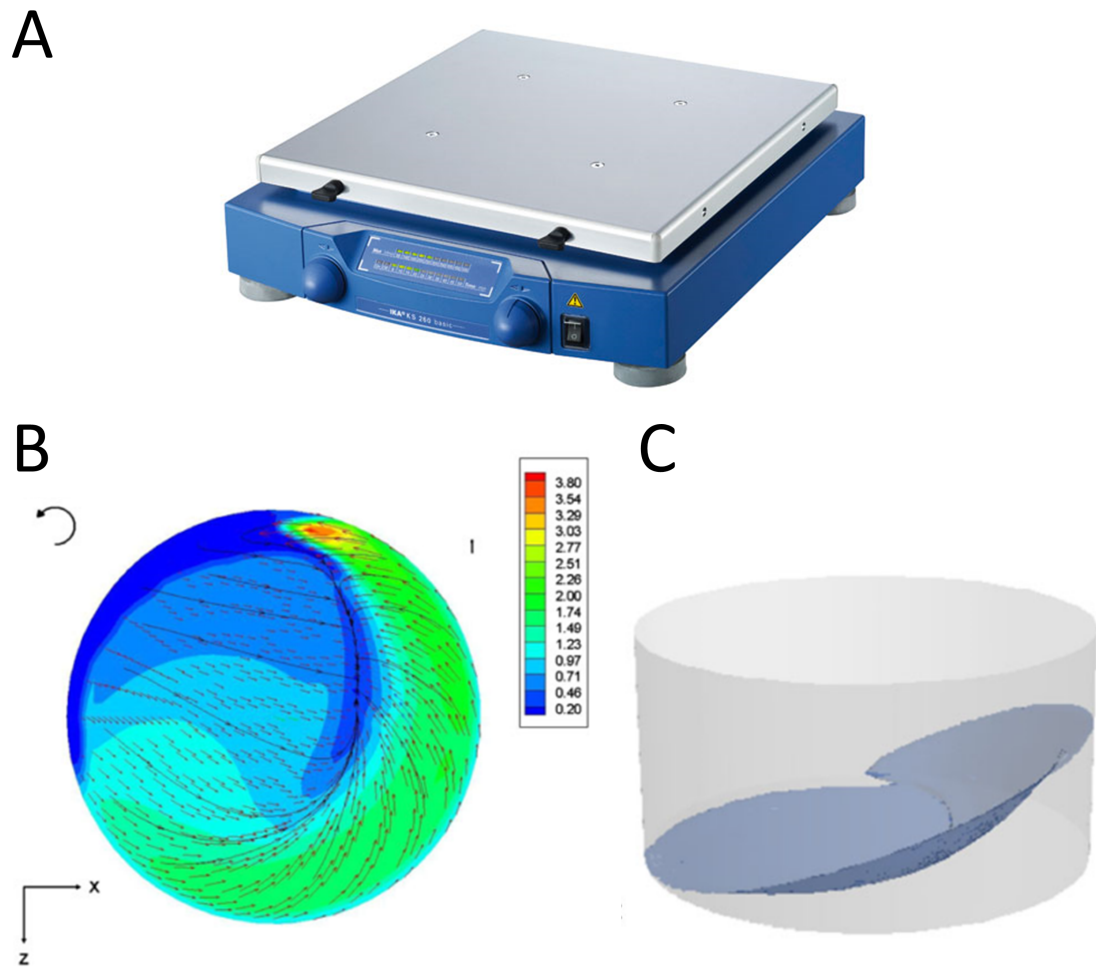
Figure 3.8: Generation of fluid shear stress with an orbital shaker.

A: Photo of orbital shaker. B: Contours of the magnitude of wall shear stress (Pa) on the bottom of a well of a 6-well plate with surface streamlines superimposed. C: 3D structure of free surfaces calculated at $t=t_0$ using a rotational speed of 200 rpm. Images B and C taken from Salek et al. (2012).

Chapter 4

Biochemical stimulation of osteocytogenesis

4.1 Introduction

Osteocytes are by far the most abundant cell type in bone. They are located deep within the mineralised bone matrix and are in contact with each other and osteoblasts on the bone surface via long cell processes and gap junctions (Yellowley et al., 2000). It is known that osteocytes are terminally differentiated osteoblasts. However, the exact mechanism guiding the osteoblast-to-osteocyte transformation process, referred to as osteocytogenesis, remains still largely unclear (Mullen et al., 2013; Prideaux et al., 2012; Holmbeck et al., 2005).

Osteocytogenesis as active process

Previously, osteocytogenesis was described primarily as a passive process controlled by the rate and duration of matrix deposition. Over time, osteoblasts would become 'buried' within their own deposited matrix or would be covered by neighbouring matrix-producing osteoblasts and turn to osteocytes (Franz-Odendaal et al., 2006; Palumbo et al., 2004). This view has shifted over the last few years and cells have been assigned a more active role in this process. For example, Holmbeck et al. (2005) described osteocytogenesis as an active invasive process which requires cleavage of collagen by matrix metalloproteinases (MMP) in order to form osteocyte processes. The importance of MMPs for osteocyte migration was further consolidated by Robin et al. (2016) using an in vitro 3D osteoid-like collagen model. In addition, tissue inhibitors of metalloproteinases (TIMPS) which are endogeneous inhibitors of MMPs are also able to regulate ECM remodelling required for osteocytogenesis (Prideaux et al., 2015). An active involvement of osteocytes in remodelling and osteocytogenesis

would also better explain their organised spatial distribution within mineralised bone (Kamioka et al., 2001).

Molecular pathways in osteocytogensis

Several different transitional stages between osteoblasts and osteocytes have been identified based on morphological, functional and molecular differences (Figure 4.1).

Early osteoblasts express markers required for osteoblast differentiation such as osterix. Following osteoblast maturation, cells begin to express osteocalcin, which plays a role in bone mineralisation and calcium ion homeostasis. In addition, these matrix-producing osteoblasts also express alkaline phosphatase (ALP) and type I collagen which are necessary for the deposition of osteoid.

The following transition towards an osteocytic phenotype is initiated by down-regulation of ALP and collagen in combination with up-regulation of MMP (Holmbeck et al., 2005), dental matrix protein 1 (Dmp1) (Toyosawa et al., 2001) and E11 (Schulze et al., 1999). While molecules such as E11 and MMPs are required for matrix remodelling to form dendrites and canaliculi, Dmp1 regulates mineralisation and mineral metabolism. During the osteoblast-to-osteocyte transition, extracellular Dmp1 can readily act as a nucleation site for hydroxyapatite crystals since it has multiple calcium binding sites (Schiavi, 2006). This function has also been confirmed in vivo with Dmp1-null mice revealing considerably lower levels of mineralised osteoid (Ling et al., 2005).

Mature osteocytes, which mark the final stage of osteocytogenesis, are characterised by the expression of sclerostin. Sclerostin is known for its anti-anabolic effect on bone formation (Bezooijen et al., 2005).

Mineralisation as trigger for osteocytogenesis

The above described molecular pathways involved in osteocytogenesis are fairly well understood. In contrast, the physical or chemical triggers which initiate osteocytic differentiation are still very vague (Robin et al., 2016). It is widely believed that mineralisation of the surrounding ECM might trigger osteocytogenesis (Robin et al., 2016; Welldon et al., 2013; Prideaux et al., 2012; Irie et al., 2008; Barragan-Adjemian et al., 2006). However, it is not clear how osteoblasts or osteocytes can sense mineralisation. Potential mechanisms include cells reacting to changes in matrix stiffness (Mullen et al., 2013), hypoxic conditions (Hirao et al., 2007) or increased mechanical forces (Zhang et al., 2006); all of which can result from increased mineralisation. In addition, proteins such as Dmp1 which control mineralisation are
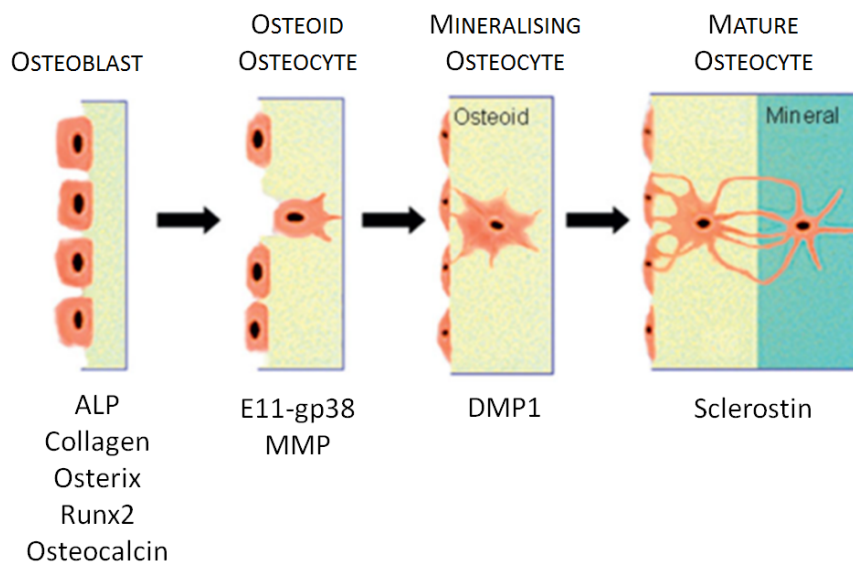
Figure 4.1: Genetic and molecular marker expression during osteocytogenesis.

Part of the osteoblast population transforms to mature osteocytes over time. During specific phases of this transformation process, referred to as osteocytogenesis, various genetic and molecular markers are expressed. The marker expression appears to coincide with the location of the osteoblast/osteocyte within the surrounding ECM, hence collagen and mineral deposition appear to play a crucial role in osteocytogenesis. Image is adapted from Bonewald (2011) and Dallas et al. (2013).

thought to regulate osteocytogenesis indirectly by down-regulating osteoblast genes (Feng et al., 2006).

Phosphate provides the chemical potential for mineral deposition. Varying the concentration of organic phosphate in bone cell culture systems is one of the most common methods to inhibit or enhance the process of mineralisation and its effect on bone cells (Tenenbaum et al., 1989). Organic phosphate is enzymatically hydrolysed to free inorganic phosphate by ALP on the cell membrane of bone cells, hence it is thought that mineralisation is closely related to the activity of ALP (Chang et al., 2000).

Studying an in vivo rat model, Irie et al. (2008) found that osteocytogenesis was triggered by mineralisation of the ECM surrounding the osteocytes. To confirm this, mineralisation of newly formed bone was inhibited by administering 1-hydroxy-ethylidene-1,1-bisphosphate (HEPB). In both the control group and the HEPB administered group, cells were found evenly spread throughout the newly formed bone. However, in the unmineralised bone of the HEPB group only immature osteoblasts, which were characterised by a 'plump' appearance and lacked cell processes, were found. In contrast, mature osteocytes, i.e. cells showing immunoreactivity to the anti-SOST antibody, could be detected in the control group. As a result, Irie et al. (2008) concluded that neither the duration since burial in the bone matrix nor the distance from the bone surface but the mineralisation of the matrix surrounding the osteocytes caused differentiation towards mature osteocytes.

The role of mineralisation for regulating osteocytogenesis was further investigated in an in vitro study by Prideaux et al. (2012). In order to decide whether mineralisation is a driver of osteocyte formation in the cell line MLO-A5, they inhibited ECM mineralisation by omitting phosphate or adding sodium pyrophosphate which is an inhibitor of hydroxyapatite formation. Both methods resulted in a lower expression of E11 and other osteocyte markers including Dmp1, CD44 and SOST. In contrast, markers associated with osteoblasts such as OCN and Col1a increased when mineralisation was inhibited. They further concluded that not only the availability of phosphate but also its incorporation within a collageneous matrix is essential for osteocyte differentiation. This was confirmed by lower levels of E11 when cells were cultured in the absence of ascorbic acid which prevented the formation of an organised collagen matrix.

Strontium ranelate enhances osteocytogenesis

In addition to ascorbic acid and phosphate, other compounds are also thought to enhance osteocytic differentiation. Examples include vitamin K (Atkins et al., 2009), retinoic acid (Song et al., 2005), fibroblast growth factor-2 (Gupta et al., 2010) and strontium ranelate (Choudhary et al., 2007). Latter has also been used for treating postmenopausal osteoporosis. Strontium ranelate (SrR) increased bone mineral density and serum levels of bone ALP in clinical studies, which resulted in a reduced risk of vertebral and hip fractures (Meunier et al., 2002). More recently, however, the use of SrR has been restricted due to cardiovascular side effects (Reginster et al., 2015).

In vitro studies showed that SrR has a dual effect on bone remodelling. It is thought that it stimulates bone formation through its positive effect on osteoblast differentiation and function, while also preventing bone resorption through inhibition of osteoclast differentiation and function (Bonnelye et al., 2008). However, the molecular mechanism involved in the effects of SrR are not fully understood yet. Extracellular calcium-sensing receptors (CaSR) (Brown and MacLeod, 2001) and pathways which are independent of these receptors might both play a role (Fromigué et al., 2009).

Although several in vitro studies have demonstrated that SrR modifies osteoblast function (Table 4.1), some of the responses are in disagreement and require more research. For example, SrR treatment increased the expression of the osteoblast marker ALP (Atkins et al., 2009; Barbara et al., 2004; Bonnelye et al., 2008; Querido et al., 2015), increased the expression of the osteocyte marker Dmp1 (Atkins et al., 2009; Bakker et al., 2013), and elevated osteoblast proliferation (Atkins et al., 2009; Caverzasio, 2008; Querido et al., 2015). Researchers also reported an increase in mineralisation (Atkins et al., 2009; Bonnelye et al., 2008; Choudhary et al., 2007; Querido et al., 2015). In contrast, some studies reported no change in mineralisation (Barbara et al., 2004) or even an inhibition of mineralisation upon treatment with SrR (Wornham et al., 2014). Such variability might be caused by the application of different cellular models including rodent and human cell cultures and the treatment with very different strontium concentrations (Nardone et al., 2015; Verberckmoes et al., 2004). In addition, different analysis methods ranging from staining techniques to phase-contrast image analysis might have also contributed to the different results (Table 4.1).

Novel cell models for observing osteocytogenesis

Observing osteocytogenesis has been made a lot easier after identifying the majority of genetic markers involved in the differentiation process. In particular the

Table 4.1: Effect of strontium on osteoblast behaviour in vitro.

Cell type	Strontium concentration	Results	Reference
Rat	0.01 to 1mM	CP ↑, Coll ↑	Canalis et al., 1996
Rat	0.01 to 100μg/ml	CP ↔, multiphasic: ALP and MS[2*, 4, 6,7]	Verberckmoes et al., 2003
MC3T3	1mM	ALP ↑, collagen ↑, MS[2,3] ↔	Barbara et al., 2004
MSC, OB-6	0.1 to 3mM	MS[1] ↑	Zhu et al., 2007
Mouse	0.1, 0.3, 1mM	ALP ↑, OCN ↑, BSP ↑, MS[1,2] ↑	Bonnelye et al., 2008
MC3T3	1, 2, 5, 10mM	CP ↑	Caverzasio, 2008
NHBC	1, 5, 10mM	CP ↑, ALP ↑, OPG/RANKL ↑, Dmp1 ↑, sclerostin ↑, MS[1,2] ↑	Atkins et al., 2009
MSC	2mM	ALP ↑, Coll ↑, MS[1,2] ↑	Yang et al., 2011
MC3T3	0.1 to 3mM	Dmp1 ↑, ALP ↔, CP ↑	Bakker et al., 2013
Rat	1μM to 1mM	MS[2*,4] ↓	Wornham et al., 2014
Mouse	0.05, 0.5mM	Change in composition and crystal structure of apatite	Querido et al., 2014
MSC	1, 3mM	ALP ↑, OCN ↑, PGE$_2$ ↑, MS[4,5,6] ↑	Querido et al., 2015
MC3T3	0.05, 0.1, and 0.5mM	CP ↓ and ↔, MS[2,5] ↑	Almeida et al., 2016

Primary cells were used unless a specific cell type is stated. Assessment method for mineralisation is marked with numbers: [1] - von Kossa staining, [2] - Image analysis, [2*] - Image analysis distinguishing between mineralised and unmineralised matrix, [3] - Measurement of calcium content in mineral, [4] - Measurement of calcium ions in medium, [5] - Alizarin red staining, [6] - Fourier transform infrared spectroscopy, [7] - X-ray. ALP - alkaline phosphatase, BSP - bone sialoprotein, CP - cell proliferation, Coll - Collagen, Dmp1 - dentin matrix protein 1, MS - mineralisation, MSC - mesenchymal stem cell, OCN - osteocalcin, OPG - osteoprotegerin, PGE$_2$ - prostaglandin E$_2$, RANKL - receptor activator of nuclear factor kappa-B ligand.

development of transgenic mouse models in which the Dmp1 promoter drives the expression of the green fluorescent protein (GFP) has been a great advancement for osteocyte research. The cell line IDG-SW3 has been derived from such transgenic mice and is able to cover the full osteogenic differentiation profile from osteoblast to late osteocyte. IDG-SW3 cells express GFP and fluoresce green after they have differentiated to osteocyte-like cells expressing Dmp1. This characteristic of IDG-SW3 allows observation of osteocytogenesis by fluorescence microscopy (Woo et al., 2011). Similar to other osteoblast cell lines such as MLO-A5, IDG-SW3 cells also produce a collagen matrix and mineralise when treated with ascorbic acid and phosphate.

4.2 Hypothesis

Mineralisation of ECM affects osteocytogenesis. Mineralisation can be controlled with ascorbic acid, β-GP and SrR.

4.3 Aims

To determine the effect of mineralisation on osteocytogenesis, mineralisation was altered by adding or omitting ascorbic acid, β-GP and SrR. Specifically, the following aims were addressed:

1. To confirm that ascorbic acid is required for the deposition of collagen in IDG-SW3.

2. To assess whether mineralisation in IDG-SW3 is directly linked to the concentration of β-GP added to the culture medium.

3. To assess the effect of SrR on mineralisation.

4. To determine whether osteocytogenic differentiation directly depends on mineralisation in IDG-SW3.
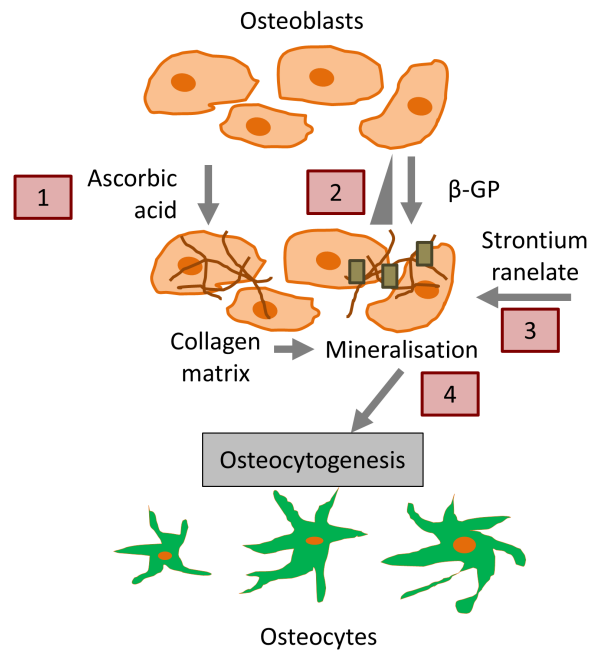
Figure 4.2: Aims of Chapter 4.

4.4 Materials and Methods

4.4.1 Materials

All reagents were purchased from Sigma-Aldrich (UK) unless otherwise stated below.

4.4.2 Methods

Cell culture

IDG-SW3 (Kerafast, USA) between passages 20 and 35 were used in this chapter. Cells were seeded at a density of 10,000 cells/well in 0.1% gelatin-coated 24-well plates. This seeding density allowed cells to become confluent within three days which is a requirement for osteogenesis in IDG-SW3 (Woo et al., 2011).For the first three days or until cells reached 100% confluence, cells were cultured at 33 °C in culture medium supplemented with 50 units/ml recombinant mouse interferon-gamma (INF-γ) (John et al., 2014). The day cells reached confluence was declared as Day 0. Temperature in the incubator was increased to 37 °C and cells were cultured in the absence of INF-γ. Culture medium was changed every two to three days. Each well contained 500 μl of cell culture medium.

Biochemical treatment

To assess the effect of biochemical stimulation on IDG-SW3, culture medium was supplemented with or without L-ascorbic acid 2-phosphate sequimagnes (AA, referred to as ascorbic acid) at a concentration of 50 μg/ml. This concentration supports collagen deposition and has been routinely used in past osteogenesis studies (Jaiswal et al., 1997). The effect of phosphate on mineralisation was assessed by adding different concentrations of β-GP (0, 2.5, 4, 5 and 10 mM) to the culture medium. 5 mM β-GP was defined as control group since this concentration has been previously enabled consistent, bone-like mineralisation in several in vitro studies (Prideaux et al., 2012; Barragan-Adjemian et al., 2006; Sittichokechaiwut et al., 2010; Staines et al., 2016).

The effect of strontium ranelate (SrR), a former leading therapeutic agent used in the treatment of postmenopausal osteoporosis, was assessed as well. Previous studies have already investigated the dose-dependency of SrR on osteoblast behaviour using a wide range of concentrations from 1 μM to 10 mM (Verberckmoes et al., 2003; Atkins et al., 2009). Therefore, this study focussed only on one concentration, i.e. 1 mM, as this dosage was not only used in most studies but also had a significant effect on osteogenesis (Canalis et al., 1996; Barbara et al., 2004; Bonnelye et al.,

2008; Bakker et al., 2013). SrR (LKT Laboratories, USA) was directly added to the culture medium at the required concentration of 1 mM on the day of experiment. Dissolution of SrR was facilitated by placing the solution for 30 min in a 37 °C water bath. All conditions are summarised in Table 4.2 and the treatment groups were compared to the control group which was supplemented with 50 µg/ml ascorbic acid, 5 mM β-GP, but no SrR.

Cellular assays

The following assays were performed to determine the effects of biochemical stimulation with β-GP, ascorbic acid and SrR on IDG-SW3 (Figure 4.3). All of these assays have been described in detail in Chapter 3.2.

- Qualitative assessment of cell morphology and Dmp1-GFP expression with phase-contrast and fluorescence microscopy.

- Quantification of Dmp1-GFP expression with microplate reader at Days 0, 7, 14 and 21.

- Quantification of metabolic activity with resazurin reduction assay at Days 0, 7, 14 and 21.

- Quantification of DNA at Days 14 and 21.

- Quantification of ALP activity at Days 14 and 21.

- Qualitative and quantitative assessment of deposited collagen with Picrosirius Red (PSR) staining at Days 14 and 21.

- Qualitative and quantitative assessment of deposited calcium with Alizarin Red S (ARS) staining at Days 14 and 21.

Statistical analysis

Data are expressed as the mean ± standard deviation (SD) of three independent experiments. Statistical analysis was performed by two way analysis of variance (ANOVA), followed by Tukey's post hoc test. p values of ≤0.05 were considered to be significant and noted '*'; p values of ≤0.001 were noted as '**'.

Table 4.2: Experimental conditions.

Condition	Ascorbic acid	β-GP	Strontium ranelate
#1 (Control)	$50\,\mu g/ml$	$5\,mM$	-
#2	$50\,\mu g/ml$	$10\,mM$	-
#3	$50\,\mu g/ml$	$4\,mM$	-
#4	$50\,\mu g/ml$	$2.5\,mM$	-
#5	$50\,\mu g/ml$	-	-
#6	$50\,\mu g/ml$	$5\,mM$	$1\,mM$
#7	-	-	-

Culture medium also contained 10% FBS and 1% PS.
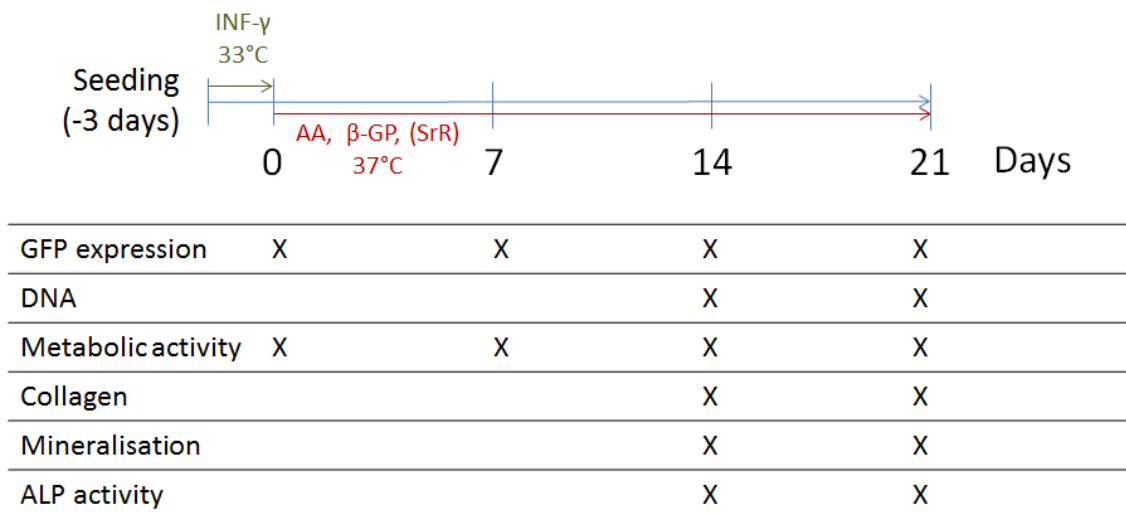
Figure 4.3: Experimental protocol for investigating the response of IDG-SW3 to biochemical stimulation.

IDG-SW3 were seeded at 10,000 cells/well in 24-well plates and grown for three days until they reached confluence in medium supplemented with INF-γ (green arrow). Cells were grown for a further 21 days in culture medium supplemented with varying concentrations of β-GP, ascorbic acid (AA) and strontium ranelate (SrR) (red arrow). Time points of the performed assays are marked in the table below.

4.5 Results

4.5.1 Metabolic activity and amount of DNA were not affected by biochemical stimulation

Cell proliferation was assessed using two different measures: metabolic activity and total DNA per well. Metabolic activity, which was measured with the resazurin-reduction assay, increased significantly between Day 0 and 7 ($p \leq 0.001$) and between Day 7 and 14 ($p \leq 0.05$), but remained constant between Day 14 and 21. No differences were found regarding the metabolic cell activity between the different conditions.

The amount of DNA was only quantified on Days 14 and 21, where no significant changes were detected between the two time points. Approximately 1 μg of DNA was detected per well which equates to roughly 400,000 cells per well. Variations in the concentration of β-GP, ascorbic acid or SrR did not affect the total DNA (Figure 4.4).

4.5.2 Collagen deposition required ascorbic acid

The amount of collagen deposited was significantly reduced when ascorbic acid (AA) was omitted from the culture medium ($p \leq 0.05$). In contrast, varying the concentration of β-GP or adding SrR to the culture medium had no effect on the amount of collagen deposited. The amount of collagen significantly increased between Day 14 and 21 ($p \leq 0.05$), except in the conditions without ascorbic acid and with added SrR where no significant increase was measured. Visual inspection of the PSR-stained samples confirmed that a layer of collagen had been deposited in the well plates at Day 14. Furthermore, the staining in the sample without ascorbic acid was less dominant and more confined to the cells themselves rather than to deposited fibres around the cells. Collagen appeared to be deposited evenly within the wells (Figure 4.5A).

4.5.3 β-GP dose-dependently enhanced mineralisation

No significant mineralisation was detected in any of the tested conditions on Day 14 as evaluated by ARS staining. On Day 21, cells deposited significant amounts of mineral as indicated by a strong red staining. The amount of deposited mineral depended on the concentration of β-GP added to the culture medium. For example, doubling the concentration of β-GP from 5 mM to 10 mM increased mineralisation by 150% ($p \leq 0.001$). On the other side of the spectrum, reducing the concentration
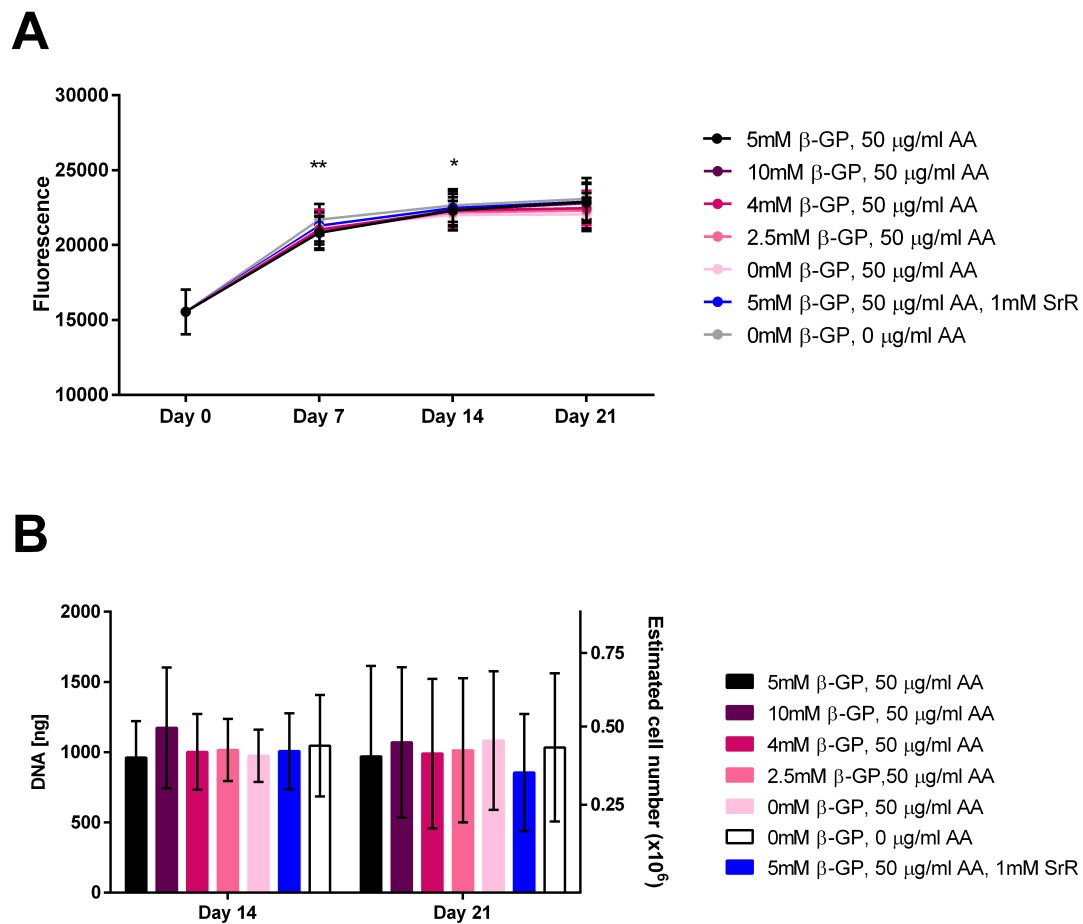
Figure 4.4: Effect of biochemical stimulation on metabolic activity and DNA.

A: Metabolic activity assessed with resazurin-reduction assay. A significant increase in metabolic activity was observed between Day 0 and 7 and between Day 7 and 14. Metabolic activity was not affected by biochemical treatment. Significantly different compared to previous time point * $p \leq 0.05$, ** $p \leq 0.001$. Mean with SD (n=3). B: Total DNA and estimated cell number per well. DNA remained constant in all conditions between Day 14 and 21. Mean with SD (n=3).

of β-GP resulted in a significant concentration-dependent decrease of mineralisation ($p \leq 0.001$). Omitting β-GP completely from the culture medium appeared to inhibit mineralisation since there was no significant increase between Day 14 and 21 in the two conditions without β-GP. Mineralisation was also inhibited following treatment with 1 mM SrR, despite the supplementation of culture medium with ascorbic acid and 5 mM β-GP (Figure 4.5B).

4.5.4 Ascorbic acid and strontium affected ALP activity

Omission of ascorbic acid and treatment with 1 mM SrR significantly inhibited ALP activity ($p \leq 0.0001$). In all other conditions ALP activity was higher at both Day 14 and 21 and increased even further between Day 14 and 21 ($p \leq 0.01$). Changes in the concentration of β-GP did not translate into significant changes in ALP activity (Figure 4.5C).

4.5.5 Dmp1-GFP expression increased over time

Expression of the osteocyte marker Dmp1 is linked to GFP fluorescence in IDG-SW3 and increased in all culture conditions from Day 0 to Day 21 ($p \leq 0.05$). Changes in the concentration of β-GP affected Dmp1 expression, i.e. higher concentrations of β-GP resulted in greater expression of GFP. For example, adding 10 mM instead of 5 mM β-GP to the culture medium increased the fluorescence by 50% on Day 21 ($p \leq 0.0001$). Reducing the concentration of β-GP or even omitting β-GP significantly decreased fluorescence on Day 21 ($p \leq 0.05$). The strongest reduction in fluorescence expression was detected when both β-GP and ascorbic acid were omitted. This decrease was significant at all three time points ($p \leq 0.0001$).

Treatment with 1 mM SrR enhanced the expression of Dmp1-GFP. While SrR did not increase Dmp1-GFP expression significantly at Day 7, the difference between the two conditions became larger over time. At Day 21 treatment with 1 mM SrR resulted in a 24% higher Dmp1-GFP expression compared to the control group without SrR ($p \leq 0.001$, Figure 4.6A).

Although absolute fluorescence values are good for measuring the increase of Dmp1-GFP expression over time, inter-experimental differences result in large standard deviations. Such differences can be minimised by normalising each value to the fluorescence of the standard condition at that day. Results in Figure 4.6B show that chemical stimulation or withdrawal of chemicals resulted in significantly different fluorescence values in all conditions compared to the control group (50 μg/ml ascorbic acid, 5 mM β-GP) at Day 21 ($p \leq 0.05$). The same trends were also observed when comparing images acquired by fluorescence microscopy.
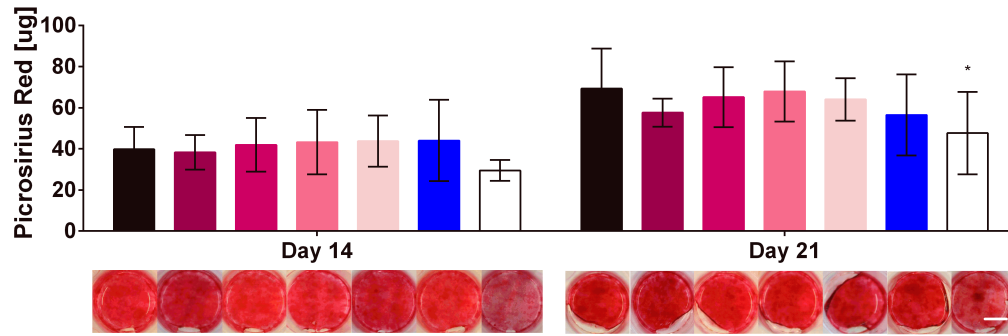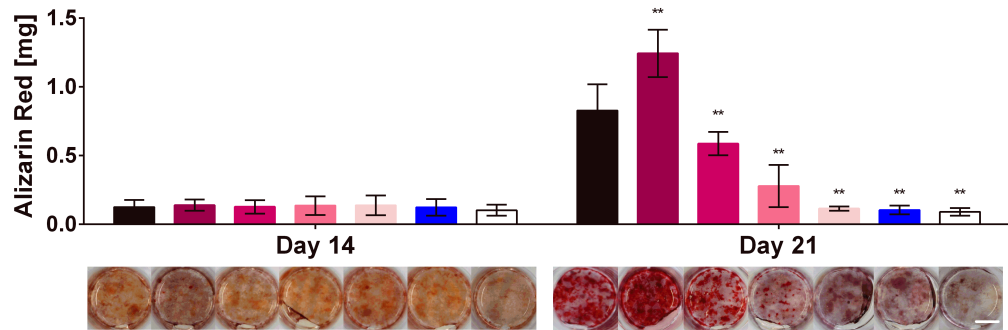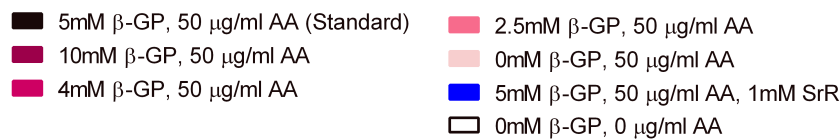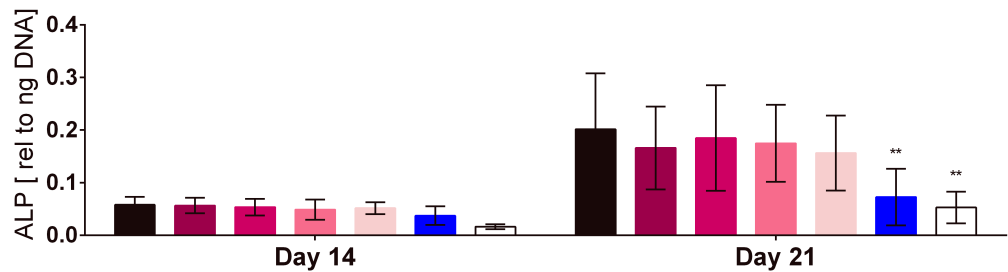
Figure 4.5: Assessment of osteogenesis in IDG-SW3.

A: Collagen deposition quantified with PSR de-stain. Images below the graph are taken from representative wells after staining for collagen. Omitting AA from the culture medium significantly reduced collagen deposition at Day 21. B: Mineralisation quantified with ARS de-stain. Images below the graph are taken from representative wells after staining for calcium. No minerals were deposited on Day 14. A positive relationship between concentration of β-GP and mineral deposition was observed on Day 21. Supplementing medium with SrR inhibited mineral deposition. C: ALP activity relative to total DNA. ALP activity at Day 21 was significantly lower in samples with 1 mM SrR or without AA. Significantly different to standard condition * $p \leq 0.05$, ** $p \leq 0.001$. Scale bar = 500 μm. Mean with SD (n=3).

Fluorescence microscopy allowed evaluation of the distribution of Dmp1-positive cells and minerals within the well (Figure 4.6B). The area of mineralisation increased with higher β-GP concentrations. Dmp1-GFP positive cells were primarily located in the mineralised areas, which also had a higher cell density than surrounding areas. Treatment with SrR prevented the formation of mineralised areas, even though small black spots were visible. However, SrR treatment did not prevent cell differentiation since many Dmp1-GFP positive cells were visible. The lack of mineralisation caused the Dmp1-GFP positive cells to be evenly distributed throughout the well, rather than clustered in the mineralised areas as seen in the mineralising conditions. Dmp1-GFP positive cells exhibited an osteocyte-like elongated morphology with several thin processes per cell in all conditions. Omission of ascorbic acid and β-GP inhibited cell differentiation completely as no Dmp1-GFP positive cells were visible.
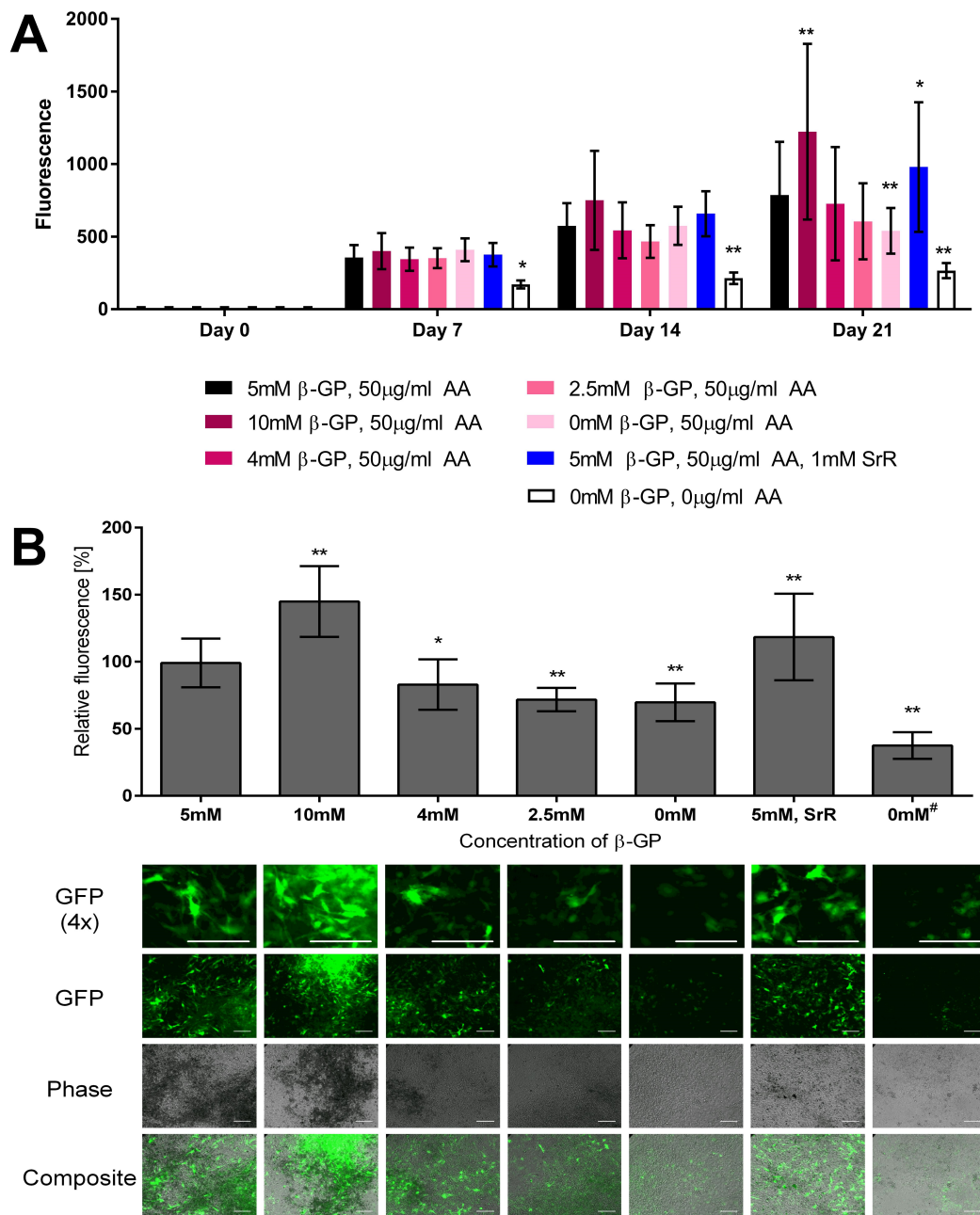
Figure 4.6: Dmp1-GFP expression and mineralisation in IDG-SW3 in response to biochemical stimulation.

A: Absolute fluorescence values measuring the expression of the osteocyte marker Dmp1-GFP. B: Relative GFP fluorescence values normalised to the standard culture condition (5 mM β-GP). All conditions contain 50 µg/ml AA except # which contains no AA. Corresponding images below were acquired at Day 21. Fluorescence images show Dmp1-GFP positive cells in green, which exhibit an osteocyte-like elongated morphology. Phase-contrast images show cell contours and mineralised areas in black. Co-localisation of highly mineralised areas and high concentrations of Dmp1-GFP positive cells can be seen in the composite images. Scale bar = 250 µm. Significantly different compared to standard condition * $p \leq 0.05$; ** $p \leq 0.001$. Mean with SD (n=3).

4.6 Discussion

This chapter investigated the effects of ascorbic acid, β-glycerophosphate (β-GP) and strontium ranelate (SrR) on mineralisation and osteocytogenesis in the murine osteoblast-osteocyte cell line IDG-SW3.

In line with previous findings, treatment with β-GP had no influence over cell metabolic activity and DNA synthesis (Chung et al., 1992; Chang et al., 2000). Similarly, treatment of IDG-SW3 with 1 mM SrR did not affect metabolic activity nor cell number of IDG-SW3 cells at any of the observed time points. While some studies support this finding (Verberckmoes et al., 2003; Wornham et al., 2014), other studies have previously shown that SrR can enhance cell proliferation and viability at concentrations ranging from 0.01 to 10 mM (Querido et al., 2015; Atkins et al., 2009; Bakker et al., 2013). It is thought that the beneficial effect of SrR on osteoblast proliferation, which had been observed in some studies, is caused by the interaction of strontium with the calcium-sensing receptor (CaSR) (Chattopadhyay et al., 2007; Brennan et al., 2009). In addition, indirect mechanisms such as the release of an autocrine growth factor in response to treatment with strontium might also enhance proliferation (Caverzasio, 2008). Canalis et al. (1996) showed in a rat calvarial culture system that 1 mM SrR but not $CaCl_2$ enhanced bone cell replication predominantly in the osteoprogenitor cell zone. Furthermore, Chattopadhyay et al. (2007) showed that both 5 and 10 mM SrR increased cell proliferation in human osteoblasts (HOBs). For the same cell line, Brennan et al. (2009) showed that also smaller concentrations of SrR (0.01 to 2 mM) increased cell replication dose-dependently. Using the cell line MC3T3-E1, Caverzasio (2008) demonstrated a similar dose-dependent increase in cell number with a small but significant increase at 1 mM, a maximal increase at 5 mM and a slightly smaller response at 10 mM. While there is a wide range of literature available which describes the positive effect of SrR on osteoblast proliferation, other in vitro studies agree with the findings from this study and have shown that SrR does not affect and might even inhibit cell proliferation. For example, Li et al. (2012c) showed that SrR at 0.1 or 1 mM inhibited cell proliferation. In another study Almeida et al. (2016) observed a dose-dependent negative effect on cell viability and proliferation in MC3T3-E1. Cells were not affected by SrR at 0.05 and 0.1 mM, but MC3T3-E1 cultures exposed to a higher concentration of 0.5 mM SrR exhibited a decrease in both measures compared to the control group. In a primary osteoblast study, Wornham et al. (2014) showed that SrR caused a moderate decrease in cell viability, but no significant effect on cell numbers. In line with the findings from the present study, Verberckmoes et al. (2003) detected no impact of strontium on DNA content and cellular proliferation in primary rat osteoblasts. In conclusion, the effect of strontium on cell proliferation appears to vary between

studies and therefore more controlled experiments are required to identify the exact mechanisms involved.

Independent of the treatment condition, high cell numbers of approximately 400,000 cells per well at Days 14 and 21 indicated complete confluence. Phase-contrast images further confirmed confluence. Cell confluence might explain why cell numbers did not further increase after Day 14. The metabolic activity also remained constant between Day 14 and 21 which further indicated that cell proliferation stopped after Day 14.

The metabolic activity at Day 0 and 7 was significantly lower compared to Day 14. Assuming that metabolic activity directly relates to number of cells, cell numbers were lower at Day 0 and kept increasing up until Day 14. However, continuous proliferation after Day 0 is in contrast to previous findings in the literature, where proliferation of the temperature-sensitive cells IDG-SW3 stopped once they were cultured at 37 °C without INF-γ (Woo et al., 2011). The same trend of continuous proliferation in IDG-SW3 was observed in Chapter 6, where the effect of mechanical stimulation on IDG-SW3 was evaluated. Since in that chapter data for both DNA and metabolic activity are available at all time points, a detailed discussion of the continuous proliferation is given in that chapter (see Chapter 6.6). However, it should be noted that the observed continuous proliferation did not appear to impair cell functions, hence it can be assumed that this difference also did not affect the overall outcome of the experiments discussed below.

Cells cultured in the absence of ascorbic acid deposited less collagen at Day 14 and Day 21 (p≤0.05). Similar amounts of collagen were deposited in all other conditions which contained 50 µg/ml ascorbic acid. Hence, collagen deposition required ascorbic acid but was independent of the concentration of β-GP or SrR. This result confirms that ascorbic acid is essential for collagen assembly (Canty and Kadler, 2005) which has also been described in more detail in Chapter 2.1.3. In brief, ascorbic acid is an essential co-factor for the hydroxylation of proline and lysine in pro-collagen chains. This modification is required for the formation of triple helical fibrils which assemble to collagen fibres (Franceschi, 1999). Although no significant differences between ascorbic acid and the more stable form ascorbic acid-2-phosphate has been observed (data not shown), the latter was used at a concentration of 50 µg/ml in line with previous studies (Jaiswal et al., 1997).

Previously SrR has been shown to have varying effects on collagen deposition in osteoblasts. In contrast to results from this experiment, some studies found that SrR was able to increase collagen production for example in rat calvaria organ cultures and rat calvaria cells (Canalis et al., 1996). Similarly, Barbara et al. (2004) reported

an increase in collagen synthesis in MC3T3-E1 in response to SrR during the first ten days of culture but not thereafter. A possible explanation for this biphasic behaviour might have been that cells at Day 14 already differentiated into mature osteoblasts and were less responsive to SrR. Almeida et al. (2016) found higher levels of collagen type I protein after 48 h of MC3T3-E1 culture, however no long-term observations regarding actual changes in collagen deposition were shown in that study. Yang et al. (2011) observed an increase in collagen deposition and col1 mRNA expression when MSCs were cultured with strontium chloride. They further confirmed the increased collagen deposition in an in vivo rat calvaria defect model implanting a collagen-strontium-substituted hydroxyapatite scaffold. In contrast, the findings by Wornham et al. (2014) were in line with the results in this chapter indicating that SrR had no apparent effect on collagen matrix formation by osteoblasts in vitro. One explanation for these contrasting results might be that pre-osteoblastic cells (e.g. MC3T3-E1, MSCs) are more responsive to SrR than late-osteoblastic cells such as IDG-SW3 or the primary osteoblasts used by Wornham et al. (2014).

Mineralisation in IDG-SW3 was dependent on the concentration of β-GP added to the culture medium. IDG-SW3 produced significantly less mineral when β-GP was omitted from the culture medium, while even a low concentration of 2.5 mM β-GP increased mineralisation significantly ($p \leq 0.001$). The finding that an external phosphate source such as hydrolysable β-GP is required to induce mineralisation in osteoblasts is consistent with the literature (Schäck et al., 2013; Chang et al., 2000; Tenenbaum et al., 1989; Chung et al., 1992; Fratzl-Zelman et al., 1998). For example, Prideaux et al. (2012) observed significantly reduced mineralisation in the osteoblast cell line MLO-A5 in the absence of β-GP compared to a control group supplemented with 5 mM β-GP.

Since the aim in tissue engineering is generally to enhance mineralisation and osteogenic differentiation, results from this study suggest that the best results, i.e. greatest mineralisation, can be achieved with the highest concentration of phosphate (10 mM). However, high phosphate concentrations have also been related to an abnormal mineralisation pattern mainly caused by spontaneous precipitation of calcium phosphates (Schäck et al., 2013). One indicator for mineral quality is the ratio between calcium and phosphate ions. Mineral in natural bone is made up mostly of carbonated hydroxyapatite consisting of calcium and phosphate ions in a ratio of approximately 1.63 (Cassella et al., 1995). In vitro studies have shown that relatively high concentrations of free phosphates reduced the calcium/phosphate ratio (Schäck et al., 2013). The concentrations of β-GP which is considered too high for biological-driven mineralisation seems to vary between different studies. While the above mentioned study observed abnormal bone formation using 10 mM β-GP

(Schäck et al., 2013), one of the first works on bone mineralisation concluded that medium supplementation with phosphate should not exceed 2 mM to prevent non-physiological mineral deposition in bone cell cultures (Chung et al., 1992). Most groups nowadays supplement their osteogenic differentiation medium with 5 mM β-GP (Prideaux et al., 2012; Barragan-Adjemian et al., 2006; Sittichokechaiwut et al., 2010; Staines et al., 2016). This concentration of phosphate has been confirmed to result in mineralisation driven by cellular activities rather than spontaneous precipitation of calcium phosphate minerals in a primary rat osteoblastic cell culture (Chang et al., 2000). In comparison, the level of inorganic phosphate in serum of adults ranges only between 0.8 and 1.5 mM (Penido and Alon, 2012). However, it is thought that concentrations of inorganic phosphate in bone likely increase during active osteoclastic resorption and might well reach the levels used in experimental studies (Ito et al., 2013).

In line with the majority of other mineralisation studies described above, a concentration of 5 mM β-GP was selected as the standard supplementation in this chapter and also in the following chapters. Interestingly, most other studies using the relatively novel cell line IDG-SW3 have used a reduced β-GP concentration of 4 mM (Woo et al., 2011; John et al., 2014; Ito et al., 2013). Both concentrations, i.e. 4 mM and 5 mM, have been investigated in this chapter. Decreasing the concentration of β-GP from 5 mM to 4 mM reduced mineralisation significantly by 30% (p≤0.001). However, it appeared that both concentrations allowed biological mineralisation with minerals primarily deposited along the collagen fibres. To further confirm the natural origin of the mineralisation in all conditions and to exclude chemically-driven precipitation, more detailed analyses of the mineralised matrix would be required. Analytical techniques including X-ray diffraction (XRD) or Fourier-transform infrared spectroscopy (FT-IR) could provide more information about the matrix material (Schäck et al., 2013). Cell-free controls with calcium and phosphate supplements could also be used in the future to check whether the minerals were formed by biologic events or spontaneous precipitation of calcium phosphate minerals (Chang et al., 2000). In conclusion, this study showed that mineralisation in IDG-SW3 increased dependent on the dose of β-GP, but further tests should be performed to confirm the natural origin of mineralisation in all conditions.

In contrast to other in vitro studies which reported increased mineralisation upon treatment with SrR (Querido et al., 2015; Atkins et al., 2009), SrR inhibited mineralisation in IDG-SW3. This finding was also in disagreement with several in vivo experiments (Delannoy et al., 2002), clinical trials (Meunier et al., 2002; Reginster et al., 2005) and the use of SrR as osteoporosis treatment where it had previously increased bone mineral density and decreased fracture risk. However, other stud-

ies also showed that SrR can block calcification in vitro (Wornham et al., 2014). Wornham and colleagues found that SrR at 0.01, 0.1 and 1 mM inhibited mineralisation dose-dependently to 59%, 98% and 100% of their control group without SrR. These differences might result from a complex multiphasic interaction between osteoblasts and strontium depending on the strontium dosage (Verberckmoes et al., 2003). Verberckmoes et al. (2003) , who investigated the effects of strontium using strontium chloride but not ranelate, found that strontium at low concentrations (0.5 and 1 μg/ml) inhibited nodule formation but still allowed normal mineralisation, hence they concluded that cell differentiation might be impaired at low concentrations of strontium. Medium concentrations of strontium (2 and 5 μg/ml) did not inhibit nodule formation or mineralisation, but also did not enhance it either in their study. High concentrations (20 and 100 μg/ml) allowed the formation of bone nodules but prevented mineralisation which might have been the result of physiochemical interactions between strontium and hydroxyapaptite formation. For example, strontium has been known to replace some of the calcium ions in hydroxyapatite and thereby increase the solubility of hydroxyapatite under standard culture conditions but also inhibit crystal growth directly (Christoffersen et al., 1997; Pan et al., 2009). The applied concentration of 1 mM SrR was equal to a concentration of 86 μg/ml strontium. Therefore, the fact that no mineralisation was detected in the samples is in line with observations by Verberckmoes et al. (2003) for high concentrations of strontium.

In addition to the SrR dosage, variations in the mineralisation assessment methods might have also contributed to the different results described above. Calcium and phosphate staining are commonly performed with Alizarin red (Almeida et al., 2016) or van Kossa (Bonnelye et al., 2008; Atkins et al., 2009) respectively, which are then followed by counting the number of mineral nodules and measuring the surface area of the nodules (Barbara et al., 2004; Atkins et al., 2009). Such image analysis methods however often contain a certain bias. For example, confluence of the mineralised colonies makes it hard to visibly separate the clusters and count bone nodules (Zhu et al., 2007), hence conclusions solely based on image analysis involving counts of bone nodules or mineralised area measurements should be interpreted with care. Furthermore, separate investigation of mineralised and non-mineralised matrix might be important for understanding the effect of strontium on mineralisation (Verberckmoes et al., 2003; Wornham et al., 2014). In this chapter, mineralisation was primarily assessed with qualitative image analysis following ARS staining and semi-quantitative ARS de-staining. Future investigations should include a wider array of assessment methods, including quantitative image analysis considering mineralised and non-mineralised areas, but also calcium ion measurements in the medium to

better understand how SrR inhibited mineralisation.

ALP activity increases during osteoblast transformation and reaches its maximum in mature osteoblasts. ALP is thought to be closely linked to mineralisation in bone cells, since it enzymatically cleaves organic phosphates such as β-GP and thereby controls and enhances the inorganic phosphate concentration (Bellows et al., 1992). Except in the SrR-treated group (discussed further below) and the group lacking ascorbic acid, ALP activity was increased in all conditions. Concentration (or even the absence) of β-GP did not seem to interfere with the ALP activity. This indicated that the collagen matrix seems to be essential in osteoblast differentiation guiding ALP expression (Langenbach et al., 2013). It is thought that osteoblast differentiation requires contact between osteoblasts and a collagen-containing ECM via interactions such as col1 and $\alpha1\beta2$ integrins (Xiao et al., 2002). This has been confirmed in a study where osteogenesis was inhibited by treating pre-osteoblasts MC3T3-E1 with collagenase (Xiao et al., 1998).

IDG-SW3 cells developed further into osteocyte-like cells as demonstrated by increased expression of the osteocyte-marker Dmp1 (Woo et al., 2011; Feng et al., 2006). Unlike ALP expression, Dmp1 expression depended significantly on the concentration of β-GP, i.e. higher concentrations of β-GP resulted in increased expression of Dmp1. Similarly, higher mineralisation also appeared to enhance osteocytic differentiation. Although there was a relationship between β-GP concentration, mineralisation and Dmp1 expression, it is difficult to distinguish whether greater phosphate concentrations directly enhanced osteocytogenesis (Rendenbach et al., 2014) or whether the increased mineralisation triggered cell differentiation towards osteocyte-like cells (Irie et al., 2008). Since Dmp1-positive cells were primarily found in highly mineralised areas, it seems more likely that mineralisation triggered osteocytogenesis as has also been previously reported (Robin et al., 2016; Irie et al., 2008; Prideaux et al., 2012). The collagen network also seemed to play a role in the osteocytic differentiation process, since Dmp1 expression was the lowest when ascorbic acid was omitted ($p \leq 0.001$). This is in line with the finding by Prideaux et al. (2012) who reported that both the availability of phosphate and its deposition within the ECM are essential for osteoblast differentiation.

Interpreting the impact SrR had on osteoblast differentiation is not straight-forward and potentially requires more analysis in future experiments. While treatment with SrR completely suppressed ALP activity, it significantly increased the expression of Dmp1. The reduced ALP activity upon incubation with strontium salts might explain the inhibition of mineralisation and has also been previously observed by Wornham et al. (2014). However, other studies have reported increased ALP activity

(Querido et al., 2015; Barbara et al., 2004; Li et al., 2012c) and increased ALP mRNA expression (Bonnelye et al., 2008) in response to treatment with 0.1 to 1 mM SrR. Moreover, SrR treatment has also been associated with enhanced expression of other osteoblast markers including COX-2 (Choudhary et al., 2007) and Type I collagen mRNA (Almeida et al., 2016). The mechanisms how strontium interacts with ALP are not well understood yet, therefore further research into signalling pathways and other mechanisms are required to better understand these contrasting observations.

The suppression of ALP as a marker for osteoblastic differentiation upon treatment with SrR is surprising though, since transformation of IDG-SW3 to osteocyte-like cells expressing Dmp1 was not impaired. Following the mechanism described for β-GP-treated cells, i.e. mineralisation triggering osteocytic differentiation, it was thought that expression of Dmp1 would have been inhibited in SrR-treated samples since SrR prevented mineralisation. However, the opposite was observed with SrR-treated cells expressing significantly more Dmp1 than the control group ($p \leq 0.001$). Therefore, mineralisation cannot be the only trigger for osteocytogenesis, but other factors have to be involved as well. The increase in Dmp1 expression is consistent with the findings by Bakker et al. (2013) who showed that 3 mM SrR enhanced Dmp1 expression by two-fold in MC3T3 osteoblasts at Day 16. In addition, SrR treatment at a concentration of 5 mM also increased Dmp1 mRNA in human primary osteoblasts, even though a concentration of only 1 mM SrR had no significant effect (Atkins et al., 2009).

In future experiments, examination of mRNA profiles of several osteoblast and osteocyte specific markers such as Col1, ALP, BSP, Dmp1 and SOST might help to better understand how SrR interferes with IDG-SW3. A limitation of this study might have been the consideration of only one concentration of SrR, in particular since strontium treatment might result in a multiphasic behaviour (Verberckmoes et al., 2003). The concentration of SrR found in bone is not known, however SrR concentrations of 0.12 mM have been found in the plasma of SrR-treated humans, which is relatively close to the concentration used in this study (Meunier et al., 2004). In addition, it is thought that the concentration of strontium in bone might easily be higher than 0.12 mM since strontium is a bone seeking agent and can be integrated in the mineralised matrix (Bakker et al., 2013).

4.7 Summary

- Metabolic activity and proliferation were not affected by β-GP, ascorbic acid or SrR.

- Ascorbic acid was required for the deposition of collagen and activation of ALP in IDG-SW3.

- Mineralisation in IDG-SW3 was directly linked to the concentration of β-GP added to the culture medium.

- Treatment of IDG-SW3 with $1\,\text{mM}$ SrR inhibited ALP activity and mineralisation.

- Osteocytogenic differentiation was linked to mineralisation in IDG-SW3, i.e. greater mineralisation enhanced expression of the osteocyte marker Dmp1.

- Treatment with $1\,\text{mM}$ SrR enhanced expression of Dmp1, despite inhibiting mineralisation, hence mineralisation cannot be the only factor which regulates osteocytogenesis.

Chapter 5

Impact of low fluid shear stress on MLO-A5 osteoblasts

5.1 Introduction

Osteoblast behaviour can be controlled by biochemical stimulation as demonstrated in the previous chapter. In addition, mechanical loading, in particular fluid shear stress (FSS), has also been shown to guide osteoblast function (Johnson et al., 1996; Reich et al., 1990). This mechanism, referred to as bone mechanotransduction, has been described extensively in Chapter 2.2.

Osteoblast responses to FSS can be divided into early (= short-term) and late (= long-term) responses based on the time for the assessed parameter to take effect. Early responses include the release of signalling factors such as calcium ions and prostaglandins within seconds to minutes after mechanical stimulation. There is a wide range of literature available on early osteoblast responses to FSS. Generally, it has been shown that early osteoblast responses depend greatly on the magnitude and type of fluid flow. For example, osteoblasts released more calcium in response to higher FSS (Allen et al., 2000; Jacobs et al., 1998; Hung et al., 1995; Huo et al., 2010).

It is thought that these early responses initiate long-term, osteogenic effects. However, the exact mechanisms which control this translation process and to what extent early and late responses are related are still under debate. Unlike the release of signalling molecules, osteogenic responses require several weeks to take effect. Osteogenesis, which describes the formation of bony tissue, is characterised by osteoblast-driven collagen and mineral deposition. Assessment of osteogenesis in vitro is challenging because cell culture devices have to support long-term cell

culture. In particular the combination of fluid flow stimulation and long-term cell culture is not straight-forward, hence there are only few studies which managed to successfully combine both aspects (Nauman et al., 2001; Kreke and Goldstein, 2004; Scaglione et al., 2008). For example, the experimental set-up by Delaine-Smith et al. (2012) included a see-saw rocker which applied FSS to cells cultured in 6-well plates. See-saw rockers exhibit several advantages compared to other established methods for generating FSS such as parallel-plate flow chambers. For example, rockers support cell culture over several weeks, they handle large numbers of samples running in parallel and allow straight-forward operation and cell monitoring. However, see-saw rockers can only generate very low shear stress which peaks around 0.05 Pa. Similar to see-saw rockers, orbital shakers have also been previously used to generate FSS on the bottom of well plates (Lim et al., 2014; Dardik et al., 2005). While orbital shakers share the same advantages as see-saw rockers, they can generate slightly higher FSS up to 0.83 Pa. The exact shear magnitude depends on the location within the well, rotation frequency and fluid volume per well (Salek et al., 2012).

As described above, most of the devices which support long-term cell culture are only able to generate low FSS. Although low FSS appears to mimic the natural biomechanical environment of osteoblasts (Bonewald and Johnson, 2008), more research is required on whether low FSS is actually able to directly enhance osteogenesis driven by osteoblasts. As discussed in detail in Chapter 2.2.5, only limited and often conflicting data is currently available on whether low FSS is able to increase late osteogenesis markers such as collagen deposition and mineralisation (Nauman et al., 2001; Delaine-Smith et al., 2012; Scaglione et al., 2008; Kreke and Goldstein, 2004). A positive osteogenic effect of FSS has been demonstrated in a study by Delaine-Smith et al. (2012) where they demonstrated that the mature osteoblast cell line MLO-A5 responded to low, oscillatory fluid shear stimulation through increased collagen production and mineral deposition after 21 days of culture. Based on these positive results, this study aims to further explore the connection between early and late responses and whether low fluid flow might be strong enough to not only enhance osteogenesis but also to guide collagen fibre orientation.

5.2 Hypothesis

Low FSS generated with see-saw rockers and orbital shakers enhances mineralised matrix deposition in MLO-A5 compared to static culture.

5.3 Aims

This chapter aims to assess early and late responses to FSS in the mature osteoblast cell line MLO-A5 (Figure 5.1). In particular the following aims are addressed:

- To optimise cell culture conditions for mechanical stimulation in 6-well plates for 1 h per day outside a CO_2-controlled incubator over several weeks.

- To investigate whether MLO-A5 respond immediately to low FSS by releasing Ca^{2+} and PGE_2.

- To investigate the effect of low FSS on osteogenesis, in particular changes in cell number, ALP activity, mineralisation and collagen deposition.

- To investigate whether MLO-A5 respond differently to FSS generated with rocking or orbital shaking.
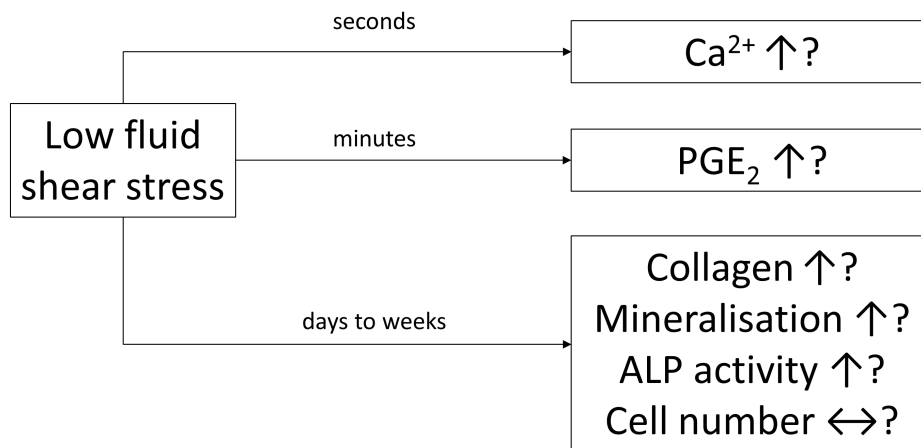
Figure 5.1: Aims of Chapter 5.

5.4 Methods

5.4.1 Cell culture

Two different batches of MLO-A5 cells were used in this chapter. One batch was a kind donation by Dr Gwendolen Reilly, University of Sheffield who previously acquired the cells from Dr Lynda Bonewald, University of Missouri. This batch of cells was used between passages 25 and 30 to asses the effect of an extremely low initial seeding density and HEPES buffering. Preliminary experiments showed that cells seeded at 10,000 cells/well could only be maintained with difficulties for more than 21 days. In order to investigate whether a lower seeding density would support longer experiments, the cell density was reduced forty-fold to 250 cells/well. The same seeding density of 250 cells/well was applied to evaluate the impact of CO_2-buffering with 25 mM HEPES on cell metabolism.

The main experiments which assessed the effect of rocking and orbital shaking on MLO-A5 cells used a different batch of cells. These cells were kindly donated by Prof Alicia El Haj, Keele University who also previously acquired them from Dr Lynda Bonewald and which were used between passages 58 and 62. Following the experimental protocol by Delaine-Smith et al. (2012), cells were seeded at a density of 10,000 cells/well on 6-well plates. This seeding density was also selected since lower seeding densities had no benefits (e.g. better survival, more consistent mineralisation) over the already established seeding density of 10,000 cells/well. In line with the study by Delaine-Smith et al. (2012), well plates were coated with 0.1% gelatin and each well contained 2 ml of proliferation medium (Table 3.2). At Day 3 of culture, proliferation medium was supplemented with 50 μg/ml ascorbic acid and 5 mM β-GP. Medium was changed every 2 days.

5.4.2 Fluid shear experiments

In this chapter, the same experimental settings which have been previously used in a study by Delaine-Smith et al. (2012) were applied to subject cells to FSS generated by a see-saw rocker. Well plates were rocked on a see-saw rocker (Stuart, UK) five times a week for 1 h following the protocol by Delaine-Smith et al. (2012). Intermittent stimulation is thought to have a greater effect since continuous stimulation may decrease cellular mechanosensitivity (Donahue et al., 2003b). Rocking was performed at two different frequencies: 0.75 Hz (45 cycles/min) and 1 Hz (60 cycles/min) generating a maximum shear stress of 0.041 Pa and 0.054 Pa respectively. The rocking frequency of 0.75 Hz was selected in line with the study by Delaine-Smith et al. (2012) where it enhanced mineralisation in MLO-A5. The

slightly higher rocking frequency of 1 Hz was added to test whether osteogenesis could be further enhanced.

In addition to see-saw rocking, FSS was also generated with an orbital shaker (IKA, Germany) as this method is able to generate even higher FSS on the bottom of a six-well plate. The orbital shaker was set to 200 rpm and each well was filled with 2 ml of culture medium which generated a maximum shear stress of 0.83 Pa. This condition was selected as it created maximum shear stress while still ensuring that the well bottom was covered by culture medium. Salek et al. (2012) showed in a computer model that higher rpm would expose parts of the well bottom affecting cell culture conditions.

Fluid flow in the six-well plates was applied outside a CO_2-controlled incubator at room temperature. Static controls were placed outside the incubator for the same duration as mechanically stimulated samples. Cell culture medium was changed every two days prior to mechanical stimulation.

5.4.3 Cellular assays

The following assays were performed to determine the effects of low FSS on MLO-A5 (Figure 5.2). All of these assays have been described in detail in Chapter 3.2.

- Qualitative assessment of cell morphology with phase-contrast microscopy.

- Quantification of DNA at Days 7, 14 and 21.

- Quantification of metabolic activity with PrestoBlue assay at Days 7, 14 and 21.

- Quantification of ALP activity at Days 7, 14 and 21.

- Quantification of extracellular PGE_2 on Day 21. Samples were collected 1 h after rocking in two out of three experiments.

- Qualitative and quantitative assessment of deposited collagen with Picrosirius Red (PSR) staining at Days 7, 14, and 21.

- Qualitative and quantitative assessment of deposited calcium with Alizarin Red S (ARS) staining at Days 7, 14, and 21.

- Visualisation of collagen deposition and organisation with SHG imaging at Day 21.

In addition, the release of intracellular calcium in response to unidirectional flow was assessed using ibidi flow chambers as described in Chapter 3.2.7. Responses to
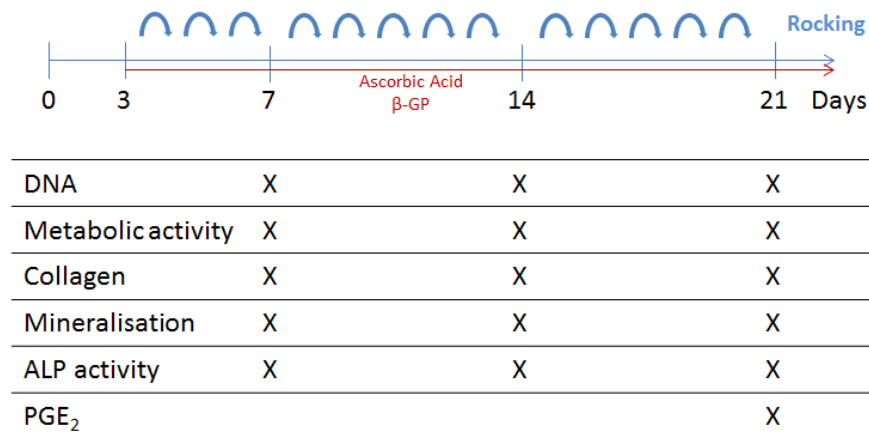
Figure 5.2: Experimental protocol investigating the response of MLO-A5 to low fluid shear stress.

MLO-A5 were cultured for 21 days. Culture medium was supplemented with β-GP and ascorbic acid from Day 3 of culture (red arrow). Mechanical stimulation was applied five times per week for 1 h either with a see-saw rocker or an orbital shaker (blue curved arrow). DNA, metabolic activity, collagen deposition, mineralisation and ALP activity were measured on Days 7, 14 and 21.

two different shear rates (0.3 Pa and 1.5 Pa) were compared with each other.

5.4.4 Statistics

Data are expressed as the mean $\pm$ standard deviation (SD) of three independent experiments unless otherwise stated. Statistical analysis was performed by two way analysis of variance (ANOVA), followed by Tukey's post hoc test. p values of ≤ 0.05 were considered to be significant and noted '*'; p values of ≤ 0.001 were noted as '**'.

5.5 Results

5.5.1 Optimisation of culture conditions

Mechanical stimulation was applied for 1 h per day outside a CO_2-controlled incubator which caused a pH reduction as indicated by the colour change of the culture medium. Although the addition of HEPES buffer provided extra buffering capacity and prevented a significant pH change, metabolic activity in MLO-A5 was significantly reduced ($p \leq 0.001$) in medium buffered with 25 mM HEPES both under static and dynamic conditions (Figure 5.3A). HEPES buffering further resulted in lower mineralisation and collagen deposition per well which was probably linked to the lower metabolic activity. Consequently, all other experiments in this chapter were performed without additional HEPES buffering.

Two different cell seeding densities were evaluated for the relatively fast-growing MLO-A5 cells. A low seeding density of 250 cells/well resulted in a patchy distribution of cells within the well. Even after 14 days of culture, no confluent monolayer covering the whole well surface was formed (Figure 5.3B). Instead, cells agglomerated which resulted in higher chances of apoptosis and cell layer detachment. In contrast, a higher seeding density of 10,000 cells/well enabled the formation of a confluent monolayer on the bottom of the well within five days. Culture medium had to be changed every two days since less frequent medium changes were found to contribute to apoptosis of these highly metabolically active cells.

5.5.2 Cell proliferation was not affected by fluid flow

Oscillating fluid flow generated with a see-saw rocker had no effect on MLO-A5 cell numbers and their metabolic activity (Figure 5.4). While there was a significant increase in DNA between each time point ($p \leq 0.001$), there was no difference in the amount of DNA between static and rocked conditions. Metabolic activity also increased over time. However, the increase was only significant between Day 7 and 14 ($p \leq 0.001$). Following the same increasing trend as DNA, metabolic activity did not differ between static and rocked samples.

5.5.3 Mechanical stimulation with see-saw rocker had no effect on osteogenesis

Collagen deposition and ALP activity, which are both osteoblastic markers, were not affected by mechanical stimulation at any of the analysed time points (Figure 5.5). Collagen deposition increased significantly between Day 7 and 14 ($p \leq 0.001$).
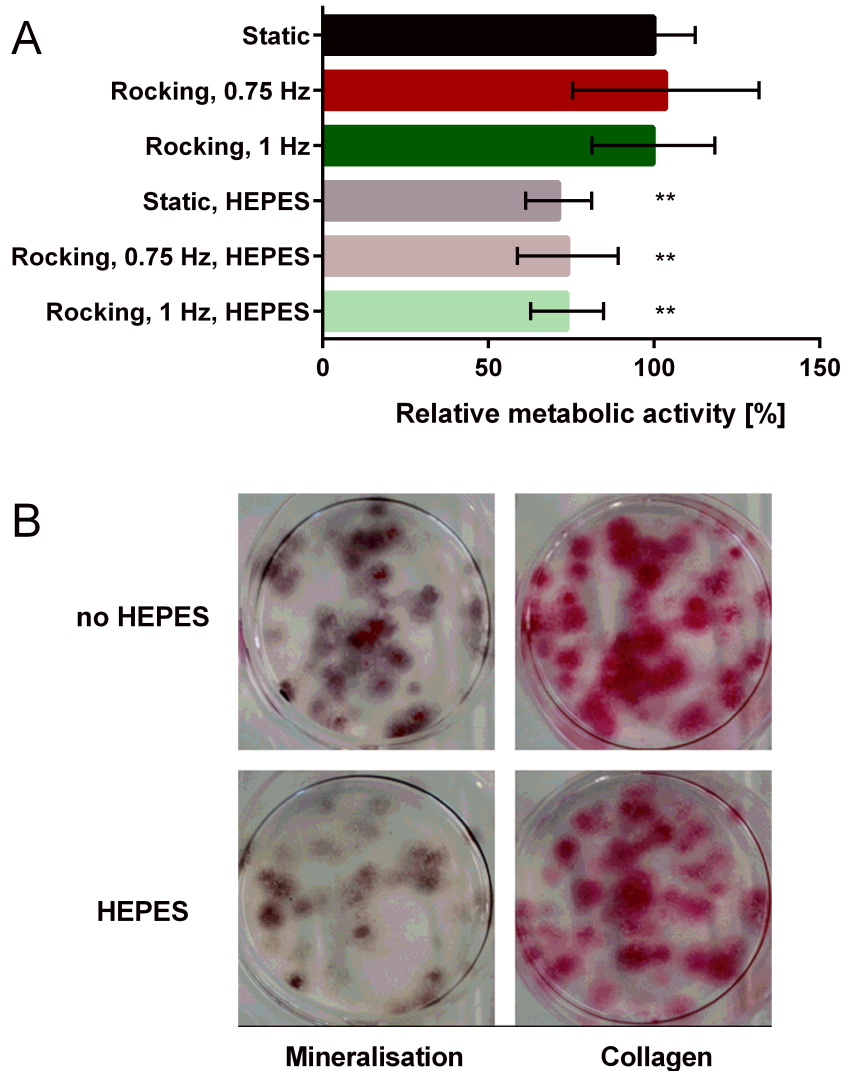
Figure 5.3: Effect of HEPES buffer and seeding density on MLO-A5.

A: Effect of HEPES buffer. HEPES buffer reduced metabolic activity of cells. Metabolic activity of cells on Day 7 and Day 14 were normalised to the corresponding metabolic activity of static samples cultured without HEPES. Cells cultured with 25 mM HEPES buffer had a significantly lower metabolic activity compared to static control without HEPES buffer. Significantly different to static control without HEPES buffer at ** $p \leq 0.001$. Mean with SD (n=6). B: Effect of seeding density. Mineralisation and collagen deposition at Day 14 were reduced in HEPES supplemented cultures as visualised with ARS and PSR staining of fixed cells. A seeding density of 250 cells/well resulted in a patchy cell distribution and failure to form a monolayer covering the whole well.
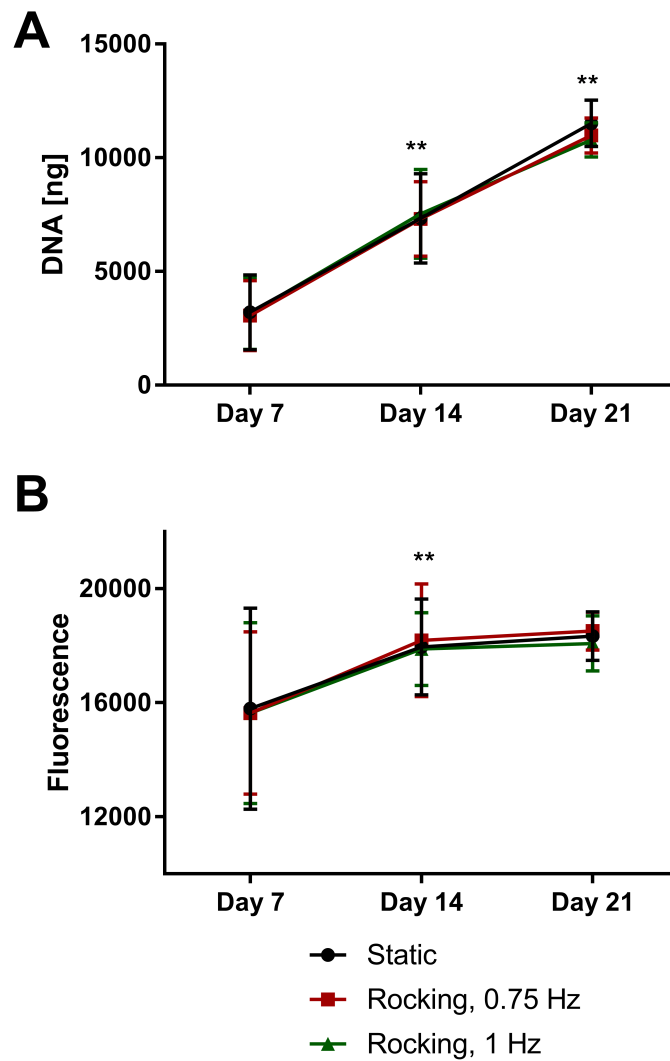
Figure 5.4: Total DNA amount and metabolic activity in MLO-A5 in response to rocking.

A: Total DNA increased significantly from Day 7 to Day 14 and from Day 14 to Day 21 in all the three conditions. B: Metabolic activity increased significantly from Day 7 to Day 14 in all three conditions. Significantly different compared to previous time point ** $p \leq 0.001$. Mean with SD (n=3).

At Day 14, wells were completely covered with collagen as demonstrated by PSR staining. The amount of collagen did not further increase after Day 14. ALP activity normalised to DNA remained constant between Day 7 and 21.

Mineralisation was negligible at Day 7 in all conditions, but increased greatly towards Day 14. At Day 21, wells were completely covered with calcium minerals in all conditions as visualised with ARS staining (Figure 5.6). The only significant difference between static and rocked cultures was measured at Day 14, when rocking at 0.75 Hz significantly increased mineralisation compared to static culture ($p \leq 0.05$). However, this increase was no longer significant at Day 21.

5.5.4 Mechanical stimulation with orbital shaker had no effect on osteogenesis

Similar to the results obtained with see-saw rocking, orbital shaking had also no effect on osteogenesis in MLO-A5 (Figure 5.7). The amount of DNA increased significantly between each time point in both conditions ($p \leq 0.001$). Following the same pattern as observed with rocking, collagen deposition increased significantly between Day 7 and 14 but did not further increase towards Day 21. ALP activity was consistently high at all time points with no difference between static culture and orbital shaking. Mineralisation increased over time, but orbital shaking had no effect on the amount of calcium minerals deposited.

5.5.5 Collagen fibre orientation was not guided by fluid flow

Collagen was visualised using SHG imaging (Figure 5.8) and fluorescence microscopy after fixed cells had been stained with PSR (Figure 5.9). Both methods showed that collagen was not evenly distributed throughout the wells. However, no consistent pattern emerged, e.g. there were no differences between the edges and the centre of the well or locations of high and low FSS. In addition, the direction of fluid flow did not influence cell orientation or orientation of deposited collagen fibres. Collagen fibres were deposited in 'honeycomb'-like structures which were orientated independent of flow or cell orientation (Figure 5.10 and 5.9).
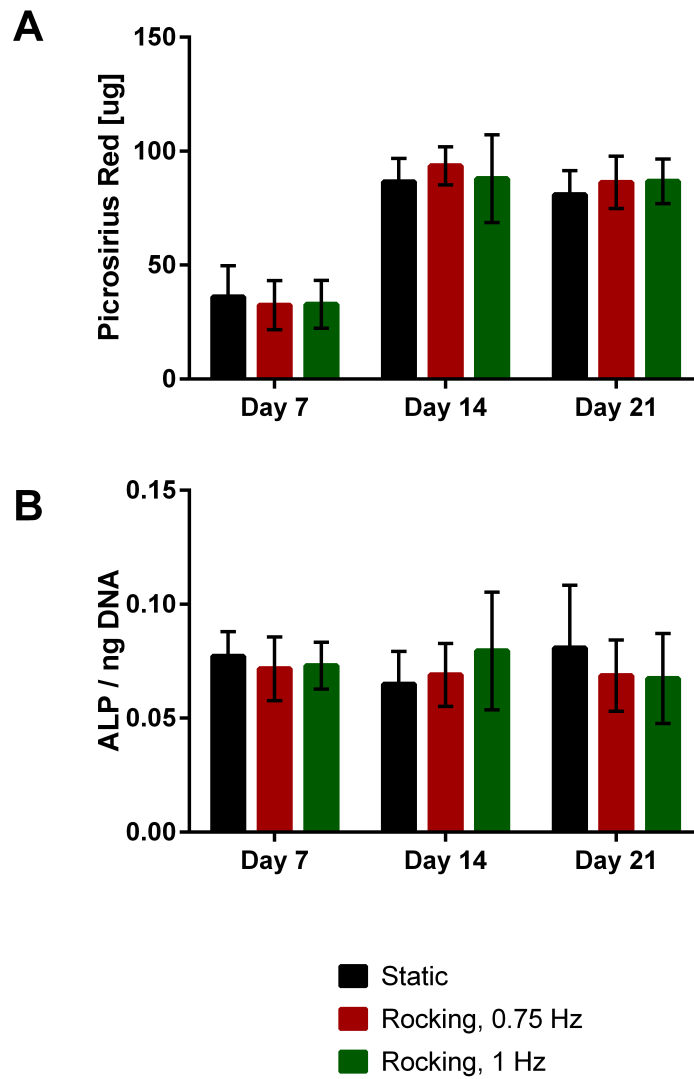
Figure 5.5: Collagen deposition and ALP activity in MLO-A5 in response to rocking.

A: Collagen deposition increased between Day 7 and Day 14. B: ALP activity normalised to DNA remained constant in all conditions. Mean with SD (n=3).
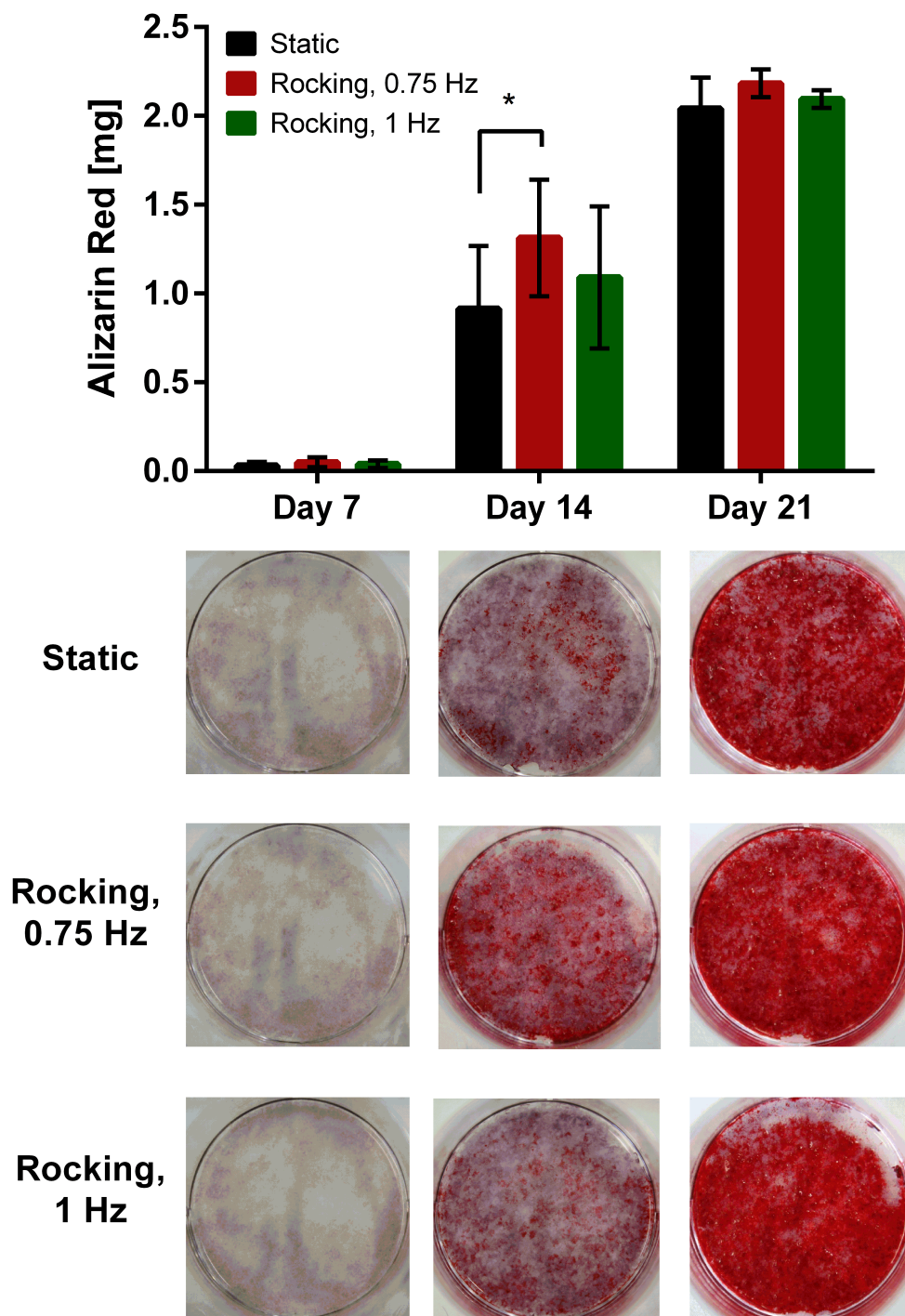
Figure 5.6: Mineralisation of MLO-A5 in response to rocking.

Quantification of mineralisation by ARS de-stain. Below are the corresponding images of fixed cells stained with ARS. Mineralisation increased over time. Low rocking frequency (0.75 Hz) significantly increased mineralisation compared to static culture at Day 14. All images are representative ones of three independent experiments. Significantly different to static control * $p \leq 0.05$. Mean with SD (n=3).
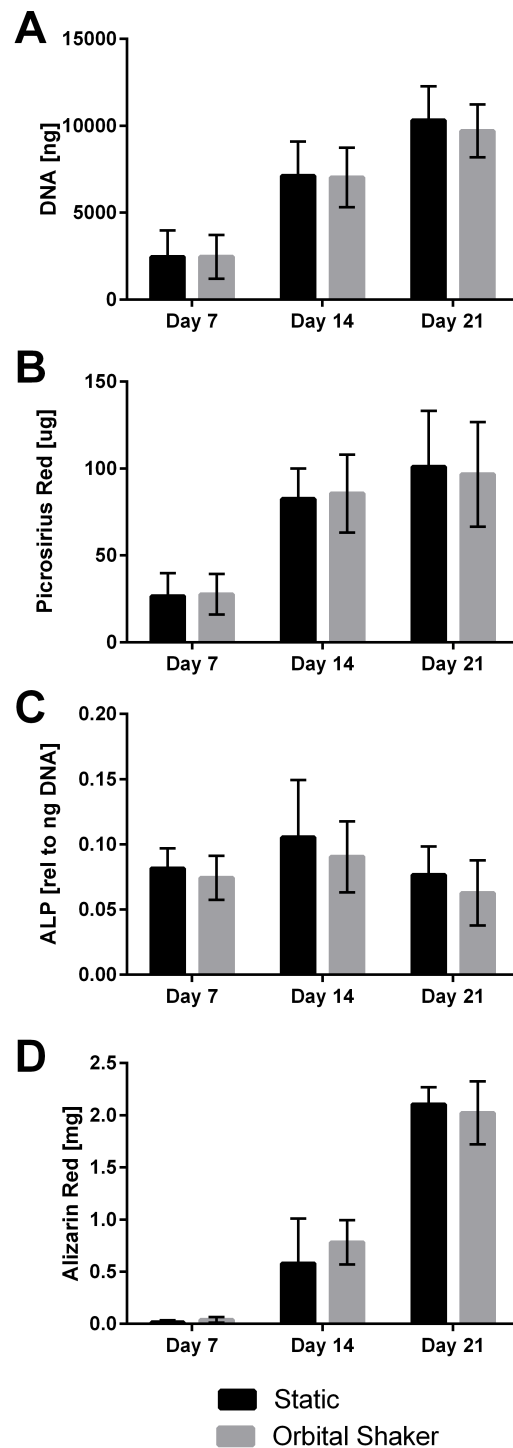
Figure 5.7: Effect of orbital shaking on MLO-A5 osteogenesis.

A: Amount of DNA increased over time. B: Collagen deposition increased between Day 7 and Day 14. C: ALP activity normalised to DNA remained constant. D: Mineralisation increased over time. No differences between static culture and intermittent orbital shaking were detected. Mean with SD (n=3).

Static

Orbital shaking, 200 rpm
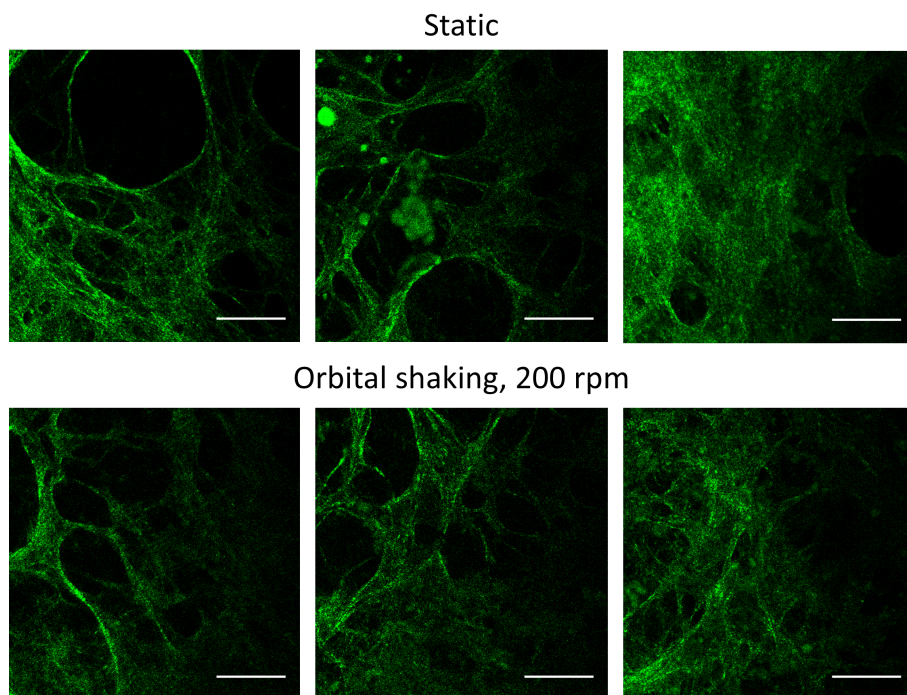
Figure 5.8: SHG images of collagen deposition.

SHG images of collagen fibres at Day 14 of static culture and dynamic culture with orbital shaking. No differences were detected in the amount and orientation of collagen fibres between static and dynamic culture. All images are representative ones from centre of the well of three independent experiments. Scale bar = 50 µm.

Picrosirius Red + DAPI   only Picrosirius Red
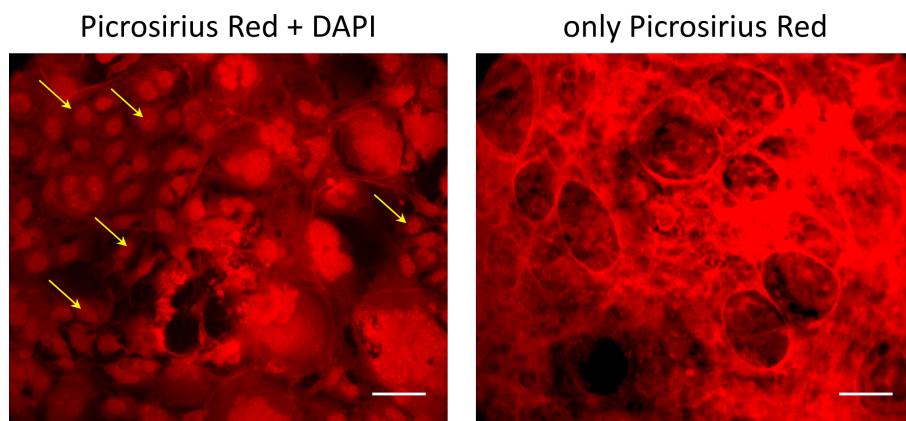
Figure 5.9: Fluorescence images of collagen deposition.

Fluorescence images of fixed cells stained with PSR and/or DAPI at Day 14. Combination of both stains allows exact localisation of cell nuclei (yellow arrows) relative to the collagen fibres. These images show that honeycomb structures were independent of the shape and orientation of underlying cells. Scale bar = 50 µm.
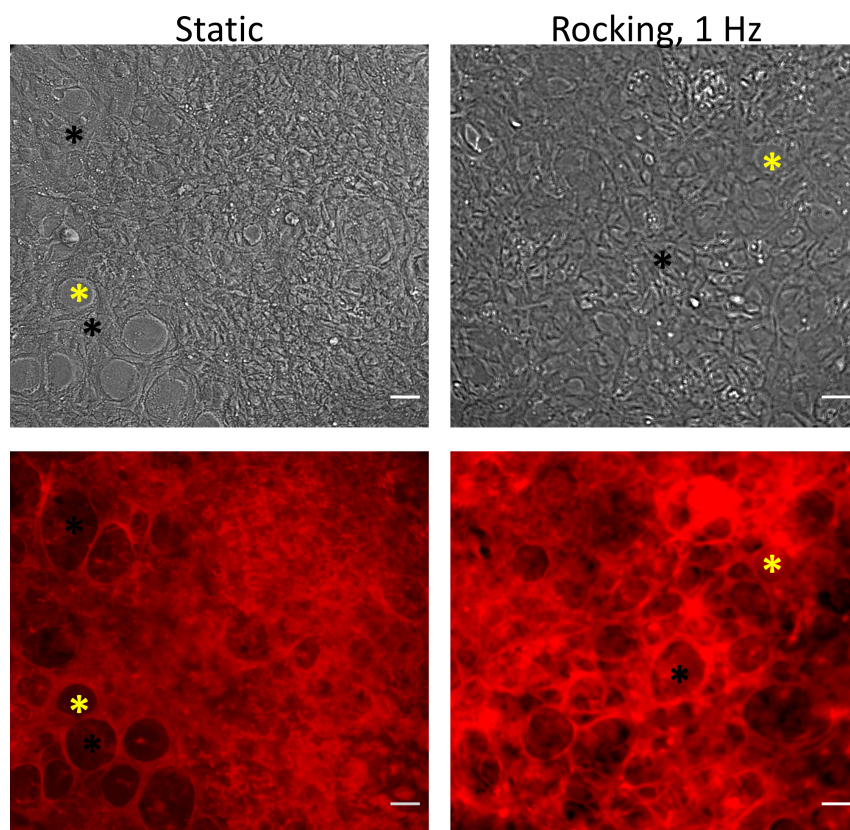
Figure 5.10: Honeycomb collagen networks produced by MLO-A5 after 14 days of culture.

Collagen orientation was the same in static (left) and mechanically stimulated culture (right). Top: Phase-contrast image. Bottom: Fluorescence image of fixed cells stained with PSR. Occasionally orientation of collagen fibres appeared to follow cell orientation (yellow asterisk). In most cases however, collagen orientation was independent of cell orientation (black asterisk). All images are representative ones from the centre of the well of three independent experiments. Images obtained from rocking at 1 Hz were similar to images from rocking at 0.75 Hz and orbital shaking. Scale bar = 50 μm.

5.5.6   Short-term effects of mechanical stimulation

Intracellular calcium (Ca^{2+}) and PGE_2 release by MLO-A5 were measured to assess the short-term responsiveness of these cells to FSS.

Calcium release was dependent on magnitude of fluid shear stress

MLO-A5 cells released more calcium in response to high FSS compared to low FSS (Figure 5.11). Cells responded strongly to high FSS of 1.5 Pa. The maximum response was detected 20 s after the onset of flow with 62% out of the total number of 37 cells increasing their fluorescence in response to flow. In detail, 32% of cells in the analysed image increased greatly in fluorescence, 30% increased moderately in fluorescence and the rest of cells did not change their fluorescence in response to fluid flow. Fluorescence signals decreased back to their initial low intensity after 80 s. The response of MLO-A5 to low FSS of 0.3 Pa was much weaker. The majority of cells (88% out of a total of 44 cells) did not increase their fluorescence at all. The remaining cells responded to fluid flow only 40 s after flow was initiated.

Minimal PGE_2 release in response to rocking

PGE_2 was measured in two experiments on Day 21. In one experiment, PGE_2 release could not be detected in any of the assessed conditions. In the other experiment, detectable levels of PGE_2 were released under mechanical stimulation but not under static culture (Table 5.1). Out of the three mechanical stimuli, low frequency rocking induced the highest PGE_2 release, followed by orbital shaking and high frequency rocking. However, small sample sizes did not allow statistical analysis of these findings.

Table 5.1: Concentration of PGE_2 in cell culture supernatants.

	Static	Rocking, 0.75 Hz	Rocking, 1 Hz	Orbital shaking
Sample 1	29.2	74.6	45.1	97.8
Sample 2	ND	72.6	62.1	68.6
Sample 3	ND	–	35.9	34.8
Average	ND	73.6	47.7	67.1

Samples were measured as three-fold dilution. All concentrations are in pg/ml and samples have been measured in duplicates. ND - not detectable: PGE_2 was below detection limit.
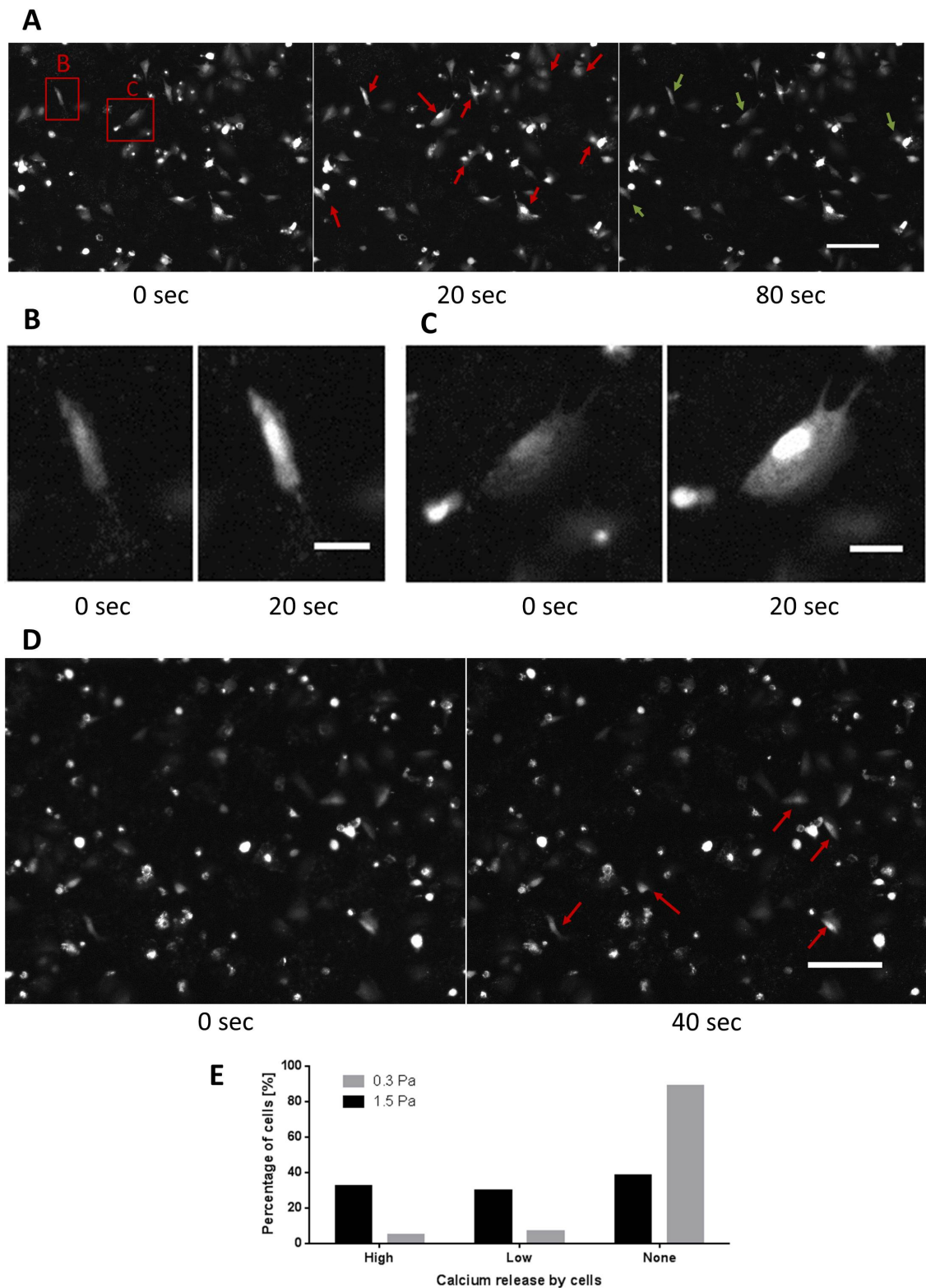
Figure 5.11: Calcium release by MLO-A5 in response to unidirectional fluid flow.

A: Cell responses to high FSS (1.5 Pa, n=37) at three different time points. B, C: Details of image A. D: Cell responses to low FSS (0.3 Pa, n=44) at two different time points. E: Percentage of cells responding to fluid flow in above images. Red arrows indicate increase and green arrows show decrease in fluorescence intensity of cells compared to previous time point. n = number of cells per condition. Scale bar = 10 μm.

5.6 Discussion

This chapter investigated the response of MLO-A5 cells to low FSS. Fluid flow was generated by placing well plates on a see-saw rocker or an orbital shaker. Both stimuli failed to enhance osteogenesis as assessed through quantifying collagen deposition and mineralisation over several weeks. These findings are in contrast to previous work done by Delaine-Smith et al. (2012), where MLO-A5 cells responded to see-saw rocking by increased collagen deposition and mineralisation at Day 21. A detailed analysis why both studies - even though they used similar methods - resulted in different outcomes, will be provided at the end of this chapter.

Prior to starting long-term experiments with MLO-A5, the effect of seeding density was assessed. MLO-A5 are fast growing cells with a doubling time of less than two days (data not shown). Experiments showed that, especially when confluent, MLO-A5 occasionally died for no apparent reason. It was thought that reducing the seeding density might allow more consistent cell culture results by avoiding apoptosis in these very metabolically active cells. However, reducing the seeding density to only 250 cells/well resulted in very patchy cell growth which prevented the formation of a monolayer all together. Since most osteoblast cultures require confluence to mineralise (Boskey and Roy, 2008), a higher seeding density of 10,000 cells per well was used. This density created a confluent monolayer approximately five days after seeding and the same density had also been applied successfully by Delaine-Smith et al. (2012) in their MLO-A5 study.

In contrast to the work done by Delaine-Smith et al. (2012), this study also included immediate responses to shear stress. Consistent with the finding that low FSS failed to increase mineralisation and collagen deposition, early responses to low FSS, i.e. release of intracellular calcium and PGE$_2$, were also minimal.

Although MLO-A5 responded to fluid flow by releasing Ca^{2+}, their response depended greatly on the magnitude of FSS. More cells responded to FSS of 1.5 Pa than 0.3 Pa. This finding is consistent with the literature (Allen et al., 2000; Jacobs et al., 1998; Hung et al., 1995; Huo et al., 2010). For example, Donahue et al. (2001) demonstrated that a higher proportion of rat primary osteoblast cells responded to 2 Pa shear stress than 1 Pa. In addition, a delayed calcium response was observed under low shear stress which is also in line with previous research (Kou et al., 2011). While cells under high shear responded 20 s after flow initiation, cells exposed to 0.3 Pa required 40 s or longer to release Ca^{2+}. Although all presented calcium signalling results are in line with previous literature, the experiment should be repeated several times more to draw statistically significant conclusions.

FSS generated through rocking may have been below most of the cells' activation threshold for calcium signalling, since only five out of 44 cells (11.4%) responded to low FSS of 0.3 Pa generated in the ibidi slides. Although some studies describe very low thresholds for primary rat osteoblasts between 0.03 Pa and 0.3 Pa (Kou et al., 2011), it is also known that thresholds vary between cell types and sources (Donahue et al., 2001). Medium conditions, in particular serum concentration, are also thought to play a role. For example, Allen et al. (2000) reported a relatively high threshold of more than 0.4 Pa in serum-free medium using rat primary cells. Pre-treating the same cells with low-serum concentrations (2%) increased their responsiveness dramatically and reduced the activation threshold to below 0.02 Pa. However, higher serum concentrations of 10%, which match the serum concentration used in this study, were shown to decrease cell response to FSS.

It was not possible to observe calcium signalling directly within the well plates, since Ca^{2+} release is one of the earliest responses to mechanical stimulation and happens within seconds of stimulation (Hung et al., 1995). Consequently, cell responses had to be monitored continuously before and during stimulation on a microscope stage using commercially available parallel-plate flow chambers. Results generated with the ibidi slides could only give an indication on how cells in the well plates responded to FSS due to the differences in flow magnitudes and flow patterns between the two culture systems. Even though the tested low shear condition of 0.3 Pa in the ibidi channel was similar to the average shear stress generated on the orbital shaker (0.78 Pa), it was roughly a magnitude higher compared to the peak shear stress generated with the see-saw rocker (0.05 Pa). In addition, flow in the ibidi channels was uniform and steady whereas rocking generated oscillating flow. Since oscillating flow has been reported to be an even less potent stimulator of bone cells than steady flow (Jacobs et al., 1998), calcium signalling might be even further reduced when cells were cultured in 6-well plates on rocking platforms. Therefore, the lack of calcium signalling might explain why osteogenesis was not enhanced when cells were cultured under oscillating flow conditions on the see-saw rocker and orbital shaker.

Intracellular calcium acts as a second messenger and plays a role in a number of metabolic pathways in bone formation, for example through the activation of first messengers such as PGE_2 (Jacobs et al., 1998). Low calcium signalling might explain the low levels of PGE_2 which were detected in the cell culture medium. PGE_2 measurements were taken in two out of three experiments at Day 21 of culture 1 h after rocking. However, PGE_2 could only be detected in one of the two experiments. In the first experiment, PGE_2 ranged from 87 pg/ml in the static controls to 220 pg/ml under low frequency rocking. Such low levels of PGE_2 were below

previously reported values of released PGE_2 (Klein-Nulend et al., 1997). Successful detection and measurement of PGE_2 in one experiment indicated that mechanical stimulation might have increased the concentration of PGE_2 compared to static controls, which is in agreement with previous findings (Reich et al., 1990; Klein-Nulend et al., 1997). However, the low number of samples prevented a statistical analysis of these results. No PGE_2 was detected in the second experiment. This is surprising, since the release of PGE_2 upon mechanical stimulation has been widely reported in osteoblasts. It should be noted however that most other studies apply higher shear rates or flow over longer time. For example, Reich et al. (1990) reported the release of PGE_2 under unidirectional flow with a shear stress of 0.6 Pa. Pulsatile flow has also been shown to induce release of prostaglandins, which can be detected as early as 15 min after flow has been initiated (Klein-Nulend et al., 1997; Bakker et al., 2001). In addition, Liegibel et al. (2004) also reported increased release of PGE_2 under low shear stress in the micro-pascal range, but in that case osteoblasts were subjected to flow for more than 6 h.

There are several possibilities why no PGE_2 was detected in any of the experiments. First, consistent with the previously described low release of Ca^{2+}, mechanical stimulation was too low to induce a significant release of PGE_2. Alternatively, experimental problems might have also contributed towards not detecting PGE_2. For example, all samples were diluted three-fold prior to analysis following the manufacturer's protocol. However, it might have been better not to dilute the samples, because of the low initial concentration of PGE_2 and relative large ratio between volume of culture medium to cells. In addition, cell culture medium was changed directly after rocking and samples were collected 1 h following incubation without mechanical stimulation. Potentially, more significant results could have been achieved if the fresh medium had been added prior to rocking and these samples had been collected afterwards.

Collagen deposition and mineralisation are essential markers for assessing osteogenesis. Considering these markers, the results of this work demonstrate that the application of intermittent, low FSS was not able to enhance osteogenesis in MLO-A5. At the same time, MLO-A5 followed the expected behaviour of mature osteoblasts regarding cell proliferation, collagen deposition and mineralisation during the 21 days of culture (Barragan-Adjemian et al., 2006; Kato et al., 2001). For example, collagen deposition was observed prior to mineralisation which is consistent with previous findings. It is known that a collagen type I network is required for bio-mineralisation acting as a scaffold for calcification (Golub, 2009). At Day 7, all samples demonstrated strong and evenly distributed staining with PSR which binds to collagen fibres. The amount of collagen further increased from Day 7 to Day

14, but no more collagen was deposited afterwards. In line with previous research by Barragan-Adjemian et al. (2006), SHG imaging and fluorescence microscopy of MLO-A5 stained with PSR showed a 'honeycomb' collagen pattern. The honeycomb structure in MLO-A5 is different to mineralisation patterns found in primary osteoblasts and other osteoblast cell lines which mineralise in nodules (Dallas et al., 2000; Ghosh-Choudhury et al., 1996). It should be highlighted that SHG only shows extracellular collagen fibres. In contrast, it has been found that PSR to some extent also stains intra-cellular pro-collagen molecules, hence distinguishing between intra- and extra-cellular collagen is more difficult with this method. Another advantage of SHG imaging is that it can also be performed on live cells.

Mechanical stimulation influenced neither the amount of collagen deposited nor the orientation of collagen fibres. The latter is in line with findings by Delaine-Smith et al. (2012). In addition, no difference in terms of collagen organisation or fibre lengths could be observed when comparing static and mechanically stimulated samples. Interestingly, Delaine-Smith et al. (2012) were able to observe such changes when using human mesenchymal stem cells (hMSC). However, mesenchymal stem cells are located in the bone marrow where fluid flow is thought to be lower (Gurkan and Akkus, 2008). Therefore, hMSC might be more sensitive to low shear stress compared to mature osteoblasts such as MLO-A5.

Following the deposition of a collagen network, matrix mineralisation was initiated. Although collagen deposition was already visible at Day 7, mineral deposition at that time was still negligible. In the following two weeks however, mineralisation increased greatly indicating a mature osteoblast cell type. The mature osteogenic phenotype of MLO-A5 was further confirmed by the consistently high ALP activity per cell throughout the whole culture period. ALP activity is commonly used as an early marker of osteogenic differentiation (Golub and Boesze-Battaglia, 2007). Interestingly, Delaine-Smith et al. (2012) were not able to show increased ALP activity in their rocked samples, even though they reported enhanced collagen deposition and mineralisation at Day 21 under fluid stimulation. This suggests that ALP activity and mineral deposition are not necessarily that closely linked with each other.

Mineralisation at Day 14 was higher under low frequency rocking compared to static culture ($p \leq 0.05$). Yet, mineralisation was not significantly increased at Day 14 in the other two mechanically stimulated groups, i.e. high frequency rocking and orbital shaking. Furthermore, low frequency rocking failed to continuously enhance mineralisation until Day 21. In combination with the relatively high standard deviations at Day 14, it is difficult to assess the actual effect of low frequency rocking on MLO-A5 mineralisation. In addition, it can be argued that long-term effects of rock-

ing, i.e. observations at Day 21, are more relevant than intermediate observations for applications such as tissue engineering.

Cell numbers kept increasing in all conditions throughout the whole culture period as demonstrated in the constant rise of total DNA. Metabolic activity plateaued at Day 21, which can be explained by the assay reaching its saturation point, with too many cells per well. Future experiments should make sure that the assay can deal with such high cell numbers by reducing the incubation time or increasing the amount of reagent. Nevertheless, both assays showed that mechanical stimulation did not affect cell numbers, which is in line with results obtained by Delaine-Smith et al. (2012).

In contrast to the study by Delaine-Smith et al. (2012), mechanical stimulation failed to enhance osteogenesis in MLO-A5. This was demonstrated both in see-saw rocking and orbital shaking. All experiments were performed in triplicate and similar cell behaviour was observed in each individual experiment making the observations very convincing. The question remains, what caused the differences between the present study and the study by Delaine-Smith et al. (2012), which have been both performed in the same laboratory only five years apart.

A potential explanation might be a change of phenotype in MLO-A5 making them less sensitive to FSS. Such a phenotype change can be caused by several factors. First, a higher passage number might change cell behaviour (American Type Culture Collaction, 2010). However, Delaine-Smith et al. (2012) used cells between passages 25 to 30, which were the same passage number as used in this study. Since the doubling rate and metabolic activity of MLO-A5 used in this study appeared to be higher than previously observed (Kato et al., 2001) and cells occasionally died between experiments, it was decided to try another batch of MLO-A5 cells from a research group at Keele University. This group reported normal cell behaviour even though their cells already reached a passage number of 55. Experiments were undertaken with both cell batches, but cells exhibited very similar behaviour both in terms of metabolic activity and unresponsiveness to fluid stimulation.

A change in cell phenotype might have also been caused by the choice of serum added to the culture medium. Cells have been shown to be very sensitive to the kind of serum and its concentration in culture medium (Allen et al., 2000). The present work used the same batch of heat-inactivated FBS in all experiments and cell culture medium was always supplemented with 10% of FBS. Delaine-Smith et al. (2012) also worked with 10% FBS. In contrast, the original research paper which introduced the cell line MLO-A5 was actually using a combination of 5% FBS and 5% calf serum (CS) for cell culture (Kato et al., 2001). They reported that

this mixture allowed proliferation but not de-differentiation of cells, in particular mixing FBS and CS prevented the loss of dendritic processes. Hence, the lack of responsiveness to fluid stimulation may have been caused by incorrect culture of cells only with FBS resulting in a change of phenotype. The only way to solve this question, would have been to obtain a new batch of the original cell line. However, due to time constraints this was not possible during this work. If results would be different with the original cell line, polymerase chain reaction (PCR) could give interesting hints to how cells changed over time and which genetic changes made them less responsive to fluid flow.

Besides the possibility of an altered cell phenotype, the rocking platform itself might have also influenced the results. For example, this study used a different rocker model compared to the rocking platform applied by Delaine-Smith et al. (2012). One of the main difference being that the rocking angle was not adjustable, therefore the angle was slightly higher than the maximum angle which would have ensured coverage of the whole well with fluid at all time. However, visual observation showed that a thin layer of fluid always covered the cells and all cells - even around the potentially exposed edges - remained alive throughout the whole experiment. Hence, even though the slightly higher rocking angle might have increased the FSS by a couple of millipascal it most likely did not influence cell behaviour as a whole. In addition, Delaine-Smith (2013) showed enhanced osteogenesis even for lower rocking speeds (30 cycles/min) and longer rocking times (2 h). This indicated that small variations in shear stress, for example caused by a slightly different rocking angle, should not explain the consistent unresponsiveness of cells in this study. Most importantly, MLO-A5 did also not respond to FSS on the orbital shaker, even though estimated shear stresses were considerably higher than on the see-saw rocker.

In addition to the rocking platform, temperature, humidity and carbon dioxide levels are other critical parameters affecting cell behaviour. Carbonate-buffered cell culture medium and incubators with elevated CO_2 levels normally ensure a stable cell culture environment. However, in line with the study by Delaine-Smith (2013), mechanical stimulation for up to 1 h per day was performed outside the cell culture incubator in normal room air. Rocking within the incubator was further prevented as both sea-saw rocker and orbital shaker were not designed to be placed inside an incubator with high humidity. Visual analysis of cell morphology and cell growth confirmed that cell culture outside the incubator for a maximum of 1 h had no obvious negative effect on MLO-A5 behaviour.

Although in contrast to the work published by Delaine-Smith et al. (2012), the unresponsiveness of mature osteoblasts to low FSS is not completely surprising.

Primarily because it has not been established yet whether a FSS threshold exists above which mature osteoblasts enhance collagen deposition and mineralisation. Even though it is assumed that FSS surrounding osteoblasts is considerably lower compared to shear stress sensed by osteocytes within the lacunar-canalicular system (McGarry et al., 2005; Bonewald and Johnson, 2008), there is the possibility that both platforms were not able to create high enough or not the right type of FSS for MLO-A5 cells to respond. In conclusion, more research on the behaviour of bone cells under the influence of low FSS is required. In particular, more detailed studies of genetic changes and how FSS impacts the transformation from osteoblasts to osteocytes might yield interesting insights into bone cell biology.

5.7 Summary

- Seeding cells at a high density of 10,000 cells/well and without HEPES buffer allowed long-term culture of MLO-A5 in 6-well plates even when placed for 1 h per day outside an incubator.

- Ca^{2+} release in response to fluid flow was dependent on the magnitude of FSS. Ca^{2+} and PGE_2 signalling was reduced under low FSS.

- Low FSS failed to enhance osteogenesis. There was no difference in ALP activity, mineralisation and collagen deposition between static and mechanically stimulated groups, which is in contrast to previously published results by Delaine-Smith et al. (2012).

- Although the generated FSS magnitudes differed considerably between see-saw rocker (0.05 Pa) and orbital shaker (0.78 Pa), both platforms resulted in similar cell behaviour and did not enhance osteogenesis in MLO-A5.

Chapter 6

Impact of low fluid shear stress on IDG-SW3 osteoblasts

6.1 Introduction

This chapter aims to explore whether bone matrix deposition and osteoblast-to-osteocyte transformation (= osteocytogenesis) can be enhanced by mechanical stimulation in the cell line IDG-SW3. Results in Chapter 4 have already demonstrated that IDG-SW3 are sensitive to biochemical stimulation. For example, the concentration of β-GP regulated mineralisation and differentiation towards an osteocyte-like cell type in IDG-SW3. However, in particular for tissue engineering applications it would be beneficial to be able to induce osteogenesis also without biochemical treatment to prevent any unwanted side effects caused by the chemicals.

Fluid shear stress (FSS) has been shown to stimulate osteoblasts to release osteogenesis-related signalling molecules such as calcium and prostaglandins (Reich et al., 1990; Genetos et al., 2004). Although the mechanisms which link the release of these molecules and long-term osteogenesis are not fully understood yet, some studies have also shown that FSS directly affects osteogenesis in bone cell monolayers (Mai et al., 2013b; Scaglione et al., 2008; Kreke and Goldstein, 2004). The outcome of these experiments, however, depended on many factors including the cell type, the magnitude and type of flow and the duration of flow (for a more detailed review see Chapter 3.2). For example, Delaine-Smith et al. (2012) showed that FSS enhanced mineral deposition in the osteoblast cell line MLO-A5, while results in Chapter 5 showed no impact of low FSS on osteogenesis in MLO-A5. Contrasting results such as these suggest that more data is required to determine the impact FSS has on both early responses but also on long-term osteogenesis and osteocytogenesis.

IDG-SW3 were selected as cell model in this chapter since they not only deposit collagen and mineral but they also differentiate over time from an osteoblast to a mature osteocyte population. Moreover, the transition process can also be easily observed by fluorescence microscopy as only osteocyte-like cells express the fluorescent Dmp1 promoter. Therefore, IDG-SW3 are a more advanced model than MLO-A5 to study osteogenesis and the transition from osteoblasts to osteocytes in vitro (Woo et al., 2011). In addition, IDG-SW3 might be more sensitive to low FSS than the osteoblast cell line MLO-A5 because osteocytes are thought to be more mechanosensitive than osteoblasts and have the ability to regulate bone formation through paracrine signalling with osteoblasts (Bonewald and Johnson, 2008).

To the author's knowledge, this study is the first one which investigates the impact of low, oscillating fluid flow on IDG-SW3 monolayer cultures. The experimental set-up involved a see-saw rocker platform which had been previously used by Delaine-Smith et al. (2012) and in Chapter 5. Knowledge gained from this study could help to better understand bone cell biology and the osteoblast-osteocyte-transition in particular.

6.2 Hypothesis

Low FSS generated with a see-saw rocker enhances deposition of mineralised matrix and osteocytogenesis in the cell line IDG-SW3 in comparison to static culture.

6.3 Aims

This chapter aims to assess early and late responses to FSS in the osteoblast/osteocyte cell line IDG-SW3 (Figure 6.1). In particular the following aims are addressed:

- To optimise cell culture conditions for mechanical stimulation in 6-well plates over several weeks and for up to 5 h per day outside a CO_2-controlled incubator.

- To investigate whether IDG-SW3 respond immediately to low FSS by releasing Ca^{2+}, nitric oxide (NO) and PGE_2.

- To investigate the effect of low FSS on osteogenesis, in particular changes in cell number, ALP activity, mineralisation and collagen deposition.

- To investigate the effect of low FSS on osteocytogenesis, in particular through the expression of the osteocyte marker Dmp1-GFP.

- To determine whether mineralisation and osteocytogenesis are linked.
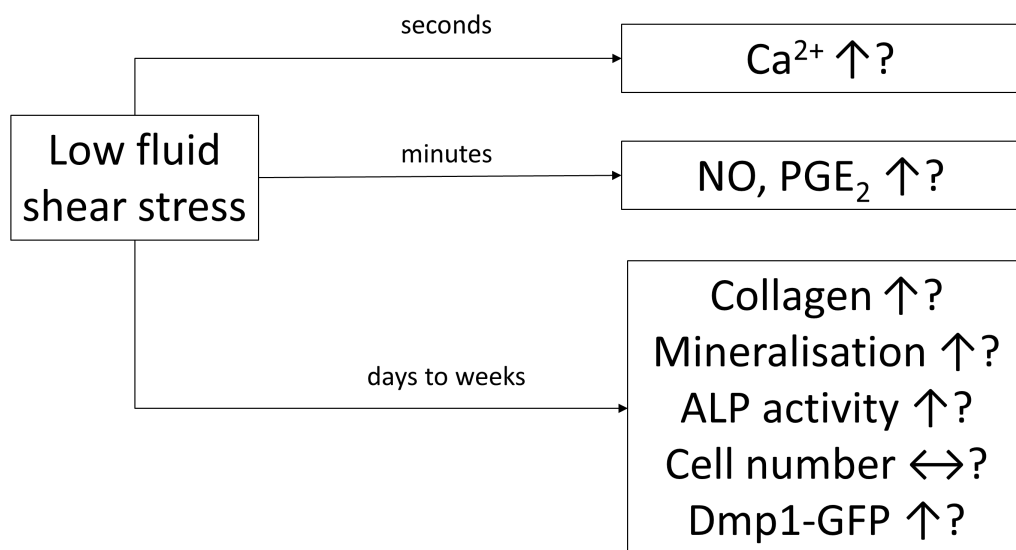
Figure 6.1: Aims of Chapter 6.

6.4 Methods

6.4.1 Cell culture

IDG-SW3 between passages 20 and 35 were used in this chapter. Cells were seeded sub-confluent at a density of 100,000 cells/well on 0.1% gelatin-coated 6-well plates. Alternatively, well plates were not coated or coated with 0.15 mg/ml collagen I rat-tail solution (Thermo Fisher Scientific, UK) dissolved in 20 mM acetic acid to determine the best coating conditions. This seeding density was chosen to allow cells to become confluent within three days which is a requirement for osteogenesis in IDG-SW3 (Woo et al., 2011). For the first three days until cells reached 100% confluence, cells were cultured at 33 °C in culture medium supplemented with 50 units/ml recombinant mouse interferon-gamma (INF-γ) (John et al., 2014). The day cells reached confluence was declared as Day 0. Temperature in the incubator was increased to 37 °C and culture medium was supplemented with 25 mM HEPES buffer, 50 µg/ml ascorbic acid, 5 mM β-GP but without INF-γ (Table 3.1). Culture medium was changed every two to three days. Each well contained 2 ml of cell culture medium.

To compare IDG-SW3's ALP activity to an established osteocyte cell line, MLO-Y4 cells were seeded at a density of 1,000 cells/well in collagen-coated 6-well plates and cultured for eleven days. ALP activity was assessed at Day 11 following the same protocol used for ALP measurement in IDG-SW3.

6.4.2 Fluid shear experiments

The experimental settings for generating FSS with a see-saw rocker were based on the previous chapter and a study by Delaine-Smith et al. (2012), in which mineralisation in MLO-A5 cells was enhanced by see-saw rocking five times a week for 1 h. In this chapter, IDG-SW3 cells were subjected to FSS on five days a week using two different rocking frequencies on a see-saw rocker (Stuart, UK) with a maximum rocking angle of approximately 7°. In line with the previous chapter, rocking was performed at a high frequency of 1 Hz (60 cycles/min) for 1 h per day, which generated a maximum shear stress of 0.054 Pa on the bottom of the well. The lower rocking frequency of 0.7 Hz (42 cycles/min) generated a maximum shear stress of 0.038 Pa and was similar to the frequency used by Delaine-Smith et al. (2012). Rocking was performed for either 1 h or 5 h per day. Flow stimulation for 5 h previously facilitated cell alignment (Prodanov et al., 2013), hence the extended stimulation period of 5 h was added in this chapter to investigate whether see-saw rocking could also initiate cell and possibly collagen alignment in IDG-SW3. Since the rocker could not be placed

inside a humidified and CO_2-controlled incubator, fluid flow was applied outside the incubator. To compensate for cells being outside a temperature- and CO_2-controlled incubator for up to 5 h, well plates were placed in temperature-controlled egg incubators (King Suro Max-20, Rcom, USA) during rocking. Static controls were also placed in an egg incubator for 1 h per day. Moreover, HEPES buffer was added to the culture medium to prevent pH changes when outside the incubator. Cell culture medium was changed every two to three days prior to rocking.

To exclude that cell culture outside a CO_2-controlled incubator had a negative impact on cell behaviour, the final experiment was performed on a different rocker model (MIX4230, IKA, Germany) which could be placed inside the incubator but was only available at the end of the study. The maximum rocking angle on that rocker was set to 5° as this ensured that the bottom of the well was constantly covered by culture medium. To compensate for the lower rocking angle, FSS was generated with a higher rocking frequency of 1.3 Hz (80 cycles/min) for 1 h per day at five days per week over 21 days. A maximum shear stress of approximately 0.052 Pa was generated, which was comparable to the shear stress described in the rocking regime above, i.e. rocking frequency of 1 Hz at a rocking angle of 7° (0.054 Pa).

6.4.3 Cellular assays

The following assays were performed to determine the effects of low FSS on IDG-SW3 (Figure 6.2). All of these assays have been described in detail in Chapter 3.2.

- Qualitative assessment of cell morphology with phase-contrast and fluorescence microscopy.

- Quantification of GFP expression with microplate reader at Days 0, 7, 14, 21 and 28.

- Quantification of DNA at Days 0, 7, 14, 21 and 28.

- Quantification of metabolic activity with PrestoBlue assay at Days 0, 7, 14, 21 and 28.

- Quantification of ALP activity at Days 0, 14, 21 and 28.

- Quantification of extracellular PGE_2 on Day 21. Samples were collected 1 h after rocking in two out of three experiments.

- Quantification of nitric oxide (NO) on Day 1 and Day 21. Samples were collected during rocking in one out of three experiments.

- Qualitative and quantitative assessment of deposited collagen with Picrosirius Red (PSR) staining at Days 14, 21 and 28.

- Qualitative and quantitative assessment of deposited calcium with Alizarin Red S (ARS) staining at Days 7, 14, 21 and 28.

- Visualisation of collagen deposition and organisation with SHG imaging at Day 21.

In addition, the release of intracellular calcium in response to unidirectional and oscillating flow was assessed using ibidi flow chambers as described in Chapter 3.2.7. Responses to two different shear rates ($0.3\,\mathrm{Pa}$ and $1.5\,\mathrm{Pa}$) were compared with each other.

6.4.4 Statistics

Data are expressed as the mean $\pm$ standard deviation (SD) of three independent experiments unless otherwise stated. Statistical analysis was performed by two way analysis of variance (ANOVA), followed by Tukey's post hoc test. p values of ≤ 0.05 were considered to be significant and noted '*'; p values of ≤ 0.001 were noted as '**'.

	0	7	14	21	28
GFP expression	X	X	X	X	X
DNA	X	X	X	X	X
Metabolic activity	X	X	X	X	X
Collagen			X	X	X
Mineralisation		X	X	X	X
ALP activity	X	X	X	X	X
PGE$_2$, NO				X	
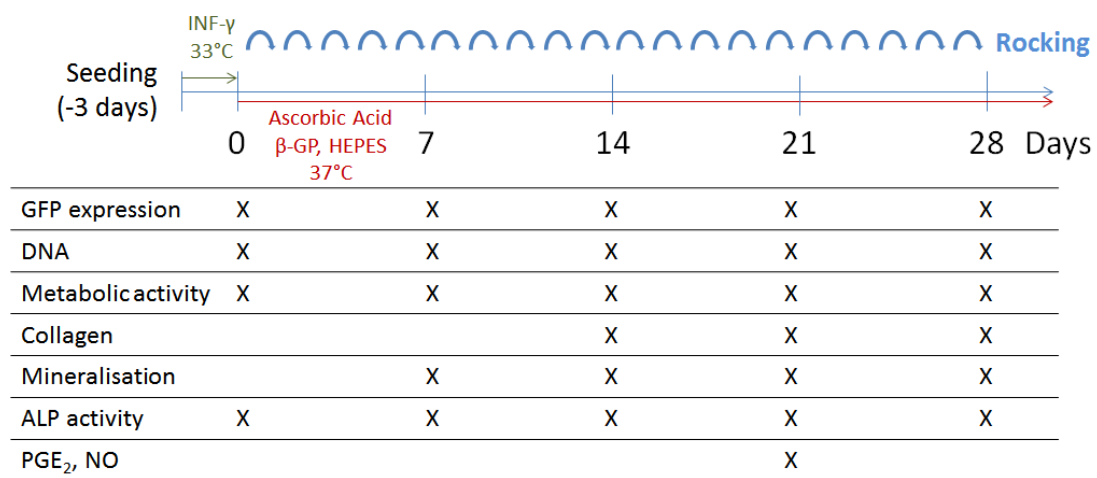
Figure 6.2: Experimental protocol for investigating the response of IDG-SW3 to low fluid shear stress.

IDG-SW3 were seeded at 100,000 cells/well in 6-well plates and grown until they reached confluence, i.e. for approximately three days. Cells were grown for a further 28 days in culture medium supplemented with β-GP, ascorbic acid and HEPES buffer (red arrow). FSS was generated by a see-saw rocker and applied five times per week for 1 h or 5 h (blue curved arrows). The time points of the assays are marked in the table below.

6.5   Results

6.5.1   Gelatin coating was required for cell attachment

Coating of culture wells with gelatin or collagen solution was required to ensure cell attachment during the whole culture period. Cell growth was reduced and more patchy in uncoated wells. The type of coating, i.e. whether wells were coated with gelatin or collagen solution, did not influence cell morphology or growth behaviour (Figure 6.3A). When wells were not coated with gelatin or collagen solution, cell layers easily detached and peeled off during culture or when performing assays such as staining for collagen with PSR. This effect was enhanced in rocked conditions (Figure 6.3B).

Supplementing culture medium with HEPES buffer supported IDG-SW3 in maintaining their cell function even when they were placed outside a CO_2-controlled incubator for 1 h or more per day. The lower CO_2 concentration outside the incubator had no significant adverse effect on proliferation or Dmp1-GFP expression (Figure 6.3C and D).

6.5.2   No effect of low fluid shear stress on DNA and metabolic activity

No significant differences between static and mechanically stimulated samples were detected at any time point considering both DNA and metabolic activity (Figure 6.4).

The amount of DNA significantly increased from Day 0 to Day 21 of culture ($p \leq 0.001$). Towards the end of culture, cell numbers slightly decreased from Day 21 to Day 28 ($p \leq 0.01$). Approximate cell numbers could be derived from the detected DNA. For example, in the static control group the following cell numbers were estimated from a standard curve: 0.1×10^6 cells at Day 0, 1.0×10^6 cells at Day 7, 1.5×10^6 cells at Day 14, 2.4×10^6 cells at Day 21 and 1.9×10^6 cells at Day 28.

Metabolic activity of cells was significantly higher on Day 0 compared to Day 7 ($p \leq 0.01$). From Day 7, metabolic activity increased in line with the increase in DNA until Day 21 and remained constant between Day 21 and Day 28.

6.5.3   Fluid flow did not enhance osteogenesis

IDG-SW3 did not enhance osteogenesis or osteocytogenesis in response to low FSS which was generated by a see-saw rocker using two different rocking frequencies (0.7 Hz and 1 Hz) for either 1 h or 5 h.
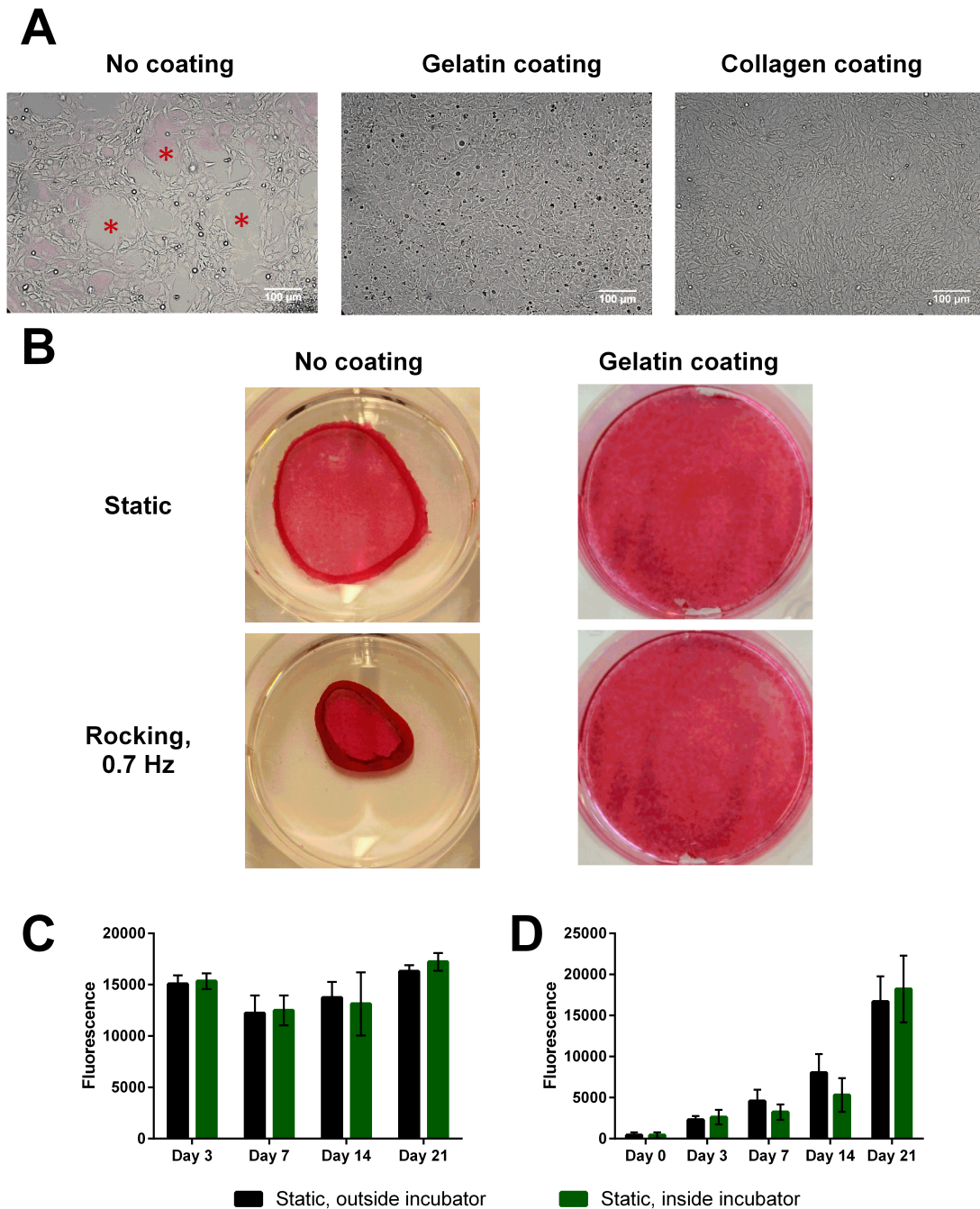
Figure 6.3: Optimisation of IDG-SW3 culture conditions.

A: Cell distribution at Day 2 of culture with no coating (left), gelatin coating (middle) and collagen coating (right). Red asterisks mark empty spots in uncoated wells. B: PSR stain at Day 7. Cell layers started to detach in wells without any coating. This effect was further enhanced in mechanically stimulated samples. Comparison of metabolic activity (C) and Dmp1-GFP expression (D) of cells cultured inside and outside a CO_2-controlled incubator for 1 h per day. Mean with SD (n=3 and n=2 at Day 21).
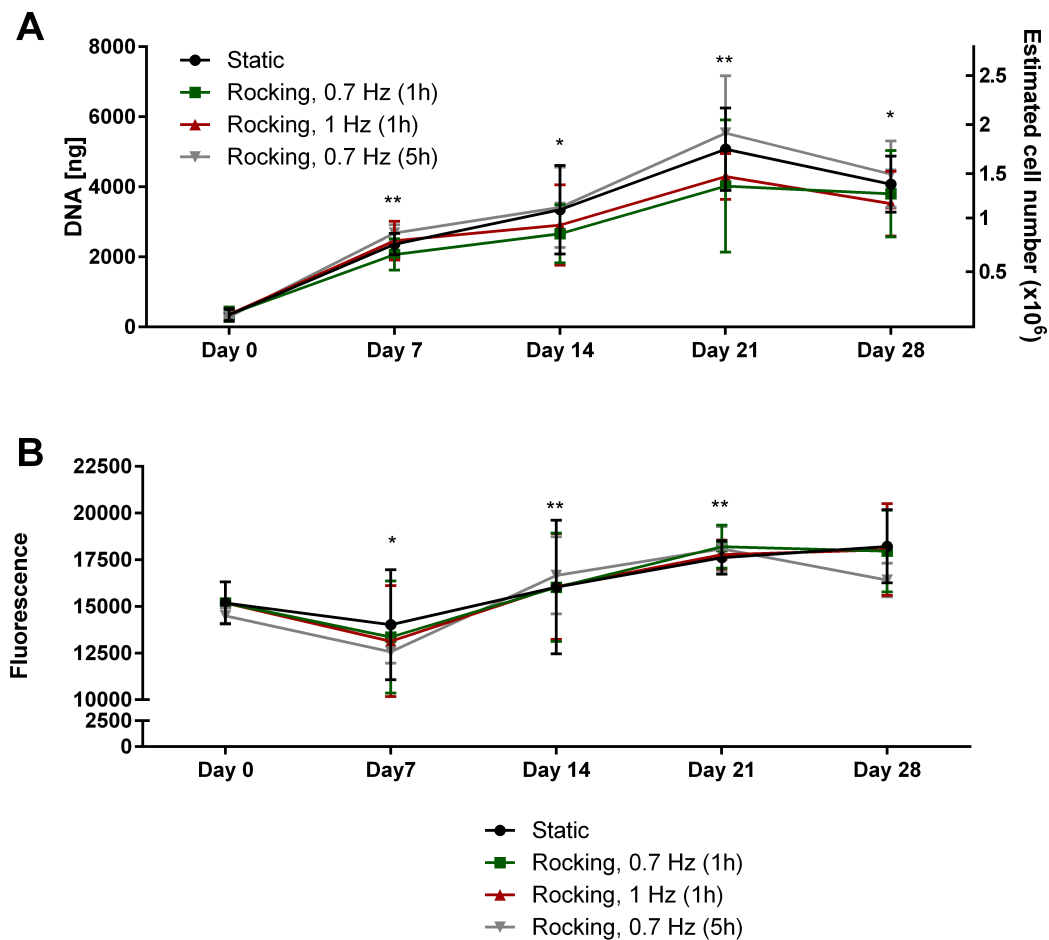
Figure 6.4: Cell proliferation of IDG-SW3 in response to FSS.

A: Amount of DNA per well. Increase in DNA from Day 0 to Day 21 and slight decrease from Day 21 to Day 28. Amount of DNA and cell numbers can be related to each other. B: Metabolic activity. Metabolic activity was lowest at Day 7 and increased towards Day 21 where it plateaued. There were no significant differences between static and rocked groups. Statistically different to previous time point * $p \leq 0.05$ or ** $p \leq 0.001$. Mean with SD (n=3).

Collagen amount and fibre orientation were not affected by low shear stress

Collagen deposition increased significantly between Day 14 and Day 28 in all conditions (p≤0.001). Mechanical stimulation failed to increase the amount of collagen deposited at any of the observed time points (Figure 6.5).

Collagen was deposited throughout the whole well. Fluorescence microscopy of PSR stained samples allowed visualisation of extracellular collagen fibres (Figure 6.6). At Day 0 and Day 3 PSR staining was mainly linked to the cell body. From Day 7, extracellular fibres became visible and their number significantly increased up to Day 28 confirming semi-quantitative results from PSR de-staining.

The thickness of the collagen networks was assessed using SHG imaging (Figure 6.7). Stacked images in the z-direction showed collagen networks which were several micrometres thick. SHG images also showed that the thickness of collagen layers varied greatly between different locations in the same well. However, no links between 'high' FSS areas and increased collagen deposition or vice versa could be drawn. In addition, cell and fibre orientation also did not seem affected by any of the tested FSS regimes. Collagen fibres were arranged in honeycomb structures which appeared to be independent of the underlying cell orientation or the direction of fluid flow.

Strong mineralisation was observed in all conditions

Mineral deposition increased significantly over time in all conditions. The amount of mineral was negligible at Day 7, with no detectable red-stained mineral in the wells following ARS staining. Mineralisation increased significantly between Day 14 and Day 21 (p≤0.001) and only slightly between Day 21 and Day 28 in all conditions. Rocking did not significantly enhance mineralisation compared to the static control group. ARS staining showed that minerals were distributed evenly in the wells (Figure 6.8).

ALP activity increased over time

ALP activity was not significantly different between static control groups and mechanically stimulated samples. ALP activity relative to DNA increased in all conditions from Day 0 to Day 28 (Figure 6.9). There was a significant increase in ALP activity between Day 0 and Day 14 (p≤0.001). For example, ALP activity in static control groups increased from 0.006 to 0.300 nM p-nitrophenol/ng DNA/min between Day 0 and Day 14. ALP activity in IDG-SW3 at Day 14 was more than
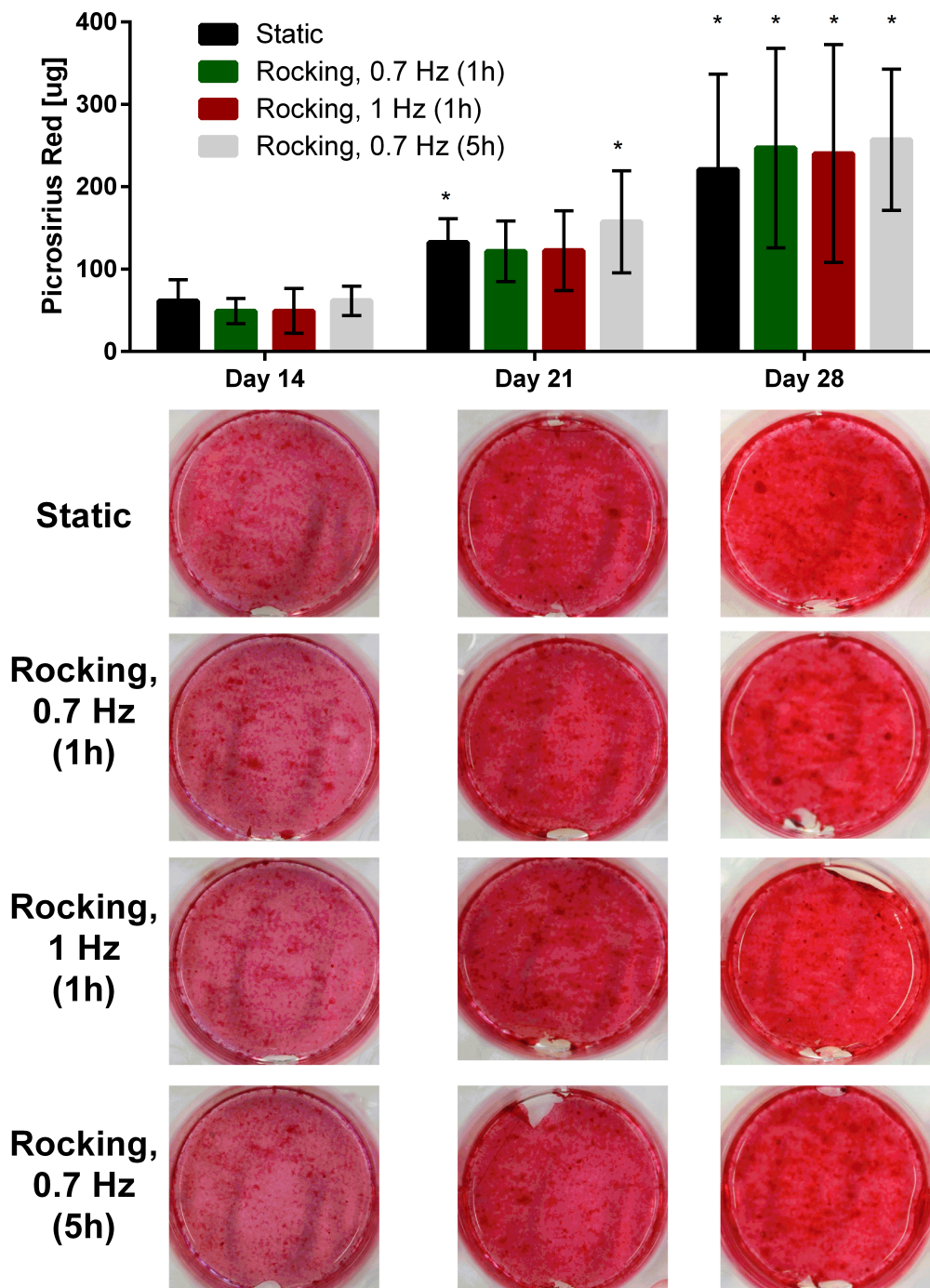
Figure 6.5: Collagen deposition of IDG-SW3 under low FSS.

Top: Quantitative assessment of collagen deposition using PSR destain. The amount of collagen increased in all conditions from Day 14 to Day 28. There were no significant differences between static and rocked groups. Bottom: Photographs of individual wells after staining with PSR. Statistically significant compared to previous time point * p≤0.05. Mean with SD (n=3).
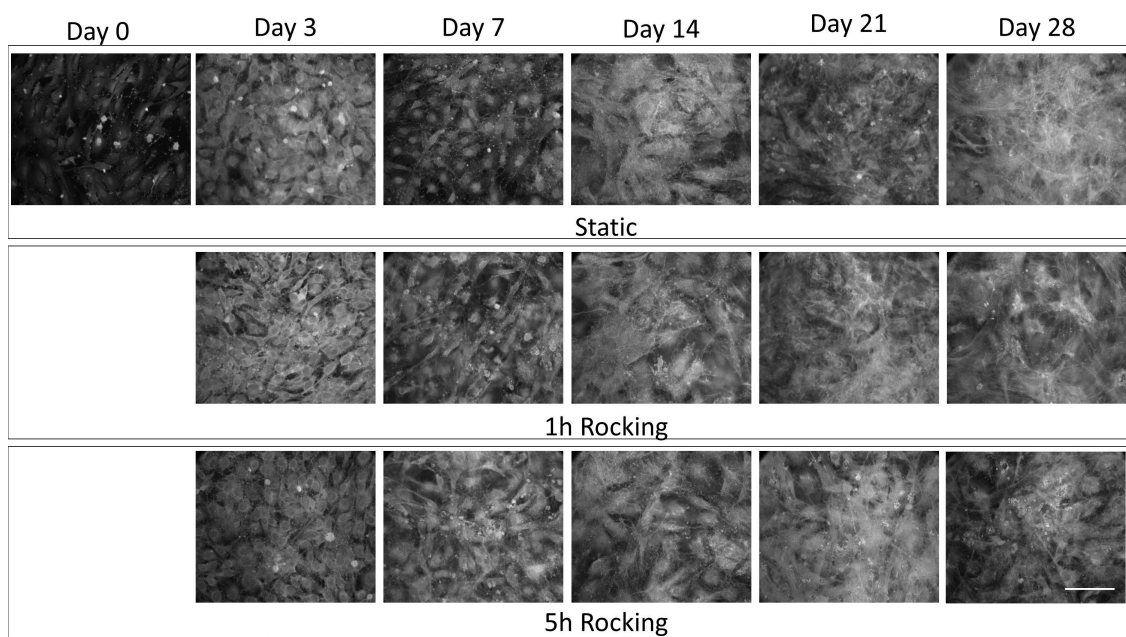
Figure 6.6: Fluorescence microscopy images of PSR-stained samples.

Intracellular pro-collagen and and extracellular collagen fibres can be visualised with red fluorescent light after staining with PSR. The amount of extracellular collagen fibres increased over time. There were no differences in fibre or cell orientation when comparing static and rocked conditions (0.7 Hz). Scale bar = 50 μm.

Static   **Rocking, 0.7 Hz**   **Rocking, 1 Hz**

10 μm

8 μm

6 μm

4 μm

2 μm

0 μm
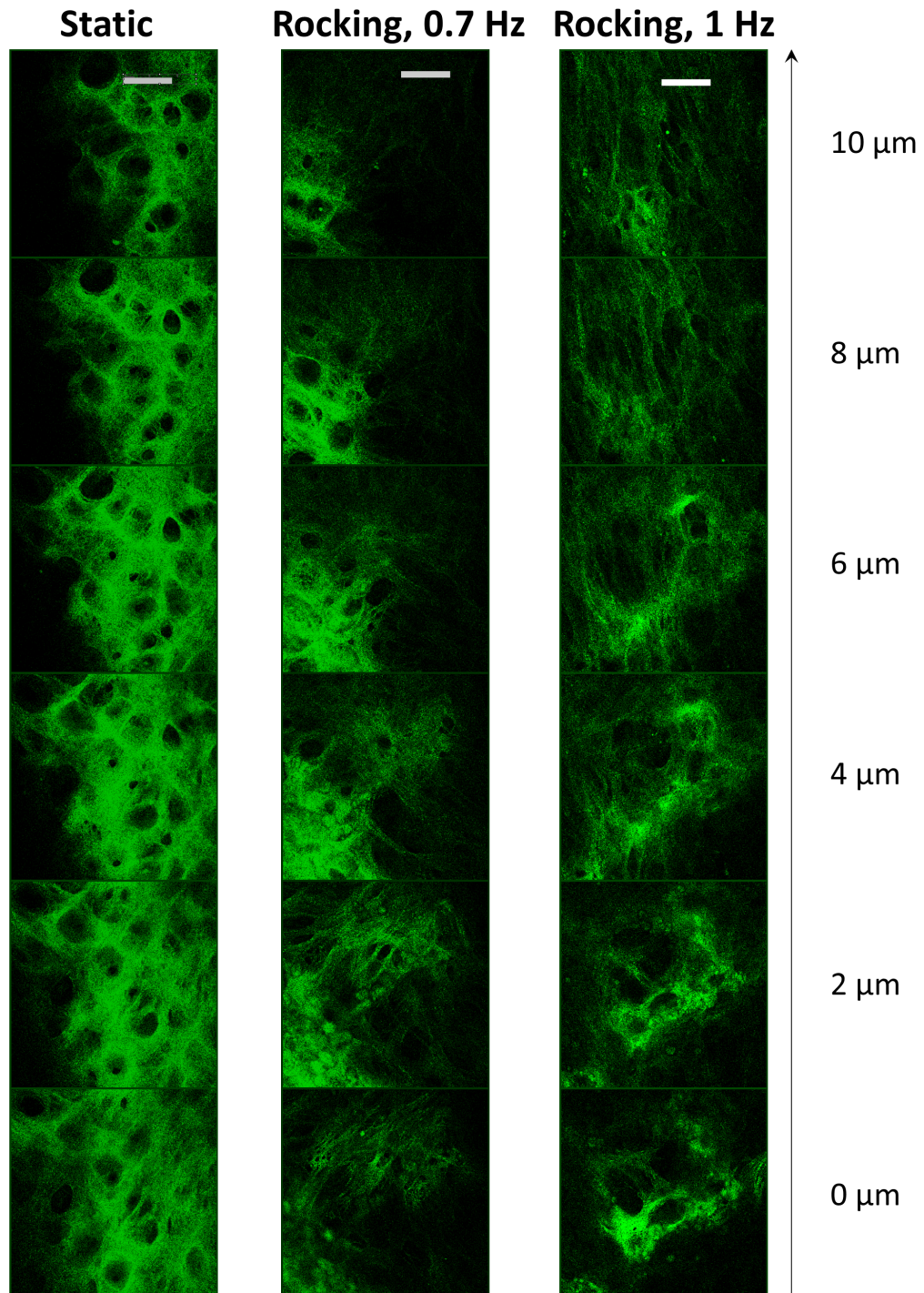
Figure 6.7: Visualisation of collagen fibres with SHG imaging at Day 21 of culture.

Extracellular collagen networks formed honeycomb structures which were several micrometres thick. Collagen deposition varied in different locations in the same well, however there were no significant differences between static and rocked groups. Displayed are z-stack images with a 2 μm step between each image. Scale bar = 50 μm.
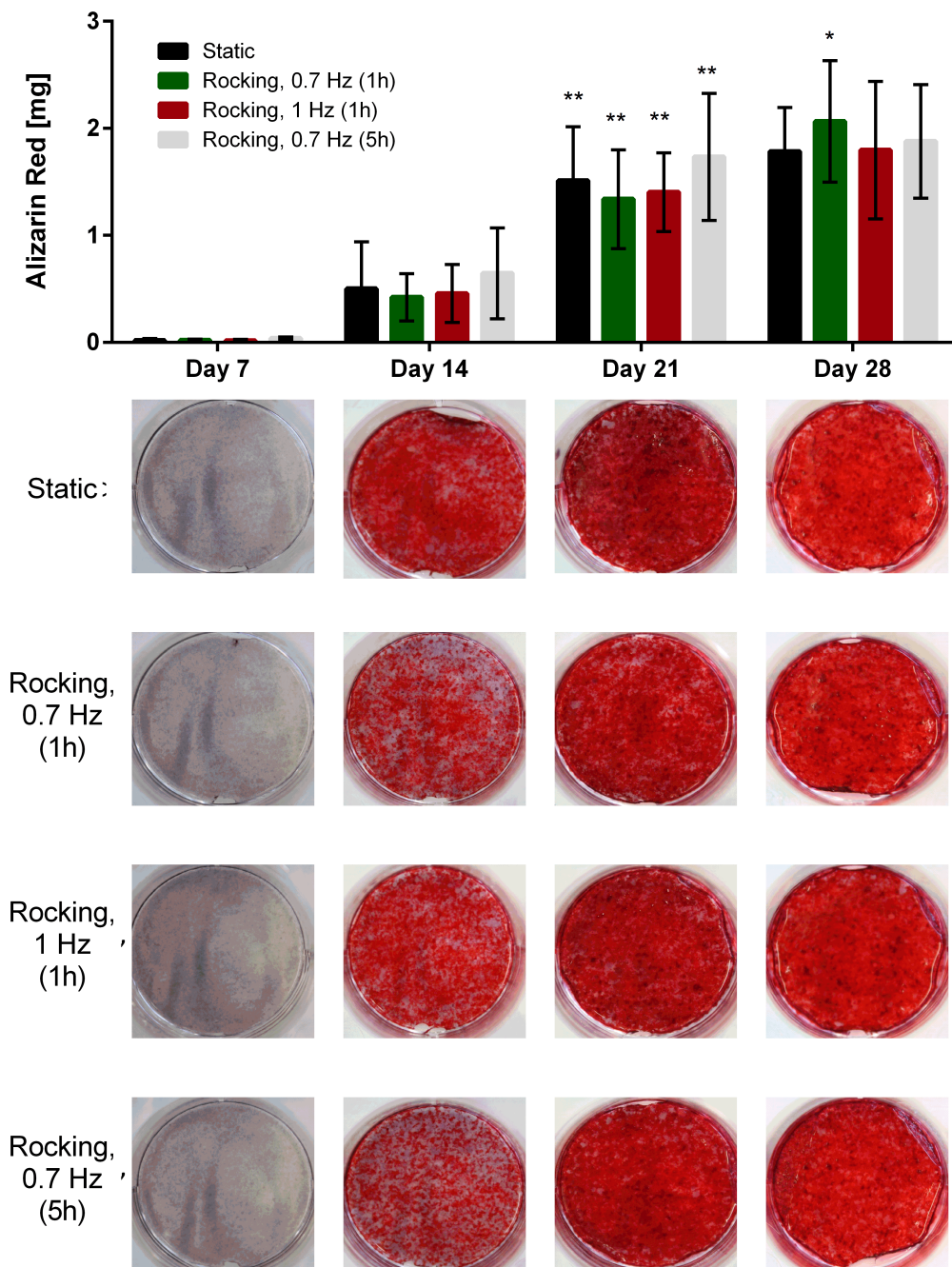
Figure 6.8: Mineralisation of IDG-SW3 in response to low FSS.

Top: Quantitative assessment of mineralisation. Mineralisation increased in all conditions from Day 7 to Day 28, with the highest increase between Day 14 and Day 21. There were no significant differences between static and rocked groups. Bottom: Photographs of individual wells after staining with ARS. Statistically significant compared to previous time point * $p \leq 0.05$ and ** $p \leq 0.001$. Mean with SD (n=3).

two magnitudes greater compared to the activity measure in the osteocyte cell line MLO-Y4 at Day 11 of culture (0.0002 nM p-nitrophenol/ng DNA/min). ALP activity further increased in IDG-SW3 between Day 21 and Day 28 up to a value of 0.739 nM p-nitrophenol/ng DNA/min ($p \leq 0.001$).

Osteocytogenesis was not affected by fluid flow

The transformation from osteoblast-like cells to osteocyte-like cells was assessed by expression of the fluorescent Dmp1-GFP marker. Fluorescence increased significantly over time in all conditions. There was no difference between static controls and mechanically stimulated groups. This trend was observed both using fluorescence readings acquired with a microplate reader and measurements taken from fluorescence microscope images (Figure 6.10).

Fluorescence images showed that Dmp1-GFP positive cells were primarily located in strongly mineralised areas. DAPI staining further indicated that these areas exhibited also the highest concentration of cells. Dmp1-GFP positive cells had a thin, spindle-like morphology and often exhibited thin processes (Figure 6.11).

Non-responsiveness was independent of rocking platform, HEPES buffer and CO_2-concentration

The use of a different rocker model enabled a better control of rocking angle and frequency. In addition, the other rocking platform allowed continuous culture inside a CO_2-controlled incubator without the need of HEPES supplemented culture medium. However, even in such a well-controlled environment, rocking had no effect on Dmp1-GFP expression, collagen deposition and mineralisation (Figure 6.12).

6.5.4   Short-term responses to mechanical stimulation

Early markers of osteogenesis include the release of calcium, PGE_2 and nitric oxide. Release of these early signalling factors in response to low oscillatory FSS were assessed in addition to the late responses considered above.

For the quantification of PGE_2 and nitric oxide, culture medium samples were taken directly from the 6-well plates. PGE_2 measurements were performed at Day 21 in two different experiments (n=2). The concentration of PGE_2 was below the detection limit of the assay in all tested samples, hence no differences between static and mechanically stimulated groups can be stated.
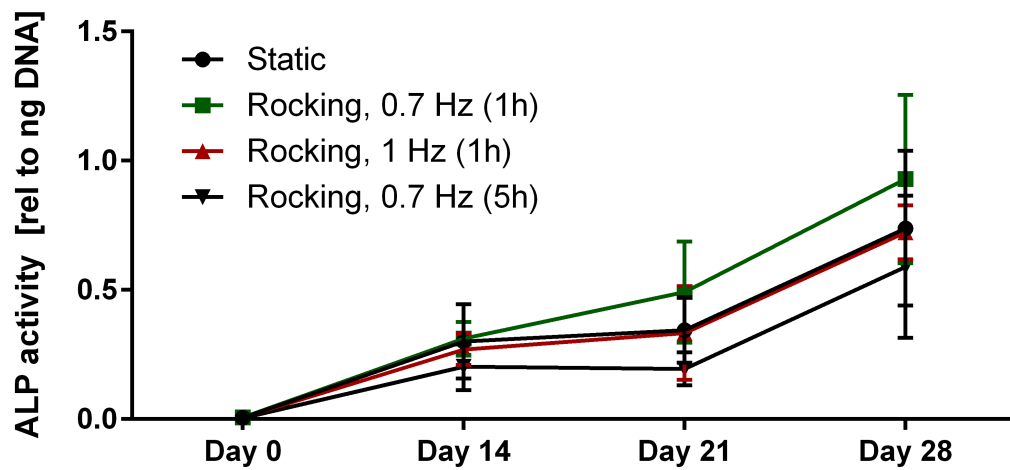
Figure 6.9: ALP activity relative to DNA in IDG-SW3.

ALP activity increased over time. ALP activity was not significantly different between static controls and rocked samples. Mean with SD (n=3).
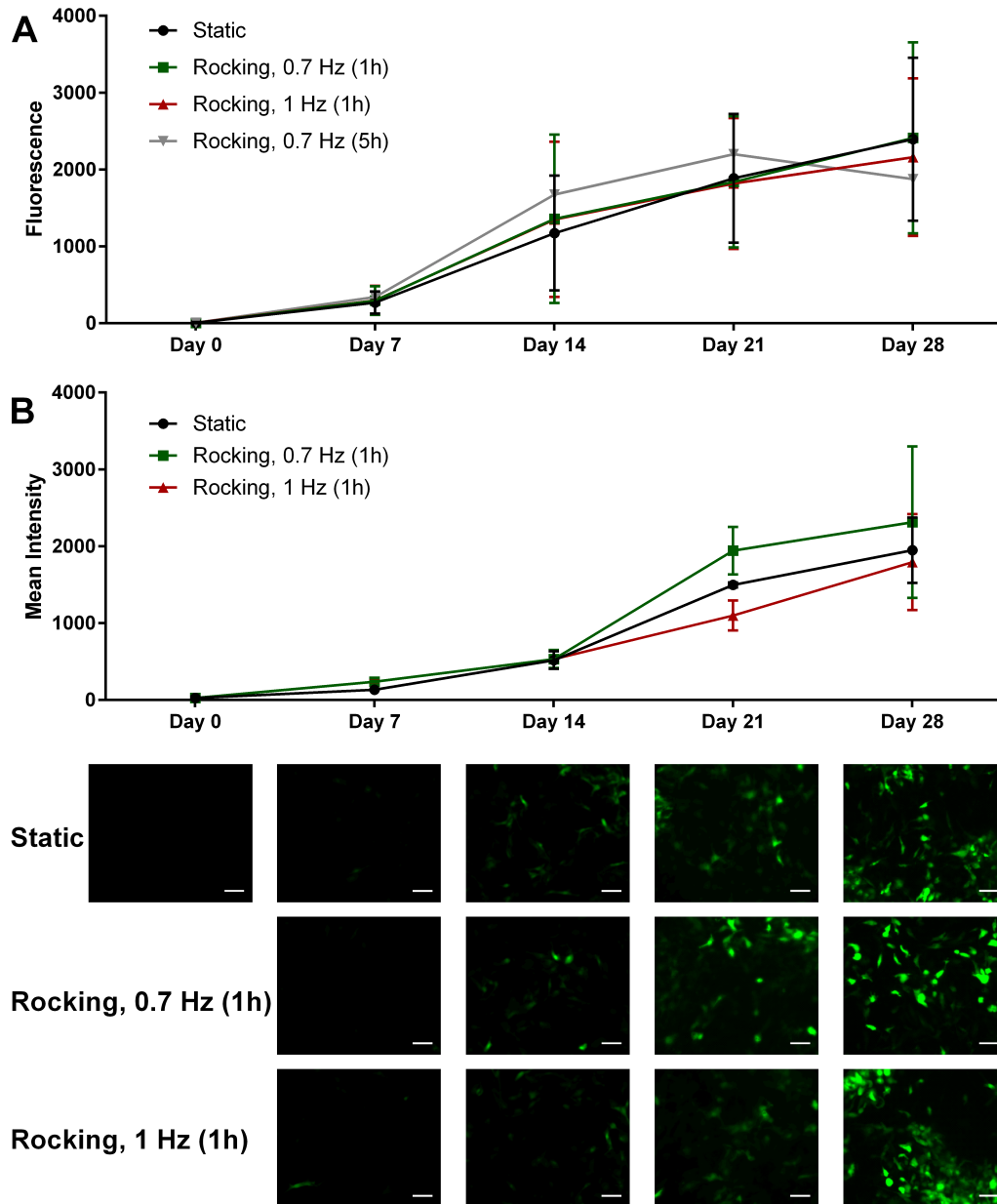
Figure 6.10: Osteocytogenesis in response to low FSS.

Osteocytogenesis was measured through the expression of the fluorescent Dmp1 promoter. A: Fluorescence signals acquired with microplate reader increased significantly over time in all four conditions. Mean with SD (n=3). B: Fluorescence image analysis. Top: Mean fluorescence values acquired from five individual fluorescence images per condition increased over time. Bottom: Corresponding representative fluorescence images. Scale bar = 100 μm. Mean with SD.
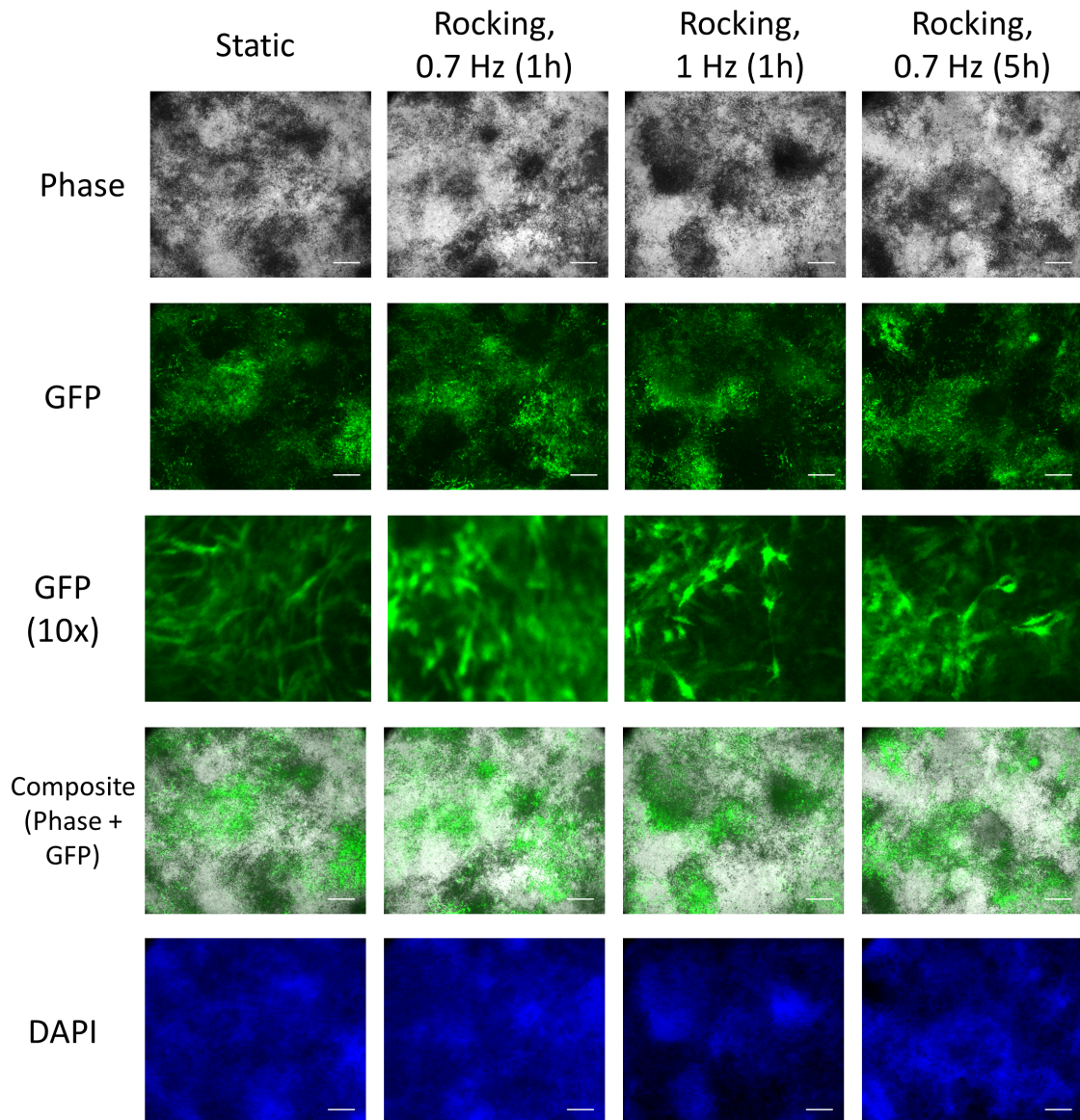
Figure 6.11: Co-localisation of minerals and Dmp1-GFP positive cells.

In all four conditions mineral deposition and Dmp1-GFP positive cells were co-localised. The black areas in the phase-contrast images are the mineralised areas. Dmp1-GFP positive cells exhibit a spindle-like morphology with processes in all conditions. A higher concentration of DAPI-stained cell nuclei can be found in mineralised areas. All images were taken at Day 28 and are representative ones from the centre of the well of three independent experiments. Scale bar = 500 μm.
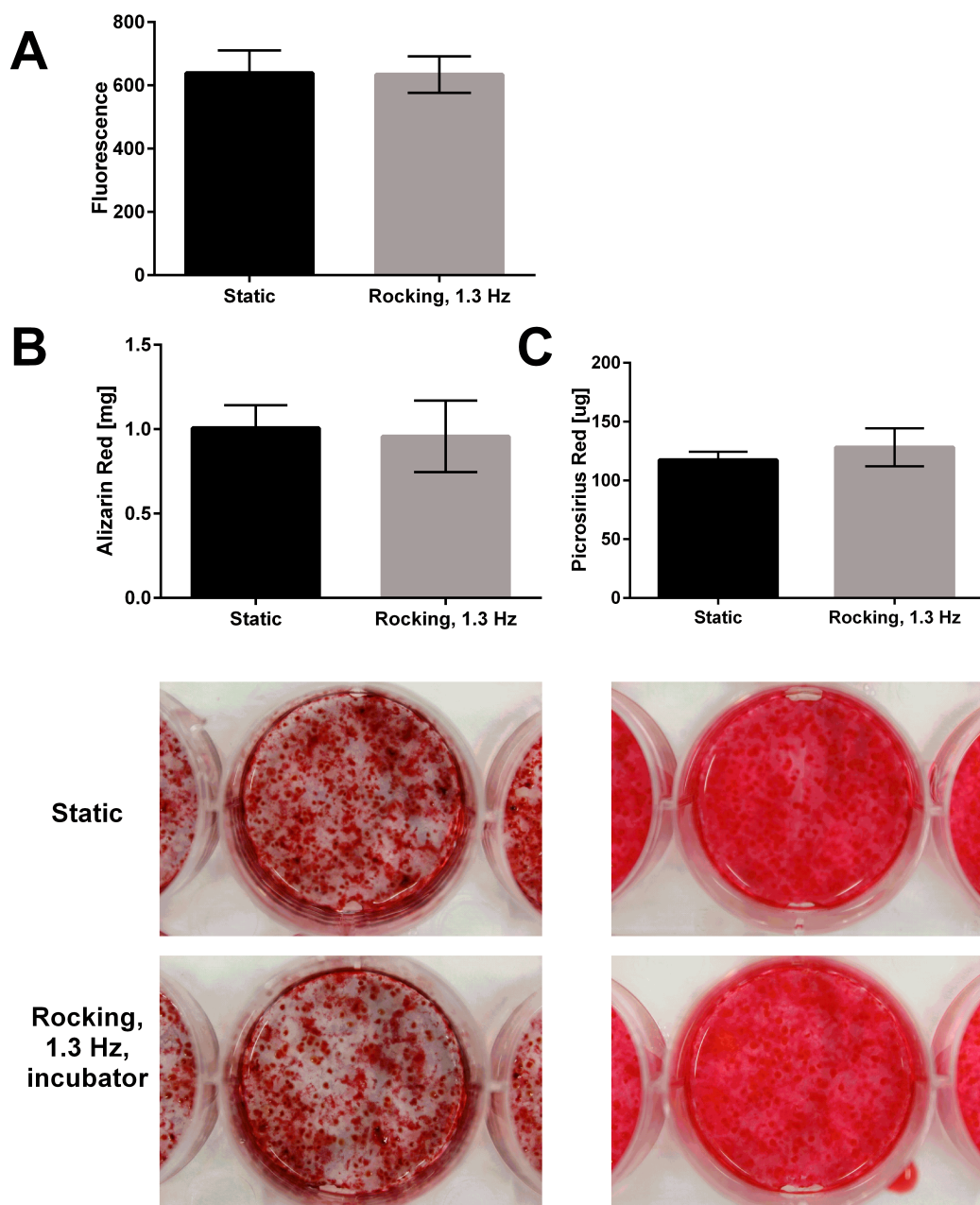
Figure 6.12: Application of FSS inside a CO_2-controlled incubator.

A: Dmp1-GFP expression was not significantly different between static and rocked conditions at Day 21. Mean with SD (n=3). B: Mineralisation. Quantitative (top) and qualitative (bottom) assessment of mineralisation following ARS staining showed no significant differences between static and rocked samples at Day 21. Mean with SD (n=2). C: Collagen deposition. Quantitative (top) and qualitative (bottom) assessment of collagen deposition following PSR staining showed no significant differences between static and rocked samples at Day 21. Mean with SD (n=3).

Nitrite is a stable product of nitric oxide and was assessed using the Griess assay. No nitrite was detected in the culture medium at all tested time points ranging from 5 min to 30 min. Samples were taken at Day 1 and Day 21 during rocking.

Calcium release was assessed using ibidi flow chambers. Two different shear rates (1.5 Pa, 0.3 Pa) under two different flow regimes (unidirectional and oscillating flow at 1 Hz) were applied. Calcium release was detected in all conditions except oscillating flow which generated a shear stress of 0.3 Pa (Figure 6.13). High fluid shear stress (1.5 Pa) triggered a calcium response both under unidirectional and oscillatory flow (Figure 6.14). Maximum fluorescence intensity was detected slightly earlier under unidirectional flow (16 s after onset of flow) compared to oscillatory flow (23 s after onset of flow). The relative fluorescence intensity however was slightly higher and more uniform over time under oscillatory flow.

Similar to the high FSS condition, intracellular calcium release was also increased in response to unidirectional, lower fluid flow which generated a shear stress of 0.3 Pa (Figure 6.15). The maximum fluorescence signal was reached around 23 s after the onset of flow. Most of the cells reacted in a very uniform fashion resulting in the greatest relative change in fluorescence intensity out of the four tested conditions.

In contrast, low, oscillating flow (0.3 Pa, 1 Hz) appeared to have no effect on intracellular calcium release, since fluorescence intensity was highest right at the beginning of fluid stimulation and only decreased thereafter. Interestingly, there were still few cells which responded to fluid flow with calcium release. But unlike the other conditions where a maximum response was reached around 20 s after flow initiation, under lower, oscillatory flow cells required more than 2 min to respond. In addition, most of the responding cells seemed to be in the process of detachment.
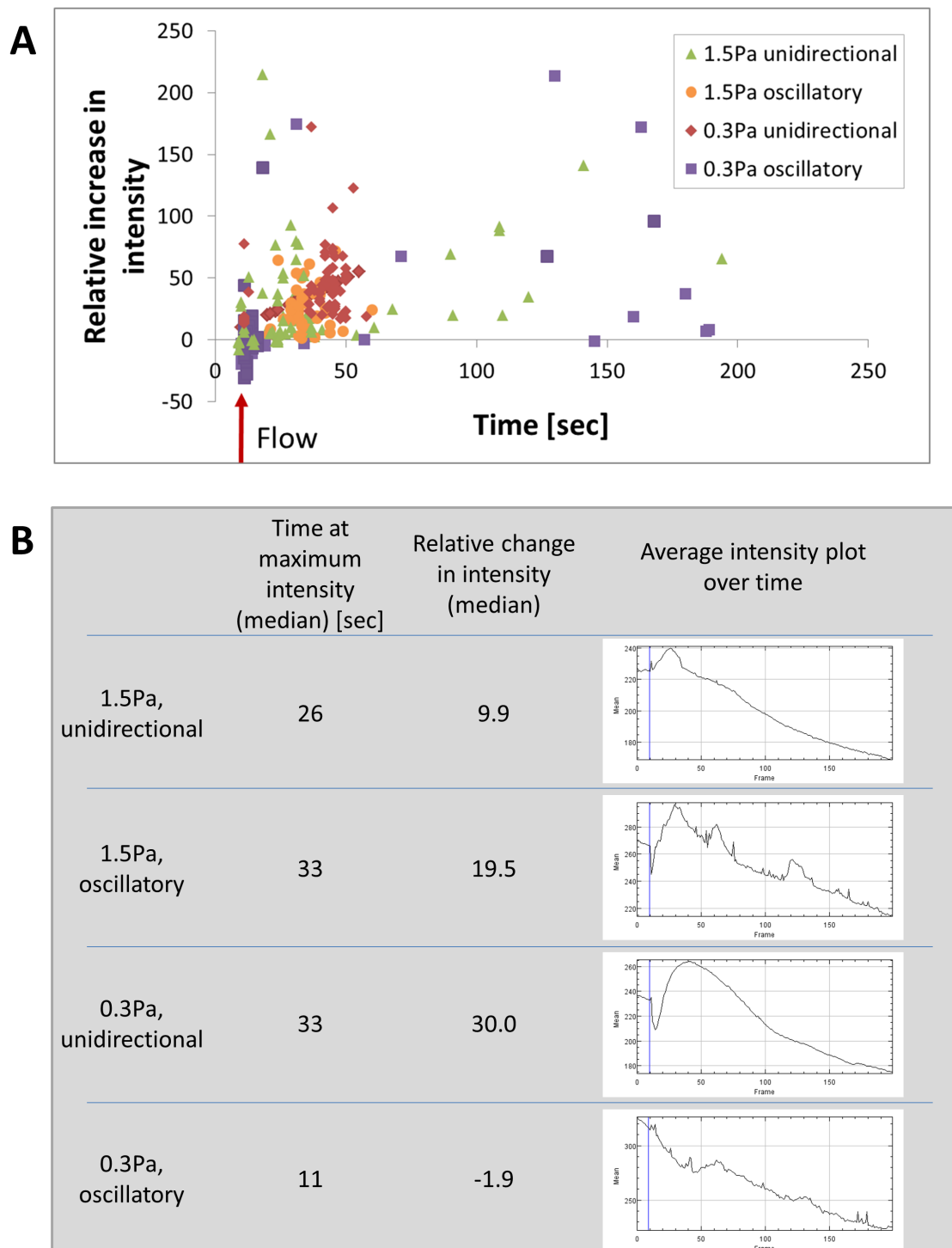
Figure 6.13: Calcium release in IDG-SW3 in response to FSS.

A: Maximum relative increase in fluorescence intensity. Assessed were 50 cells per condition in two independent experiments. The red arrow indicates the onset of flow at 10 s. B: Comparison of median time when the maximum intensity was detected and the magnitude of the fluorescence change between the four different conditions. Mean intensity profile of one cell which was representative of the majority of cells in this flow condition. Blue line in the profile indicated the start of fluid flow.
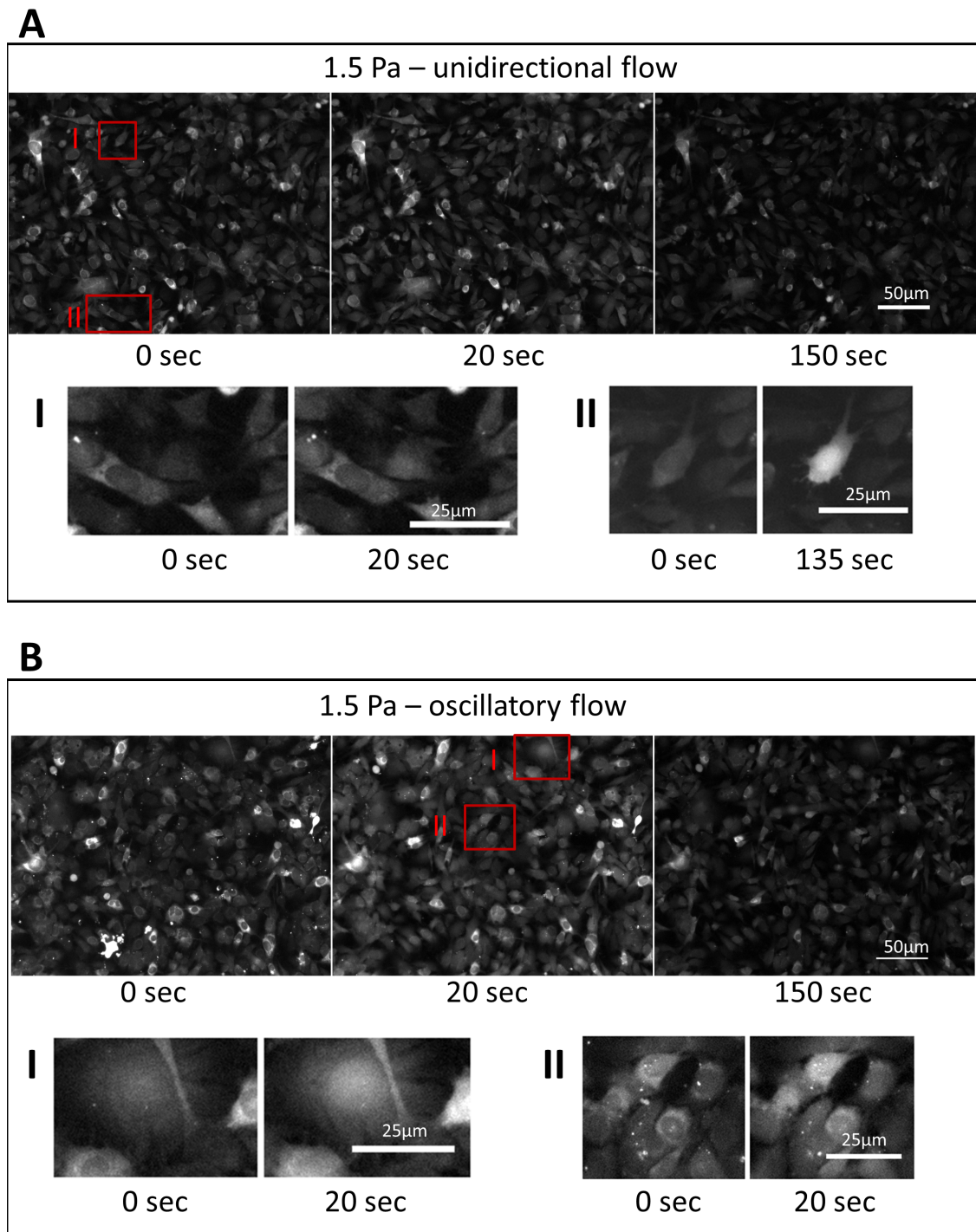
Figure 6.14: Calcium release in IDG-SW3 in response to high FSS (1.5 Pa).

A: Unidirectional flow. B: Oscillating flow (1 Hz). 0 s represents the start of flow. Red squares marked with I and II represent cells which are magnified below.
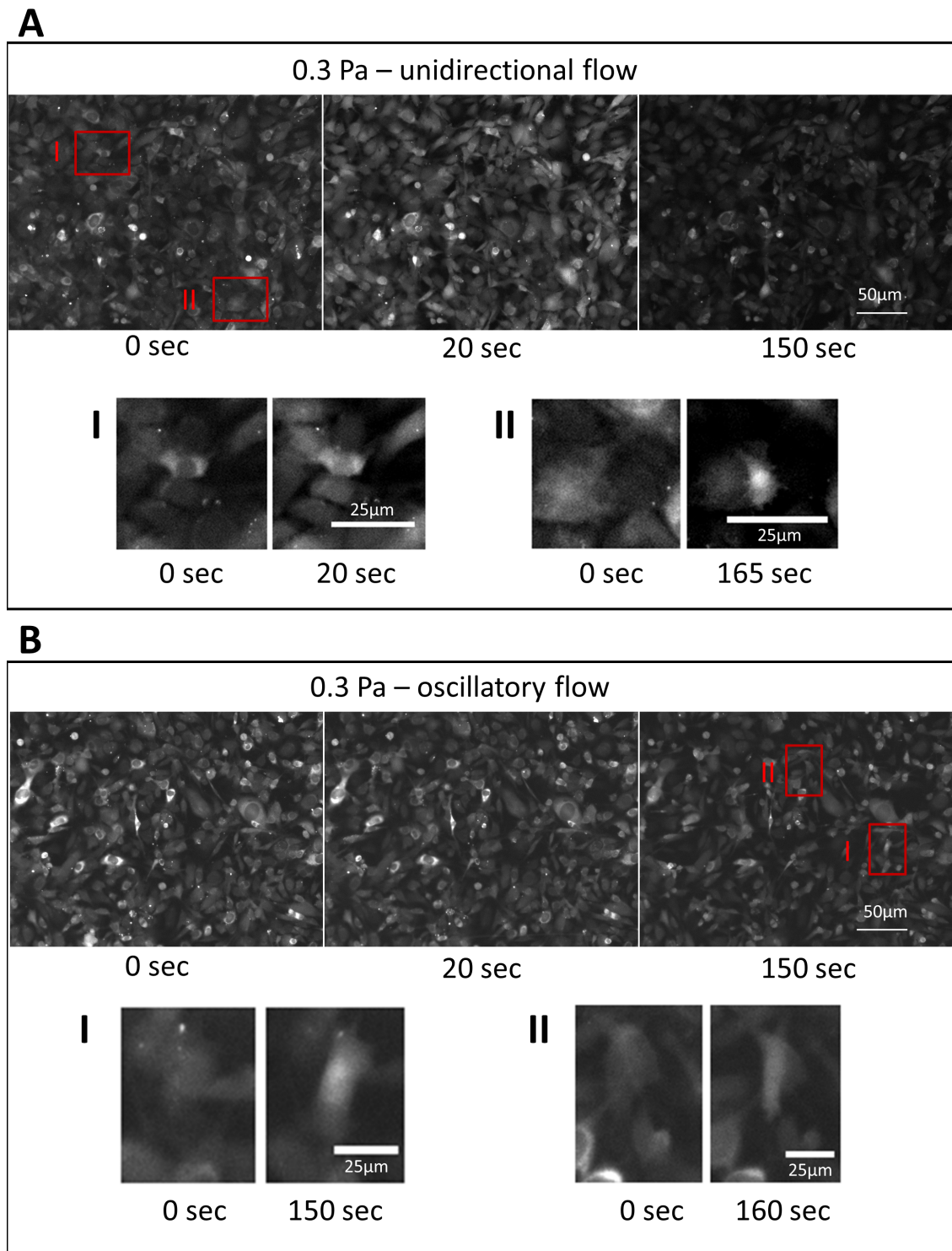
Figure 6.15: Calcium release in IDG-SW3 in response to low FSS (0.3 Pa).

A: Unidirectional flow. B: Oscillating flow (1 Hz). 0 s represents the start of flow. Red squares marked with I and II represent cells which are magnified below.

6.6 Discussion

This chapter investigated early and late responses of IDG-SW3 monolayer cells to FSS. A see-saw rocking platform generated low, oscillatory fluid flow similar to the one described in the previous chapter and by Delaine-Smith et al. (2012).

IDG-SW3 cells were successfully cultured in collagen- and gelatin-coated wells for more than 28 days. However, since collagen coating has the potential to interact with the detection of deposited collagen fibres and was more expensive, wells were coated with gelatin solution instead to facilitate cell attachment. To prevent a pH drop of the culture medium, HEPES buffer was added to the medium which allowed culture outside a CO_2-controlled incubator for 5 h without affecting the cells' viability.

Proliferation and metabolic activity of IDG-SW3 were not influenced by FSS. Although some studies reported higher proliferation in response to FSS (Aisha et al., 2015; Xing et al., 2014), other ones also found that low FSS had no effect on cell numbers (Delaine-Smith et al., 2014; Kreke and Goldstein, 2004). Cell numbers in both static and rocked samples increased up to Day 21. Day 0 was defined as the time point that cells reached confluence, i.e. when cells covered the complete surface of the well. Continuing proliferation meant that cells started to form high-density cell clusters and occasionally grew on top of each other. The increase in cell numbers was confirmed by measurements of DNA and metabolic activity but also through comparison of DAPI stained nuclei at different time points (Figure 6.16A). Continuous proliferation after Day 0 was in contrast to how IDG-SW3 were described in the literature. According to the literature, proliferation and immortalisation in IDG-SW3 is regulated through a temperature-sensitive mutant of the SV40 large tumour antigen (Woo et al., 2011). This antigen is regulated by the INF-γ inducible H-2K^b promoter, hence IDG-SW3 should only proliferate in the presence of INF-γ at 33 °C, but stop proliferating after Day 0 when they were cultured at 37 °C in the absence of INF-γ. Woo et al. (2011), who first characterised the cell line IDG-SW3, did not directly quantify proliferation rates. Instead, they compared the number of DAPI stained nuclei at several time points and came to the conclusion that the number of nuclei remained constant over time. However, when looking at some of their published images the number of nuclei seems to increase similar to what has been observed in this experiment, in particular between Day 0 and 14 (Figure 6.16C).

The variation in proliferation could result from a different seeding technique. To seed cells at the same, very confluent density which Woo et al. (2011) had used, i.e. 80,000 cells/cm² or 760,000 cells/well, a huge number of cells would have been required for each experiment. For example, a standard experimental set-up comprised of

more than 144 wells, i.e. four different conditions each consisting of three different assays at four different time points which were performed in triplicate. As a result, more than 100 million cells would have been required in order to seed cells in a confluent state. To avoid production of such large amounts of cells, the initial seeding density was decreased and cells were cultured at 33 °C until they reached confluence within the well plates (John et al., 2014). Cells were seeded at 10,500 cells/cm^2 (= 100,000 cells/well) and then kept for three days to proliferate and reach confluence. Interestingly, DNA measurements indicated that only around 100,000 cells were found per well at Day 0 , even though cells definitely proliferated between seeding and Day 0. One explanation might be that not all of the seeded cells attached initially, i.e. less than 100,000 cells successfully attached after seeding.

It should also be mentioned that in preliminary experiments cells appeared to follow the mechanism described in the literature. However, even though cells in preliminary experiments stopped proliferating at 37 °C, they also failed to mineralise or deposit a collagen matrix. Therefore, data from these experiments were not considered further (Figure 6.16B). It is not yet known why no mineralisation and no proliferation were observed during the first three independent experiments, but why both were observed in all following experiments. Possible explanations include changes in the biochemical composition of the culture medium, e.g. lower concentration of ascorbic acid or β-GP, or impairment of the SV40 antigen during freeze-thaw cycles and in higher passages.

To better understand the impact of initial seeding density and cell density when temperature is switched to 37 °C, more studies should quantitatively investigate proliferation in this relatively new cell line. In future experiments, cells might be given more time to proliferate at 33 °C to make sure cells reach a very confluent state already at Day 0. It is remarkable however, how Woo et al. (2011) mention such a high initial seeding density even though their DAPI images look very similar to Day 0 images acquired in this study (Figure 6.16C).

Overall, continued proliferation of cells did not seem to affect their viability, osteoblastic activity or ability to express Dmp1-GFP. Metabolic activity plateaued between Day 21 and Day 28 and the amount of DNA even slightly decreased in the same time span. At Day 21, cells had reached more than 2 million cells per well, which can be classed as over-confluent. Hence, over-confluence might have finally stopped proliferation and even initiated cell apoptosis. The question remains, why only confluence and not withdrawal of INF-γ or the temperature switch stopped cell proliferation.

Interestingly, on Days 0 and 7 metabolic activity and DNA content did not follow
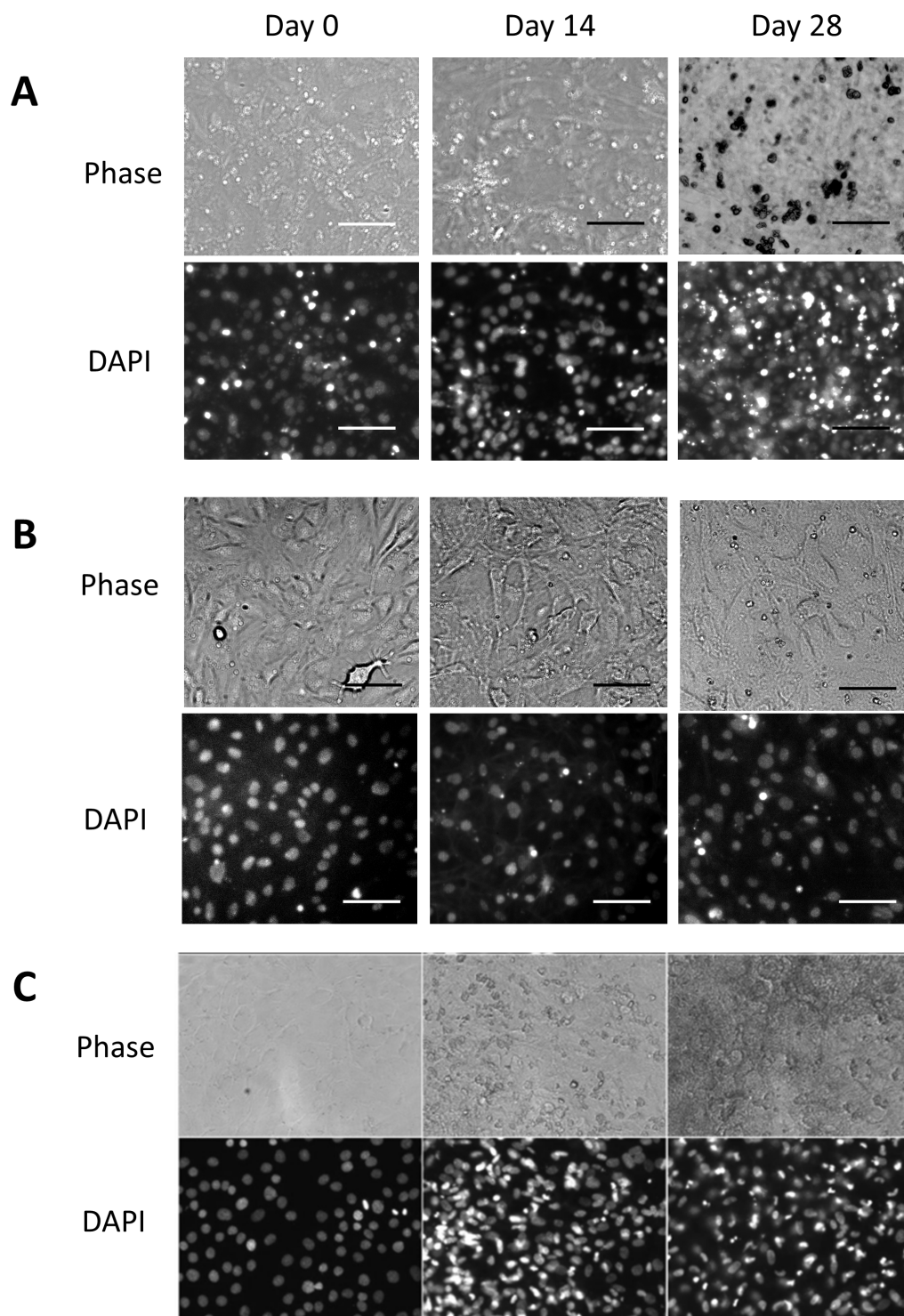
Figure 6.16: Phase-contrast and fluorescence images of DAPI-stained cell nuclei.

A: Images taken from experiments used in this chapter. Mineral deposition increased over time (black dots in phase-contrast images). Number of DAPI-stained nuclei (blue dots) also increase over time. B: Images taken from non-mineralising cultures which were not used in this study. Number of DAPI-stained nuclei remained constant over time. C: Published images by Woo et al. (2011). Despite claiming that cell numbers did not change after Day 0, their images indicate more DAPI-stained cells in Day 14 compared to Day 0. Scale bar = 50 μm.

the same trend. While more DNA was detected at Day 7 than at Day 0, metabolic activity was higher at Day 0 compared to Day 7. This anomaly might indicate that IDG-SW3 at Day 0 were more metabolic active since they were still exhibiting their immortalised, proliferative phenotype which is characteristic of IDG-SW3 cultured at 33 °C and with INF-γ (Woo et al., 2011). Differences between metabolic activity and DNA are in line with previous studies. DNA content is known to be a more tightly controlled indicator of cell numbers than metabolic activity, since metabolic activity has been shown to vary greatly throughout the life cycle of cells and with cell densities (Quent et al., 2010). Although metabolic activity was able to further confirm that cells did not respond to low FSS, this data shows that metabolic activity might not be a suitable assay for comparing cell numbers between different days.

The osteoblastic phenotype of IDG-SW3 was assessed using ALP activity as a marker. IDG-SW3 displayed significantly increased ALP levels throughout the whole culture period which was in contrast to the osteocyte cell line MLO-Y4 that had nearly undetectable ALP levels at Day 11 of culture. ALP activity increased over time and at Day 28 it reached levels which were comparable to ALP values found in the late-osteoblast cell line MLO-A5 (see Chapter 5). However, the continuous increase in ALP activity over 28 days was in contrast to findings by Woo et al. (2011). They described a peak ALP activity at Day 14 which was followed by a decline towards Day 21 when the majority of cells started to display an osteocytic phenotype. It has to be noted however that a direct comparison with their ALP values was not possible, since Woo et al. (2011) normalised ALP activity to protein content and not DNA content. Continuous proliferation (as discussed above) might explain the high ALP activity throughout the whole culture period. Potentially, the number of constantly newly formed osteoblast-like cells overruled the effects of already differentiated osteocyte-like cells. Even though osteocyte-like cells existed, fluorescence microscopy indicated that at no time did they made up the majority of cells. Alternatively, differentiation towards an osteocytic phenotype might have just been delayed. While Woo et al. (2011) observed a strong increase in ALP activity just before ALP activity decreased, i.e. between Day 7 and 14, the present data showed the strongest increase between Day 21 and 28. This delay might suggest that a decrease in ALP activity might also have been delayed and followed after more than 28 days of culture.

Another marker for osteoblastic activity of bone cells is the deposition of collagen type I. In line with the previously described high ALP activity of IDG-SW3, these cells also continuously deposited new collagen. Fluorescence microscopy of PSR-stained samples revealed the appearance of the first extracellular collagen fibres around Day 7 and their number increased further over the coming weeks (Figure

6.6). Cells formed a several micrometer thick collagen network which exhibited a honeycomb structure similar to the collagen network developed by MLO-A5 in Chapter 5 and which has been described by Woo et al. (2011) for IDG-SW3. When comparing collagen production of IDG-SW3 to MLO-A5 at Day 21 of culture, both cell types produced very similar amounts of collagen matrix. Fluid flow did not affect collagen production and its deposition pattern. Potentially, the relatively thick collagen layers which covered the cells might have even prevented the cells from sensing fluid flow towards the end of culture.

Mineralisation of the collagen network increased over time. In contrast to the work by Delaine-Smith et al. (2012), who observed enhanced mineralisation in response to FSS in MLO-A5, mineralisation was not affected by mechanical stimulation in IDG-SW3 cultures. This finding was in line with MLO-A5 data from the previous chapter. The combination of findings from this and the previous chapter strongly suggests that bone cells are unable to respond to low, oscillatory fluid flow in particular in terms of long-term effects such as collagen deposition and mineralisation.

Mineralisation and osteocytogenesis are thought to be linked, as previous studies (Robin et al., 2016; Prideaux et al., 2012; Irie et al., 2008) and findings from Chapter 4 suggest. Since FSS was not able to enhance mineralisation, it was hypothesised that mechanical stimulation would also have no effect on the expression of Dmp1-GFP as a marker of osteocytogenesis. Our results confirm this hypothesis and show that FSS had no effect on osteocytogenesis. In addition, the location of Dmp1-GFP positive, osteocyte-like cells matched the location of highly mineralised areas in the wells. This further suggests that mineral deposits are required for osteocytogenesis or vice versa: early osteocytes expressing Dmp1-GFP contribute positively to the mineralisation of their surrounding matrix.

Overall, expression of the osteocyte marker Dmp1-GFP increased over time in all conditions. To evaluate fluorescence progression, 36 readings were taken per well with a fluorescence reader. Since the microplate reader was only able to take fluorescence readings from the top, the lid of the well plate had to be removed and cell culture medium was replaced by HBSS to reduce the impact of background noise generated by the cell culture medium. Validity of this technique was confirmed by image analysis, whereby both methods produced very similar results. Simultaneous investigation of cell morphology and cell distribution was one of the advantages of image analysis. However, quantitative image analysis required consistent microscope settings over several weeks which can be challenging in a shared lab facility. In addition, image acquisition and analysis requires considerably more user input and time than the microplate reader method, hence the latter was selected as method of

choice. In contrast to other publications (Woo et al., 2011; John et al., 2014; Scully, 2015), this work is the first one which describes the use of a microplate reader to evaluate the progression of osteocytogenesis in IDG-SW3.

The analysis of short-term signalling pathways, e.g. release of calcium, can help to better understand the non-responsiveness of IDG-SW3 to low, oscillating fluid flow. Calcium signalling in IDG-SW3 has been measured using four different flow regimes in parallel-plate flow chambers. It was not possible to directly observe calcium release on the see-saw rocker as already explained in the previous chapter. The lowest possible shear stress which could be generated within the PPFC was 0.3 Pa, which was almost one magnitude higher than FSS generated on the rocker. Calcium signalling was observed in three out of four conditions: unidirectional flow (τ=1.5 Pa) and oscillating flow (τ=0.3 Pa and 1.5 Pa). The only flow regime which did not trigger widespread Ca^{2+} release in IDG-SW3 was the condition most similar to the fluid flow generated with the rocking platform, i.e. oscillating flow at 1 Hz generating a shear stress of 0.3 Pa. As discussed in the previous chapter, it was expected that oscillatory flow would induce a lower reaction compared to unidirectional flow in osteoblasts (Jacobs et al., 1998). Similar to osteoblasts, osteocytes have also been found to be more responsive to steady flow than to oscillatory flow by generating more frequent and stronger Ca^{2+} peaks (Lu et al., 2012a). In addition, a lower magnitude of FSS is also known to decrease calcium signalling (Lu et al., 2012b). Oscillating flow appeared to influence cell morphology more than unidirectional flow with a high proportion of cells shrinking in size and some even starting to detach. Detachment might have been facilitated by the relatively short incubation time of only 4 h. A significantly longer incubation time however, induced cell apoptosis caused by a lack of nutrients available in the small volume of culture medium. Future experiments might look into optimising incubation times prior to flow applications and investigate more flow rates. In addition, the current set-up investigated calcium signalling in osteoblast-like IDG-SW3 cells, since cells were tested only hours after seeding. While experimentally challenging, it might be interesting to culture cells over several days prior to flow application to investigate the response of osteocyte-like IDG-SW3 cells. In conclusion, while more data should be gathered the presented results already indicate that low, oscillating fluid flow fails to activate calcium signalling in IDG-SW3. This might explain the non-responsiveness of IDG-SW3 also in terms of long-term osteogenesis markers such as mineralisation and collagen production.

It was also not possible to detect any NO or PGE_2 upon stimulation of IDG-SW3 on the see-saw rocking platform. The non-responsiveness was in line with the other previously described findings. At the same time, possible measurement errors might

have also prevented the detection of PGE_2 and NO. Possible limitations for PGE_2 have already been discussed in the previous chapter. In brief, higher PGE_2 values might have been achieved without sample dilution or if samples would have been retrieved during the rocking stage.

Nitric oxide (NO) was determined with the Griess assay which estimates the total NO concentration via nitrite (NO_2^-) analysis. Although the Griess assay is inexpensive and readily available commercially, it also has a fairly high detection limit of around $2.5\,\mu M$, hence preventing the detection of very low levels of NO. More sensitive detection methods include chemiluminescence or electrochemical sensors, but they are more expensive and require specialist equipment and therefore could not be applied in this study (Hunter et al., 2013). Another limitation of the Griess assay is that it only measures nitrite which is only one of the stable metabolites of NO. The other metabolite is nitrate (NO_3^{2-}). In future experiments, potentially more accurate and higher readings could be generated by treating the incubation medium with nitrate reductase before applying the Griess reagent (Kuchan and Frangos, 1994; Johnson et al., 1996).

While the magnitude of shear stress is an important regulator of bone mechanotransduction, duration of force application and rest periods are also thought to play an essential role (Kreke et al., 2008). In this study, cells were stimulated once per day either for $1\,h$ or $5\,h$. A stimulation period of $1\,h$ has been previously applied in bone cell studies and yielded increased mineralisation (Delaine-Smith et al., 2012) and enhanced osteogenic differentiation (Mai et al., 2013b). In addition, cells were subjected to $5\,h$ of flow per day, hoping that longer flow stimulation would facilitate cell and collagen alignment. For example, Prodanov et al. (2013) showed that MC3T3 cells aligned in perpendicular direction from the direction of fluid flow (τ=0.7 Pa) after $3\,h$ and $5\,h$ but not after $1\,h$ of flow. However, no cell or collagen alignment was observed in any of the observed flow regimes in this study.

Continuous stimulation of bone cells has been known to decrease cellular mechanosensitivity, while inserting rest periods can recover and enhance this ability again. The underlying cellular mechanism are not yet fully understood, hence recommendations of rest periods range from a couple of seconds up to several hours or even days (Batra et al., 2005; Donahue et al., 2003a; Robling et al., 2001; Jacobs et al., 1998; Gong et al., 2014; Kreke et al., 2008). For example, the most distinct calcium release in response to flow can be observed directly after loading and it has been shown that cells can regain their mechanosensitivity within $15\,min$ (Donahue et al., 2003a). On the other hand, long-term loading is thought to control downstream responses in bone cells by generating multiple Ca^{2+} oscillations, even though they are

of lower magnitude compared to the initial response (Donahue et al., 2003a). In the present study, cells were only stimulated with a total of 20 bouts of fluid flow over a period of 28 days. Although some research has shown that even one single bout of loading was able to enhance long-term osteogenic behaviour (Mai et al., 2013b), potentially stronger osteogenic responses could have been created if fluid flow would have been applied several times a day, i.e. by reducing the rest periods from 23 h to 1 h.

Initially, it was thought that IDG-SW3 would respond stronger than MLO-A5 to low FSS since they differentiate towards mechanically more sensitive osteocytes (Bonewald and Johnson, 2008). However, IDG-SW3 also failed to respond to mechanical stimulation generated by a see-saw rocking platform. The combination of results from this and the previous chapter therefore strengthens the hypothesis that osteoblast-like and osteocyte-like cells, and the cell lines MLO-A5 and IDG-SW3 in particular, might not be able to respond to low, oscillatory fluid flow when cultured in monolayers.

6.7 Summary

- Gelatin-coating and HEPES buffering of cell culture medium ensured successful culture of IDG-SW3 in 6-well plates for more than 28 days.

- IDG-SW3 failed to release Ca^{2+}, PGE_2 and NO under low, oscillatory FSS.

- Low FSS failed to enhance osteogenesis. There was no difference in ALP activity, mineralisation and collagen deposition between static and mechanically stimulated groups. These results are in line with MLO-A5 results from the previous chapter.

- Low FSS failed to enhance expression of the osteocyte marker Dmp1-GFP.

- Co-localisation of Dmp1-GFP positive, osteocyte-like cells and mineral indicated a link between mineralisation and osteocytogenesis.

Chapter 7

3D culture of IDG-SW3 in collagen gels under low fluid flow

7.1 Introduction

The preceding chapters have investigated osteoblast and osteocyte biology with cells cultured as monolayers on well plates made of polystyrene. However, flat polystyrene dishes provide a very different environment compared to the complex, three-dimensional (3D) environment that bone cells find in vivo. This potentially affects cellular functions such as the cells' ability to sense and respond to mechanical forces.

Interactions between cells and matrix

Previous research has demonstrated that the behaviour of cells is strongly linked to the properties of their surrounding matrix, such as the rigidity of the substrate (Trappmann et al., 2012; Chatterjee et al., 2010), the pore size of the scaffold (O'Brien et al., 2005) and whether the cells were cultured as a monolayer or in a 3D scaffold (Sun et al., 2006). For more than 40 years, the standard approach for culturing cells used culture vessels with flat surfaces made from polystyrene or glass (**mcguigan2008**). However, monolayer cell culture does not accurately represent the environment of most cells, since they often reside inside the extra-cellular matrix (ECM). It has been shown that receptor expression, transcriptional expression, cellular migration, and apoptosis differ significantly between cells cultured as monolayer and in 3D scaffolds (**haycock2011**).

Fibroblasts for example, which are the most common cells in animal connective tissue, have been shown to exhibit a more elongated morphology similar to that

found in vivo when cultured in 3D (Yamada and Cukierman, 2007; Sung et al., 2013). Fibroblasts in 3D also better synthesize tropocollagen, a component of the ECM and a forerunner of collagen (Lee et al., 2001).

A more in vivo-like behaviour has also been observed in cancer cells cultured in 3D. For example, the cervical cancer cell line HeLa formed cellular spheroids and showed a higher proliferation rate and enhanced matrix metalloproteinase (MMP) expression in a 3D environment compared to culture on flat substrates (Zhao et al., 2014). MMPs have been linked to multiple stages of cancer progression including increased cancer-cell invasion and metastasis since they can degrade various components of the ECM (Egeblad and Werb, 2002). 3D cancer cell cultures also showed increased resistance to chemotherapy (Zhao et al., 2014). This might be due to cells inside the 3D constructs being better protected from the drug than cells on the outside or due to different proliferation rates caused by the oxygen, nutrient, and growth factor gradients across the spheroid (Lin and Chang, 2008; Loessner et al., 2010).

Three-dimensional bone cell culture in collagen gels

3D models have also become increasingly popular for in vitro bone cell culture. Different materials have been used as scaffolds including stiff titanium fibre meshes (Bancroft et al., 2002), porous chitosan scaffolds (Su et al., 2014), polymerised high internal phase emulsions (PolyHIPEs) (Owen et al., 2016) and non-fibrillar hydrogels such as poly(ethylene glycol) (PEG) (Chatterjee et al., 2010). To study the differentiation of human primary osteocytes, ceramic particles which closely resemble the mineral composition of mature bone have also been used (Boukhechba et al., 2009). Most studies, however, which investigated the osteoblast-to-osteocyte transformation, i.e. the process by which osteoblasts become embedded within the fibrillar, collageneous osteoid matrix, used type I collagen gels as scaffold (Woo et al., 2011; Prideaux et al., 2014; Murshid et al., 2007; Parreno et al., 2008; Matthews et al., 2014; Vazquez et al., 2014). Similar to what has been observed in vivo, osteoblasts seeded on top of a collagen gel were able to migrate into the gel, where they extended their dendritic processes to neighbouring cells, synthesised collagen fibrils and initiated mineralisation and thereby formed structures closely related to the natural lacunar-canalicular system (Uchihashi et al., 2013). Most importantly for the scope of this thesis, cell differentiation from osteoblasts to osteocytes can be directed by 3D culture in collagen gels (Parreno et al., 2008; Prideaux et al., 2014; Murshid et al., 2007; Woo et al., 2011). For example, IDG-SW3 cells differentiated into osteocyte-like cells expressing Dmp1-GFP and sclerostin when grown in 3D collagen gels and sponges (Woo et al., 2011; Scully, 2015). Compared to a monolayer culture, mineral deposition and the induction of osteoblast marker genes was
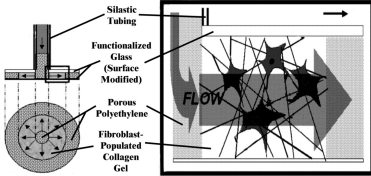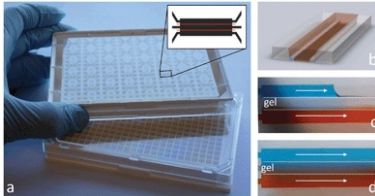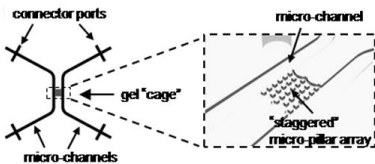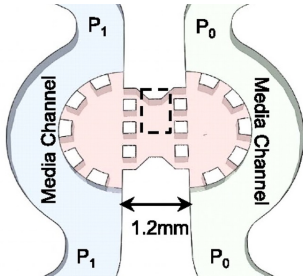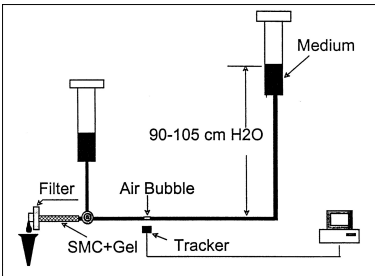
initiated earlier in 3D collagen cultures of MC3T3-E1 (Matthews et al., 2014). 3D culture in collagen systems also changed the morphology of osteoblasts into a more dendrite-like osteocyte morphology (Murshid et al., 2007).

Mechanical loading of 3D collagen substrates

To truly mimic the natural environment of bone cells, biomechanical stimulation is required in addition to the three-dimensional environment provided by the collagen gels. As previously described in Chapter 2.2, biomechanical forces are an essential stimuli controlling cell behaviour. Fluid flow-induced shear stress is thought to be the dominant force acting on bone cells in vivo (McGarry et al., 2005). Most of the 3D collagen models described above, however, investigated only the impact of collagen scaffolds on cell behaviour without exposing the cells to mechanical loading (Murshid et al., 2007; Prideaux et al., 2014; Matthews et al., 2014). The weak mechanical properties of collagen hydrogels might be one reason why not many studies combined 3D collagen culture with mechanical loading. In particular, the high water content of collagen gels makes handling the gels very challenging. Vazquez et al. (2014) overcame this difficulty by confining collagen gels in a silicone plate and applying cyclic compression to the plate. The resulting loading of 4000 to 4500 microstrains increased the release of PGE_2 by osteocytes embedded within the gel and also enhanced the release of type I pro-collagen in a co-culture with osteoblasts and osteocytes (Vazquez et al., 2014). While this model is suitable for studying the effect of strain on bone cells, it is difficult to establish the effect of FSS using this system.

To assess the effect of FSS itself, it would be best to utilise a system which enables fluid flow through collagen gel with almost no compression of the collagen scaffold. Perfusion of collagen is very challenging due to its weak mechanical properties with a very low Young's modulus between 0.5 to 12 kPa depending on its concentration (Raub et al., 2010). Table 7.1 shows an overview of current systems where collagen gel has been used as a scaffold in flow models. Solutions for maintaining the collagen's mechanical integrity include nylon fibres (Wang and Tarbell, 2000), porous polyethylene as barrier (Ng et al., 2005), PDMS stamps which create a 'cage' structure (**polacheck2011**; Vickerman et al., 2008), or 'phaseguides' which utilise the surface tension of the gel (Trietsch et al., 2013). The low flow rates required for interstitial flow through the collagen gel were normally generated by hydrostatic pressure differences, i.e. the height difference of the medium between inlet and outlet (Wang and Tarbell, 2000; Ng et al., 2005).

Table 7.1: 3D collagen in vitro assays investigating the effect of fluid flow.

Description of system	Image of system
Radial interstitial flow tissue culture chamber Collagen gel (2 mg/ml) with dermal fibroblast was sandwiched between two glass cover slips and held in place by acid-treated porous polyethylene. Fibroblasts aligned perpendicular to the direction of interstitial flow (Ng and Swartz, 2003) and differentiated to contractile myofibroblasts (Ng et al., 2005).	
Microfluidic titer plate by MIMETAS A 384-well plate has been modified to create inlets, outlets and cell culture chambers connected by microfluidic channels. Channels are separated by phaseguides allowing controlled co-culture. Matrigel is sucked into the microfluidic chambers by capillary forces. Invasion and aggregation models with breast cancer cells, 3D cell culture of hepatocytes under continuous perfusion, a rifampicin toxicity assay and co-culture with fibroblasts have been demonstrated (Trietsch et al., 2013).	
Microinjection of scaffold in 'gel cage' Two parallel microfluidic channels delivered cell culture medium to a central gel cage consisting of a micro-pillar array made of PDMS. Cell-seeded collagen gel (2 mg/ml) was injected into the cage. Endothelial cells formed open lumen-like structures when cultured under flow conditions (Vickerman et al., 2008).	
Cell-laden gel area between two fluid channels The microfluidic system consisted of two fluid channels separated by an area containing cells suspended in collagen gel (2 mg/ml). It was found that the direction of the migration of breast carcinoma cells was influenced by interstitial flow (0.3 µm/s to 3.0 µm/s) (**polacheck2011**).	
Gel supported by nylon fibres Collagen gel (2.5 mg/ml) containing cells was placed in a silicone tube and supported by nylon fibres to prevent compaction under flow. Smooth muscle cells showed elevated levels of prostaglandin compared to culture under static conditions but lower than cultured in 2D (Wang and Tarbell, 2000).	

Images on the right show the set-up of the models. All images are taken from the corresponding papers.

Mathematical description of flow through porous scaffolds

Characterising the fluid shear stress sensed by the cells within a scaffold is essential for understanding how fluid flow affects cell behaviour in 3D. Mathematical models such as the Navier-Stokes equation or Darcy's Law can be used to describe fluid flow through porous scaffolds such as collagen gels. The Navier-Stokes equation is able to predict the flow behaviour on a microscale level taking into account the precise location and dimensions of cells and fibres. As a result, flow predicted with the Navier-Stokes equation is locally discontinuous and inhomogeneous. However, lack of an exact knowledge of spatial and geometrical information regarding fibres and cells within collagen gels combined with the increased computational expenditure, justifies in most cases the use of the less demanding Darcy's Law as approximation to describe flow in porous materials (Swartz and Fleury, 2007).

Darcy's Law is a continuum approximation which mathematically predicts the average fluid velocity $\bar{v}$ through a porous medium:

$$\bar{v} = \frac{-k\nabla P}{\mu},\tag{7.1}$$

where k is the permeability of the medium, ∇P is the pressure gradient and μ is the viscosity of the flow medium. The actual fluid velocity v, which a particle travelling through the porous medium would experience, can be derived by dividing the average fluid velocity $\bar{v}$ by the porosity n of the medium.

Darcy's Law can also be formulated in a way which includes the flow rate Q through the porous medium:

$$Q = \frac{-kA\Delta P}{\mu L},\tag{7.2}$$

where A is the cross-sectional area of flow, ΔP is the total pressure drop, and L is the length over which the pressure drop is taking place. The negative sign indicates that the fluid flows from high to low pressure.

Based on the value of the Darcy permeability k of the cell-laden scaffold, the shear stress τ on the cell surface can be estimated with an equation derived by Brinkman (1949) for spheres and further developed by Wang and Tarbell (2000) for cylindrical cells,

$$\tau = B\frac{\mu \times (Q/A)}{\sqrt{k}},\tag{7.3}$$

where B is a factor which considers the geometry of the objects, such as $\frac{3}{\pi}$ for spheres or $\frac{4}{\pi}$ for cylindrical cells (Brinkman, 1949; Wang and Tarbell, 1995). Since cells are neither perfect cylinders nor spheres and B is very close to 1 in both cases anyway, the equation for shear stress τ can be simplified to the following (Wang and Tarbell, 2000):

$$\tau \approx \frac{\mu \times (Q/A)}{\sqrt{k}}. \tag{7.4}$$

According to Equation 7.4, knowledge of the permeability k of the scaffold is required to estimate the FSS sensed by cells within the porous scaffold. Table 7.2 lists the results of some studies which measured the permeability of different concentrations of collagen. The permeability of collagen varied between different studies which might have been due to varying collagen concentration, different crosslinking methods and variations in the sourcing of the collagen (e.g. bovine, rat-tail).

Table 7.2: Permeability measurements of collagen gels.

Type of collagen	Permeability [m^2]	Pressure drop [cmH$_2$O]	Method	Source
3.5 mg/ml rat tail collagen	2.7x10^{-13}; 1.6x10^{-14}(cells)	3.5	Collagen gel was fixed between acid-treated polyethylene to prevent contraction	(Ng and Swartz, 2003)
10 mg/ml bovine collagen (ultra-centrifugation)	1x10^{-15}	5-15	Flow rate was measured by monitoring a small air bubble	(Ramanujan et al., 2002)
2 mg/ml collagen type I	1x10^{-13}	n.a.	Tracking of 200 nm fluorescent beads	(**polacheck2011**)
2.5 mg/ml rat tail collagen type I (with nylon fibres)	9.24x10^{-13}	13	Flow rate was measured by monitoring a small air bubble	(Wang and Tarbell, 2000)

7.2 Hypothesis

A 3D collagen model where osteoblasts are embedded within a type I collagen gel that supports fluid perfusion represents a useful in vitro model for investigating the impact of interstitial flow on osteogenesis and osteoblast-to-osteocyte differentiation.

7.3 Aims

To investigate this hypothesis, the following aims were considered:

- To establish and characterise a novel in vitro 3D collagen model which supports fluid perfusion.

- To determine the impact of flow on IDG-SW3 embedded within the 3D collagen scaffold regarding cell numbers, mineral deposition, osteocytogenesis and cell-driven ECM remodelling.

7.4 Methods

7.4.1 Preparation of transwell model

The 3D model consisted of a modified transwell insert which contained collagen gel. IDG-SW3 were embedded within the gel and fluid perfusion through the gel was driven by hydrostatic pressure difference between the transwell insert and the bottom well (Figure 7.1).

Modification of transwell inserts

Sterile transwell inserts (Thincert, greiner bio-one, UK) with a transparent polyester (PET) membrane (0.4 μm pore size) were pierced 20 times with a sterile scalpel to allow fluid flow through the membrane. Care was taken when piercing the membrane that the cuts were roughly the same length (approximately 1 mm) and evenly distributed mainly over the central part of the membrane and avoiding the edge of the membrane. This modification enabled fluid flow through the membrane while still providing support for the soft collagen hydrogel.

Collagen gel preparation

Previous works by Woo et al. (2011) and Scully (2015) showed that rat-tail type I collagen gel supports survival of IDG-SW3. Following the protocol by Scully (2015), IDG-SW3 were embedded in rat-tail type I collagen hydrogel (2 mg/ml) at a final cell concentration of 3.5×10^5 cells/ml. To prepare the collagen hydrogel of 2 mg/ml, rat-tail collagen type I solution (3 mg/ml, Thermo Fisher Scientific, UK) was diluted in 10x PBS, 1 M NaOH and the appropriate volume of cell suspension. All preparation and mixing steps were performed on ice to prevent early cross-linking.

Cell seeding in transwell inserts

150 μl of the cell-collagen solution was added to each modified transwell insert, hence approximately 52,500 cells were seeded per transwell insert. The transwell inserts were placed in a 24-well plate and transferred to a humidified incubator (33 °C) for 45 min for the collagen gel to cross-link. After 45 min of incubation, culture medium was carefully added to the wells. In case of the 'no flow' condition, 1.1 ml of medium was added directly to the well and 100 μl of medium was added on top of the collagen gel. In case of the 'flow' condition, only 800 μl of medium was added directly to the well but 400 μl was added on top of the gel in the transwell insert. The height difference between medium in the insert and medium in the surrounding well in the 'flow' condition created a hydrostatic pressure difference which initiated
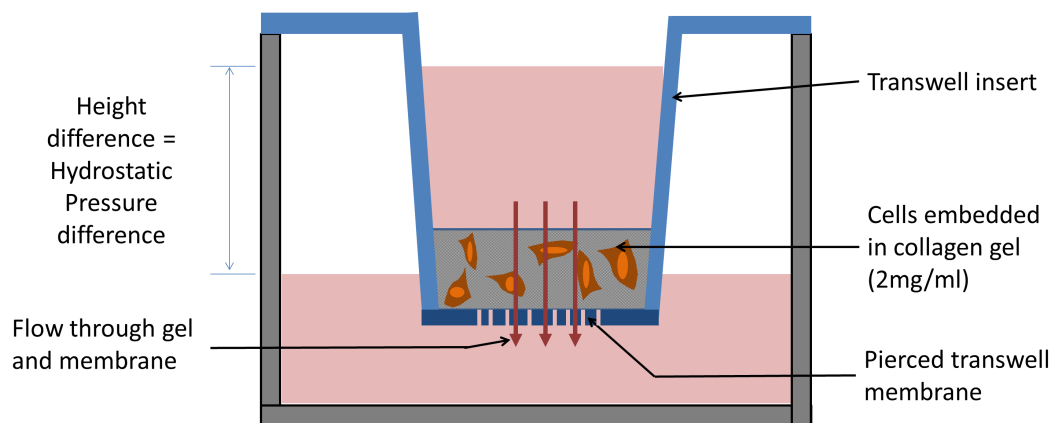
Figure 7.1: Schematic drawing of modified transwell insert.

IDG-SW3 cells were embedded in collagen gel and cultured in a modified transwell insert. Small holes had been pierced in the transwell membrane to allow fluid flow through the collagen gel and the membrane. The hydrostatic pressure difference between the culture medium in the insert and the culture medium in the surrounding well was the driving force for the fluid flow.

slow fluid flow through the collagen gel and the pierced transwell membrane. In contrast, the level of culture medium in the 'no flow' wells was roughly the same in well and insert, hence no flow through the gel was initiated.

Cell culture

For the first three days, IDG-SW3 were cultured at 33 °C in proliferation medium, i.e. culture medium containing INF-γ (Table 3.1). Three days after seeding, defined as Day 0, culture medium was changed to induce osteogenic differentiation by replacing INF-γ with 50 μg/ml ascorbic acid and 5 mM β-GP. The temperature was also increased to 37 °C in the humidified incubator. Cells were cultured for a further 21 days and culture medium was changed every two to three days by adding the same medium volumes as described above. In the 'flow condition', hydrostatic pressure-driven flow was applied for 1 h once a day at 5 days per week. To maintain fluid flow, roughly every 15 min culture medium was transferred back from the bottom of the well into the transwell insert with the aim of maintaining a similar hydrostatic pressure gradient of approximately 1 cm H_2O for 1 h per day.

7.4.2 Characterisation of 3D collagen scaffold

The collagen scaffold was characterised regarding changes in volume and permeability over time. These parameters were used to estimate the shear stress sensed by cells within the porous collagen scaffold.

Measurement of collagen volume

Collagen volume was measured directly after cross-linking and at Day 21. It was assumed that the collagen scaffold had a cylindrical shape and therefore the volume V of the collagen gel was calculated using the following equation:

$$V = A \times \pi \times r, \tag{7.5}$$

where A is the area of the vertical cross-section of the scaffold and r is the radius of the transwell membrane. The vertical cross-sectional area was estimated by analysing photos of the collagen within the transwell inserts in ImageJ.

Permeability measurement of collagen hydrogel

Permeability of the collagen gel was measured at Day 7 and 21 of culture in cell-free samples and cell-containing samples. To calculate the permeability of the gels,

the volume of culture medium passing through the collagen gel in a defined time was determined. Following the procedure described above, a hydrostatic pressure gradient of $1\,\text{cm}$ H_2O was created by adding $800\,\mu\text{l}$ of culture medium to the bottom compartment of the well and by filling the transwell insert completely with culture medium ($\approx 400\,\mu\text{l}$). Well plates were carefully transferred back to the incubator. After $15\,\text{min}$ some of the culture medium had passed through the collagen gel. The inserts were again completely filled with medium and the volume of culture medium which had to be added to the insert (= the medium which had passed through the collagen gel) was noted. To ensure that each well always contained a total volume of $1.2\,\text{ml}$ of culture medium, the medium for re-filling the transwell inserts was taken directly from the bottom well.

The volume of medium which had passed through the collagen gel in $15\,\text{min}$ was used to calculate the flow rate Q. The permeability k of the cell-containing collagen gels was calculated using Darcy's Law (Equation 7.2):

$$k = \frac{Q\mu L}{A\Delta P}, \tag{7.6}$$

where Q is the flow rate through the collagen gel, μ is the viscosity of the flow medium, L is the length over which the pressure drop is taking place, A is the horizontal cross-sectional area of flow, and ΔP is the total pressure drop.

The pressure drop ΔP is calculated using the following equation:

$$\Delta P = L \times \rho \times g, \tag{7.7}$$

where, L is the height of the water column in the transwell insert (= length over which the pressure drop is taking place), ρ is the density of the flow medium and g is the gravitational constant. Therefore, Equation 7.6 can be simplified and used to calculate the permeability k of the collagen scaffold:

$$k = \frac{Q\mu}{A\rho g}. \tag{7.8}$$

Shear stress calculation

Based on the calculated permeability k of the collagen hydrogel, shear stress τ which is sensed by cells within the collagen gel was estimated using Equation 7.4.

7.4.3   Assessment of osteoblast behaviour in 3D

In addition to characterising the collagen scaffold, osteoblast behaviour was also assessed. Collagen scaffolds were fixed and cryosectioned to analyse cell distribution, collagen deposition and mineralisation. Lysis of the cell-collagen constructs was required to determine the DNA content and ALP activity (Figure 7.2).

Fixing of cells in collagen gels

Cells in collagen gels were fixed prior to sectioning. At Day 21, culture medium was completely removed from the wells. The transwell membrane was carefully cut out of the transwell insert using a scalpel. Care was taken that the membrane and the collagen gel did not detach and that the collagen gel was not damaged. The collagen-membrane constructs were placed in new well plates and fixed with 1 ml of 10% formalin for 30 min at room temperature. Following fixation, the formalin solution was removed and the collagen gels were washed four times with DPBS over a period of 30 min. Fixed samples were stored in PBS at 4 °C until required for sectioning.

Cryosectioning of collagen gels

Collagen gels were orientated into square plastic moulds, embedded in freezing media (Cryo-M-Bed, Bright Instruments, UK) and quickly frozen to −20 °C. Specimens were then removed from the mould and mounted on a cryostat chuck. 8 μm transverse sections, showing the top of the gel down to the membrane of the transwell insert, were cut at −20 °C using a CM3050 cryostat (Leica, Germany) and a stainless steel Feather S35 microtome blade (pfm medical, Germany). Three sections were placed onto individual microscope slides. A minimum of 24 sections was taken from each collagen sample. Slides were stored at −20 °C prior to staining and for long-term storage.

Collagen staining of gel sections

Collagen staining was performed with picrosirius red (PSR) solution which was applied to at least six sections per sample for 1 h. PSR solution was made by dissolving direct red 80 in saturated picric acid (1%w/v). After 1 h, the staining solution was removed and the samples were washed gently four times with deionised water. Images of the stained samples were taken by bright-field microscopy and fluorescence microscopy using a red filter.
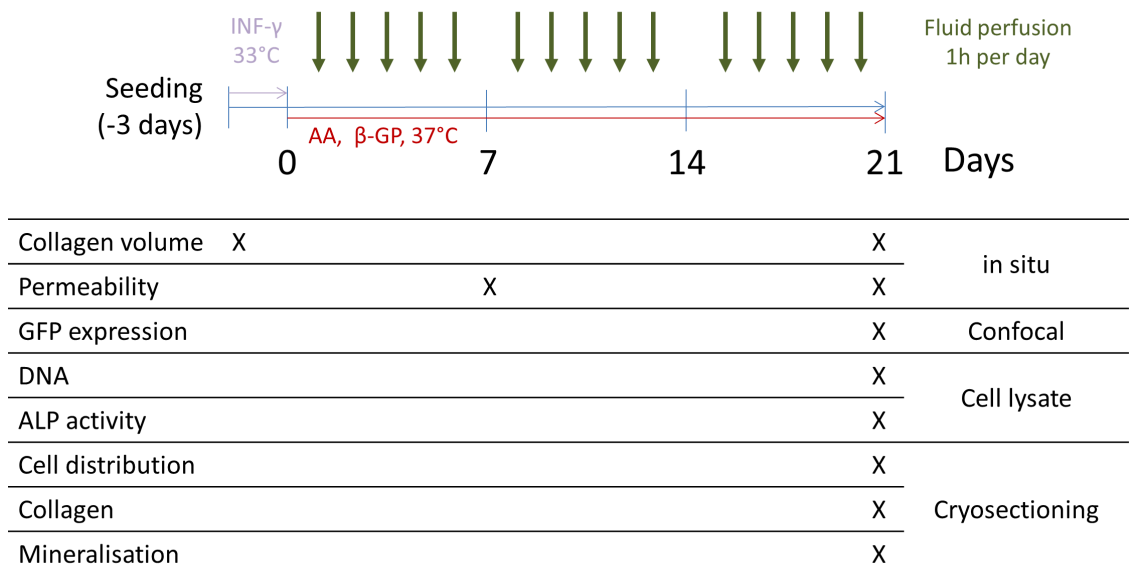
Figure 7.2: Experimental protocol investigating the response of IDG-SW3 to fluid perfusion embedded within 3D collagen hydrogels.

IDG-SW3 cells were embedded in collagen gel and cultured for three days at $33\,°C$ in culture medium supplemented with INF-γ (purple arrow). Subsequently, the temperature was increased to $37\,°C$ and cells were cultured for a further 21 days in culture medium supplemented with β-GP and ascorbic acid (AA) (red arrow). Fluid perfusion was driven by hydrostatic pressure difference and applied five times per week for $1\,h$ (green arrows). Time points of the assays are marked in the table below.

Mineral staining of gel sections

Calcium minerals in the cryosections were stained with alizarin red S (ARS). On the day of analysis, ARS powder was added to distilled water (1%w/v) and filtered through a 0.45 μm filter to remove any undissolved particles. A drop of ARS solution was added to at least six sections per sample for 1 h. Following incubation, the dye was removed and the samples were washed four times with distilled water. Images of the stained samples were taken by bright-field microscopy.

DAPI staining of gel sections

Cell nuclei were stained with 4',6-diamidino-2-phenylindole (DAPI) solution (BD Biosciences, USA) at a concentration of 5 μg/ml diluted in PBS. The solution was added either to fixed sections or to whole collagen gels containing live cells. Fixed sections were incubated in the dark for 30 min. Following incubation, the sections were washed several times in water to remove the DAPI solution. Images of the stained sections were taken by fluorescence microscopy. DAPI staining was also directly applied to live cells embedded in whole collagen gels. Following a 10 min incubation in the dark, the whole gels were washed in PBS several times and imaged by confocal microscopy.

Measurement of DNA and ALP activity of embedded cells

For the measurement of cellular DNA and ALP activity, DNA had to be released from the cells using the same method as described in detail in Chapter 3.2.3. In brief, collagen gels were transferred from the transwell inserts to 1.5 ml microcentrifuge tubes using a spatula. 1 ml of digestion buffer was added to each gel. To facilitate the release of cellular DNA, collagen gels were broken down as much as possible using mechanical agitation with pipette tips. Cell lysates were also briefly vortexed and subjected to a freeze-thaw cycle for three times (10 min at $-80\,°C$, 15 min at $37\,°C$). Finally, the lysates were centrifuged at 10,000 rpm for 5 min. Lysates were stored at $-80\,°C$. DNA was measured using the same method as described in Chapter 3.2.5. ALP activity was determined following the procedure described in Chapter 3.2.12.

7.4.4 Statistics

Data are expressed as the mean $\pm$ standard deviation (SD) of two independent experiments performed in triplicate. Statistical analysis was performed by two way analysis of variance (ANOVA). p values of ≤ 0.05 were considered to be significant and noted '*'; p values of ≤ 0.001 were noted as '**'.

7.5 Results

7.5.1 Development of novel 3D collagen perfusion model

The developed 3D collagen model is one of only a few in vitro models which supports fluid perfusion of a soft collagen matrix. Perfusion was enabled by modifying a commercially available transwell insert. Holes were pierced in the transwell membrane which were big enough to allow medium to flow through the membrane, but small enough to support and stabilise collagen hydrogel within the inserts (Figure 7.3). Cells survived for at least 21 days within the collagen hydrogel. They also appeared to actively remodel the collagen scaffolds as indicated for example by contraction of the collagen scaffold and a significantly lower permeability of cell-containing collagen gels compared to cell-free samples as presented later.

7.5.2 Characterisation of collagen scaffolds

Properties of the collagen scaffolds such as their volume and permeability changed over time. These changes also affected the estimated fluid shear stress sensed by the cells within the collagen scaffolds.

Cells contracted collagen gels

A volume of $151.3\,\text{mm}^3$ of solidified collagen gel was measured in the transwell insert directly following cross-linking. Since $150\,\mu\text{l}$ ($150\,\text{mm}^3$) of liquid collagen solution had been originally added to the transwell insert, the similarity of both values validated the applied measurement method which was based on image analysis.

Both acellular and cellular collagen gels contracted between Day 0 and 21. But only cellular gels reduced their volume significantly by 50% (p≤0.001). In contrast, the shrinkage of acellular gels to around 83% of their original volume was not significant at Day 21. Fluid perfusion did not affect the collagen volume as there was no significant difference between static and flow-mediated samples. In the majority of samples, the gels contracted in the centre of the membrane forming a short 'dome-like' structure. However, sometimes compaction of the gels was also more off-centre or the resulting structures were relatively flat. No defining pattern was observed when comparing the geometry of compacted collagen gels under static or flow conditions (Figure 7.4A).

Permeability decreased in cellular gels over time

Permeability in acellular collagen gels increased slightly from $5.17 \times 10^{-14}\,\text{m}^2$ at Day 7 to $5.93 \times 10^{-14}\,\text{m}^2$ at Day 21 (Figure 7.4B). In contrast, permeability decreased
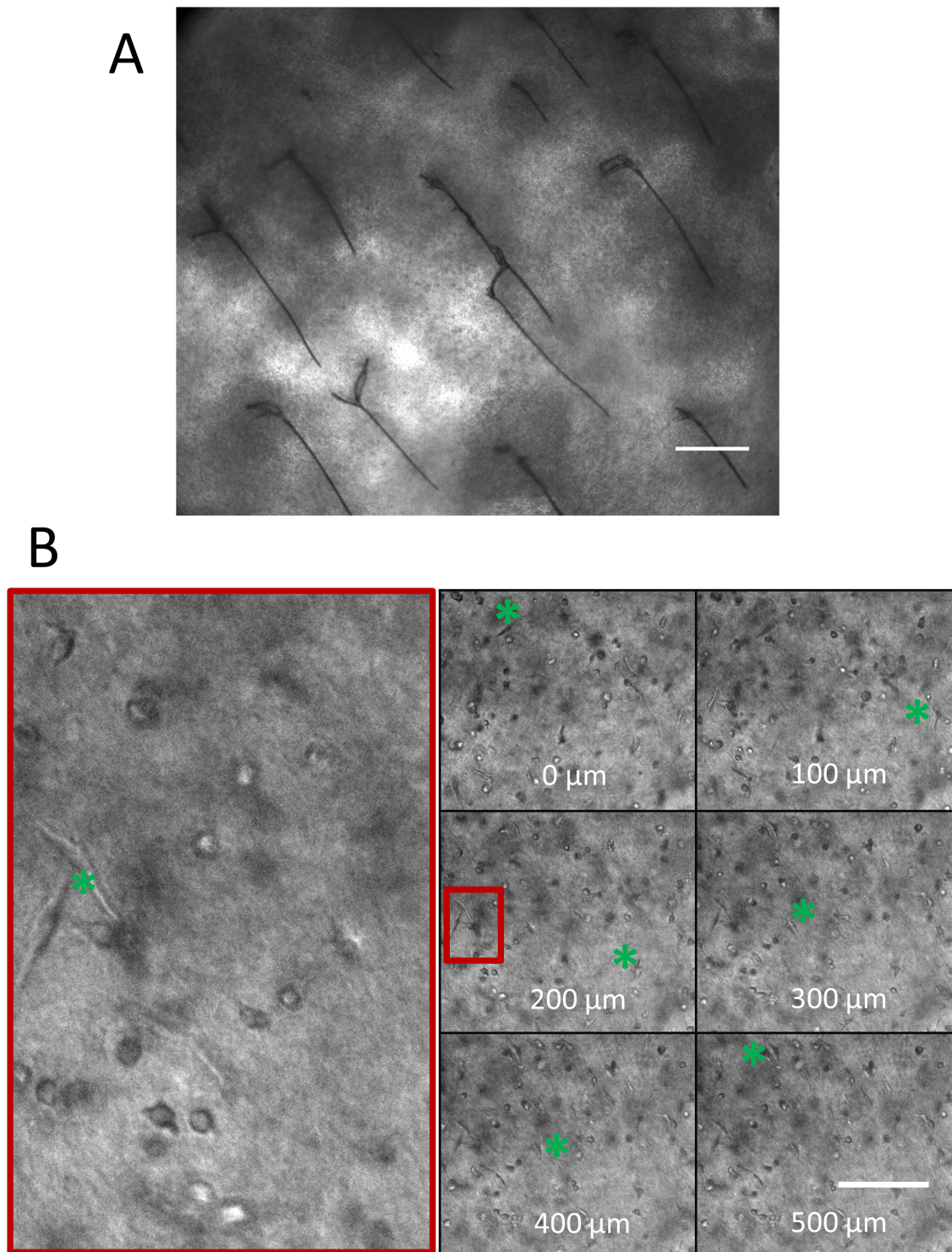
Figure 7.3: Modified transwell insert enabled perfusion of collagen hydrogel.

A: Pierced membrane. Phase-contrast image of membrane with scalpel cuts (black lines). Scale bar = 500 μm. B: Z-stack phase-contrast image of IDG-SW3 embedded in collagen at Day 0. Cells were evenly distributed throughout the collagen hydrogel. Some cells were elongated (green asterisk), while others were rounded up. Panels show every 10th optical slice throughout the z-stack (depth from the first slice is indicated in each panel). The whole file is composed of 50 z-slices that encompass a total thickness of 500 μm. Magnification of part of a panel can be seen on the left in the red-framed image. Scale bar = 100 μm.

significantly over time in collagen gels containing cells from $4.27 \times 10^{-14}\,\mathrm{m^2}$ at Day 7 to $1.21 \times 10^{-14}\,\mathrm{m^2}$ at Day 21 (p≤0.01). Moreover, while permeability was not significantly different between cellular and acellular gels at Day 7, permeability of cellular gels was significantly reduced at Day 21 (p≤0.01).

Fluid shear stress within gels was very low

Fluid shear stress within the collagen hydrogel was estimated using Equation 7.4. At Day 7, the shear stress τ was approximately 1.9 mPa. The reduced permeability of the collagen hydrogel at Day 21 generated higher shear stress of approximately 3.7 mPa within the collagen.

7.5.3   Assessment of osteoblast behaviour in 3D

Cell distribution and proliferation, ALP activity and the deposition of collagen and minerals were assessed to evaluate the effect of 3D culture and fluid flow on IDG-SW3 function.

Fluid flow did not affect cell distribution

Cell distribution was assessed in DAPI stained cryosections (Figure 7.5). Cells were primarily distributed around the edge of the gels. In particular, complete cell layers were found close to the transwell membrane. These cell layers appeared to form a very tight boundary layer which in some locations had a thickness of more than five cells. Interestingly, cells did not only appear on top of the transwell membrane, i.e. the side facing the collagen gel, but also on the bottom of the transwell membrane. The centre of the collagen scaffold was relatively sparsely populated with cells at Day 21. Quantitative assessment of the cell distribution was not feasible as the collagen gels did not always remain intact following cryosectioning. In general, the shape of the collagen and the cell distribution varied widely between samples. No significant differences between fluid-perfused and static samples could be observed both in terms of cell distribution and number of DAPI-stained nuclei.

Fluid flow did not affect DNA content or ALP activity

The amount of measured DNA at Day 21 was not significantly different between static and fluid-perfused samples (Figure 7.6A). The amount of DNA was equivalent to around 500,000 cells per gel. No DNA was detected in cell-free samples (data not shown).

ALP activity which was normalised to the respective DNA measured in the well, was the same when comparing 'flow' and 'no flow' conditions (Figure 7.6B).
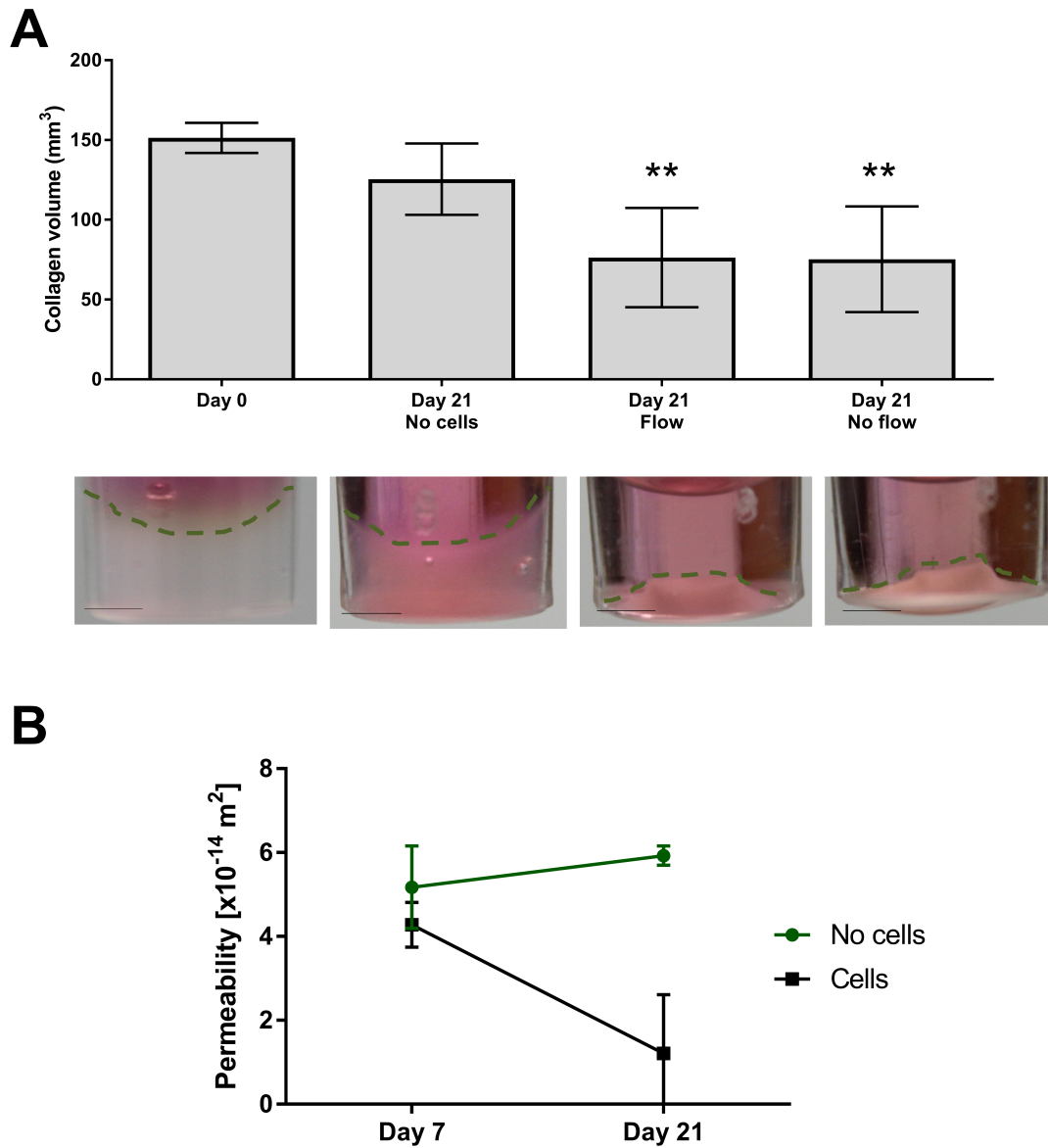
Figure 7.4: Collagen remodelling by IDG-SW3 in 3D culture model.

A: Contraction of collagen following 21 days of culture. Collagen volume was significantly decreased comparing cellular collagen gel volumes at Day 0 and Day 21. There was no significant difference between 'flow' and 'no flow' condition. Images below are representative for each condition and show the collagen in the transwell insert. The edge of the collagen gel is marked with a green dashed line. Scale bar = 2 mm. Significantly different to Day 0 ** $p \leq 0.001$. Mean with SD (n=2-3). B: Permeability of collagen hydrogels. Permeability of cell-containing collagen hydrogels decreased significantly from Day 7 to Day 21 and was also significantly lower than the permeability of cell-free control collagen scaffolds. Mean with SD (n=3).
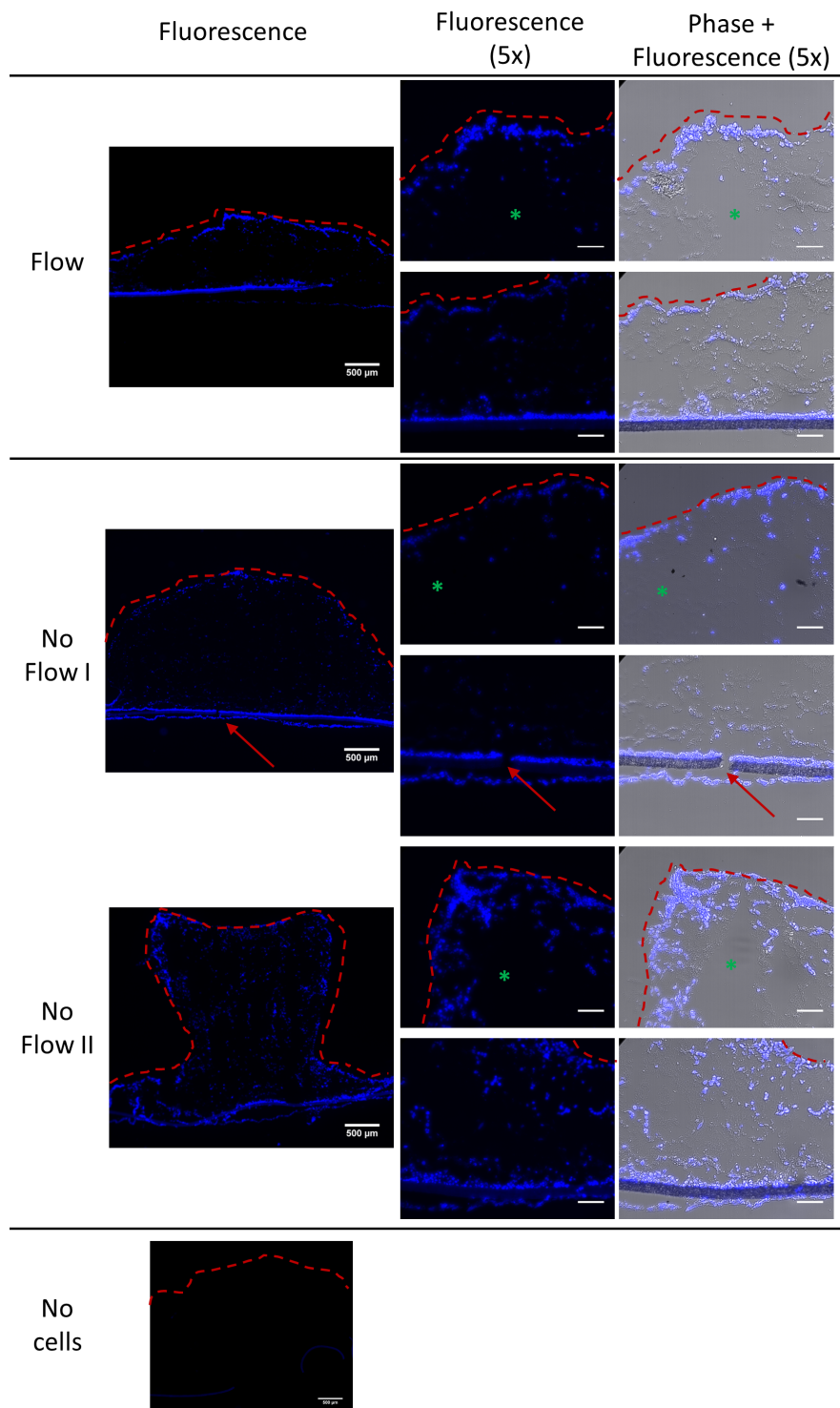
Figure 7.5: Staining of cell nuclei with DAPI in sectioned samples.

Sectioned samples were stained with DAPI at Day 21 and imaged with fluorescence and phase-contrast microscopy. Cells were primarily located around the edge of the gel (red dashed line) and near the membrane. Fewer cells were located within the collagen gel, some samples were also damaged during sectioning (green astrisk). No DAPI stain was detected in the 'no cell'-control. Some images also show the holes in the transwell membrane (red arrow). Scale bar $= 100\,\mu\text{m}$ unless otherwise stated.
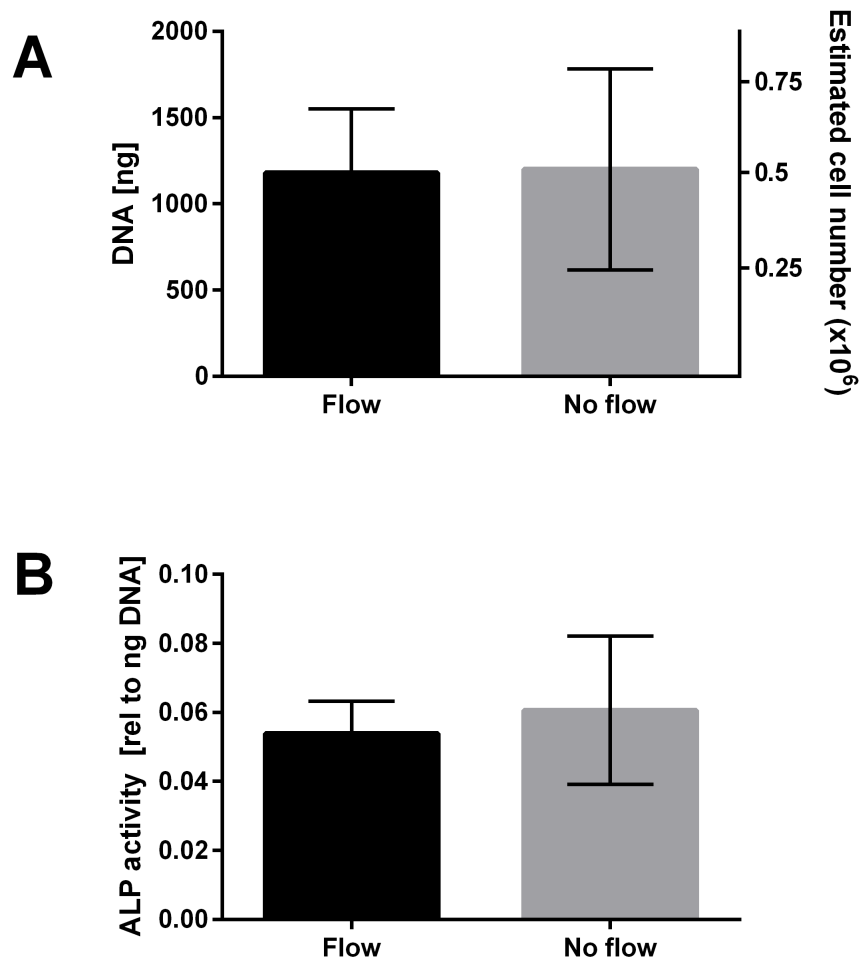
Figure 7.6: Effect of fluid flow on amount of DNA and relative ALP activity at Day 21.

A: Total DNA and estimated cell numbers per well. B: ALP activity relative to DNA per well. No significant differences between static and flow-mediated groups were observed. Mean with SD (n=3).

Collagen staining was more intense in cellular scaffolds

Since PSR stains all collagens and the scaffolds were composed of collagen them-
selves, it was not possible to distinguish exactly between collagen making up the
scaffolds and collagen deposited by the cells. However, the staining for collagen was
stronger in cell-containing samples compared to cell-free samples (Figure 7.7). The
staining was particularly intense in areas where cells were found in high densities
(e.g. around the edge and close to the membrane). Staining of gels which were
subjected to flow appeared to be slightly more intense than static gels. While the
difference in stain between cellular and acellular gels was obvious, the difference
between static and flow conditions was more subtle. Lack of an adequate assess-
ment method prevented a quantitative comparison between static and mechanically
stimulated groups in terms of collagen deposition.

Mineralisation was only observed in cellular collagen gels

Qualitative comparison between cell-containing and cell-free samples showed that
cells were essential for mineralisation. No mineral staining was detected in the acel-
lular samples (Figure 7.8). High intensities of mineral stains were found at similar
locations which also exhibited high cell concentrations, i.e. around the edges of the
collagen gel and near the membrane. Image comparison indicated that there was
no qualitative difference in mineral deposition between 'flow' and 'no flow' samples,
however a quantitative assessment could not be performed with ARS staining.

Osteocytogenesis was not affected by fluid perfusion in 3D cultures

Dmp1-GFP positive cells have been used in this project as a way to assess the
progression of osteocytogenesis in IDG-SW3. Both cell fixing and cryosectioning,
however, have been found to destroy the GFP fluorescence. Confocal imaging of live
cells embedded within the collagen scaffolds was used to image Dmp1-GFP positive
cells (Figure 7.9). Images obtained with this method showed Dmp1-GFP positive
cells in both static and flow conditions. Since not all cells were Dmp1-GFP positive,
it was concluded that not all cells had turned into osteocyte-like cells by Day 21.
The images which had been acquired showed a random distribution of cells which did
not appear to differ between static and flow condition. Dmp1-GFP cells expressed
an osteocyte-like morphology with each cell having several long cell processes.
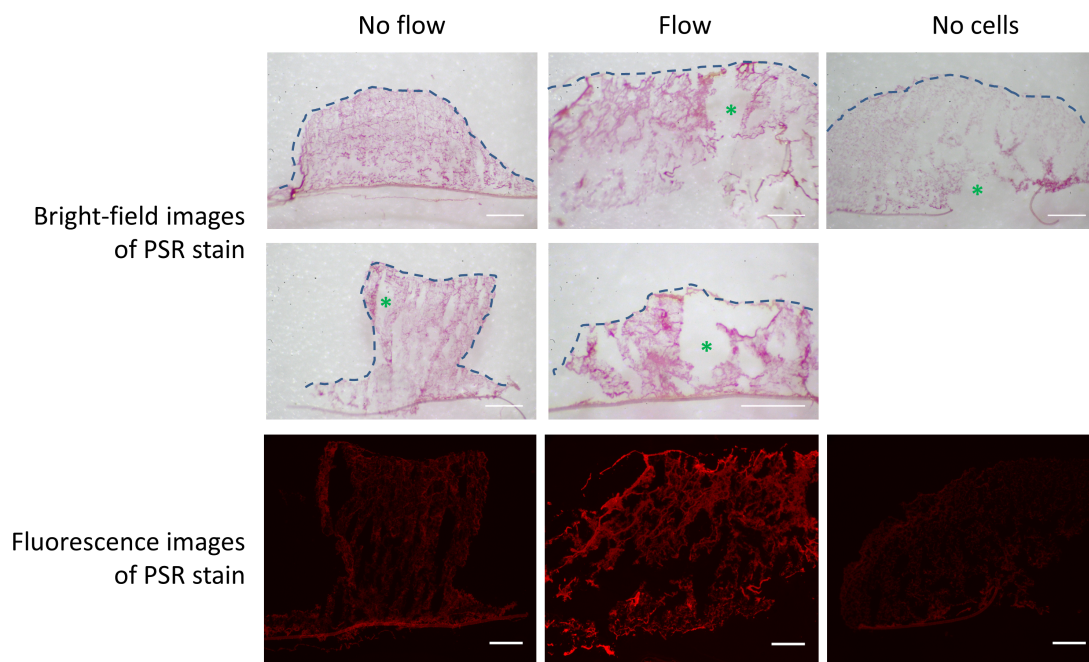
Figure 7.7: Collagen staining in sectioned samples.

Sectioned samples were stained with PSR at Day 21 and imaged with bright-field microscopy and fluorescence microscopy. Less staining could be detected in the 'no cell'-control. Samples became easily damaged during sectioning (green asterisk). The border of the collagen has been marked with a blue dashed line in the bright-field images. Scale bar $= 500\,\mu m$.
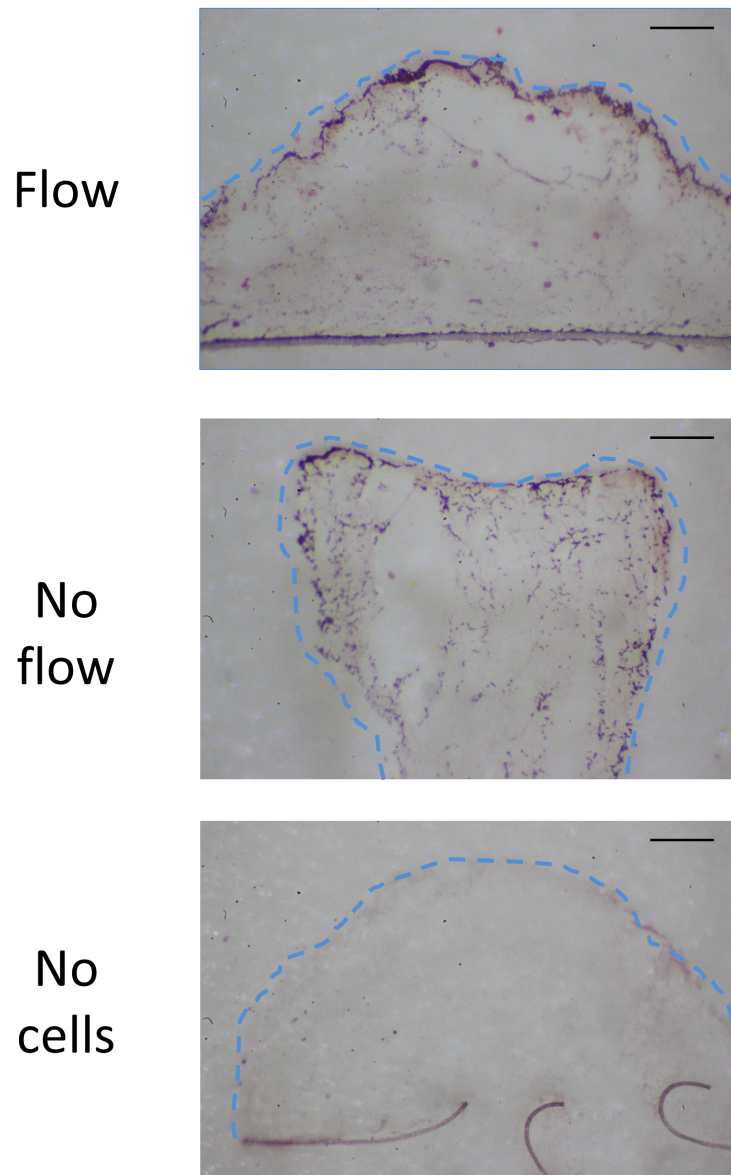
Figure 7.8: Staining of calcium minerals with Alizarin Red S dye in sectioned samples.

Sectioned samples were stained with ARS at Day 21 and imaged with bright-field microscopy. Staining was primarily detected around the edge of the gel (blue dashed line) and near the membrane. No mineral staining was detected in the 'no cell'-control. Scale bar = 250 µm.
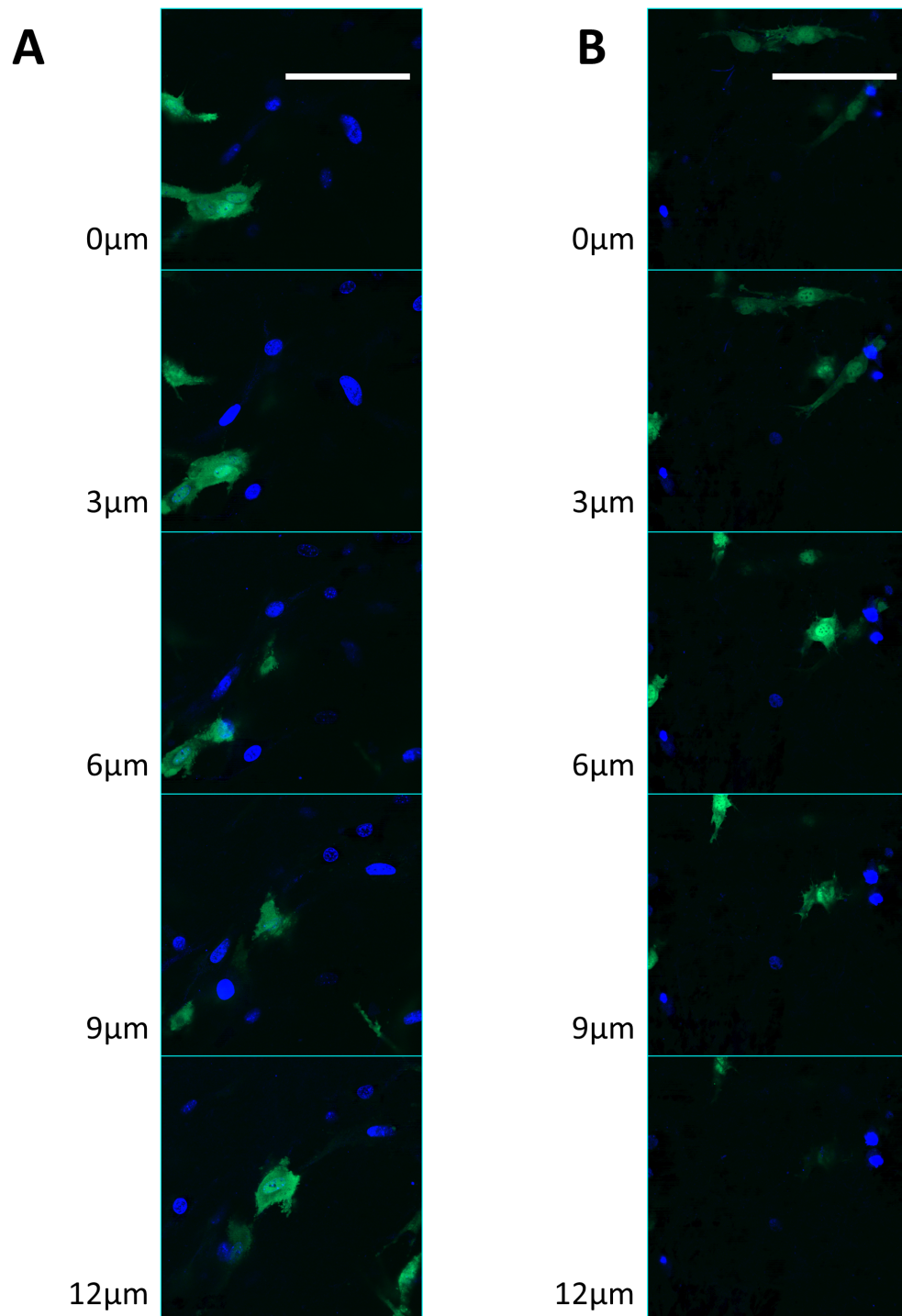
Figure 7.9: Confocal z-stack images of IDG-SW3 in collagen gels stained with DAPI.

A: Flow. B: No flow. Cell nuclei are stained with DAPI (blue) and Dmp1-GFP positive cells fluoresce in green. Z-stack of images of live cells were acquired with a confocal microscope at Day 21. Panels show every 3rd optical slice throughout the z-stack (depth from the first slice is indicated in each panel). The whole file is composed of 13 z-slices that encompass a total thickness of 13 µm. Scale bar = 100 µm.

7.6   Discussion

Collagen is the most abundant protein in connective tissue and therefore used as scaffold in a wide range of in vitro 3D studies (Wang and Tarbell, 2000; Sumanasinghe et al., 2006; Buchanan et al., 2013). However, its weak mechanical properties make it a very challenging substrate to work with, especially in combination with fluid flow. One of the main challenges when working with collagen hydrogel is maintaining its mechanical integrity by preventing compaction of the hydrogel or channelling of the fluid around instead of through the gel (Ng and Swartz, 2003). The few systems, which successfully supported perfusion of collagen gels, maintained their mechanical integrity by anchoring the gel to porous polyethylene (Ng and Swartz, 2003; Ng et al., 2005) or encasing it within PDMS stamps (**polacheck2011**; Vickerman et al., 2008).

The 3D model developed here is the first model to use a commercially available transwell insert for maintaining the mechanical integrity of soft collagen under low fluid perfusion. Transwell inserts are commonly used in co-culture applications, for example to study transport, absorption and secretion of molecules and growth factors (Spector et al., 2002). While the pores in the transwell membrane allow exchange of small molecules, they are too small to support unimpeded fluid flow. This barrier function had to be significantly reduced in order to use transwell inserts for flow studies. Piercing the transwell membrane with a scalpel was found to be a quick and cost-effective way to achieve this goal. Cutting 20 small holes in the membrane resulted in a rapid flow through the membrane. Therefore, it could be assumed that the modified membrane did not significantly reduce the overall permeability of the collagen-transwell membrane construct. Most importantly for this application, the pierced membrane was still effective in maintaining the collagen hydrogel within the transwell insert.

Since piercing the membranes effectively destroyed the original function of transwell inserts, it could be argued that an alternative method avoiding the use of the relatively expensive transwell inserts should be found. However, the use of commercially available, easy-to-use and sterile inserts hugely benefited a prototype development with consistent results. Moreover, the transparent transwell membranes also facilitated microscopy of the collagen layer close to the membrane. A disadvantage of the current fabrication method was the use of a scalpel to randomly pierce holes in the membrane. With this approach no completely identical transwell inserts could be created. Despite this limitation, similar flow rates through the gels were achieved in all samples. Therefore, small variations in the size of the cuts did not appear to affect the overall performance of the inserts. Instead, the flow rate primarily

depended on the permeability of the collagen hydrogel.

Determining the permeability of the collagen-cell substrates was relatively easy with this model applying Darcy's Law (Equation 7.2). Permeability of cell-containing gels decreased significantly from Day 7 to Day 21. This finding is in line with a study by Ng and Swartz (2003) who investigated collagen remodelling by fibroblasts. They hypothesised that the reduction in permeability was due to matrix synthesis and remodelling of the ECM. In line with this hypothesis, stronger collagen staining in cellular gels compared to acellular gels had been observed in this chapter (Figure 7.7). Permeability of cell-free gels on the other hand slightly increased over time, which has also been shown by Ng and Swartz (2003). The increase in permeability might have been caused by slow degradation of the collagen hydrogel, which might also explain the small (but not significant) volume reduction in acellular collagen gels towards Day 21 (Figure 7.4A). Overall, collagen permeability values determined with this method were in the same range as previously obtained values (see Table 7.2).

The ability of this transwell 3D model to estimate scaffold permeability in situ without having to sacrifice the sample is a great feature of this model. In particular since permeability can also be seen as an indirect monitor of matrix integrity. For example, an extremely high permeability indicated that the fluid was not flowing through the collagen gel any more but rather through a hole in the membrane which became exposed due to shrinkage of the collagen gels. Such samples, which failed due to excessive contraction of the gels, had to be excluded from further analysis. Future experiments could take permeability readings at more frequent intervals to gain a better understanding about the remodelling process over time. Such knowledge could be of particular interest as other studies have found that changes in permeability (Ng and Swartz, 2003) or contraction (Parreno et al., 2008) are greatest at the beginning of culture but level off after a couple of days.

As described above, shrinkage of collagen gels due to cell-related contraction is a common complication when working with collagen gels. Cell-induced contraction of ECM is a physiological phenomenon and plays for example a significant role in wound healing (Tomasek et al., 2002) and has also been shown to alter osteoblastic differentiation in vitro (Parreno et al., 2008). In this study, contraction of collagen gels by 50% were observed. Results indicated that cells were the driving force behind the gel contraction as the volume reduction in acellular scaffolds was not significant. The ability of cells to contract collagen gels has been previously reported (Sumanasinghe et al., 2006; Parreno et al., 2008; Sung et al., 2009; Tan and Desai, 2003; Uchihashi et al., 2013). Collagen contraction depends on a variety of factors

such as collagen concentration and cell density (Nirmalanandhan et al., 2006), but results in this study indicated that perfusion of the collagen matrix was not one of them.

Normal osteoblast behaviour, including the deposition of a collagen matrix, mineralisation and increased ALP activity could be confirmed for IDG-SW3 embedded in collagen. For example, collagen staining appeared to be significantly stronger in cellular sections compared to cell-free sections. Although PSR stained both the collagen scaffold and cell-deposited collagen, the increased collagen staining of cell-seeded constructs indicated that cells deposited additional collagen and/or that the collagen concentration was increased due to contraction of the collagen matrix (Figure 7.7). Mineral staining was only observed in cellular collagen gels, demonstrating the ability of IDG-SW3 to mineralise their surrounding collageneous matrix (Figure 7.8). Moreover, ALP activity in IDG-SW3 at Day 21 was also relatively high, even though it was about five times lower compared to the ALP activity of IDG-SW3 cultured in monolayers (Chapter 6).

The expression of Dmp1-GFP in osteocyte-like cells allows straightforward assessment of osteocytogenesis and is one great feature of the cell line IDG-SW3 (Woo et al., 2011). In Chapters 4 and 6, where cells were cultured as monolayers, expression of the fluorescent marker Dmp1-GFP had been successfully quantified with a fluorescence plate reader and by fluorescence microscopy. The two methods, however, could not be applied for IDG-SW3 embedded in 3D collagen gels as the high background noise created by the thick collagen layer prevented accurate measurements or good image acquisition. Although better image resolution of 3D samples could be achieved with confocal microscopy, drawbacks of this technique included that gels had to be removed from the transwell inserts and that only small areas instead of the whole thickness of the gels could be visualised. Despite these limitations, confocal microscopy of DAPI-stained live cells confirmed that part of the IDG-SW3 cells differentiated towards an osteocyte-like Dmp1-GFP positive cell type (Figure 7.9). Furthermore, Dmp1-GFP positive cells exhibited osteocyte-specific dendrites. Overall, the morphology and the expression of Dmp1-GFP by IDG-SW3 embedded in collagen gel was comparable to IDG-SW3 cultured as monolayers in previous chapters. This similarity between monolayer and 3D culture had also been observed by Woo et al. (2011) who cultured IDG-SW3 on collagen gels and sponges.

In contrast to confocal microscopy, cryosectioning allowed a better overview of the cell distribution over the whole cross-section of the gel. The weak material properties of collagen, however, meant that some sections were destroyed during cutting. Moreover, the contours of the collagen scaffolds after 21 days of culture differed

greatly between samples. Both of these limitations meant that quantitative analysis (e.g. number of cells per section, ratio of cells near the gel boundary relative to the centre of the gel) were not feasible or would not provide comparable values. Despite not being able to quantify cell distribution, comparison of different sections showed that cells at Day 21 were distributed in all samples throughout the gels. Even though the distribution was not very evenly, this indicated that the culture medium perfused the whole scaffold as intended. Cells appear most evenly distributed shortly after seeding as shown in z-stack images (Figure 7.3B). In contrast, cryosections obtained at Day 21 of culture showed that the majority of cells were found close to the boundary of the gels. Potentially, nutrient and oxygen concentration might have been lower in the centre of the collagen gels similar to what has been previously observed in spheroid models (Zanoni et al., 2016). These gradients might have initiated cell migration towards the boundaries as osteoblasts are able to migrate within collagen gels (Woo et al., 2011). Moreover, cells might have also preferred the stiffer properties of the transwell membrane compared to the soft collagen gel (Chatterjee et al., 2010). In future experiments, samples should be taken at several time points throughout the culture to be able to better evaluate the temporal progression of cell migration.

Except ALP activity, the transwell 3D model did not facilitate direct comparison between monolayer and 3D culture. Although previous studies have shown that osteoblast differentiation can be enhanced when cultured in 3D scaffolds (Matthews et al., 2014), a wider range of quantitative methods is required to confidently assess the effect of 3D culture on IDG-SW3.

Previous studies have also demonstrated that osteoblasts respond very differently to fluid flow in a 3D environment (Ng and Swartz, 2003). Although IDG-SW3 cultured as monolayer have failed to respond to low FSS generated with a see-saw rocker in Chapter 6, the hypothesis for the present chapter was that IDG-SW3 would be more sensitive to fluid flow in 3D. However, results from this chapter suggest that IDG-SW3 also did not respond to low fluid flow when embedded in a 3D collagen matrix. Qualitative image analysis, for example, indicated that fluid stimulation had no effect on cell distribution, cell morphology and the proportion of Dmp1-GFP positive cells (Figure 7.9). DNA measurements further confirmed that fluid stimulation had no effect on the number of cells per scaffold. This finding was in line with the monolayer results from Chapter 4 and 6, where cell numbers were also not affected by mechanical stimulation. In 3D culture, estimated cell numbers increased from originally 52,500 cells per insert to approximately 500,000 cells per insert at Day 21. This rate of increase was similar to the one observed when IDG-SW3 were cultured as monolayers in Chapter 6. ALP activity was also

not significantly different between static and flow conditions. Moreover, collagen staining and mineral staining did not qualitatively differ between the two groups, however quantitative assessment methods should be explored further in the future.

Although flow rate measurement through the collagen was relatively straight-forward, tracking the fluid pathway was more challenging and has not been achieved yet. Therefore, no information can be provided on whether fluid evenly diffused the collagen scaffold or whether it followed primarily certain 'routes' through the collagen. Tracking of air bubbles (Wang and Tarbell, 2000; Ramanujan et al., 2002) or fluorescent beads (**polacheck2011**) could provide a solution for visualising the fluid pathway in the future. However, in contrast to **polacheck2011** who tracked the horizontal movement of fluorescent particles through a very thin layer of collagen in a microfluidic set-up, vertical fluid flow through a several hundred micrometer thick collagen layer hindered such analysis in this chapter. Therefore, only bulk properties of the collagen gel could be generated and calculations of the shear stress were based on these bulk properties only.

Based on the bulk properties, shear stress within the collagen hydrogel was estimated to be only a few millipascal ($<3.7\,\mathrm{mPa}$). Such low shear stress levels have also been calculated in other 3D perfusion reactors (Sikavitsas et al., 2005; Wang and Tarbell, 2000). Compared to a maximum shear stress of $50\,\mathrm{mPa}$ generated with the seesaw rocker in Chapter 6, shear stress in the 3D collagen scaffold was estimated to be more than one magnitude smaller. However, this is a very rough estimation of the shear stress which assumes for example even perfusion of the collagen hydrogel. Furthermore, a direct comparison of shear stress between monolayer cells and 3D scaffolds may not be relevant as the mechanical environment is more complex in 3D. For example, shear stress in 3D can also be transmitted to ECM fibres leading to ECM strain and thus cytoskeletal strain transmitted via integrins which can further increase the stress sensed by cells in 3D (Ng and Swartz, 2003).

Collagen's weak bulk mechanical strength and its low mass fraction are limitations of the current model (Cross et al., 2010). In particular, contraction of the gel during culture resulted in very different scaffold shapes making analysis and comparison between different samples challenging. One way to improve the biomechanical properties of collagen scaffolds might be the use of pre-compressed collagen scaffolds instead of highly hydrated collagen gels which would also produce a more in vivo-like high mass fraction matrix (Serpooshan et al., 2010).

The main limitation of the current transwell model is the use of a thick collagen layer which hindered effective cell assessment in situ. For example, visualisation of Dmp1-GFP positive cells was only possible using confocal microscopy which required

sacrificing the samples. Moreover, assessing the mineralisation required cryosectioning which easily damaged the samples and thus prevented quantitative analysis. Cryosectioning is also not well suited for high-throughput approaches. Another limitation caused by the thick collagen layer was the failure to precisely characterise fluid flow within the collagen gel. Hence, it was difficult to estimate the mechanical environment of the cells. Finally, migration of some of the cells towards the boundary layer of the collagen indicated that conditions within the gel were not homogeneous probably due to its size. Embedding cells in a thinner collagen layer might help to solve several of the previously mentioned problems. For example, thin gels would provide similar culture conditions throughout the whole sample and facilitate in situ observation. However, thin gels are also more likely to break in particular in combination with fluid flow.

In conclusion, to better understand the effects of low FSS on bone cells, an in vitro transwell 3D model was developed. Although this model was initially tested with osteoblast-like cells, it has the potential to be also used with other cells experiencing interstitial flow. Similarly, instead of collagen other hydrogels could be used as matrices. The main design features of the presented model were: 1) it facilitated easy set-up by using commercially available transwell inserts, 2) it allowed tracking of matrix remodelling via changes in permeability, 3) it allowed measuring the contraction of the ECM, and 4) it could be maintained over long periods of time to allow observation of cell and matrix organisation changes. Moreover, this model replicated very well the in vivo environment of osteoblasts, which become embedded within collageneous osteoid before they differentiate towards osteocytes.

7.7 Summary

- A novel 3D model which supported fluid perfusion of a collagen scaffold using a modified transwell insert was developed.

- The model allowed in situ measurements of permeability and contraction of the collagen scaffold.

- Cell viability was maintained for more than 21 days.

- Hydrostatic pressure-driven flow had no impact on cell numbers, collagen deposition, mineralisation, ALP activity, osteocytogenesis and cell-driven ECM remodelling in the cell line IDG-SW3.

- A limitation of the model was the thickness of the collagen scaffold which prevented quantitative assessment of cell distribution, mineralisation, collagen deposition and expression of the osteocyte marker Dmp1-GFP.

Chapter 8

Modular assembly of a microfluidic 3D collagen bioreactor

8.1 Introduction

In the previous chapter a 3D collagen model was developed to investigate whether interstitial fluid flow can enhance osteoblast-to-osteocyte differentiation. The model consisted of a commercially available transwell insert which maintained the collagen's mechanical integrity under fluid flow. Despite the model supporting fluid perfusion of the collagen scaffold and cell viability for over three weeks, it had a number of limitations which prevented effective assessment of cell behaviour. The thickness of the collagen layer was one of the main drawbacks and hampered cell imaging and observation of the fluid pathway through the gel. The latter could have provided valuable information on whether uniform perfusion of the collagen gel was achieved despite there only being very few, randomly distributed holes in the transwell membrane. In addition, quantitative comparison of different samples was challenging due to contraction of the scaffolds and their weak mechanical properties. Moreover, fluid flow could not be controlled easily as it was solely driven by hydrostatic pressure. Aiming to address most of these limitations, this chapter explores ways to improve the model by creating a microfluidic 'organ-on-a-chip'.

Organs-on-chips are in vitro models which go further than conventional 3D models (Huh et al., 2011). Organs-on-chips try to resemble the natural environment of cells as a whole. They aim to mimic all critical tissue functions including mechanical stimulation and cell-extracellular matrix (ECM) interactions, but also cell-cell communication as well as replicating biochemical gradients (Huh et al., 2012). Another important feature of organs-on-chips is their small size.

Miniaturisation provides great opportunities for biological assays since it reduces the required volumes of expensive compounds and also decreases transport distances of molecules which results in faster reaction times. Considering that conventional screening methods for new drugs from huge libraries are costly and time-consuming, miniaturisation can provide an advantage in drug discovery (Xu et al., 2011). Moreover, smaller length scales are more relevant to the natural environment of cells for example when considering transport distances of oxygen and nutrients. The physical conditions in miniaturised devices are also different compared to experiments performed on a macroscale and have been extensively studied and reviewed by Beebe et al. (2002).

Techniques which were originally developed for the fabrication of integrated circuits on computer chips can decrease the size of in vitro test devices by creating structures in the micrometer range. Unlike in vitro devices, computer chips are made of silicon wafers using additive and etching processes as well as photolithography. Such techniques require specialised equipment as well as a clean room environment and are therefore not suited for most biological labs. In addition, silicon is a stiff material which is very different from the natural environment of most cells. Therefore, elastomers such as polydimethyl siloxane (PDMS) are preferred for micro-engineering biological testing devices (Berthier et al., 2012). Elastomers have the additional advantage that defined micro-structures can be easily created with soft lithography (Figure 8.1). In this technique an initially liquid pre-polymer is poured into a mould which then readily converts into a solid elastomer by cross-linking (Xia and Whitesides, 1998). Soft lithography is not only remarkable for its simplicity but is also characterised by its low cost and adaptability to a wide range of elastomeric biomaterials. These materials can be further patterned with molecules to provide cellular niches for different cell types (Whitesides et al., 2001).

Integration of microfluidic systems in organs-on-chips ensures continuous delivery of nutrients, removal of waste and a defined mechanical stimulation in form of shear stress to cultured cells. Due to the small size of the microchannels on organs-on-chips, laminar flow is the dominant flow regime in microfluidic channels. Microfluidic systems have several magnitudes higher surface area to volume ratio compared to macroscale systems. Although this benefits faster reaction times, the absorption of molecules in the surrounding material becomes also more important. This might be a problem when using PDMS, since this material is known for its ability to absorb hydrophobic small molecules (Toepke and Beebe, 2006). Furthermore, capillary forces become the dominant forces in microfluidic systems due to the increased surface tension in microchannels. Gravitational forces on the other hand, which directed fluid flow in the previous chapter, can often be neglected on this length
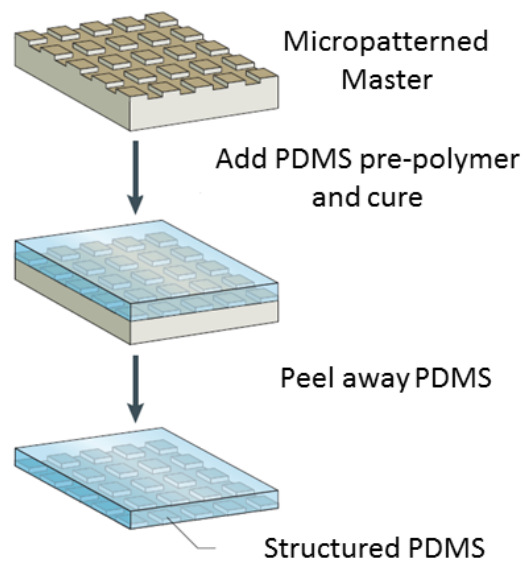
Figure 8.1: Fabrication process to generate micropatterned structures with soft lithography.

Soft lithography requires the fabrication of a micropatterned master (= mould). Liquid pre-polymer PDMS is poured on the master, thermally cured and peeled away. The resulting layer of PDMS has the micro-structure embossed in its surface and the same mould can often be used multiple times. Image adapted from Weibel et al. (2007).

scale due to the use of small volumes (Tabeling, 2010).

In addition to mimicking the physiological conditions, organs-on-chips also aim to be compatible with high-throughput strategies. This is an essential requirement in the pharmaceutical industry and had not been sufficiently achieved with the system in the previous chapter. Key features of high-throughput systems include easy assembly and set-up but also automated analysis of cell behaviour using techniques such as light or fluorescence microscopy and microplate reader assays. This is another reason why transparent materials, in particular the previously described elastic PDMS, are used as materials for organs-on-chips (**huh2010**; **kim2012**). Despite the use of transparent materials, combination of conventional hydrogel-based 3D culture with high-throughput applications remains challenging since assessment of cellular viability and phenotype often still requires specialised histology and optical techniques (Su et al., 2014).

Modular assembly of 3D structures might be one way to solve the high-throughput issue while still mimicking the natural 3D multi-cellular environment found in the body. The idea of modular assembly has been applied for example in the 'Cells-in-Gels-in-Paper' approach (Deiss et al., 2013) and has been further refined in the 'Cells-in-Gels-in-Mesh' approach (Simon et al., 2014; Simon et al., 2015). Both methods generated 3D cultures by stacking approximately 200 µm thick paper sheets or meshes filled with cell-containing hydrogels on top of each other. Co-culture of different cell types in spatially defined areas was enabled by stacking sheets containing different cell types. Moreover, easy visualisation was supported by the possibility to take apart ('de-stack') these stacks. Since meshes had relatively big openings, the 'Cells-in-Gels-in-Mesh' approach even supported light microscopy. Furthermore, patterning of the sheets with wax or parafilm created compartments similar to 96-well plates which supported a high-throughput analysis. The 'Cells-in-Gels-in-Paper' method has been used to develop a model for cardiac ischemia by establishing a gradient of oxygen and glucose (Mosadegh et al., 2014). However, neither of the two methods has been combined with mechanical stimulation yet. Therefore, combination of a modular 'Cells-in-Gels-in-Mesh' approach with an integrated microfluidic system could be used to generate an organ-on-a-chip which mimics the natural, dynamic environment of osteoblasts embedded in osteoid within the bone.

A wide range of organ-on-a-chip systems have been successfully developed which try to mimic critical functions of organs such as the lung (**huh2010**), gut (**kim2012**), liver (Nakao et al., 2011; Li et al., 2014), heart (Agarwal et al., 2013), kidney (Jang and Suh, 2010; Wilmer et al., 2016) and brain (Park et al., 2015). Even multi-organ models which combine for example liver and skin models (Wagner et al., 2013)

have already been created. However, only few systems try to resemble the bone microenvironment. Bersini et al. (2014) developed a bone model where they cultured osteo-conditioned stem cells in collagen gels to study the invasiveness of highly metastatic cancer cells. Another study investigated the osteoblast mechanosensitivity by comparing static and flow-mediated culture of osteoblasts (Altmann et al., 2014). The study by Gu et al. (2015) focussed on recreating 3D osteocyte networks in mature bone by assembling osteocytes with microbeads in a microfluidic culture chamber. A bone marrow-on-a-chip has also been developed in which bone marrow was generated first in mice in vivo and then explanted and maintained in vitro within a microfluidic device (Torisawa et al., 2014). However, to the author's knowledge a bone-on-a-chip which specifically focusses on the osteoblast-to-osteocyte transformation and the stage where osteoblasts embed themselves in soft osteoid has not been developed yet.

8.2 Hypothesis

A modular approach is better suited than conventional 3D models for investigating the effect of fluid flow on cells embedded within a three-dimensional collagen scaffold.

8.3 Aims

To investigate this hypothesis, the aim was to create an organ-on-a-chip mimicking soft tissue by further advancing the Cells-in-Gels-in-Mesh model through the addition of a microfluidic perfusion system. Specifically, the following features were defined for the microfluidic 3D collagen bioreactor:

- The mesh should support the mechanical integrity of collagen but also facilitate light microscopy.

- The mesh-sheet should consist of a hydrophilic region that allows seeding of cells embedded in collagen gel and hydrophobic barriers that confine the seeded cells.

- The cell culture platform should consist only of materials that are non-toxic to cells and are easy to sterilise.

- The thickness of the mesh-sheet should be $<200\,\mu m$ to not limit the mass transport of oxygen and other nutrient molecules or waste products within a single sheet and to facilitate light microscopy.

- In situ cell observation should be supported using transparent materials and a reversible assembly method.

- Controlled perfusion of the the mesh-sheet should be enabled by integrating a microfluidic circuit.

8.4 Materials and Methods

8.4.1 Materials

All materials and reagents were purchased from Sigma-Aldrich (UK) unless otherwise stated.

8.4.2 Methods

Design concept for microfluidic 3D collagen model

Cells were embedded within a thin collagen layer. The collagen layer was supported by a woven polylactic acid (PLA) mesh which suited this application best compared to other meshes which had also been tested (see 8.5.1). The PLA mesh was partly encased in a PDMS sheet to provide more structure to the mesh. Wrapping the mesh in PDMS also controlled the size and thickness of the collagen scaffold. Moreover, the PLA mesh also allowed the culture of two different cell types on either side of the mesh, hence providing spatially controlled co-culture conditions. Fluid flow was guided through the collagen layer by placing two thin PDMS sheets containing microfluidic channel structures above and below the collagen layer. Overall, the device consisted of three thin PDMS sheets containing a microfluidic channel, a collagen scaffold and another microfluidic channel from top to bottom (Figure 8.2).

Preparation of moulds

The three PDMS sheets, which made up the microfluidic device, were created by soft lithography (Figure 8.1). This technique required the fabrication of moulds which were made of vinyl stickers, duct tape and laser printer transparency film.

After assessing several materials, duct tape was selected as the best material to create a mould for the PLA mesh-based PDMS sheet. Two rectangular pieces (0.5 mm x 4 mm) of duct tape (3M, USA) were applied to opposite sides of a PLA mesh (Yamanaka, Japan). The duct tape was cut with a desktop digital craft cutter (Robocut, Graphtec, Japan). The duct tape pieces which masked part of the mesh would create a PDMS-free zone on the PLA mesh. A rectangular duct tape frame (20 mm x 50 mm) defined the border of the mould. The bottom of the mould was formed by a laser printer transparency film (3M, USA) to which the duct tape frame was firmly attached. The PLA mesh was placed on top and held in place by another duct tape frame which was firmly attached to the frame below (Figure 8.3A).

Vinyl stickers with a very smooth surface were used as material for the flow channel moulds. Outlines of the channels were cut from vinyl sticker sheets with a desktop
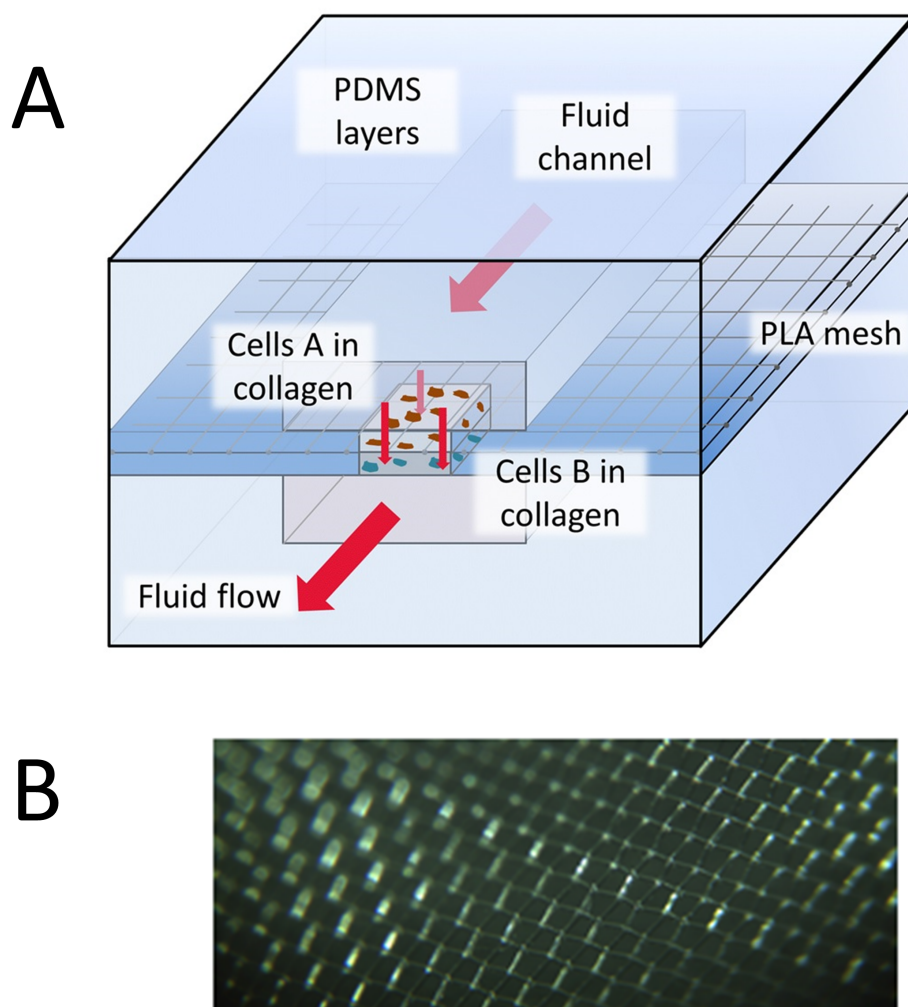
Figure 8.2: Design concept for microfluidic 3D collagen bioreactor.

A: Schematic drawing of stackable 3D collagen model. The bioreactor consisted of three thin PDMS sheets containing a microfluidic channel, a collagen scaffold and another microfluidic channel from top to bottom. Red arrows symbolise the direction of fluid flow which perfused the collagen layer. B: Photograph of woven PLA mesh. The PLA mesh maintained the mechanical integrity of the cell-laden collagen layer under fluid perfusion. The woven, transparent mesh had 250 µm big openings.

digital craft cutter. The channel designs were created using the free and open source vector graphics software Inkscape (available from http://inkscape.org). The fluid channel on the top was 0.8 mm wide, 30 mm long and 160 µm high. The fluid channel on the bottom had the same dimensions but was 15 mm longer. The height of the channels was determined by the number of vinyl stickers stacked on top of each other. Since one layer of vinyl was approximately 80 µm thick, two vinyl stickers were stacked on top of each other before cutting. To create the moulds, the vinyl channels were attached to a laser printer transparency film, making sure that no air bubbles or wrinkles were trapped. A 2 mm high rectangular PDMS frame (20 mm x 75 mm) formed the border of the mould and was placed around the vinyl channels on top of the transparency film (Figure 8.3B).

Polydimethyl siloxane casting

PDMS pre-polymer was prepared by thoroughly mixing elastomer and curing agent at a 10 parts to 1 part ratio (Sylgard 184, Dow Corning, USA). The mixture was placed in a vacuum desiccator (Diener, Germany) for around 15 min to remove entrapped air bubbles from the solution. The highly viscous pre-polymer solution was cast in the previously prepared moulds and returned to the vacuum chamber for a further 15 min. A laser printer transparency film was carefully added on top of the moulds ensuring that no air bubbles were trapped between the two transparency films. The construct was then sandwiched between two microscope glass slides which were hold together tightly by at least two foldback clips aiming to create smooth and even PDMS surfaces. PDMS was cured for 30 min at 100 °C in an oven (Frigidaire, UK). PDMS in PLA mesh-containing moulds was cured at lower temperatures (<80 °C) for at least 1 h to prevent melting of the PLA mesh. After all parts were fully cured and had cooled down, the moulds were taken apart, vinyl stickers and duct tape were removed and 20 mm wide and 75 mm long PDMS rectangles were cut. To enable fluid flow through the device, four 2 mm holes were punched in the top microfluidic PDMS sheet and and two holes in the mesh-containing PDMS sheet respectively (Figure 8.3C and D).

Cleaning and sterilisation of parts

PDMS sheets were cleaned with acetone, ethanol and water successively. Dust particles and fine fibres were removed from the PDMS sheets with Scotch Tape (3M, US). To increase hydrophilicity, PDMS surfaces which were later in contact with fluids were air plasma treated for 30 s in a plasma machine (Diener, Germany) and stored in deionised water until assembly. All parts including the tubing, were
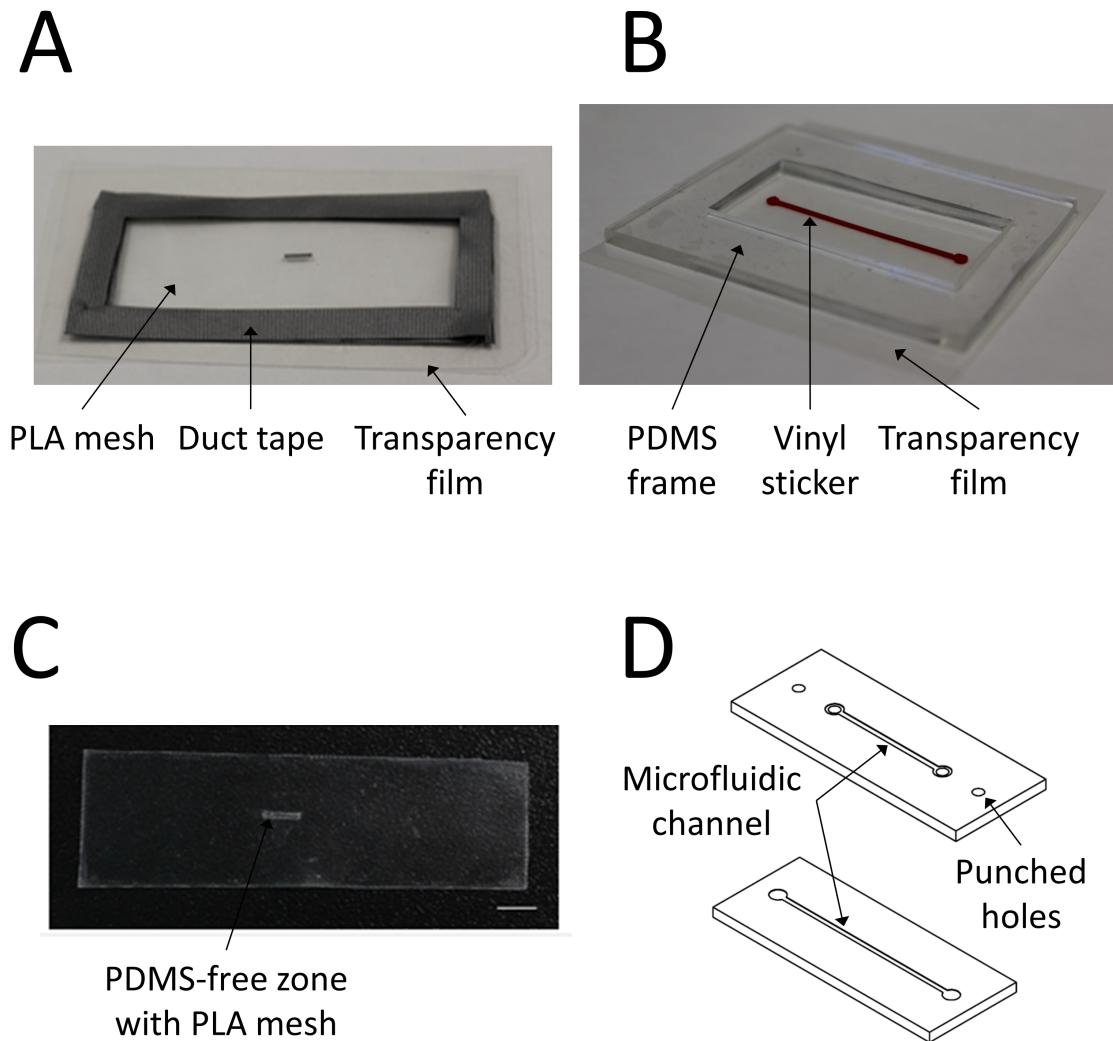
Figure 8.3: Fabrication of PDMS sheets for microfluidic bioreactor.

A: Mould for PDMS casting of mesh-containing sheets. Part of the mesh was masked by duct tape to create a PDMS-free zone. B: Mould for PDMS casting of microfluidic channels. C: PDMS sheet after casting and curing. Duct tape created a PDMS-free zone on the PLA mesh for the application of collagen D: CAD drawing of PDMS sheets with microfluidic top and bottom channels. Scale bar $= 500\,\mu\mathrm{m}$.

sterilised by washing them with 70% ethanol and rinsing them with sterile water. Moreover, all parts were exposed to ultra violet light for 10 min.

Filling of mesh-based PDMS sheets with collagen

In Chapter 7, IDG-SW3 were embedded in 2 mg/ml rat-tail collagen hydrogel. Initial experiments with the same hydrogel showed that a concentration of 2 mg/ml provided insufficient mechanical stability to maintain the gel's integrity within the mesh-based PDMS sheet. To increase the stiffness of the collagen gel, a collagen gel of higher concentration was required. Since bovine collagen solution was available at a higher initial concentration of 5 mg/ml (Thermo Fisher Scientific, UK), bovine instead of rat-tail collagen solution was selected for this experiment. Preliminary experiments suggested that cell behaviour was not significantly different between rat-tail and bovine based collagen gels and that both mechanical integrity and cell spreading were well supported in bovine collagen gel of 3 mg/ml. Collagen gel was prepared by adding 10x PBS, 1 M NaOH and water or cell suspension at the appropriate volumes. The final cell concentration of 5×10^5 cells per ml gel was slightly higher than in Chapter 7 to ensure a sufficient number of cells per chamber. MLO-A5 were used as cell model and were cultured in proliferation medium (see Table 3.2). Alternatively, the cell suspension was replaced by yellow-green fluorescent microspheres with a diameter of 2 μm (FluoSpheres, Thermo Fisher Scientific, UK) in case no cells were embedded. 1.5 μl of the collagen solution was applied per chamber using a micropipette. A PDMS frame which could easily be sterilised and placed in a petri dish raised the PDMS-collagen sheet from the ground and thereby enabled even filling of the chamber. A small drop of water was added to the petri dish to prevent drying of the collagen gel during incubation. The petri dish with the collagen-PDMS sheet was sealed with parafilm to prevent evaporation of water and was placed in an incubator for 30 min for cross-linking (Figure 8.4A).

For static culture, the collagen-filled PDMS sheets were cultured in 35 mm-diameter petri dishes filled with proliferation medium for 96 h. Alternatively the sheets could be used for perfusion experiments within the microfluidic device.

For co-culture experiments, chambers on either side of the mesh were filled independently of each other. After filling the first chamber following the procedure described above, the PDMS slab was placed in the incubator for 20 min to initiate gelling of the collagen. Next, the PDMS slab was turned over and the other chamber was filled with collagen solution and returned back to the incubator for another 30 min. To differentiate between the two collagen solutions, yellow-green beads were added to one of the solutions and red beads were added to the other one.

Assembly of microfluidic device

Two PDMS sheets with microfluidic channels and one PDMS sheet containing the collagen-cell scaffold were assembled by placing them on a regular microscope glass slide. The top of the bioreactor was formed by a 3 mm thick acrylic sheet (25 mm x 60 mm) which contained 3 mm diameter holes for inlets and outlets. These holes were filled with PDMS. After the PDMS was cured, 1 mm holes were punched into the silicone enabling optimal sealing of the tubes which would later pass through these holes. Microscope slide, PDMS sheets and acrylic sheet were tightly held together by four 12 mm foldback clips (Figure 8.4B).

Fluid perfusion

Tubing made of fluorinated ethylene propylene with an outer diameter of 1 mm (Fisher Scientific, UK) was connected to the device through the holes in the acrylic sheet. The two inlets were attached to a needle (25G, Greiner Bio-One Ltd, UK) and a 5 ml syringe (Thermo Fisher Scientific, UK) on the other side. Fluid perfusion was regulated with programmable syringe pumps (AL1000-220, World Precision Instruments, UK). Cell culture medium was degassed in a vacuum chamber overnight prior to each experiment to decrease the chance of bubble formation. After initiating the fluid flow, the complete assembly was transferred to a humidified 37 °C incubator for long-term culture. Syringe pumps were placed in a customised airtight container protecting the pumps from high humidity in the incubator.

Cell viability assay

The PDMS sheets with the cell-laden collagen gels were cultured for 96 h under static conditions in a petri dish. A live/dead cell viability assay was performed to assess the survival rate of cells within the collagen gels. Cell sheets were washed twice with DPBS and stained with 200 µl solution of 2 µM calcein AM (Thermo Fisher Scientific, UK) dissolved in dimethyl sulfoxide (DMSO) and 4 µM ethidium homodimer-1 (EthD-1). The sheets were incubated for 30 min in the dark at room temperature. Cells were washed twice with DPBS. Labelled cell sheets were observed under a fluorescence microscope. Live cells converted the non-fluorescent cell-permeable calcein AM to the intensely fluorescent calcein (excitation 495 nm, emission 515 nm). EthD-1 could only enter dead cells through damaged membranes and produced a bright red fluorescence when binding to nucleic acids in dead cells (excitation 528 nm, emission 617 nm).
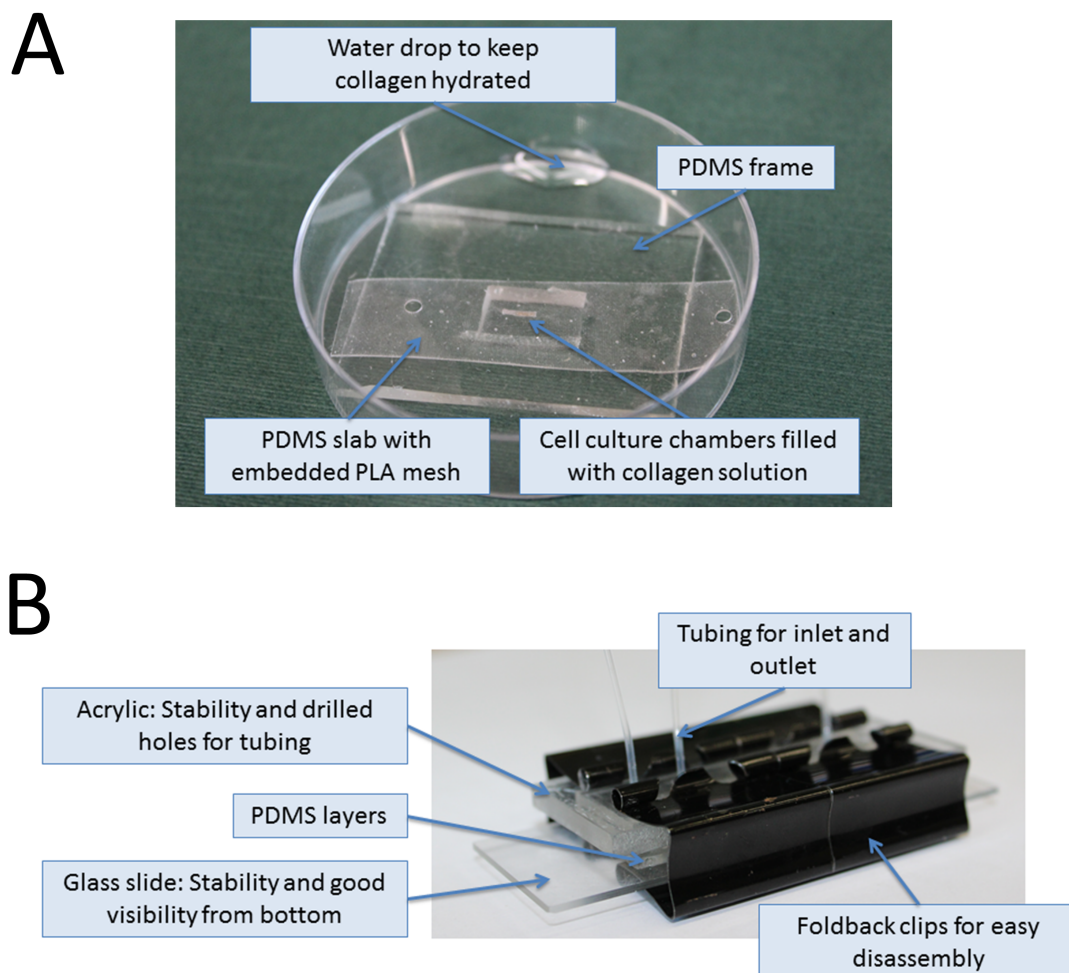
Figure 8.4: Assembly of microfluidic chamber.

A: Photo of set-up for filling the mesh-based PDMS sheet with cell-collagen solution. The PDMS sheet was raised using a customised PDMS frame to prevent contact between PLA mesh and the bottom of the petri dish. A drop of water was placed in the petri dish to prevent drying of the collagen during cross-linking. B: Photo of microfluidic bioreactor after assembly. Foldback clips allowed a secure positioning of the different parts while also enabling easy disassembly.

8.5 Results and Discussion

The aim of this chapter was to improve the 3D transwell collagen model from the previous chapter by using thin collagen sheets instead of bulk collagen. 3D structures have been previously created by assembling thin hydrogel sheets which were supported by paper or polymer meshes (Deiss et al., 2013; Simon et al., 2014).

8.5.1 Woven mesh was selected as collagen support

Unlike paper, mesh has the advantage that it can be combined with microscopy as its openings are normally big enough to prevent light scattering. Therefore, a polymer mesh was considered most suitable as support for collagen gel. A previous study by Simon et al. (2014) has assessed several polymer meshes regarding their suitability for being stackable and supporting hydrogels. They found poly(ethylene terephthalate) (PET) the most suitable material compared to polymer meshes made of poly(propylene), nylon and PEEK. PLA is another biomaterial which is not only characterised by its excellent biocompatibility and transparency, but also by its processability which allows the easy production of thin threads and meshes. Therefore, this study investigated whether PLA could be used as barrier substrate by comparing it to two other materials. In total four different mesh types were evaluated regarding their suitability to support the mechanical integrity of collagen while also facilitating in situ light microscopy. The investigated materials were (1) a woven PLA mesh with 250 µm openings, (2) a PLA mesh with irregular openings of around 30 µm which had been created by manually pushing the threads of the PLA mesh together, (3) a woven polypropylene mesh with 105 µm openings, and (4) a knitted nylon mesh with average openings of 30 µm taken from a pair of commercially available tights (Figure 8.5).

The pores of the knitted nylon mesh and the irregular openings of the PLA mesh were too small to facilitate light microscopy. Although the polyethylene mesh had slightly bigger openings (105 µm), microscopy was still impeded due to the thickness of the polyethylene threads. In contrast, the transparent, biocompatible PLA mesh with its regular pore size of 250 µm facilitated light microscopy and cell culture. PLA was also able to maintain the mechanical integrity of the collagen gel better than polypropylene and nylon, which is in line with a study by Simon et al. (2014) who reported that the adhesion between mesh and gel was not as good in polypropylene and nylon meshes compared to other meshes. Therefore, the regular PLA mesh was selected as collagen support in this study.
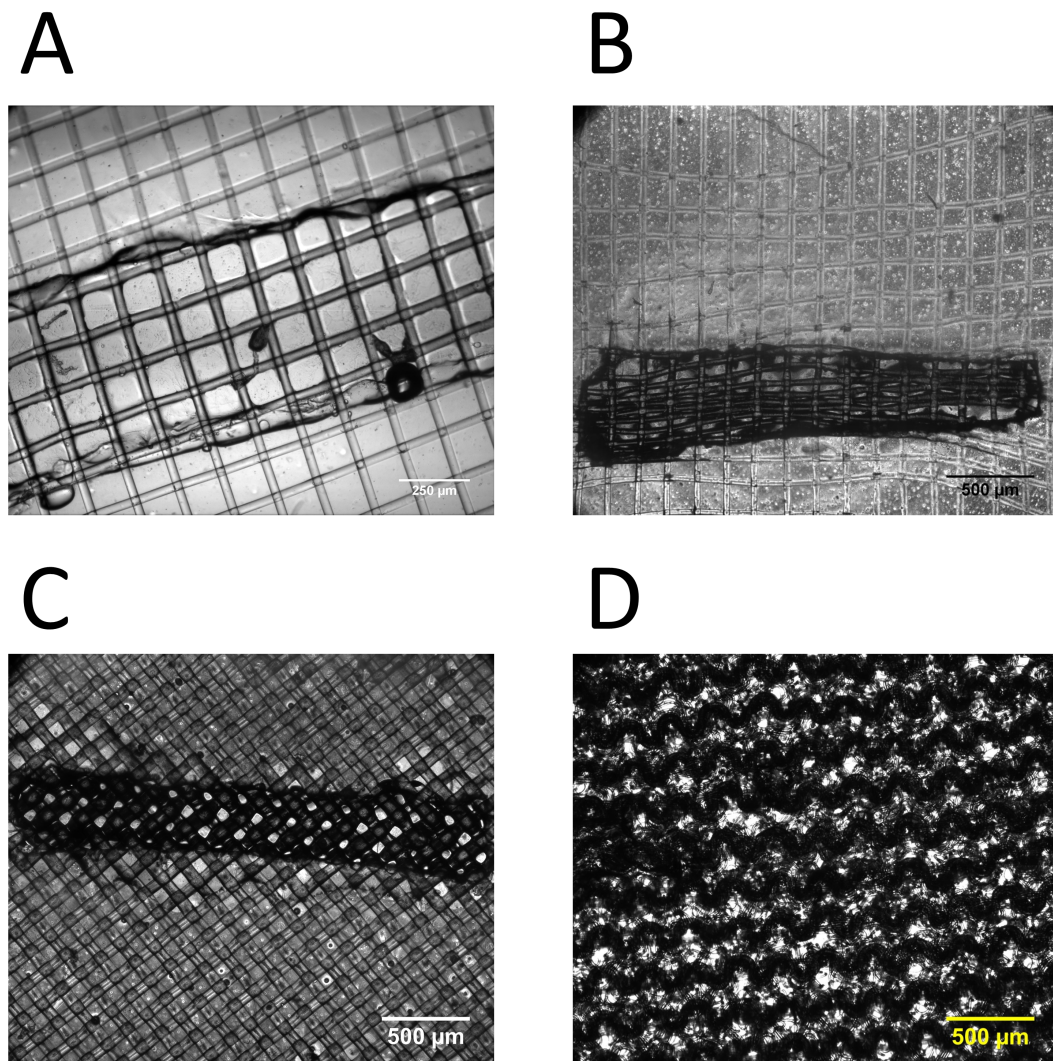
Figure 8.5: Phase-contrast images of mesh alternatives.

A: Woven PLA mesh with openings of 250 µm. B: Woven PLA mesh with manually compacted threads to create smaller openings. C: Polypropylene mesh with openings of 105 µm. D: Knitted nylon mesh of commercially available tights.

8.5.2 Maskless soft lithography was chosen as fabrication method

PDMS was selected as material to create most parts of the microfluidic device and also the hydrophobic barriers on the mesh. PDMS is a common material for microfluidic bioreactors due to its transparency and biocompatibility (Zheng et al., 2010; Leclerc et al., 2006; Lu et al., 2012b). However, its high compliance (low stiffness) can lead to deformations, including bulging or sagging of channels which can potentially alter the fluid flow in the bioreactor (Berthier et al., 2012). The absorption of small hydrophobic molecules by PDMS can be a further limitation in particular in pharmaceutical studies (Toepke and Beebe, 2006; Domansky et al., 2013). PDMS is still a suitable material for prototyping applications as it is inexpensive and can easily be cast in a variety of different shapes using soft lithography (Montanez-Sauri et al., 2011).

The first step in soft lithography is the fabrication of a suitable mould ('master copy', see Figure 8.1). Conventionally, a mould is created by spin-coating photoresist on a silicon wafer and its thickness determines the height of the structure. A mask (= transparency film with printed pattern) is placed on top of the layer of photoresist. Exposure to UV light transfers the pattern from the mask to the photoresist and uncross-linked polymer is washed off. Since the creation of the mask requires specialised equipment and expertise, research has been focussing on the development of 'maskless' soft lithography technologies (Menon et al., 2005). In particular, the use of a cutting plotter to rapid prototype micro-structures made of a wide range of materials, including vinyl tape (Bartholomeusz et al., 2005), double-sided pressure sensitive adhesive tape (Yuen and Goral, 2010) and cyclic olefin polymer sheets (Do et al., 2011) has been shown promising results.

The PDMS sheets which form the bioreactor in this chapter were also created using maskless soft lithography. The quality of the maskless mould depends on many factors including the cutting material but also the sharpness of the blade and the cutting settings, e.g. speed and force (Yuen and Goral, 2010). To select the best substrate for masking areas on the PLA mesh, several adhesive materials were compared regarding their (1) adhesiveness to the PLA mesh, (2) ease of removal from the PLA mesh, (3) surface quality, (4) temperature resistance and (5) shape stability of the adhesive (Table 8.1). Vinyl duct tape produced by 3M fulfilled all of these criteria best. In contrast to the duct tape by Unibond (UK), the duct tape by 3M adhered well to the PLA mesh and could also be easily removed after the PDMS was cured. Furthermore, duct tape by 3M maintained its shape during cutting and resisted temperatures up to 120 °C which facilitated rapid PDMS curing at high

Table 8.1: Advantages and disadvantages of different adhesive substrates for 'mask-less' soft lithography.

Adhesive material	Thickness in μm	Advantages	Disadvantages
Foam stickers	300	Good adhesion to mesh	Foam produces bubbles in PDMS, too thick, not compatible with craft cutter
Masking tape	60	Easy to cut	Absorbs liquid and is not able to create moulds
Vinyl stickers	80	Easy to cut, smooth surface	Low adhesion to mesh
Electrical insulation tape	100	Easy to cut, good tape-tape adhesion	Low adhesion to mesh
Duct tape (Unibond)	100	Easy to cut, good adhesion on tape and mesh	Very ductile, could not resist high temperatures
Duct tape (3M)	100	Easy to cut, good adhesion on tape and mesh, resistant to high temperatures	No smooth surface

temperatures.

Despite duct tape being the best choice for masking areas on the PLA mesh, it was not suitable for the fabrication of smooth microfluidic channels due to its structured surface. In addition, certain vinyl sheets could not be used since they prevented complete curing of PDMS and left 'sticky' surfaces behind. Potentially, this effect might have been triggered by surface modifications of the colour-coated vinyl sheets as the effect appeared to depend on the colour and was reduced after several PDMS casts. Despite having problems with some vinyl materials, other vinyl sheets or normal cellular tape did not prevent curing of PDMS. Consequently, adhesive vinyl sheets with a thickness of 80 μm were selected since they were most compatible with the desktop cutter (Figure 8.6).

8.5.3   Plasma treatment enabled filling of PDMS sheets with cell-collagen solution

Following the successful fabrication of thin PDMS sheets, cell-collagen solution was added to the PDMS-free zone on the mesh-based sheets. The hydrophobic properties of both PLA mesh and PDMS made spreading of collagen gel difficult. Instead of evenly filling the mesh in the PDMS-free zone, the liquid collagen solution beaded on the native PLA fibres and formed drops. However, air plasma treatment turned the mesh-based PDMS sheets hydrophilic and allowed the collagen solution to easily fill the whole PDMS-free mesh zone (Figure 8.8A). Collagen solution inside the mesh transformed from a liquid to a gel after incubation at 37 °C for 30 min. At this stage of the project 3D cultures of cells were constructed using only single sheets of collagen-containing mesh. In the future, however, multiple gelled sheets could be stacked together to create thicker 3D constructs. Furthermore, preliminary experiments with fluorescent beads demonstrated that this system can support spatially-defined cell co-culture when filling both sides of the mesh independently (Figure 8.7).

8.5.4   Clamping supported reversible assembly of bioreactor

The three PDMS sheets were joined together by foldback clips. In contrast to air plasma bonding which is commonly used for microfluidic systems made of PDMS (Eddings et al., 2008), clamping facilitated de-stacking of the sheets (Land et al., 2011). Plasma treatment would have also not worked for this complex set-up, since cells were already embedded within the PDMS sheets and would have not survived plasma treatment. For the assembly, it was essential to place stiff materials around
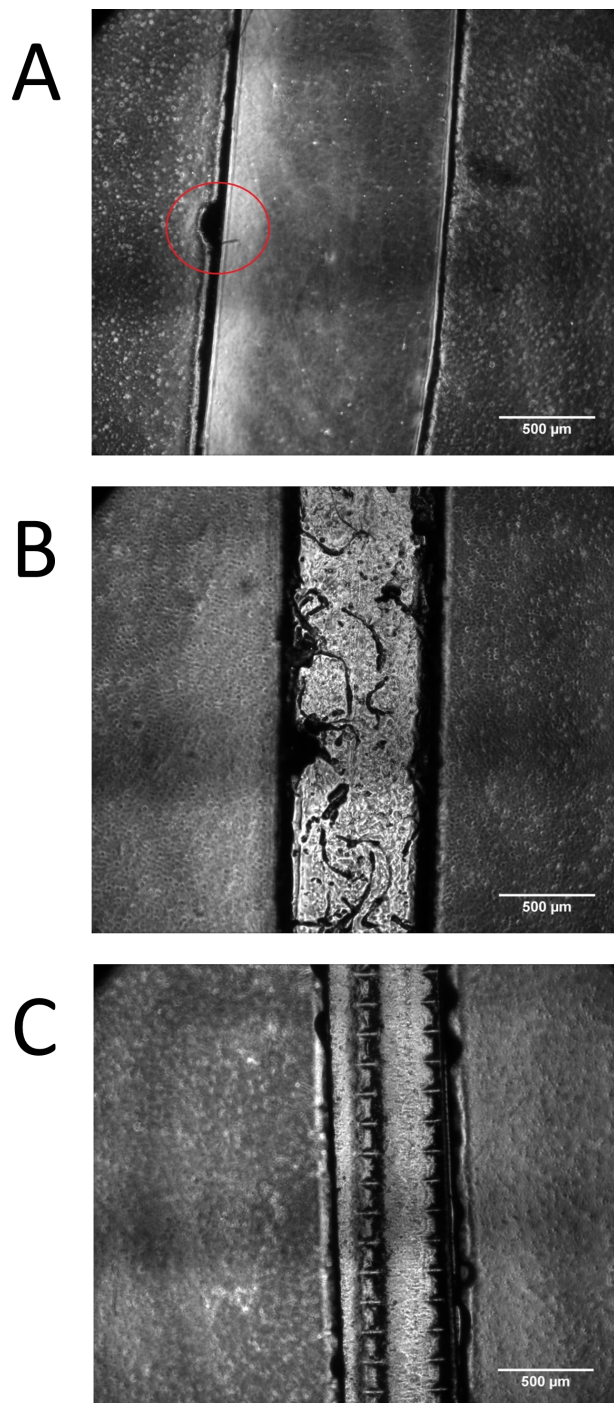
Figure 8.6: Phase-contrast images of cured PDMS using different tapes as moulds.

A: Cellular tape. Despite the smooth surface of the channel, small entrapped bubbles created uneven borders (red circle) B: Adhesive vinyl sheet. Some vinyl coatings prevented curing of PDMS and left behind a non-transparent and 'sticky' surface. C: Duct tape. Transparency was affected by pattern of duct tape. Scale bar = 500 μm.
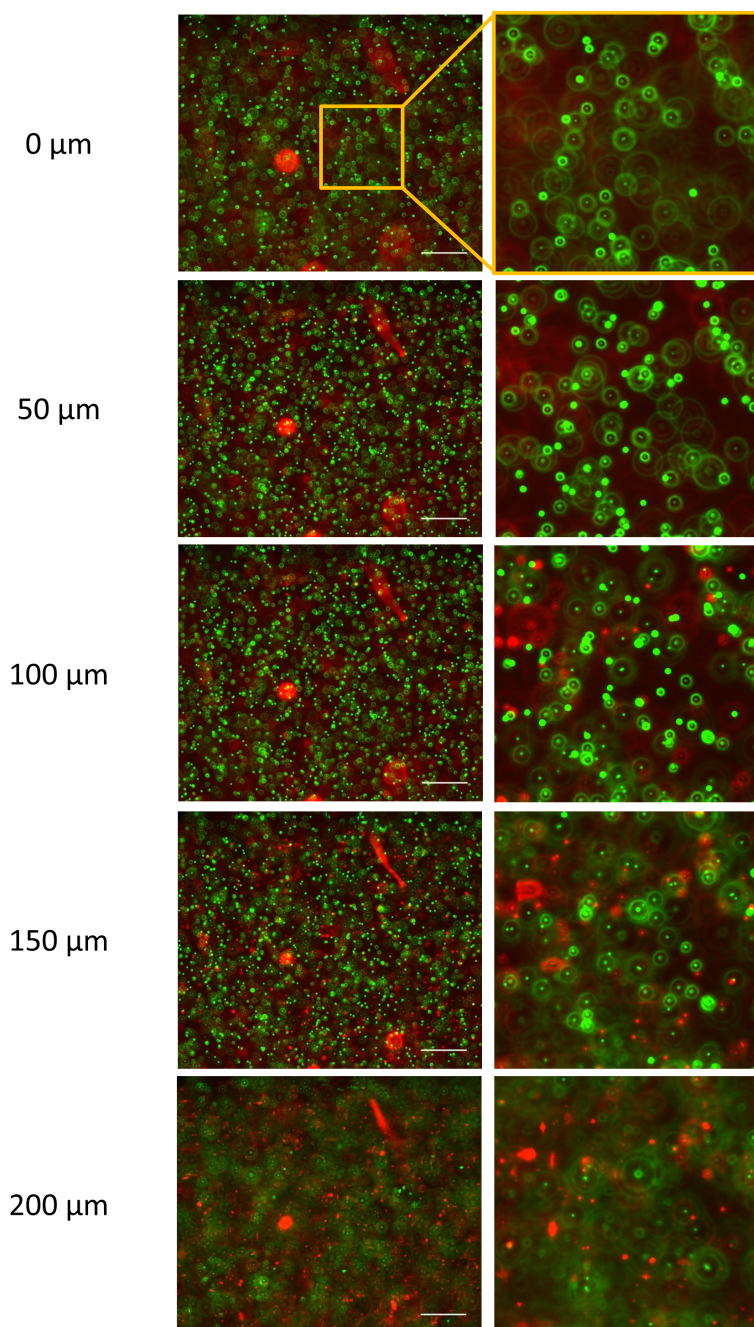
Figure 8.7: Fluorescence images showing spatially-defined separation of fluorescent beads by PLA mesh.

Fluorescent z-stack of images of yellow-green and red fluorescent beads embedded in collagen gel were acquired with a fluorescence microscope and merged. Panels show every 2nd optical slice throughout the z-stack (depth from the first slice is indicated in each panel). Green fluorescent beads are in focus between $0\,\mu m$ and $100\,\mu m$. Red fluorescent beads are in focus between $100\,\mu m$ and $200\,\mu m$. The mesh is located around $100\,\mu m$ and is able to separate both layers. Scale bar $= 250\,\mu m$. Images on the right side are enlargements of images on the left.

the PDMS sheets on the top and bottom to distribute the high forces from the clamps equally. A microscope glass slide was selected as bottom part because of its excellent optical characteristics. A transparent acrylic sheet was selected instead of glass for the top to facilitate drilling of holes which were required to connect the bioreactor with its perfusion system (Figure 8.4B).

8.5.5 Pre-filling of reactor was required to prevent dehydration of collagen

Collagen sheets dried within minutes when not in contact with liquid. It was very important to keep the collagen sheets hydrated at all times to prevent them losing their three-dimensional structure and becoming thin and brittle. This was straightforward when cultured under static conditions in a petri dish. However, it was more challenging to keep the collagen sheets hydrated within the microfluidic bioreactor as the reactor had to be pre-filled with cell culture medium without destroying the fragile collagen layer. Two different approaches for pre-filling the microfluidic chamber were tested.

Initially, a microfluidic bioreactor consisting of only one inlet and one outlet was used (Figure 8.9A). Channels were manually filled with culture medium before assembling the device. Approximately 10 µl of fluid was transferred with a pipette to the bottom channel, followed by carefully placing the cell-containing collagen sheet on top of the fluid. The next step was to align the top fluid channel, which also had been pre-filled with approximately 10 µl of medium. Finally all layers were clamped together. Despite being as careful as possible, the clamping created really high fluid pressure inside the channels. This caused the fluid not only to go through the inlets and outlets, but also to burst through the collagen layer which left the collagen in great parts damaged or completely destroyed (Figure 8.8B).

Therefore, an alternative bioreactor design with two inlets and two outlets was developed which allowed separate filling of bottom and top channel after assembly (Figure 8.9B). To fill the bottom channel, the inlet and outlet of the top channel were blocked and fluid was added to the bottom channel at a rate of 30 µl/min. After the bottom channel was filled, the blockage of the top channel was released and the inlet and outlet of the bottom channel were blocked. The top channel was filled at the same rate. This approach allowed a more even filling of the top and bottom channels without destroying the collagen layer in the pre-filling phase. Although the success rate was higher compared to the initial design, still in about 50% of the devices fluid broke through the collagen layer leaving behind a hole (Figure 8.9C). All of the damaged devices had to be discarded as the flow would have always followed the
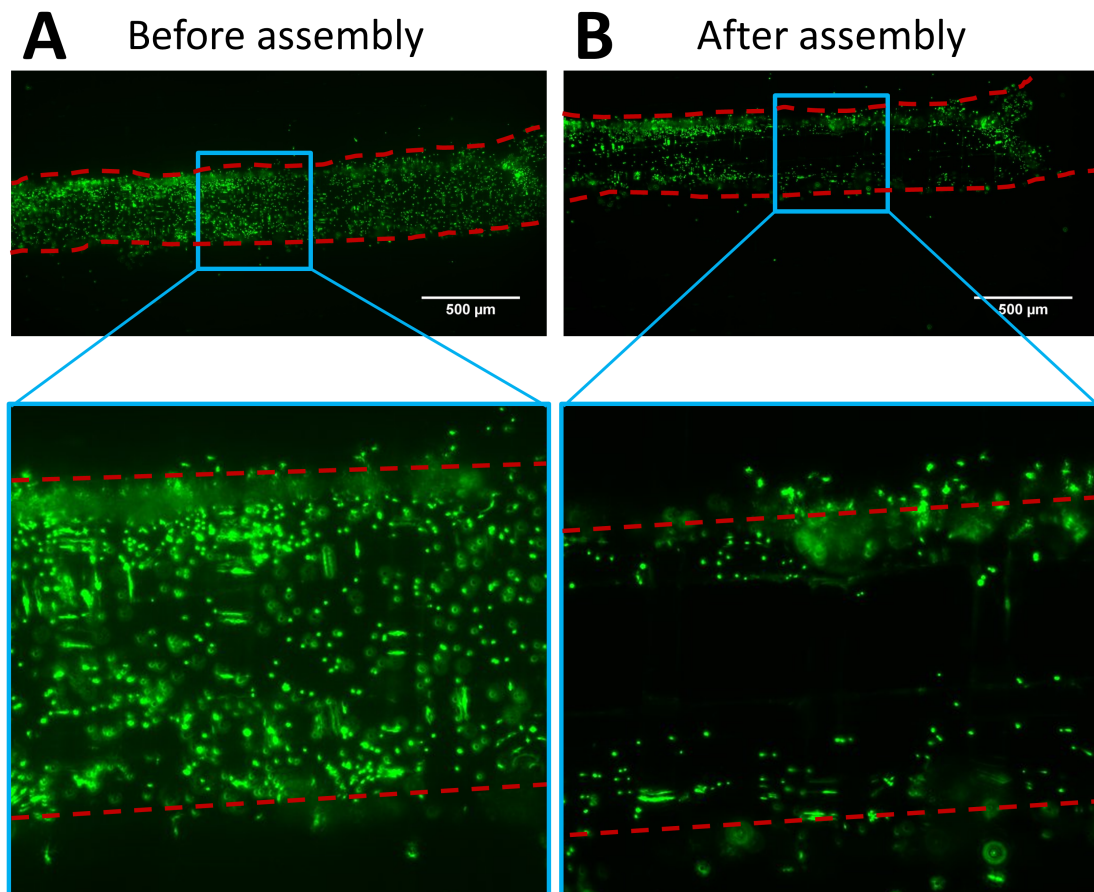
Figure 8.8: Fluorescence image of collagen layer before and after assembly.

A: Intact collagen layer before assembly. B: Damaged collagen layer after assembly. After assembling the bioreactor, the collagen layer stayed intact only on the edges of the chamber. The high fluid pressure during assembly washed away the collagen in the centre of the chamber. The location of the collagen gel was visualised by embedding yellow-green fluorescent beads ($2\,\mu m$ diameter). The edge of the PDMS-free zone is marked with a red-dashed line.

path of least resistance and gone through the hole instead of passing evenly through the whole collagen layer. This high failure rate demonstrates the difficulties when working with soft collagen hydrogel. A method to protect the soft and very fragile collagen layer and which could be used in the future has been described by Haessler et al. (2012). They added Matrigel, which has a higher flow resistance than collagen, around the collagen layer and were able to protect the collagen layer and achieved constant perfusion of the collagen hydrogel avoiding adverse effects such as fluid channelling.

8.5.6   Bubble formation prevented perfusion of system

After pre-filling the bioreactor, slow perfusion of the collagen scaffold was generated with syringe pumps. Two tubes, e.g. the outlet of the top channel and inlet of the bottom channel were blocked, and culture medium was added to the bioreactor through the top channel at a constant rate (Figure 8.9B). Despite trying a wide range of flow rates (1 µl/min to 50 µl/min), continuous perfusion of the bioreactor has not been achieved yet. The biggest obstacle preventing the perfusion of the device was the formation of bubbles inside the fluid channels, in particular just above the collagen-filled cell culture chamber (Figure 8.11A).

Bubble formation is a common problem in microfluidics due to the enclosed channel geometries, small dimensions and constant introduction of new culture media (Kim et al., 2007). Bubbles can have several serious effects. For example, they can cause cell apoptosis as the surface tension of the air-liquid interface within a microfluidic channel becomes large enough to destroy cell membranes (Michaels et al., 1996). In addition, bubbles worsen the optical characteristics of the system preventing image acquisition near bubbles. Bubbles also change the fluid flow dramatically which increases the pressure within the channel and in this set-up can damage the weak collagen layer.

The complex design of this device prevented the application of commonly used methods to avoid bubbles. For example, devices are commonly pre-filled with low surface tension liquids such as ethanol prior to adding cell culture medium to the channels (Kim et al., 2007). This method was not suitable as cells were already seeded in the device and ethanol would have killed the cells. 'Blind-filling' is another approach in which residual air bubbles are flushed out by filling the system first under high pressure (>5 Pa). However, such high pressure would have destroyed the very weak collagen layer. It has also been reported that 'pulling' the medium through microfluidic systems by applying negative pressure created less bubbles compared to 'pushing' the medium through the system. The very weak collagen layer, however,
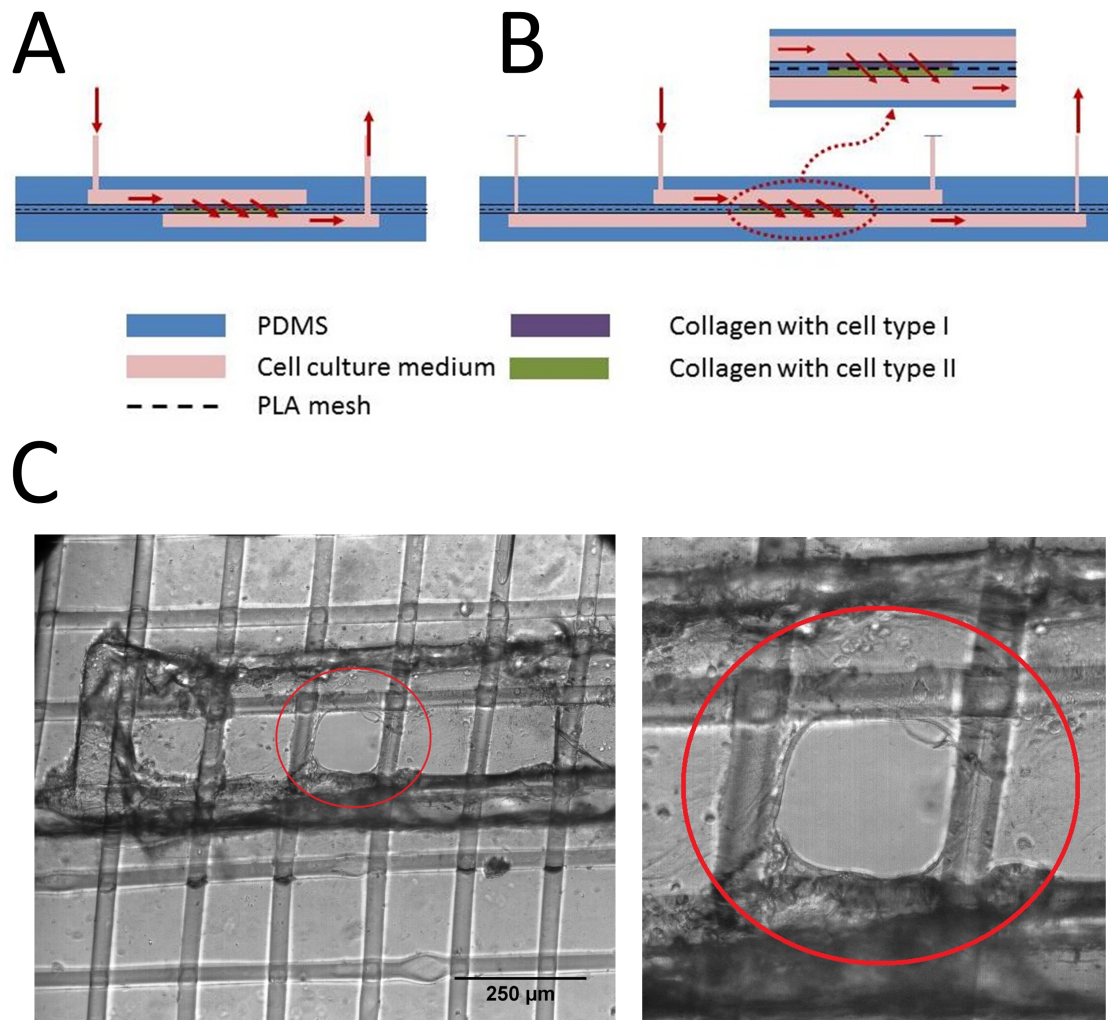
Figure 8.9: Pre-filling of microfluidic bioreactor to keep collagen sheets hydrated.

A: Schematic drawing of the original bioreactor design consisting of only one inlet and outlet. The high fluid pressure build-up in the channels repeatedly destroyed the collagen sheet during assembly and therefore this design was excluded from further testing. B: Schematic drawing of the final bioreactor design consisting of two inlets and outlets enabling separate pre-filling of bottom and top channel. The red arrows symbolise the direction of fluid flow through the device following assembly. C: Phase-contrast image of damaged collagen layer. In about 50% of the designs the collagen sheet broke during assembly leaving behind a hole (red circle). Devices with broken collagen sheets had to be discarded as they prevented even perfusion of the collagen hydrogel.

was destroyed repeatedly under the application of negative pressure.

Since bubbles are thought to nucleate at deformation sites, several measures were taken to avoid defects in the PDMS, tears in fluidic interconnects and irregular geometries (Kim et al., 2007). For example, PDMS was degassed in a vacuum chamber before curing to remove any air bubbles which might have been entrapped in the pre-polymer after mixing. Furthermore, inlet and outlet holes were created with very sharp biopsy punchers. Sharp scalpels were used to cut tubing to prevent any micro-damage. Despite these measures, bubbles still formed. This could have been caused by the modular design which might have created tiny gaps between sheets where bubbles could nucleate. Moreover, 'maskless' soft lithography compared to traditional approaches prevented the fabrication of completely flawless channel borders as air was easily entrapped between vinyl stickers and transparency film creating tiny defects in the PDMS (Figure 8.6A).

Degassing of culture medium prior to the experiment was another attempt to reduce the potential of bubble formation. Air bubbles form more easily at higher temperatures as the solubility of gases in fluids is dependent on temperature. A temperature dependent increase in kinetic energy leads to more motion in the gas molecules, breaking intermolecular bonds and allowing gasses to escape from solution (Florence and Attwood, 2011). Despite a reduction in bubble formation, degassing also failed to completely eliminate bubbles.

In addition, PDMS sheets were treated with air plasma prior to assembly to reduce surface tension and facilitate filling of the microchannels. PDMS is natively a hydrophobic material due to the repeating $OSi(CH_3)_2)O$-units, which leads to high surface tensions and impedes flow through microchannels. Air or oxygen plasma treatment can replace the methyl groups ($Si\text{-}CH_3$) with silanol groups ($Si\text{-}OH$) and convert the surface of PDMS into a hydrophilic material (Zahn, 2009). However, the surface returns to being hydrophobic after only a couple of minutes ('hydrophobic recovery') when the PDMS polymer chains diffuse back from the bulk to the surface and replace the silanol groups (Eddington et al., 2006). To use the hydrophilic advantages of plasma-treated PDMS, all PDMS parts had to be plasma treated just before the experiment adding further to the already fairly complicated and lengthy preparation process for each experiment.

As a last measure, bubble traps were added to the system as another attempt to prevent bubbles reaching the sensitive cell culture chamber (Zheng et al., 2010; Buchanan et al., 2013; Huesa et al., 2010; Leclerc et al., 2006). Two different versions, one outside the bioreactor and one integrated into the chip were tested

(Figure 8.10). The first bubble trap was located outside the bioreactor and was connected in series with the syringe pump and the inlet for the bioreactor. A well with a volume of approximately 200 μl was cut into a piece of PDMS. An inlet and outlet hole were punched into the well and the PDMS piece was plasma bonded to a small glass slide. Although this system could contain a large air volume and stopped bubbles reaching the chamber, it was not able to sufficiently prevent bubbles forming within the system. Alternatively, a bubble trap was integrated into the design and was placed directly on the glass slide between the inlet hole and the cell culture chamber. The trap was created by removing a small piece of PDMS (approximately 3 mm x 5 mm) from the top PDMS sheet. This created a well with a volume of around 30 μl for trapping bubbles. Although this delayed the formation of bubbles within the device, it could not prevent the formation of bubbles in particular on top of the collagen gel altogether.

Despite applying a variety of measures, bubble nucleation directly above the collagen was not prevented. Since bubbles changed the flow profile and also hindered microscopic analysis of the cells, cell culture within the microfluidic device failed (Figure 8.11). It is not clear, why bubbles preferred to form on top of the collagen. Potentially, culture medium followed the path of least resistance and preferred the hydrophilic PDMS surface to the collagen gel. Consequently, culture medium trapped air above the collagen while flowing around the collagen chamber. Moreover, the relatively complex design which included many different materials further facilitated bubble formation. Finally, it appears that set-ups which successfully combined collagen 3D culture with microfluidic perfusion used a horizontal set-up rather than vertical flow (**polacheck2011**; Haessler et al., 2012; Trietsch et al., 2013). The disadvantage of a horizontal set-up where fluid layer and collagen layers are next to each other is that it cannot be easily modified, hence this chapter aimed to create a vertical system.

Compared to the successful passive perfusion of bulk collagen in the previous chapter, more difficulties were encountered when trying to achieve vertical perfusion of thin collagen layers using a microfluidic approach. Bubbles or collagen breakage was no hindrance in the previous chapter which used a thick collagen layer. This might indicate that 'milli-systems', i.e. systems whose dimensions are in the millimetre range rather than in the micrometre range, might be more suitable for the complex work with soft hydrogels (Sbrana and Ahluwalia, 2012).

A
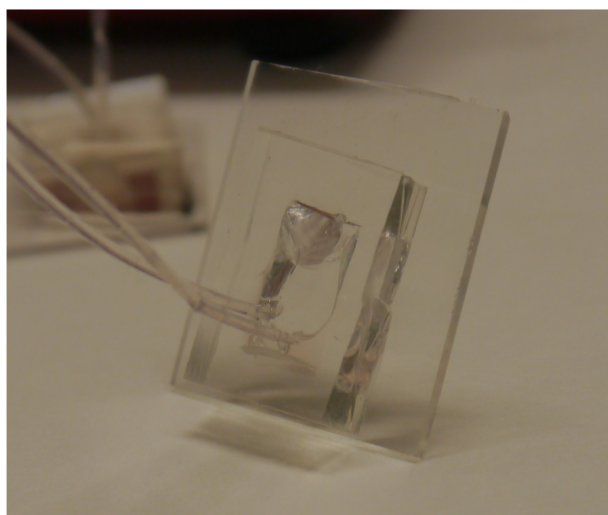
B
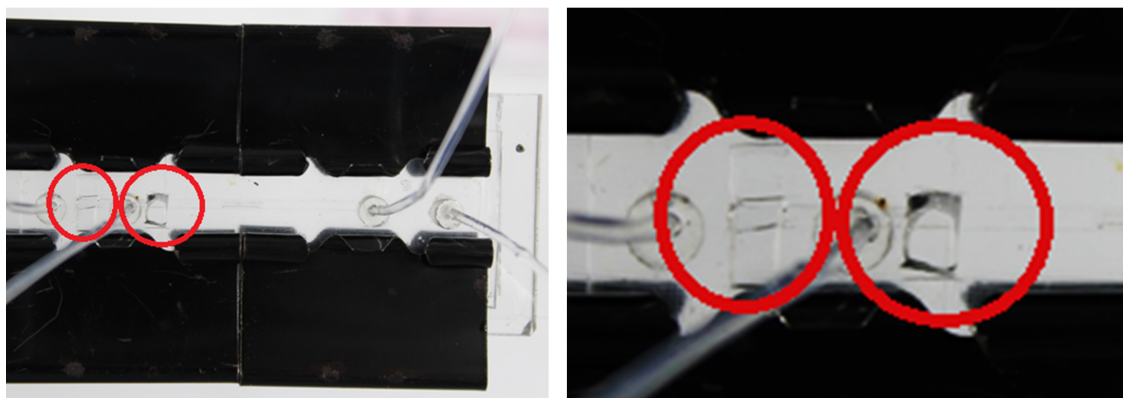
Figure 8.10: Photos of bubble traps.

A. Photo of external bubble trap installed between syringe pump and inlet. B: Photo of integrated bubble trap created by removing some PDMS on top of the microfluidic channels. Bubble traps are highlighted with red circles.
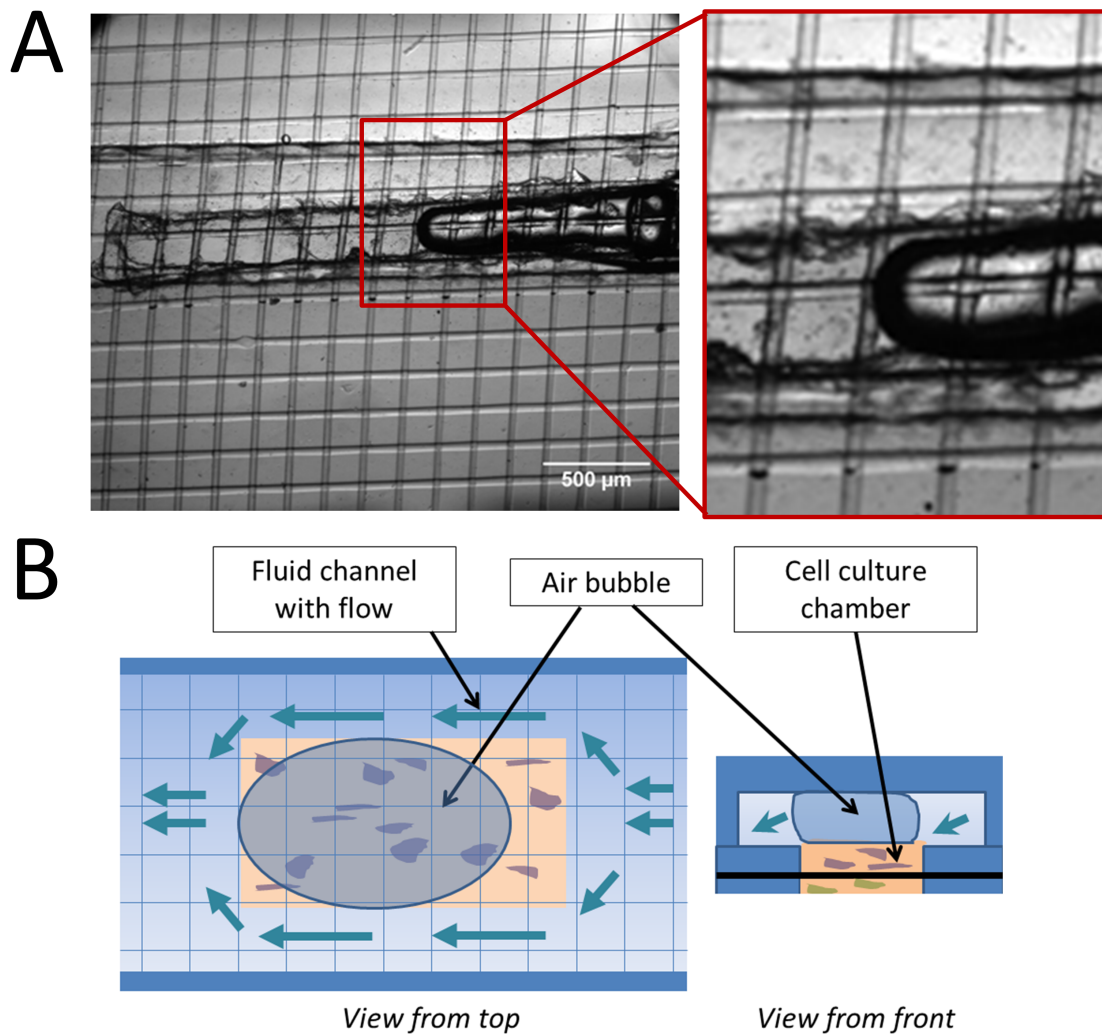
Figure 8.11: Bubble formation above collagen chamber.

A: Phase-contrast image of bubble forming directly over collagen channel. B: Schematic drawing explaining bubble formation above the collagen chamber. Cell culture medium might have preferred to flow (blue arrows) around the collagen chamber (orange) and thereby trapped air above the collagen.

8.5.7 Successful cell culture was achieved under static conditions

Although perfusion of the chamber was not achieved, cells were successfully cultured under static conditions in the mesh-based PDMS sheet embedded in collagen for at least 96 h (Figure 8.12). Cells elongated and migrated within the collagen gel confirming that none of the materials were cytotoxic. Live-dead staining further confirmed cell survival within the collagen gel. The collagen layer with its thickness of around 200 µm was thin enough to permit nutrient supply and waste removal based on diffusion, hence no active perfusion was required. As originally intended, it was possible to observe both the density and morphology of labelled and non-labelled cells using optical and fluorescence microscopy without having to section the gel. In contrast to Chapter 7 where cells migrated towards the surface of the collagen hydrogel which resulted in an uneven cell distribution, cells remained evenly distributed throughout the thin collagen scaffold for 96 h. Longer experiments would be required to assess whether cells would eventually contract the collagen scaffold and thereby destroy the integrity between collagen layers and PDMS sheets. Extensive contraction would potentially further complicate operation of the microfluidic device.
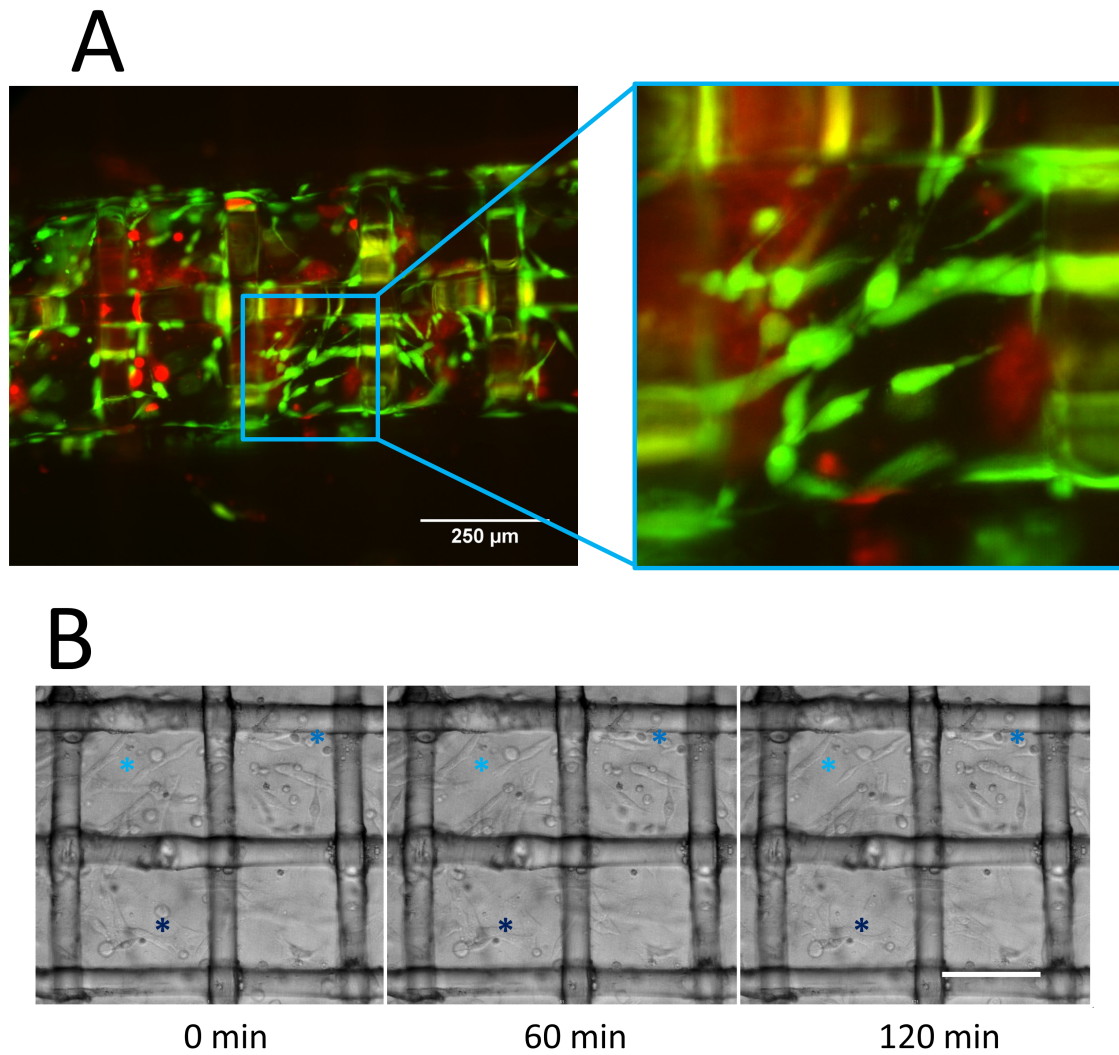
Figure 8.12: Cell viability in mesh-supported collagen gel after 96 h of static culture.

A: Fluorescence microscopy image of live (green) and dead (red) cells after cell viability assay. B: Time-lapse phase-contrast images show migration of cells within the collagen gel. Migrating cells are marked with blue asterisks. Scale bar = 250 µm.

8.6   Summary

- All of the individual parts of the bioreactor were successfully fabricated with 'maskless' soft lithography.

- A woven PLA mesh was selected for this bioreactor since it supported best the mechanical integrity of cell-seeded collagen hydrogels and facilitated light microscopy.

- The PLA mesh-based PDMS sheet supported cell viability in collagen scaffolds for at least 96 h under static conditions.

- Cell culture inside the bioreactor has not been achieved due to the weak mechanical properties of collagen in combination with technical difficulties such as bubble formation within the microfluidic system.

Chapter 9

General discussion and future work

Cell behaviour is determined by a multitude of factors which are acting at the same time. To understand such complexity is a major challenge in cell biology (Prodanov et al., 2013). Bone, in particular, is a complex tissue containing different cell types that are located in a three-dimensional environment ranging from stiff mineralised bone tissue to non-mineralised osteoid and soft bone marrow. Previous studies have shown that mechanical stimulation and specifically FSS can regulate bone metabolism (Bakker et al., 2001; Genetos et al., 2004). However, only few studies have focussed on the long-term effects of FSS (Kreke and Goldstein, 2004; Delaine-Smith et al., 2012). Therefore, the main aim of this research project was to investigate how FSS guides osteogenesis (e.g. collagen deposition, mineralisation) and osteoblast-to-osteocyte differentiation using 2D and 3D models.

Despite many studies showing that bone cells are sensitive to a wide range of mechanical stimulation (Reich et al., 1990; Klein-Nulend et al., 1997; Delaine-Smith et al., 2012; Aisha et al., 2015), the results of this work indicate that bone cells do not respond to all types of forces. Specifically, low FSS, as it was generated in this study with a see-saw rocker and an orbital shaker, did not affect cellular behaviour in the osteoblast cell lines MLO-A5 (Chapter 5) and IDG-SW3 (Chapter 6). On the other hand, IDG-SW3 osteoblasts responded as expected to biochemical stimulation (Chapter 4).

There are several possible explanations for why MLO-A5 and IDG-SW3 did not respond to mechanical loading in this study. One of the most likely reason is that these cell lines were not sensitive to the applied magnitude and type of loading. Although previous studies have demonstrated that a wide spectrum of shear stress

ranging from less than 0.01 Pa to more than 2 Pa can alter bone cell behaviour, it is difficult to directly extrapolate these findings to the present study as other loading platforms, cell types and analysis methods were used (Scaglione et al., 2008; Ajubi et al., 1999; Jing et al., 2013). Only a study by Delaine-Smith et al. (2012) used a very similar set-up, but in contrast to the findings of this thesis they were able to show that mineralisation in MLO-A5 increased following mechanical stimulation. Explanations which try to explain the differences between the present study and the study by Delaine-Smith et al. (2012) have already been discussed in detail in Chapter 5.6.

The present study focussed on the application of low, interstitial-like fluid flow, since the see-saw rocking platform was only able to produce low shear stress of less than 0.05 Pa (Zhou et al., 2010). The use of microfluidic parallel-plate flow chambers, which are commonly applied in flow experiments and can produce significantly higher shear rates, was not possible since long-term culture of matrix-producing cells in tiny channels is extremely challenging (Anderson et al., 2006). Most importantly, it is believed that low FSS mimics best the native environment of osteoblasts, even though the exact shear range is still under debate (Bonewald and Johnson, 2008). Because of the limited knowledge regarding the in vivo flow environment in bone, future experiments should investigate a wider range of shear stress to find out whether IDG-SW3 and MLO-A5 might respond stronger to higher shear forces. Preliminary results indicated that greater shear stress might be more effective in these cell lines as calcium release was strongest under high shear forces of 1.5 Pa (see Chapter 5.5.6 and 6.5.4). However, such high shear forces could not be generated with the see-saw rocker. Although slight changes of shear stress in the range of several millipascals could be achieved by varying the rocking frequency and tilt angle of the see-saw rocking platform, these variations did not significantly affect cell behaviour. Since the results on the see-saw rocker were in contrast to the findings by Delaine-Smith et al. (2012), MLO-A5 cells were also exposed to substantially higher shear stress (0.87 Pa) on the orbital shaker hoping that this would enhance osteogenesis. However, the enhanced shear stress was also not able to modulate osteoblast behaviour. Potentially, supplementing culture medium with dextran, which increases its viscosity, could provide an alternative method to modulate the FSS on the rocking platform without changing any other parameters (Bakker et al., 2001). To allow investigation of an even wider range of shear stress regimes would require the development of novel in vitro culture systems which can facilitate long-term culture better than conventional PPFC. The development of such a microfluidic system based on the design criteria for a stackable organ-on-a-chip was attempted in the previous chapter. However, several difficulties including bubble formation were encountered

which prevented the use of this device for long-term culture. Therefore, in order to use microfluidic systems in the future better solutions have to be developed which prevent bubble formation and channel clogging by growing cells.

Although previous flow studies have demonstrated mechanosensitivity of bone cells, part of these studies produced contradicting results. For example, some studies found that cells are more sensitive to oscillatory fluid flow (Jaasma and O'Brien, 2008), while other studies showed a stronger cell response to steady, unidirectional flow (Lu et al., 2012a; Ponik et al., 2007). The majority of data in the literature cannot be easily compared due to the different testing regimes. Moreover, comparison between results from this study and data from the literature is even more difficult as most studies assessed only short-term effects or used parallel-plate flow chambers with a well-defined fluid flow (Bacabac et al., 2004; Vezeridis et al., 2006). In this study, however, see-saw rocker and orbital shaker produced temporal and spatial varying FSS. This made the estimation of the average shear stress experienced by the cells challenging. Shear stress magnitudes and flow profiles are based on analytical and numerical methods from the literature (Zhou et al., 2010; Salek et al., 2012), but have not been validated in this study. The FSS estimates depend on several factors. Most of them, such as the volume of culture medium added per well, the rocking frequency and medium viscosity, can be controlled relatively easy. Other parameters are harder to control. For example, it has not yet been explored what effect the extensive matrix deposition on top of the cells has on the flow profile and on the cells' ability to sense the flow. Future work should explore ways to better characterise the forces cells experience on the rocking platforms.

Better characterisation of fluid flow and the generated fluid shear forces are also required for the 3D collagen model. Currently, shear forces were estimated using bulk equations developed by Wang and Tarbell (2000), which did not provide information about the specific mechanical environment of individual cells. To gain more information about the microenvironment, a better understanding of the fluid pathway through the collagen would be required.

Besides variations in loading platforms and cell types, contrasting results may also be explained by the cells' sensitivity to growth factors within the cell culture medium. For example, FBS is a biological reagent with slightly different properties depending on its batch. Therefore, future experiments might want to consider whether a different batch of FBS or lower FBS concentrations can increase the mechanosensitivity of MLO-A5 and IDG-SW3 (Allen et al., 2000).

The lack of osteogenic response to mechanical stimulation might have also been due to the low frequency of fluid flow application. Fluid flow might have to be generated

more than once a day to achieve an osteogenic response. Although rest periods in between mechanical stimulation have been shown to be beneficial in vitro, their optimum duration is still under debate (Batra et al., 2005; Robling et al., 2001; Gong et al., 2014). Consequently, future work should not only investigate the type and magnitude of loading but also the most appropriate loading frequency and the optimum time point of loading.

This study concentrated on the long-term effects as these were considered to be most relevant for in vitro bone models or tissue engineering applications. But as mentioned earlier, the majority of studies report short-term responses of bone cells to fluid stimulation focussing primarily on changes in their gene expression (Bakker et al., 2013; Jaasma and O'Brien, 2008; Kreke et al., 2008) or signalling molecules such as PGE_2 (Klein-Nulend et al., 1997; Kou et al., 2011). Only very few studies considered late responses such as collagen deposition and mineralisation (Scaglione et al., 2008; Delaine-Smith et al., 2012). Further investigation is required whether early mechanosensitive responses, such as changes in gene expression or release of signalling molecules, automatically result in increased collagen deposition and mineralisation several days or weeks later. In order to gain a better understanding of the signalling cascade involved in osteogenesis, future studies should combine measurements of collagen deposition and mineralisation with analysis of gene expression and measurements of signalling factors. Analysis of gene expression would also provide an alternative method to track osteocytogenesis in IDG-SW3 in addition to fluorescence measurements of Dmp1-GFP positive IDG-SW3 cells. Although measurements of PGE_2 and NO were attempted in this project, future improvements are required since the current assays were not sensitive enough to provide statistically significant results.

One of the hypotheses of this project was that FSS does not only increase the amount of ECM deposited but that it can also control cell orientation and the orientation and structure of collagen fibres. Despite being able to see cell outlines in phase contrast microscopy images, the high cell density and the primarily cuboidal shape of osteoblasts made assessment of cell orientation difficult. Potentially, fluorescence labelling of actin fibres could provide more information on the cells' orientation in the future. In contrast, identifying the shape of Dmp1-GFP positive cells by fluorescence microscopy was straight-forward, but no dominant orientation of cell processes could be discovered in these osteocyte-like cells. SHG imaging allowed visualisation of collagen fibres which had been deposited in randomly orientated honeycomb patterns by both MLO-A5 and IDG-SW3 (Kato et al., 2001; Woo et al., 2011). In conclusion, mechanical stimulation lasting up to five hours was not able to influence cell and collagen organisation in both cell lines (Chapter 5.5.5 and

6.5.3). Potentially, the periodically changing fluid flow prevented cell and collagen fibre alignment. Future studies could investigate whether scaffold guidance is more potent in regulating cell and collagen fibre orientation than fluid flow (Matsugaki et al., 2015b).

Despite IDG-SW3 not responding to mechanical stimulation, biochemical variations in the culture medium affected cellular behaviour significantly. Specifically, a dose-dependent increase in mineralisation was observed following supplementation with β-GP (Chapter 4). The detection of changes in cellular function confirmed not only that cells were sensitive to their environment, but also that the analysis methods used in this study were able to detect changes in cellular behaviour. Analysis methods could be further refined by assessing the quality of the deposited minerals using techniques such as Fourier-transform infra-red spectroscopy (Schäck et al., 2013).

One limitation of this study might be the use of only two murine cell lines which were both derived from long bones of transgenic mice (Kato et al., 2001; Woo et al., 2011). Future studies might consider using mesenchymal stem cells as an alternative cell model as they have been reported to be sensitive to low fluid flow as well (Delaine-Smith et al., 2012). Moreover, the use of human cells might be more relevant than animal cells, particularly if screening for novel therapeutic agents with a clinical application. However, variations in the differentiation potential of human and animal mesenchymal stem cells have to be considered when transitioning between in vitro and in vivo studies (Markides et al., 2015).

All experiments in Chapters 4, 5 and 6 have been repeated independently of each other for three times ensuring reliability of the data. However, even though data trends were consistent in independent experiments, significant cross-experiment variability was observed on several occasions. For example, average calcium deposition by IDG-SW3 on Day 21 of culture using standard conditions varied between 0.84 mg per well in Repeat 1 and 1.16 mg per well in Repeat 3, which is a 37% increase (Chapter 4). An even larger difference of 75% was observed in Chapter 6, where collagen deposited by IDG-SW3 at Day 14 ranged from 97 μg per well in Repeat 3 to 171 μg per well in Repeat 2. This variability might have been caused by differences in cell numbers which appeared to have a huge effect on collagen deposition and mineralisation. Specifically, a lower cell density at Day 0 might have resulted in less or delayed collagen deposition which also delayed mineralisation. Despite attempting to keep the seeding density constant between experiments, different passage numbers possibly resulted in faster or slower growth which affected the cell numbers at Day 0. To omit this problem in the future, cells could be seeded directly at a very high density of 80,000 cells/cm^2 resulting in confluence straight away (Woo et al., 2011).

However, this approach would require the preparation of huge numbers of cells for each experiment. In addition, preliminary experiments have shown that MLO-A5 cells tend to die if cultured over extended periods at very high densities. Biological variability in IDG-SW3 experiments could have also been caused by their proliferation behaviour which differed to what has been described in the literature (Woo et al., 2011). This discrepancy has already been extensively discussed in Chapter 6.6. It can be concluded that more research regarding the cell biology of the fairly new cell line IDG-SW3 is still required.

Non-responsiveness to fluid flow was not only detected when the two cell lines were cultured as monolayers in 2D, but also when IDG-SW3 were cultured within 3D collagen scaffolds (Chapter 7). Despite successful cell culture in the newly developed 3D collagen transwell model, one of the shortcomings of this model was that assessment of cell distribution and mineralisation was hindered by the thickness of the collagen layer in the transwell insert. Chapter 8 attempted to overcome this limitation by developing a 'bone-on-a-chip' device based on a modular assembly of cell-filled collagen sheets. Although static culture of cells within the collagen sheets was successful, the combination of soft collagen layers and a microfluidic flow system was too ambitious and failed. Future studies might want to evaluate whether soft collagen hydrogel is indeed the optimum scaffold to be used in such applications. In particular since higher collagen concentrations or pre-compressed collagen sheets might be easier to handle and would create a more natural environment for osteocytogenesis (Serpooshan et al., 2010). Despite failing to achieve cell culture within the microfluidic device, Chapter 8 provided a good foundation for future work. In particular, the idea of culturing two cell types together in one collagen sheet but spatially separated by a mesh should be explored further. Such a co-culture set-up would have the potential to study paracrine signalling between two cell types such as osteoblasts and osteocytes and thereby create a more native environment for bone cells. The study of osteoblast and osteocyte interactions would be particularly interesting for flow studies as osteocytes are thought to be more sensitive to mechanical loading than osteoblasts (Bakker et al., 2013).

Chapter 10

Conclusion

This thesis demonstrated the sensitivity of the osteoblast cell line IDG-SW3 to biochemical triggers such as β-GP, ascorbic acid and strontium ranelate. In contrast to biochemical stimulation, low FSS generated with a see-saw rocking platform and an orbital shaker did not enhance osteogenesis in the osteoblast cell lines MLO-A5 and IDG-SW3. 3D culture in a collagen scaffold in combination with mechanical stimulation by slow fluid flow perfusion did also not enhance osteogenesis in IDG-SW3. Non-responsiveness of cells to low fluid shear stress was concluded after comparing collagen deposition, mineralisation, cell proliferation, ALP activity and the expression of the osteocyte marker Dmp1-GFP in mechanically stimulated and static samples. Potentially, the application of higher or more frequent fluid flow would be required for osteoblasts to respond. To allow 3D culture in combination with fluid perfusion, a modular assembly approach based on cell-containing collagen sheets was also explored in this thesis. Unfortunately, technical challenges such as bubble nucleation and the weak mechanical properties of the collagen scaffold prevented successful operation of this device. Future work should aim to improve current in vitro system to gain a better understanding of cell responses to mechanical loading. This thesis highlights that cellular responses appear to depend on a multitude of factors including the type and magnitude of loading, but also the cell type and whether early responses (e.g. release of signalling molecules, genetic changes) or late responses (e.g. collagen deposition, mineralisation) are assessed. This studies is one of the first ones to combine the analysis of osteogenesis and osteocytogenesis with fluid flow.

Bibliography

Agarwal, A. et al. (2013). "Microfluidic heart on a chip for higher throughput pharmacological studies". In: *Lab on a Chip* **13**.18, p. 3599.

Aisha, M. D., M. N. K. Nor-Ashikin, A. B. R. Sharaniza, H Nawawi and G. R. A. Froemming (2015). "Orbital fluid shear stress promotes osteoblast metabolism, proliferation and alkaline phosphates activity in vitro." In: *Experimental cell research* **337**.1, pp. 87–93.

Ajubi, N. E., J. Klein-Nulend, M. J. Alblas, E. H. Burger and P. J. Nijweide (1999). "Signal transduction pathways involved in fluid flow-induced PGE2 production by cultured osteocytes". In: *Am J Physiol Endocrinol Metab* **276**.1, E171–178.

Al Nazer, R, J Lanovaz, C Kawalilak, J. D. Johnston and S Kontulainen (2012). "Direct in vivo strain measurements in human bone-a systematic literature review." In: *Journal of biomechanics* **45**.1, pp. 27–40.

Allen, F., C. Hung, S. Pollack and C. Brighton (2000). "Serum modulates the intracellular calcium response of primary cultured bone cells to shear flow". In: *Journal of Biomechanics* **33**.12, pp. 1585–1591.

Almeida, M. M., E. P. Nani, L. N. Teixeira, D. C. Peruzzo, J. C. Joly, M. H. Napimoga and E. F. Martinez (2016). "Strontium ranelate increases osteoblast activity". In: *Tissue and Cell* **48**.3, pp. 183–188.

Altmann, B., A. Löchner, M. Swain, R.-J. Kohal, S. Giselbrecht, E. Gottwald, T. Steinberg and P. Tomakidi (2014). "Differences in morphogenesis of 3D cultured primary human osteoblasts under static and microfluidic growth conditions". In: *Biomaterials* **35**.10, pp. 3208–3219.

American Type Culture Collaction (2010). *Technical Bulletin No 7: Passage Number Effects In Cell Lines*. Tech. rep., p. 3.

Anderson, E. J., T. D. Falls, A. M. Sorkin and M. L. Knothe Tate (2006). "The imperative for controlled mechanical stresses in unraveling cellular mechanisms of mechanotransduction." In: *Biomedical engineering online* **5**, p. 27.

Anderson, H. C. (1995). "Molecular biology of matrix vesicles." In: *Clinical orthopaedics and related research* 314, pp. 266–80.

Anderson, H. C. (2003). "Matrix vesicles and calcification". In: *Current Rheumatology Reports* **5**.3, pp. 222–226.

Aryaei, A. and A. C. Jayasuriya (2015). "The effect of oscillatory mechanical stimulation on osteoblast attachment and proliferation". In: *Materials Science and Engineering: C* **52**, pp. 129–134.

Atkins, G. J., K. J. Welldon, P Halbout and D. M. Findlay (2009). "Strontium ranelate treatment of human primary osteoblasts promotes an osteocyte-like phenotype while eliciting an osteoprotegerin response." In: *Osteoporosis international* **20**.4, pp. 653–64.

Bacabac, R. G., T. H. Smit, M. G. Mullender, S. J. Dijcks, J. J. W. A. Van Loon and J. Klein-Nulend (2004). "Nitric oxide production by bone cells is fluid shear stress rate dependent." In: *Biochemical and biophysical research communications* **315**.4, pp. 823–9.

Bacabac, R. G., T. H. Smit, S. C. Cowin, J. J. W. A. Van Loon, F. T. M. Nieuwstadt, R. Heethaar and J. Klein-Nulend (2005). "Dynamic shear stress in parallel-plate flow chambers." In: *Journal of biomechanics* **38**.1, pp. 159–67.

Bakker, A. D. and J. Klein-Nulend (2012). "Osteoblast isolation from murine calvaria and long bones." In: *Methods in molecular biology (Clifton, N.J.)* **816**, pp. 19–29.

Bakker, A. D., K. Soejima, J. Klein-Nulend and E. H. Burger (2001). "The production of nitric oxide and prostaglandin E2 by primary bone cells is shear stress dependent". In: *Journal of Biomechanics* **34**.5, pp. 671–677.

Bakker, A. D., B. Zandieh-Doulabi and J. Klein-Nulend (2013). "Strontium ranelate affects signaling from mechanically-stimulated osteocytes towards osteoclasts and osteoblasts." In: *Bone* **53**.1, pp. 112–9.

Ban, Y., Y.-y. Wu, T. Yu, N. Geng, Y.-y. Wang, X.-g. Liu and P. Gong (2011). "Response of osteoblasts to low fluid shear stress is time dependent." In: *Tissue & cell* **43**.5, pp. 311–7.

Bancroft, G. N., V. I. Sikavitsas, J. van den Dolder, T. L. Sheffield, C. G. Ambrose, J. A. Jansen and A. G. Mikos (2002). "Fluid flow increases mineralized matrix deposition in 3D perfusion culture of marrow stromal osteoblasts in a dose-dependent manner." In: *Proceedings of the National Academy of Sciences of the United States of America* **99**.20, pp. 12600–5.

Barbara, A, P Delannoy, B. G. Denis and P. J. Marie (2004). "Normal matrix mineralization induced by strontium ranelate in MC3T3-E1 osteogenic cells." In: *Metabolism: clinical and experimental* **53**.4, pp. 532–7.

Barragan-Adjemian, C, D Nicolella, V Dusevich, M. R. Dallas, J. D. Eick and L. F. Bonewald (2006). "Mechanism by which MLO-A5 late osteoblasts/early osteocytes mineralize in culture: similarities with mineralization of lamellar bone." In: *Calcified tissue international* **79**.5, pp. 340–53.

Bartholomeusz, D. A., R. W. Boutté and J. D. Andrade (2005). "Xurography: rapid prototyping of microstructures using a cutting plotter". In: *Journal of Microelectromechanical Systems* **14**.6, pp. 1364–1374.

Batra, N. N., Y. J. Li, C. E. Yellowley, L. You, A. M. Malone, C. H. Kim and C. R. Jacobs (2005). "Effects of short-term recovery periods on fluid-induced signaling in osteoblastic cells". In: *Journal of Biomechanics* **38**.9, pp. 1909–1917.

Beebe, D. J., G. A. Mensing and G. M. Walker (2002). "Physics and applications of microfluidics in biology". In: *Annual review of biomedical engineering* **4**.1, pp. 261–286.

Bellows, C., J. Heersche and J. Aubin (1992). "Inorganic phosphate added exogenously or released from β-glycerophosphate initiates mineralization of osteoid nodules in vitro". In: *Bone and Mineral* **17**.1, pp. 15–29.

Bersini, S., J. S. Jeon, G. Dubini, C. Arrigoni, S. Chung, J. L. Charest, M. Moretti and R. D. Kamm (2014). "A microfluidic 3D invitro model for specificity of breast cancer metastasis to bone". In: *Biomaterials* **35**.8, pp. 2454–2461.

Berthier, E., E. W. K. Young and D. Beebe (2012). "Engineers are from PDMS-land, Biologists are from Polystyrenia". In: *Lab on a Chip* **12**.7, pp. 1224–1237.

Bezooijen, R. L. van et al. (2005). "SOST/sclerostin, an osteocyte-derived negative regulator of bone formation." In: *Cytokine & growth factor reviews* **16**.3, pp. 319–27.

Birk, D. E., M. V. Nurminskaya and E. I. Zycband (1995). "Collagen fibrillogenesis in situ: fibril segments undergo post-depositional modifications resulting in linear and lateral growth during matrix development." In: *Developmental dynamics* **202**.3, pp. 229–43.

Bonewald, L. F. (2011). "The amazing osteocyte." In: *Journal of bone and mineral research* **26**.2, pp. 229–38.

Bonewald, L. F. and M. L. Johnson (2008). "Osteocytes, mechanosensing and Wnt signaling." In: *Bone* **42**.4, pp. 606–15.

Bonivtch, A. R., L. F. Bonewald and D. P. Nicolella (2007). "Tissue strain amplification at the osteocyte lacuna: a microstructural finite element analysis." In: *Journal of biomechanics* **40**.10, pp. 2199–206.

Bonnelye, E., A. Chabadel, F. Saltel and P. Jurdic (2008). "Dual effect of strontium ranelate: stimulation of osteoblast differentiation and inhibition of osteoclast formation and resorption in vitro." In: *Bone* **42**.1, pp. 129–38.

Bose, S., M. Roy and A. Bandyopadhyay (2012). "Recent advances in bone tissue engineering scaffolds". In: *Trends in Biotechnology* **30**.10, pp. 546–554.

Boskey, A. L. (2007). "Mineralization of Bones and Teeth". In: *Elements* **3**.6, pp. 385–391.

Boskey, A. L. (2013). "Bone composition: relationship to bone fragility and antiosteoporotic drug effects." In: *BoneKEy reports* **2**, p. 447.

Boskey, A. L. and R. Roy (2008). "Cell Culture Systems for Studies of Bone and Tooth Mineralization". In: *Chemical reviews* **108**.11, pp. 4716–4733.

Boukhechba, F., T. Balaguer, J.-F. Michiels, K. Ackermann, D. Quincey, J.-M. Bouler, W. Pyerin, G. F. Carle and N. Rochet (2009). "Human Primary Osteocyte Differentiation in a 3D Culture System". In: *Journal of Bone and Mineral Research* **24**.11, pp. 1927–1935.

Bouxsein, M. L. and E. Seeman (2009). "Quantifying the material and structural determinants of bone strength." In: *Best practice & research. Clinical rheumatology* **23**.6, pp. 741–53.

Boyce, B. F. and L. Xing (2008). "Functions of RANKL/RANK/OPG in bone modeling and remodeling." In: *Archives of biochemistry and biophysics* **473**.2, pp. 139–46.

Boyle, W. J., W. S. Simonet and D. L. Lacey (2003). "Osteoclast differentiation and activation". In: *Nature* **423**.6937, pp. 337–342.

Brennan, T., M. Rybchyn, W Green, S Atwa, A. Conigrave and R. Mason (2009). "Osteoblasts play key roles in the mechanisms of action of strontium ranelate". In: *British Journal of Pharmacology* **157**.7, pp. 1291–1300.

Breslin, S. and L. O'Driscoll (2013). "Three-dimensional cell culture: the missing link in drug discovery". In: *Drug Discovery Today* **18**.5, pp. 240–249.

Brinkman, H. C. (1949). "A calculation of the viscous force exerted by a flowing fluid on a dense swarm of particles". In: *Applied Scientific Research* **1**.1, pp. 27–34.

Brommage, R. (2015). "Genetic Approaches To Identifying Novel Osteoporosis Drug Targets". In: *Journal of Cellular Biochemistry* **116**.10, pp. 2139–2145.

Brown, E. M. and R. J. MacLeod (2001). "Extracellular calcium sensing and extracellular calcium signaling." In: *Physiological reviews* **81**.1, pp. 239–297.

Buchanan, C. F., E. E. Voigt, C. S. Szot, J. W. Freeman, P. P. Vlachos and M. N. Rylander (2013). "Three-Dimensional Microfluidic Collagen Hydrogels for Investigating Flow-Mediated Tumor-Endothelial Signaling and Vascular Organization." In: *Tissue engineering. Part C, Methods.*

Burger, E. H. and J. Klein-Nulend (1999). "Mechanotransduction in bone—role of the lacuno-canalicular network". In: *FASEB J* **13**.9001, pp. 101–112.

Burra, S., D. P. Nicolella and J. X. Jiang (2011). "Dark horse in osteocyte biology". In: *Communicative & Integrative Biology* **4**.1, pp. 48–50.

Canalis, E, M. Hott, P. Deloffre, Y. Tsouderos and P. Marie (1996). "The divalent strontium salt S12911 enhances bone cell replication and bone formation in vitro". In: *Bone* **18**.6, pp. 517–523.

Canty, E. G. and K. E. Kadler (2005). "Procollagen trafficking, processing and fibrillogenesis." In: *Journal of cell science* **118**.Pt 7, pp. 1341–53.

Caplan, A. I. (1991). "Mesenchymal stem cells." In: *Journal of orthopaedic research* **9**.5, pp. 641–50.

Caplan, A. I. and S. P. Bruder (2001). "Mesenchymal stem cells: building blocks for molecular medicine in the 21st century". In: *Trends in Molecular Medicine* **7**.6, pp. 259–264.

Cartmell, S. H., B. D. Porter, A. J. García and R. E. Guldberg (2003). "Effects of medium perfusion rate on cell-seeded three-dimensional bone constructs in vitro." In: *Tissue engineering* **9**.6, pp. 1197–203.

Cassella, J. P., N. Garrington, T. C. B. Stamp and S. H. Ali (1995). "An electron probe X-ray microanalytical study of bone mineral in osteogenesis imperfecta". In: *Calcified Tissue International* **56**.2, pp. 118–122.

Caverzasio, J. (2008). "Strontium ranelate promotes osteoblastic cell replication through at least two different mechanisms." In: *Bone* **42**.6, pp. 1131–6.

Chan, M. E., X. L. Lu, B. Huo, A. D. Baik, V. Chiang, R. E. Guldberg, H. H. Lu and X. E. Guo (2009). "A Trabecular Bone Explant Model of Osteocyte-Osteoblast Co-Culture for Bone Mechanobiology." In: *Cellular and molecular bioengineering* **2**.3, pp. 405–415.

Chang, Y.-L., C. M. Stanford and J. C. Keller (2000). "Calcium and phosphate supplementation promotes bone cell mineralization: Implications for hydroxyapatite (HA)-enhanced bone formation". In: *Journal of Biomedical Materials Research* **52**.2, pp. 270–278.

Chatterjee, K., S. Lin-Gibson, W. E. Wallace, S. H. Parekh, Y. J. Lee, M. T. Cicerone, M. F. Young and C. G. Simon (2010). "The effect of 3D hydrogel scaffold modulus on osteoblast differentiation and mineralization revealed by combinatorial screening." In: *Biomaterials* **31**.19, pp. 5051–62.

Chattopadhyay, N., S. J. Quinn, O. Kifor, C. Ye and E. M. Brown (2007). "The calcium-sensing receptor (CaR) is involved in strontium ranelate-induced osteoblast proliferation". In: *Biochemical Pharmacology* **74**.3, pp. 438–447.

Chen, X., O. Nadiarynkh, S. Plotnikov and P. J. Campagnola (2012). "Second harmonic generation microscopy for quantitative analysis of collagen fibrillar structure". In: *Nature Protocols* **7**.4, pp. 654–669.

Choudhary, S., P. Halbout, C. Alander, L. Raisz and C. Pilbeam (2007). "Strontium ranelate promotes osteoblastic differentiation and mineralization of murine bone marrow stromal cells: involvement of prostaglandins." In: *Journal of bone and mineral research* **22**.7, pp. 1002–10.

Christoffersen, J., M. Christoffersen, N. Kolthoff and O. Bärenholdt (1997). "Effects of strontium ions on growth and dissolution of hydroxyapatite and on bone mineral detection". In: *Bone* **20**.1, pp. 47–54.

Chung, C.-H., E. E. Golub, E. Forbes, T. Tokuoka and I. M. Shapiro (1992). "Mechanism of action of b-glycerophosphate on bone cell mineralization". In: *Calcified Tissue International* **51**.4, pp. 305–311.

Clarke, B. (2008). "Normal bone anatomy and physiology." In: *Clinical journal of the American Society of Nephrology : CJASN* **3 Suppl 3**, S131–9.

Clover, J. and M. Gowen (1994). "Are MG-63 and HOS TE85 human osteosarcoma cell lines representative models of the osteoblastic phenotype?" In: *Bone* **15**.6, pp. 585–591.

Cowin, S. C. and L. Cardoso (2015). "Blood and interstitial flow in the hierarchical pore space architecture of bone tissue." In: *Journal of biomechanics* **48**.5, pp. 842–54.

Cox, G. and E. Kable (2006). "Second-harmonic imaging of collagen." In: *Methods in molecular biology* **319**, pp. 15–35.

Cross, V. L., Y. Zheng, N. Won Choi, S. S. Verbridge, B. A. Sutermaster, L. J. Bonassar, C. Fischbach and A. D. Stroock (2010). "Dense type I collagen matrices that support cellular remodeling and microfabrication for studies of tumor angiogenesis and vasculogenesis in vitro." In: *Biomaterials* **31**.33, pp. 8596–607.

Curtze, S., M. Dembo, M. Miron and D. B. Jones (2004). "Dynamic changes in traction forces with DC electric field in osteoblast-like cells." In: *Journal of cell science* **117**.Pt 13, pp. 2721–9.

Czekanska, E. M., M. J. Stoddart, R. G. Richards and J. S. Hayes (2012). "In search of an osteoblast cell model for in vitro research." In: *European cells & materials* **24**, pp. 1–17.

Dallas, S. L. (2006). "Dynamics of bone extracellular matrix assembly and mineralization." In: *Journal of musculoskeletal & neuronal interactions* **6**.4, pp. 370–1.

Dallas, S. L., D. R. Keene, S. P. Bruder, J Saharinen, L. Y. Sakai, G. R. Mundy and L. F. Bonewald (2000). "Role of the latent transforming growth factor beta binding protein 1 in fibrillin-containing microfibrils in bone cells in vitro and in vivo." In: *Journal of bone and mineral research* **15**.1, pp. 68–81.

Dallas, S. L., M. Prideaux and L. F. Bonewald (2013). "The osteocyte: an endocrine cell ... and more." In: *Endocrine reviews* **34**.5, pp. 658–90.

Dardik, A., L. Chen, J. Frattini, H. Asada, F. Aziz, F. A. Kudo and B. E. Sumpio (2005). "Differential effects of orbital and laminar shear stress on endothelial cells." In: *Journal of vascular surgery* **41**.5, pp. 869–80.

Datta, N., Q. P. Pham, U. Sharma, V. I. Sikavitsas, J. A. Jansen and A. G. Mikos (2006). "In vitro generated extracellular matrix and fluid shear stress synergistically enhance 3D osteoblastic differentiation." In: *Proceedings of the National Academy of Sciences of the United States of America* **103**.8, pp. 2488–93.

Davies, P. F. (1995). "Flow-mediated endothelial mechanotransduction." In: *Physiological reviews* **75**.3, pp. 519–60.

Deiss, F., A. Mazzeo, E. Hong, D. E. Ingber, R. Derda and G. M. Whitesides (2013). "Platform for high-throughput testing of the effect of soluble compounds on 3D cell cultures." In: *Analytical chemistry* **85**.17, pp. 8085–94.

Delaine-Smith, R. M., S MacNeil and G. C. Reilly (2012). "Matrix production and collagen structure are enhanced in two types of osteogenic progenitor cells by a simple fluid shear stress stimulus." In: *European cells & materials* **24**, pp. 162–74.

Delaine-Smith, R. M. (2013). "Mechanical and physical guidance of osteogenic differentiation and matrix production". PhD thesis. University of Sheffield.

Delaine-Smith, R. M., A. Sittichokechaiwut and G. C. Reilly (2014). "Primary cilia respond to fluid shear stress and mediate flow-induced calcium deposition in osteoblasts." In: *FASEB journal* **28**.1, pp. 430–9.

Delaine-Smith, R. M., B. Javaheri, J. Helen Edwards, M. Vazquez and R. M. H. Rumney (2015). "Preclinical models for in vitro mechanical loading of bone-derived cells". In: *BoneKEy Reports* **4**, p. 728.

Delannoy, P., D. Bazot and P. Marie (2002). "Long-term treatment with strontium ranelate increases vertebral bone mass without deleterious effect in mice". In: *Metabolism* **51**.7, pp. 906–911.

Do, J., J. Y. Zhang and C. M. Klapperich (2011). "Maskless writing of microfluidics: Rapid prototyping of 3D microfluidics using scratch on a polymer substrate". In: *Robotics and Computer-Integrated Manufacturing* **27**.2, pp. 245–248.

Domansky, K., D. C. Leslie, J. McKinney, J. P. Fraser, J. D. Sliz, T. Hamkins-Indik, G. A. Hamilton, A. Bahinski and D. E. Ingber (2013). "Clear castable polyurethane elastomer for fabrication of microfluidic devices". In: *Lab on a Chip* **13**.19, pp. 3956–3964.

Donahue, S. W., C. R. Jacobs and H. J. Donahue (2001). "Flow-induced calcium oscillations in rat osteoblasts are age, loading frequency, and shear stress dependent". In: *Am J Physiol Cell Physiol* **281**.5, pp. C1635–1641.

Donahue, S. W., H. J. Donahue and C. R. Jacobs (2003a). "Osteoblastic cells have refractory periods for fluid-flow-induced intracellular calcium oscillations for short bouts of flow and display multiple low-magnitude oscillations during long-term flow". In: *Journal of Biomechanics* **36**.1, pp. 35–43.

Donahue, T., T. Haut, C. Yellowley, H. Donahue and C. Jacobs (2003b). "Mechanosensitivity of bone cells to oscillating fluid flow induced shear stress may be modulated by chemotransport". In: *Journal of Biomechanics* **36**.9, pp. 1363–1371.

Ducy, P., R. Zhang, V. Geoffroy, A. L. Ridall and G. Karsenty (1997). "Osf2/Cbfa1: A Transcriptional Activator of Osteoblast Differentiation". In: *Cell* **89**.5, pp. 747–754.

Duncan, R. L. and C. H. Turner (1995). "Mechanotransduction and the functional response of bone to mechanical strain". In: *Calcified Tissue International* **57**.5, pp. 344–358.

Eddings, M. A., M. A. Johnson and B. K. Gale (2008). "Determining the optimal PDMS–PDMS bonding technique for microfluidic devices". In: *Journal of Micromechanics and Microengineering* **18**.6, p. 067001.

Eddington, D. T., J. P. Puccinelli and D. J. Beebe (2006). "Thermal aging and reduced hydrophobic recovery of polydimethylsiloxane". In: *Sensors and Actuators B: Chemical* **114**.1, pp. 170–172.

Egeblad, M. and Z. Werb (2002). "New functions for the matrix metalloproteinases in cancer progression". In: *Nature Reviews Cancer* **2**.3, pp. 161–174.

Elvidge, S. (2016). "Amgen/UCB build on bone franchise with anti-sclerostin antibody". In: *Nature Biotechnology* **34**.6, pp. 580–581.

Esch, E. W., A. Bahinski and D. Huh (2015). "Organs-on-chips at the frontiers of drug discovery". In: *Nature Reviews Drug Discovery* **14**.4, pp. 248–260.

Feng, J. Q. et al. (2006). "Loss of DMP1 causes rickets and osteomalacia and identifies a role for osteocytes in mineral metabolism." In: *Nature genetics* **38**.11, pp. 1310–5.

Feng, Z., Y. Wagatsuma, M. Kikuchi, T. Kosawada, T. Nakamura, D. Sato, N. Shirasawa, T. Kitajima and M. Umezu (2014). "The mechanisms of fibroblast-mediated com-

paction of collagen gels and the mechanical niche around individual fibroblasts." In: *Biomaterials* **35**.28, pp. 8078–91.

Florence, A. T. and D. Attwood (2011). *Physicochemical principles of pharmacy.* 4th ed. London: Pharmaceutical Press, p. 46. ISBN: 0 85369 608 X.

Flynn, B. P., A. P. Bhole, N. Saeidi, M. Liles, C. A. Dimarzio and J. W. Ruberti (2010). "Mechanical strain stabilizes reconstituted collagen fibrils against enzymatic degradation by mammalian collagenase matrix metalloproteinase 8 (MMP-8)." In: *PloS one* **5**.8, e12337.

Franceschi, R. T. (1999). "The developmental control of osteoblast-specific gene expression: role of specific transcription factors and the extracellular matrix environment." In: *Critical reviews in oral biology and medicine* **10**.1, pp. 40–57.

Franceschi, R. T. and B. S. Iyer (1992). "Relationship between collagen synthesis and expression of the osteoblast phenotype in MC3T3-E1 cells." In: *Journal of bone and mineral research : the official journal of the American Society for Bone and Mineral Research* **7**.2, pp. 235–46.

Frangos, J., S. Eskin, L. McIntire and C. Ives (1985). "Flow effects on prostacyclin production by cultured human endothelial cells". In: *Science* **227**.4693, pp. 1477–1479.

Franz-Odendaal, T. A., B. K. Hall and P. E. Witten (2006). "Buried alive: how osteoblasts become osteocytes." In: *Developmental dynamics* **235**.1, pp. 176–90.

Fratzl-Zelman, N., P. Fratzl, H. Hörandner, B. Grabner, F. Varga, A. Ellinger and K. Klaushofer (1998). "Matrix mineralization in MC3T3-E1 cell cultures initiated by β-glycerophosphate pulse". In: *Bone* **23**.6, pp. 511–520.

Freshney, R. I. (2010). *Culture of Animal Cells.* 6th ed. Hoboken, NJ, USA: John Wiley & Sons, Inc., pp. 57–70. ISBN: 9780470649367.

Freund, J. B., J. G. Goetz, K. L. Hill and J. Vermot (2012). "Fluid flows and forces in development: functions, features and biophysical principles." In: *Development* **139**.7, pp. 1229–45.

Fromigué, O., E. Haÿ, A. Barbara, C. Petrel, E. Traiffort, M. Ruat and P. J. Marie (2009). "Calcium sensing receptor-dependent and receptor-independent activation of osteoblast replication and survival by strontium ranelate". In: *Journal of Cellular and Molecular Medicine* **13**.8b, pp. 2189–2199.

Frost, H. M. (1987). "Bone "mass" and the "mechanostat": a proposal." In: *The Anatomical record* **219**.1, pp. 1–9.

Frost, H. M. (2003). "Bone's mechanostat: a 2003 update." In: *The anatomical record. Part A, Discoveries in molecular, cellular, and evolutionary biology* **275**.2, pp. 1081–101.

Garnero, P. (2015). "The Role of Collagen Organization on the Properties of Bone." In: *Calcified tissue international* **97**.3, pp. 229–40.

Genetos, D. C., D. J. Geist, D. Liu, H. J. Donahue and R. L. Duncan (2004). "Fluid Shear-Induced ATP Secretion Mediates Prostaglandin Release in MC3T3-E1 Osteoblasts". In: *Journal of Bone and Mineral Research* **20**.1, pp. 41–49.

Genetos, D. C., C. J. Kephart, Y. Zhang, C. E. Yellowley and H. J. Donahue (2007). "Oscillating fluid flow activation of gap junction hemichannels induces ATP release from MLO-Y4 osteocytes." In: *Journal of cellular physiology* **212**.1, pp. 207–14.

Ghosh-Choudhury, N, J. J. Windle, B. A. Koop, M. A. Harris, D. L. Guerrero, J. M. Wozney, G. R. Mundy and S. E. Harris (1996). "Immortalized murine osteoblasts derived from BMP 2-T-antigen expressing transgenic mice." In: *Endocrinology* **137**.1, pp. 331–9.

Gillespie, P. G. and U. Müller (2009). "Mechanotransduction by hair cells: models, molecules, and mechanisms." In: *Cell* **139**.1, pp. 33–44.

Giraud-Guille, M.-M., E. Belamie, G. Mosser, C. Helary, F. Gobeaux and S. Vigier (2008). "Liquid crystalline properties of type I collagen: Perspectives in tissue morphogenesis". In: *Comptes Rendus Chimie* **11**.3, pp. 245–252.

Goldstein, A (2001). "Effect of convection on osteoblastic cell growth and function in biodegradable polymer foam scaffolds". In: *Biomaterials* **22**.11, pp. 1279–1288.

Golub, E. E. and K. Boesze-Battaglia (2007). "The role of alkaline phosphatase in mineralization". In: *Current Opinion in Orthopaedics* **18**, pp. 444–448.

Golub, E. E. (2009). "Role of matrix vesicles in biomineralization." In: *Biochimica et biophysica acta* **1790**.12, pp. 1592–8.

Gong, X., Y. Fan, Y. Zhang, C. Luo, X. Duan, L. Yang and J. Pan (2014). "Inserted rest period resensitizes MC3T3-E1 cells to fluid shear stress in a time-dependent manner via F-actin-regulated mechanosensitive channel(s)". In: *Bioscience, Biotechnology, and Biochemistry* **78**.4, pp. 565–573.

Gregory, C. A., W. G. Gunn, A. Peister and D. J. Prockop (2004). "An Alizarin red-based assay of mineralization by adherent cells in culture: comparison with cetylpyridinium chloride extraction." In: *Analytical biochemistry* **329**.1, pp. 77–84.

Gu, G., M. Nars, T. A. Hentunen, K. Metsikkö and H. K. Väänänen (2006). "Isolated primary osteocytes express functional gap junctions in vitro." In: *Cell and tissue research* **323**.2, pp. 263–71.

Gu, Y. et al. (2015). "Microbead-guided reconstruction of the 3D osteocyte network during microfluidic perfusion culture". In: *J. Mater. Chem. B* **3**.17, pp. 3625–3633.

Gundberg, C. M. (2003). "Matrix proteins." In: *Osteoporosis international* **14 Suppl 5**, S37–40; discussion S40–2.

Gupta, R. R., D. J. Yoo, C. Hebert, C. Niger and J. P. Stains (2010). "Induction of an osteocyte-like phenotype by fibroblast growth factor-2." In: *Biochemical and biophysical research communications* **402**.2, pp. 258–64.

Gurkan, U. A. and O. Akkus (2008). "The mechanical environment of bone marrow: a review." In: *Annals of biomedical engineering* **36**.12, pp. 1978–91.

Hadjidakis, D. J. and I. I. Androulakis (2006). "Bone remodeling." In: *Annals of the New York Academy of Sciences* **1092**, pp. 385–96.

Haessler, U. et al. (2012). "Migration dynamics of breast cancer cells in a tunable 3D interstitial flow chamber". In: *Integr. Biol.* **4**.4, pp. 401–409.

Han, Y., S. C. Cowin, M. B. Schaffler and S. Weinbaum (2004). "Mechanotransduction and strain amplification in osteocyte cell processes." In: *Proceedings of the National Academy of Sciences of the United States of America* **101**.47, pp. 16689–94.

Harris, A. K., D. Stopak and P. Wild (1981). "Fibroblast traction as a mechanism for collagen morphogenesis". In: *Nature* **290**.5803, pp. 249–251.

Haycock, J. W. (2011). "3D cell culture: a review of current approaches and techniques". In: *3D Cell Culture*. Springer, pp. 1–15.

Heck, T. A. M., W Wilson, J Foolen, A. C. Cilingir, K Ito and C. C. van Donkelaar (2015). "A tissue adaptation model based on strain-dependent collagen degradation and contact-guided cell traction." In: *Journal of biomechanics* **48**.5, pp. 823–831.

Heino, T. J., T. A. Hentunen and H. K. Väänänen (2004). "Conditioned medium from osteocytes stimulates the proliferation of bone marrow mesenchymal stem cells and their differentiation into osteoblasts." In: *Experimental cell research* **294**.2, pp. 458–68.

Heremans, H, A Billiau, J. J. Cassiman, J. C. Mulier and P de Somer (1978). "In vitro cultivation of human tumor tissues. II. Morphological and virological characterization of three cell lines." In: *Oncology* **35**.6, pp. 246–52.

Heřt, J., P. Fiala and M. Petrtýl (1994). "Osteon orientation of the diaphysis of the long bones in man". In: *Bone* **15**.3, pp. 269–277.

Hillsley, M. V. and J. A. Frangos (1997). "Alkaline phosphatase in osteoblasts is down-regulated by pulsatile fluid flow". In: *Calcified Tissue International* **60**.1, pp. 48–53.

Hirao, M., J. Hashimoto, N. Yamasaki, W. Ando, H. Tsuboi, A. Myoui and H. Yoshikawa (2007). "Oxygen tension is an important mediator of the transformation of osteoblasts to osteocytes." In: *Journal of bone and mineral metabolism* **25**.5, pp. 266–76.

Hoey, D. A., D. J. Kelly and C. R. Jacobs (2011). "A role for the primary cilium in paracrine signaling between mechanically stimulated osteocytes and mesenchymal stem cells." In: *Biochemical and biophysical research communications* **412**.1, pp. 182–7.

Holmbeck, K. et al. (2005). "The metalloproteinase MT1-MMP is required for normal development and maintenance of osteocyte processes in bone." In: *Journal of cell science* **118**.Pt 1, pp. 147–56.

Holmes, D. F., H. K. Graham and K. E. Kadler (1998). "Collagen fibrils forming in developing tendon show an early and abrupt limitation in diameter at the growing tips." In: *Journal of molecular biology* **283**.5, pp. 1049–58.

Huesa, C., M. H. Helfrich and R. M. Aspden (2010). "Parallel-plate fluid flow systems for bone cell stimulation." In: *Journal of biomechanics* **43**.6, pp. 1182–9.

Huh, D., B. D. Matthews, A. Mammoto, M. Montoya-Zavala, H. Y. Hsin and D. E. Ingber (2010). "Reconstituting organ-level lung functions on a chip". In: *Science* **328**.5986, pp. 1662–1668.

Huh, D., G. A. Hamilton and D. E. Ingber (2011). "From 3D cell culture to organs-on-chips". In: *Trends in cell biology* **21**.12, pp. 745–754.

Huh, D., Y.-s. Torisawa, G. A. Hamilton, H. J. Kim and D. E. Ingber (2012). "Microengineered physiological biomimicry: organs-on-chips". In: *Lab on a chip* **12**.12, pp. 2156–2164.

Hulsart-Billström, G et al. (2016). "A surprisingly poor correlation between in vitro and in vivo testing of biomaterials for bone regeneration: results of a multicentre analysis." In: *European cells & materials* **31**, pp. 312–22.

Hung, C. T., S. R. Pollack, T. M. Reilly and C. T. Brighton (1995). "Real-Time Calcium Response of Cultured Bone Cells to Fluid Flow." In: *Clinical Orthopaedics & Related Research* **313**, pp. 256–69.

Hunter, R. A., W. L. Storm, P. N. Coneski and M. H. Schoenfisch (2013). "Inaccuracies of nitric oxide measurement methods in biological media." In: *Analytical chemistry* **85**.3, pp. 1957–63.

Huo, B., X. L. Lu, K. D. Costa, Q. Xu and X. E. Guo (2010). "An ATP-dependent mechanism mediates intercellular calcium signaling in bone cell network under single cell nanoindentation." In: *Cell calcium* **47**.3, pp. 234–41.

Hutmacher, D. W. (2000). "Scaffolds in tissue engineering bone and cartilage". In: *Biomaterials* **21**.24, pp. 2529–2543.

Ingber, D. E. (2006). "Cellular mechanotransduction: putting all the pieces together again." In: *FASEB journal* **20**.7, pp. 811–27.

Irie, K., S. Ejiri, Y. Sakakura, T. Shibui and T. Yajima (2008). "Matrix mineralization as a trigger for osteocyte maturation." In: *The journal of histochemistry and cytochemistry* **56**.6, pp. 561–7.

Ito, N., D. M. Findlay, P. H. Anderson, L. F. Bonewald and G. J. Atkins (2013). "Extracellular phosphate modulates the effect of 1α,25-dihydroxy vitamin D3 (1,25D) on osteocyte like cells". In: *The Journal of Steroid Biochemistry and Molecular Biology* **136**, pp. 183–186.

Jaasma, M. J. and F. J. O'Brien (2008). "Mechanical Stimulation of Osteoblasts Using Steady and Dynamic Fluid Flow". In: *Tissue Engineering Part A* **14**.7, pp. 1213–23.

Jacobs, C. R., C. E. Yellowley, B. R. Davis, Z Zhou, J. M. Cimbala and H. J. Donahue (1998). "Differential effect of steady versus oscillating flow on bone cells." In: *Journal of biomechanics* **31**.11, pp. 969–76.

Jaiswal, N, S. E. Haynesworth, A. I. Caplan and S. P. Bruder (1997). "Osteogenic differentiation of purified, culture-expanded human mesenchymal stem cells in vitro." In: *Journal of cellular biochemistry* **64**.2, pp. 295–312.

Jang, K.-J. and K.-Y. Suh (2010). "A multi-layer microfluidic device for efficient culture and analysis of renal tubular cells". In: *Lab on a Chip* **10**.1, pp. 36–42.

Jing, D., X. L. Lu, E. Luo, P. Sajda, P. L. Leong and X. E. Guo (2013). "Spatiotemporal properties of intracellular calcium signaling in osteocytic and osteoblastic cell networks under fluid flow." In: *Bone* **53**.2, pp. 531–40.

John, H. C. S., K. A. Bishop, M. B. Meyer, N. A. Benkusky, N. Leng, C. Kendziorski, L. F. Bonewald and J. W. Pike (2014). "The Osteoblast to Osteocyte Transition: Epigenetic

Changes and Response to the Vitamin D3 Hormone". In: *Molecular Endocrinology* **28**, pp. 1150 –1165.

Johnson, D. L., T. N. McAllister and J. A. Frangos (1996). "Fluid flow stimulates rapid and continuous release of nitric oxide in osteoblasts". In: *Am J Physiol Endocrinol Metab* **271**.1, E205–208.

Jones, S., A. Boyde and J. Pawley (1975). "Osteoblasts and collagen orientation". In: *Cell and Tissue Research* **159**, pp. 73–80.

Jonsson, K. B., A. Frost, O. Nilsson, S. Ljunghall and Ö. Ljunggren (2009). "Three isolation techniques for primary culture of human osteoblast-like cells: A comparison". In: *Acta Orthopaedica Scandinavica* **70**.4, pp. 365–373.

Kadler, K. E., A. Hill and E. G. Canty-Laird (2008). "Collagen fibrillogenesis: fibronectin, integrins, and minor collagens as organizers and nucleators." In: *Current opinion in cell biology* **20**.5, pp. 495–501.

Kagan, H. M. and W. Li (2003). "Lysyl oxidase: properties, specificity, and biological roles inside and outside of the cell." In: *Journal of cellular biochemistry* **88**.4, pp. 660–72.

Kalajzic, I, A Braut, D Guo, X Jiang, M. Kronenberg, M Mina, M. Harris, S. Harris and D. Rowe (2004). "Dentin matrix protein 1 expression during osteoblastic differentiation, generation of an osteocyte GFP-transgene". In: *Bone* **35**.1, pp. 74–82.

Kamel, M. A., J. L. Picconi, N. Lara-Castillo and M. L. Johnson (2010). "Activation of β-catenin signaling in MLO-Y4 osteocytic cells versus 2T3 osteoblastic cells by fluid flow shear stress and PGE2: Implications for the study of mechanosensation in bone." In: *Bone* **47**.5, pp. 872–81.

Kamioka, H, T Honjo and T Takano-Yamamoto (2001). "A three-dimensional distribution of osteocyte processes revealed by the combination of confocal laser scanning microscopy and differential interference contrast microscopy". In: *Bone* **28**.2, pp. 145–149.

Karageorgiou, V. and D. Kaplan (2005). "Porosity of 3D biomaterial scaffolds and osteogenesis". In: *Biomaterials* **26**.27, pp. 5474–5491.

Kartsogiannis, V. and K. W. Ng (2004). "Cell lines and primary cell cultures in the study of bone cell biology." In: *Molecular and cellular endocrinology* **228**.1-2, pp. 79–102.

Kato, Y., J. J. Windle, B. A. Koop, G. R. Mundy and L. F. Bonewald (1997). "Establishment of an osteocyte-like cell line, MLO-Y4." In: *Journal of bone and mineral research* **12**.12, pp. 2014–23.

Kato, Y, A Boskey, L Spevak, M Dallas, M Hori and L. F. Bonewald (2001). "Establishment of an osteoid preosteocyte-like cell MLO-A5 that spontaneously mineralizes in culture." In: *Journal of bone and mineral research* **16**.9, pp. 1622–33.

Katz, E. P., E Wachtel, M Yamauchi and G. L. Mechanic (1989). "The structure of mineralized collagen fibrils." In: *Connective tissue research* **21**.1-4, 149–54; discussion 155–8.

Kerschnitzki, M., W. Wagermaier, P. Roschger, J. Seto, R. Shahar, G. N. Duda, S. Mundlos and P. Fratzl (2011). "The organization of the osteocyte network mirrors the extra-

cellular matrix orientation in bone." In: *Journal of structural biology* **173**.2, pp. 303–11.

Khan, A. F., M. Awais, A. S. Khan, S. Tabassum, A. A. Chaudhry and I. U. Rehman (2013). "Raman Spectroscopy of Natural Bone and Synthetic Apatites". In: *Applied Spectroscopy Reviews* **48**.4, pp. 329–355.

Kim, H. J., D. Huh, G. Hamilton and D. E. Ingber (2012). "Human gut-on-a-chip inhabited by microbial flora that experiences intestinal peristalsis-like motions and flow". In: *Lab on a Chip* **12**.12, pp. 2165–2174.

Kim, L., Y.-C. Toh, J. Voldman and H. Yu (2007). "A practical guide to microfluidic perfusion culture of adherent mammalian cells". In: *Lab on a Chip* **7**.6, pp. 681–694.

Kini, U. and B. N. Nandeesh (2012). "Physiology of Bone Formation, Remodeling, and Metabolism". In: *Radionuclide and Hybrid Bone Imaging*. Ed. by I. Fogelman, G. Gnanasegaran and H. van der Wall. Berlin, Heidelberg: Springer Berlin Heidelberg, pp. 29–57.

Klein-Nulend, J., C. Semeins, N. Ajubi, P. Nijweide and E. Burger (1995a). "Pulsating Fluid Flow Increases Nitric Oxide (NO) Synthesis by Osteocytes but Not Periosteal Fibroblasts - Correlation with Prostaglandin Upregulation". In: *Biochemical and Biophysical Research Communications* **217**.2, pp. 640–648.

Klein-Nulend, J, A van der Plas, C. M. Semeins, N. E. Ajubi, J. A. Frangos, P. J. Nijweide and E. H. Burger (1995b). "Sensitivity of osteocytes to biomechanical stress in vitro." In: *FASEB journal : official publication of the Federation of American Societies for Experimental Biology* **9**.5, pp. 441–5.

Klein-Nulend, J, E. H. Burger, C. M. Semeins, L. G. Raisz and C. C. Pilbeam (1997). "Pulsating fluid flow stimulates prostaglandin release and inducible prostaglandin G/H synthase mRNA expression in primary mouse bone cells." In: *Journal of bone and mineral research* **12**.1, pp. 45–51.

Klein-Nulend, J, R. G. Bacabac and A. D. Bakker (2012). "Mechanical loading and how it affects bone cells: the role of the osteocyte cytoskeleton in maintaining our skeleton." In: *European cells & materials* **24**, pp. 278–91.

Klein-Nulend, J., A. D. Bakker, R. G. Bacabac, A. Vatsa and S. Weinbaum (2013). "Mechanosensation and transduction in osteocytes." In: *Bone* **54**.2, pp. 182–90.

Knothe Tate, M. L., R Steck, M. R. Forwood and P Niederer (2000). "In vivo demonstration of load-induced fluid flow in the rat tibia and its potential implications for processes associated with functional adaptation." In: *The Journal of experimental biology* **203**, pp. 2737–45.

Knothe Tate, M. L., J. R. Adamson, A. E. Tami and T. W. Bauer (2004). "The osteocyte". In: *The International Journal of Biochemistry & Cell Biology* **36**.1, pp. 1–8.

Kou, S., L. Pan, D. van Noort, G. Meng, X. Wu, H. Sun, J. Xu and I. Lee (2011). "A multishear microfluidic device for quantitative analysis of calcium dynamics in osteoblasts." In: *Biochemical and biophysical research communications* **408**.2, pp. 350–5.

Kreke, M. R. and A. S. Goldstein (2004). "Hydrodynamic shear stimulates osteocalcin expression but not proliferation of bone marrow stromal cells." In: *Tissue engineering* **10**.5-6, pp. 780–8.

Kreke, M. R., W. R. Huckle and A. S. Goldstein (2005). "Fluid flow stimulates expression of osteopontin and bone sialoprotein by bone marrow stromal cells in a temporally dependent manner." In: *Bone* **36**.6, pp. 1047–55.

Kreke, M. R., L. A. Sharp, Y. W. Lee and A. S. Goldstein (2008). "Effect of intermittent shear stress on mechanotransductive signaling and osteoblastic differentiation of bone marrow stromal cells." In: *Tissue engineering. Part A* **14**.4, pp. 529–37.

Kuchan, M. J. and J. A. Frangos (1994). "Role of calcium and calmodulin in flow-induced nitric oxide production in endothelial cells." In: *The American journal of physiology* **266**.3 Pt 1, pp. C628–36.

Lamers, E., X. F. Walboomers, M. Domanski, J. te Riet, F. C. M. J. M. van Delft, R. Luttge, L. A. J. A. Winnubst, H. J. G. E. Gardeniers and J. A. Jansen (2010). "The influence of nanoscale grooved substrates on osteoblast behavior and extracellular matrix deposition." In: *Biomaterials* **31**.12, pp. 3307–16.

Land, K. J., M. B. Mbanjwa, K. Govindasamy and J. G. Korvink (2011). "Low cost fabrication and assembly process for re-usable 3D polydimethylsiloxane (PDMS) microfluidic networks." In: *Biomicrofluidics* **5**.3, pp. 36502–365026.

Langenbach, F. et al. (2013). "Effects of dexamethasone, ascorbic acid and beta glycerophosphate on the osteogenic differentiation of stem cells in vitro". In: *Stem Cell Research & Therapy* **4**.5, p. 117.

Lattouf, R., R. Younes, D. Lutomski, N. Naaman, G. Godeau, K. Senni and S. Changotade (2014). "Picrosirius red staining: a useful tool to appraise collagen networks in normal and pathological tissues." In: *The journal of histochemistry and cytochemistry* **62**.10, pp. 751–8.

Leblanc, A. D., V. S. Schneider, H. J. Evans, D. A. Engelbretson and J. M. Krebs (1990). "Bone mineral loss and recovery after 17 weeks of bed rest." In: *Journal of bone and mineral research* **5**.8, pp. 843–50.

Leblond, C. P. (1989). "Synthesis and seretion of collagen by cells of connective tissue, bone and dentin". In: *The Anatomical record* **224**.2, pp. 123–329.

Leclerc, E, B David, L Griscom, B Lepioufle, T Fujii, P Layrolle and C Legallaisa (2006). "Study of osteoblastic cells in a microfluidic environment." In: *Biomaterials* **27**.4, pp. 586–95.

Lee, C. H., A. Singla and Y. Lee (2001). "Biomedical applications of collagen". In: *International journal of pharmaceutics* **221**.1, pp. 1–22.

Lee, T. C. and D. Taylor (1999). "Bone remodelling: Should we cry wolff?" In: *Irish Journal of Medical Science* **168**.2, pp. 102–105.

Leis, H. J., W Hulla, R Gruber, E Huber, D Zach, H Gleispach and W Windischhofer (1997). "Phenotypic heterogeneity of osteoblast-like MC3T3-E1 cells: changes of bradykinin-

induced prostaglandin E2 production during osteoblast maturation." In: *Journal of bone and mineral research* **12**.4, pp. 541–51.

Li, C. Y., K. R. Stevens, R. E. Schwartz, B. S. Alejandro, J. H. Huang and S. N. Bhatia (2014). "Micropatterned cell-cell interactions enable functional encapsulation of primary hepatocytes in hydrogel microtissues." In: *Tissue engineering. Part A* **20**.15-16, pp. 2200–12.

Li, D., T. Tang, J. Lu and K. Dai (2009). "Effects of flow shear stress and mass transport on the construction of a large-scale tissue-engineered bone in a perfusion bioreactor." In: *Tissue engineering. Part A* **15**.10, pp. 2773–83.

Li, J., E. Rose, D. Frances, Y. Sun and L. You (2012a). "Effect of oscillating fluid flow stimulation on osteocyte mRNA expression." In: *Journal of biomechanics* **45**.2, pp. 247–51.

Li, S., C. Van Den Diepstraten, S. J. D'Souza, B. M. C. Chan and J. G. Pickering (2003). "Vascular smooth muscle cells orchestrate the assembly of type I collagen via alpha2beta1 integrin, RhoA, and fibronectin polymerization." In: *The American journal of pathology* **163**.3, pp. 1045–56.

Li, X., C. Wittkowske, R. Yao and Y. Du (2012b). "Hydrogel as Stem Cell Niche for In Vivo Applications in Regenerative Medicine". In: *Biomaterials and Stem Cells in Regenerative Medicine*. Ed. by S. B. Murugan Ramalingam , Seeram Ramakrishna. 1st ed. CRC Press, pp. 31–54.

Li, X., C. Liu, P. Li, S. Li, Z. Zhao, Y. Chen, B. Huo and D. Zhang (2013). "Connexin 43 is a potential regulator in fluid shear stress-induced signal transduction in osteocytes." In: *Journal of orthopaedic research* **31**.12, pp. 1959–65.

Li, Y., J. Li, S. Zhu, E. Luo, G. Feng, Q. Chen and J. Hu (2012c). "Effects of strontium on proliferation and differentiation of rat bone marrow mesenchymal stem cells".

Liegibel, U. M., U Sommer, B Bundschuh, B Schweizer, U Hilscher, A Lieder, P Nawroth and C Kasperk (2004). "Fluid shear of low magnitude increases growth and expression of TGFbeta1 and adhesion molecules in human bone cells in vitro." In: *Experimental and clinical endocrinology & diabetes* **112**.7, pp. 356–63.

Lim, K. T., J. Hexiu, J. Kim, H. Seonwoo, P.-H. Choung and J. H. Chung (2014). "Synergistic Effects of Orbital Shear Stress on In Vitro Growth and Osteogenic Differentiation of Human Alveolar Bone-Derived Mesenchymal Stem Cells". In: *BioMed Research International* **2014**, pp. 1–18.

Lin, R.-Z. and H.-Y. Chang (2008). "Recent advances in three-dimensional multicellular spheroid culture for biomedical research". In: *Biotechnology Journal* **3**.9-10, pp. 1172–1184.

Ling, Y., H. F. Rios, E. R. Myers, Y. Lu, J. Q. Feng and A. L. Boskey (2005). "DMP1 depletion decreases bone mineralization in vivo: an FTIR imaging analysis." In: *Journal of bone and mineral research* **20**.12, pp. 2169–77.

Loessner, D., K. S. Stok, M. P. Lutolf, D. W. Hutmacher, J. A. Clements and S. C. Rizzi (2010). "Bioengineered 3D platform to explore cell–ECM interactions and drug resistance of epithelial ovarian cancer cells". In: *Biomaterials* **31**.32, pp. 8494–8506.

Lu, X. L., B. Huo, M. Park and X. E. Guo (2012a). "Calcium response in osteocytic networks under steady and oscillatory fluid flow." In: *Bone* **51**.3, pp. 466–73.

Lu, X. L., B. Huo, V. Chiang and X. E. Guo (2012b). "Osteocytic network is more responsive in calcium signaling than osteoblastic network under fluid flow." In: *Journal of bone and mineral research* **27**.3, pp. 563–74.

Mai, Z.-h., Z.-l. Peng, J.-l. Zhang, L. Chen, H.-y. Liang, B. Cai and H. Ai (2013a). "miRNA expression profile during fluid shear stress-induced osteogenic differentiation in MC3T3-E1 cells." In: *Chinese medical journal* **126**.8, pp. 1544–50.

Mai, Z., Z. Peng, S. Wu, J. Zhang, L. Chen, H. Liang, D. Bai, G. Yan and H. Ai (2013b). "Single bout short duration fluid shear stress induces osteogenic differentiation of MC3T3-E1 cells via integrin β1 and BMP2 signaling cross-talk." In: *PloS one* **8**.4, e61600.

Malone, A. M. D., C. T. Anderson, P. Tummala, R. Y. Kwon, T. R. Johnston, T. Stearns and C. R. Jacobs (2007). "Primary cilia mediate mechanosensing in bone cells by a calcium-independent mechanism". In: *Proceedings of the National Academy of Sciences* **104**.33, pp. 13325–13330.

Manolagas, S. C. (2000). "Birth and death of bone cells: basic regulatory mechanisms and implications for the pathogenesis and treatment of osteoporosis." In: *Endocrine reviews* **21**.2, pp. 115–37.

Markides, H., J. S. McLaren and A. J. El Haj (2015). "Overcoming translational challenges – The delivery of mechanical stimuli in vivo". In: *The International Journal of Biochemistry & Cell Biology* **69**, pp. 162–172.

Martin, R. and D. Boardman (1993). "The effects of collagen fiber orientation, porosity, density, and mineralization on bovine cortical bone bending properties". In: *Journal of Biomechanics* **26**.9, pp. 1047–1054.

Martin, R., S. Lau, P. Mathews, V. Gibson and S. Stover (1996). "Collagen fiber organization is related to mechanical properties and remodeling in equine bone. A comparsion of two methods". In: *Journal of Biomechanics* **29**.12, pp. 1515–1521.

Martínez, M. E. et al. (1999). "Influence of Skeletal Site of Origin and Donor Age on Osteoblastic Cell Growth and Differentiation". In: *Calcified Tissue International* **64**.4, pp. 280–286.

Matsugaki, A., N. Fujiwara and T. Nakano (2013). "Continuous cyclic stretch induces osteoblast alignment and formation of anisotropic collagen fiber matrix." In: *Acta biomaterialia* **9**.7, pp. 7227–35.

Matsugaki, A., G. Aramoto, T. Ninomiya, H. Sawada, S. Hata and T. Nakano (2015a). "Abnormal arrangement of a collagen/apatite extracellular matrix orthogonal to osteoblast alignment is constructed by a nanoscale periodic surface structure." In: *Biomaterials* **37**, pp. 134–43.

Matsugaki, A., Y. Isobe, T. Saku and T. Nakano (2015b). "Quantitative regulation of bone-mimetic, oriented collagen/apatite matrix structure depends on the degree of osteoblast alignment on oriented collagen substrates." In: *Journal of biomedical materials research. Part A* **103**.2, pp. 489–99.

Matthews, B. G., D. Naot, K. E. Callon, D. S. Musson, R. Locklin, P. A. Hulley, A. Grey and J. Cornish (2014). "Enhanced osteoblastogenesis in three-dimensional collagen gels". In: *Bonekey Reports* **3**.

McCoy, R. J. and F. J. O'Brien (2010). "Influence of shear stress in perfusion bioreactor cultures for the development of three-dimensional bone tissue constructs: a review." In: *Tissue engineering. Part B, Reviews* **16**.6, pp. 587–601.

McDonald, J. A., D. G. Kelley and T. J. Broekelmann (1982). "Role of fibronectin in collagen deposition: Fab' to the gelatin-binding domain of fibronectin inhibits both fibronectin and collagen organization in fibroblast extracellular matrix." In: *The Journal of cell biology* **92**.2, pp. 485–92.

McGarry, J. G., J. Klein-Nulend, M. G. Mullender and P. J. Prendergast (2005). "A comparison of strain and fluid shear stress in stimulating bone cell responses–a computational and experimental study." In: *FASEB journal* **19**.3, pp. 482–4.

McGuigan, A. P., D. A. Bruzewicz, A. Glavan, M. Butte and G. M. Whitesides (2008). "Cell encapsulation in sub-mm sized gel modules using replica molding". In: *PLOS one* **3**.5, e2258.

Menon, R., A. Patel, D. Gil and H. I. Smith (2005). "Maskless lithography". In: *Materials Today* **8**.2, pp. 26–33.

Meunier, P. J. et al. (2002). "Strontium ranelate: dose-dependent effects in established postmenopausal vertebral osteoporosis–a 2-year randomized placebo controlled trial." In: *The Journal of clinical endocrinology and metabolism* **87**.5, pp. 2060–6.

Meunier, P. J. et al. (2004). "The Effects of Strontium Ranelate on the Risk of Vertebral Fracture in Women with Postmenopausal Osteoporosis". In: *The new england journal of medicine* **350**, pp. 459–68.

Michaels, J. D., A. K. Mallik and E. T. Papoutsakis (1996). "Sparging and agitation-induced injury of cultured animals cells: Do cell-to-bubble interactions in the bulk liquid injure cells?" In: *Biotechnology and bioengineering* **51**.4, pp. 399–409.

Montanez-Sauri, S. I., K. E. Sung, J. P. Puccinelli, C. Pehlke and D. J. Beebe (2011). "Automation of three-dimensional cell culture in arrayed microfluidic devices." In: *Journal of laboratory automation* **16**.3, pp. 171–85.

Morris, H. L., C. I. Reed, J. W. Haycock and G. C. Reilly (2010). "Mechanisms of fluid-flow-induced matrix production in bone tissue engineering." In: *Proceedings of the Institution of Mechanical Engineers. Part H, Journal of engineering in medicine* **224**.12, pp. 1509–21.

Mosadegh, B., B. E. Dabiri, M. R. Lockett, R. Derda, P. Campbell, K. K. Parker and G. M. Whitesides (2014). "Three-Dimensional Paper-Based Model for Cardiac Ischemia". In: *Advanced healthcare materials*.

Mullard, A. (2016). "Merck & Co. drops osteoporosis drug odanacatib". In: *Nature Reviews Drug Discovery* **15**.10, pp. 669–669.

Mullen, C. A., M. G. Haugh, M. B. Schaffler, R. J. Majeska and L. M. McNamara (2013). "Osteocyte differentiation is regulated by extracellular matrix stiffness and intercellular separation." In: *Journal of the mechanical behavior of biomedical materials* **28**, pp. 183–94.

Mullender, M, A. J. El Haj, Y Yang, M. A. van Duin, E. H. Burger and J Klein-Nulend (2004). "Mechanotransduction of bone cells in vitro: mechanobiology of bone tissue." In: *Medical & biological engineering & computing* **42**.1, pp. 14–21.

Murshid, S. A., H. Kamioka, Y. Ishihara, R. Ando, Y. Sugawara and T. Takano-Yamamoto (2007). "Actin and microtubule cytoskeletons of the processes of 3D-cultured MC3T3-E1 cells and osteocytes". In: *Journal of Bone and Mineral Metabolism* **25**.3, pp. 151–158.

Myers, K. A., J. B. Rattner, N. G. Shrive and D. A. Hart (2007). "Osteoblast-like cells and fluid flow: cytoskeleton-dependent shear sensitivity." In: *Biochemical and biophysical research communications* **364**.2, pp. 214–9.

Nair, A. K., A. Gautieri, S.-W. Chang and M. J. Buehler (2013). "Molecular mechanics of mineralized collagen fibrils in bone." In: *Nature communications* **4**, p. 1724.

Nakao, Y., H. Ura, Y. Sakai and T. Fujii (2011). "Bile canaliculi formation by aligning rat primary hepatocytes in a microfluidic device". In: *Biomicrofluidics* **5**.2, p. 22212.

Nardone, V. et al. (2015). "In Vitro Effects of Strontium on Proliferation and Osteoinduction of Human Preadipocytes". In: *Stem Cells International* **2015**.

Nauman, E. A., R. L. Satcher, T. M. Keaveny, B. P. Halloran and D. D. Bikle (2001). "Osteoblasts respond to pulsatile fluid flow with short-term increases in PGE2 but no change in mineralization". In: *J Appl Physiol* **90**.5, pp. 1849–1854.

Ng, C. P., B Hiny and M. A. Swartz (2005). "Interstitial fluid flow induces myofibroblast differentiation and collagen alignment in vitro". In: *Journal of Cell Science* **118**.20, pp. 4731–4739.

Ng, C. P. and M. A. Swartz (2003). "Fibroblast alignment under interstitial fluid flow using a novel 3-D tissue culture model". In: *American Journal of Physiology-Heart and Circulatory Physiology* **284**.5, H1771–H1777.

Nirmalanandhan, V. S., M. S. Levy, A. J. Huth and D. L. Butler (2006). "Effects of Cell Seeding Density and Collagen Concentration on Contraction Kinetics of Mesenchymal Stem Cell–Seeded Collagen Constructs". In: *Tissue Engineering* **12**.7, pp. 1865–1872.

Niu, X., L. Wang, F. Tian, L. Wang, P. Li, Q. Feng and Y. Fan (2016). "Shear-mediated crystallization from amorphous calcium phosphate to bone apatite." In: *Journal of the mechanical behavior of biomedical materials* **54**, pp. 131–40.

O'Brien, F. J., B. A. Harley, I. V. Yannas and L. J. Gibson (2005). "The effect of pore size on cell adhesion in collagen-GAG scaffolds". In: *Biomaterials* **26**.4, pp. 433–441.

Orimo, H. (2010). "The mechanism of mineralization and the role of alkaline phosphatase in health and disease." In: *Journal of Nihon Medical School* **77**.1, pp. 4–12.

Orriss, I. R., S. E. B. Taylor and T. R. Arnett (2012). "Rat osteoblast cultures." In: *Methods in molecular biology* **816**, pp. 31–41.

Owan, I., D. B. Burr, C. H. Turner, J. Qiu, Y. Tu, J. E. Onyia and R. L. Duncan (1997). "Mechanotransduction in bone: osteoblasts are more responsive to fluid forces than mechanical strain". In: *Am J Physiol Cell Physiol* **273**.3, pp. C810–815.

Owen, R., C. Sherborne, T. Paterson, N. H. Green, G. C. Reilly and F. Claeyssens (2016). "Emulsion templated scaffolds with tunable mechanical properties for bone tissue engineering". In: *Journal of the Mechanical Behavior of Biomedical Materials* **54**, pp. 159–172.

Palumbo, C., M. Ferretti and G. Marotti (2004). "Osteocyte dendrogenesis in static and dynamic bone formation: an ultrastructural study." In: *The anatomical record. Part A, Discoveries in molecular, cellular, and evolutionary biology* **278**.1, pp. 474–80.

Pammolli, F., L. Magazzini and M. Riccaboni (2011). "The productivity crisis in pharmaceutical R&D". In: *Nature Reviews Drug Discovery* **10**.6, pp. 428–438.

Pan, H., Z. Li, W. Lam, J. Wong, B. Darvell, K. Luk and W. Lu (2009). "Solubility of strontium-substituted apatite by solid titration". In: *Acta Biomaterialia* **5**.5, pp. 1678–1685.

Park, J. et al. (2015). "Three-dimensional brain-on-a-chip with an interstitial level of flow and its application as an in vitro model of Alzheimer's disease". In: *Lab Chip* **15**.1, pp. 141–150.

Parreno, J., G. Buckley-Herd, I. De-Hemptinne and D. A. Hart (2008). "Osteoblastic MG-63 cell differentiation, contraction, and mRNA expression in stress-relaxed 3D collagen I gels". In: *Molecular and Cellular Biochemistry* **317**.1-2, pp. 21–32.

Pavalko, F. M., N. X. Chen, C. H. Turner, D. B. Burr, S. Atkinson, Y.-F. Hsieh, J. Qiu and R. L. Duncan (1998). "Fluid shear-induced mechanical signaling in MC3T3-E1 osteoblasts requires cytoskeleton-integrin interactions". In: *Am J Physiol Cell Physiol* **275**.6, pp. C1591–1601.

Pedersen, J. A., S. Lichter and M. A. Swartz (2010). "Cells in 3D matrices under interstitial flow: effects of extracellular matrix alignment on cell shear stress and drag forces." In: *Journal of biomechanics* **43**.5, pp. 900–5.

Penido, M. G. M. G. and U. S. Alon (2012). "Phosphate homeostasis and its role in bone health." In: *Pediatric nephrology* **27**.11, pp. 2039–48.

Plas, A van der and P. J. Nijweide (1992). "Isolation and purification of osteocytes." In: *Journal of bone and mineral research* **7**.4, pp. 389–96.

Poellmann, M. J., J. B. Estrada, T. Boudou, Z. T. Berent, C. Franck and A. J. Wagoner Johnson (2015). "Differences in Morphology and Traction Generation of Cell Lines Representing Different Stages of Osteogenesis." In: *Journal of biomechanical engineering* **137**.12, p. 124503.

Polacheck, W. J., J. L. Charest and R. D. Kamm (2011). "Interstitial flow influences direction of tumor cell migration through competing mechanisms." In: *Proceedings of*

the National Academy of Sciences of the United States of America **108**.27, pp. 11115–11120.

Polishchuk, R. S., E. V. Polishchuk, P Marra, S Alberti, R Buccione, A Luini and A. A. Mironov (2000). "Correlative light-electron microscopy reveals the tubular-saccular ultrastructure of carriers operating between Golgi apparatus and plasma membrane." In: *The Journal of cell biology* **148**.1, pp. 45–58.

Ponik, S. M., J. W. Triplett and F. M. Pavalko (2007). "Osteoblasts and osteocytes respond differently to oscillatory and unidirectional fluid flow profiles." In: *Journal of cellular biochemistry* **100**.3, pp. 794–807.

Prideaux, M, K. A. Staines, E. R. Jones, G. P. Riley, A. A. Pitsillides and C Farquharson (2015). "MMP and TIMP temporal gene expression during osteocytogenesis." In: *Gene expression patterns* **18**.1-2, pp. 29–36.

Prideaux, M., N. Loveridge, A. A. Pitsillides and C. Farquharson (2012). "Extracellular matrix mineralization promotes E11/gp38 glycoprotein expression and drives osteocytic differentiation." In: *PloS one* **7**.5, e36786.

Prideaux, M., A. R. Wijenayaka, D. D. Kumarasinghe, R. T. Ormsby, A. Evdokiou, D. M. Findlay and G. J. Atkins (2014). "SaOS2 Osteosarcoma cells as an in vitro model for studying the transition of human osteoblasts to osteocytes." In: *Calcified tissue international* **95**.2, pp. 183–93.

Prideaux, M., C. Schutz, A. R. Wijenayaka, D. M. Findlay, D. G. Campbell, L. B. Solomon and G. J. Atkins (2016). "Isolation of osteocytes from human trabecular bone." In: *Bone* **88**, pp. 64–72.

Prockop, D. J., A. L. Sieron and S. W. Li (1998). "Procollagen N-proteinase and procollagen C-proteinase. Two unusual metalloproteinases that are essential for procollagen processing probably have important roles in development and cell signaling." In: *Matrix biology* **16**.7, pp. 399–408.

Prodanov, L, C. M. Semeins, J. J. W. A. van Loon, J te Riet, J. A. Jansen, J Klein-Nulend and X. F. Walboomers (2013). "Influence of nanostructural environment and fluid flow on osteoblast-like cell behavior: a model for cell-mechanics studies." In: *Acta biomaterialia* **9**.5, pp. 6653–62.

Puustjärvi, K, J Nieminen, T Räsänen, M Hyttinen, H. J. Helminen, H Kröger, J Huuskonen, E Alhava and V Kovanen (1999). "Do more highly organized collagen fibrils increase bone mechanical strength in loss of mineral density after one-year running training?" In: *Journal of bone and mineral research* **14**.3, pp. 321–9.

Quent, V. M. C., D. Loessner, T. Friis, J. C. Reichert and D. W. Hutmacher (2010). "Discrepancies between metabolic activity and DNA content as tool to assess cell proliferation in cancer research." In: *Journal of cellular and molecular medicine* **14**.4, pp. 1003–13.

Querido, W., A. P. C. Campos, E. H. Martins Ferreira, R. A. S. San Gil, A. M. Rossi and M. Farina (2014). "Strontium ranelate changes the composition and crystal structure

of the biological bone-like apatite produced in osteoblast cell cultures." In: *Cell and tissue research* **357**.3, pp. 793–801.

Querido, W., M. Farina and K. Anselme (2015). "Strontium ranelate improves the interaction of osteoblastic cells with titanium substrates: Increase in cell proliferation, differentiation and matrix mineralization." In: *Biomatter* **5**.1, e1027847–1–e1027847–11.

Ramanujan, S., A. Pluen, T. D. McKee, E. B. Brown, Y. Boucher and R. K. Jain (2002). "Diffusion and Convection in Collagen Gels: Implications for Transport in the Tumor Interstitium". In: *Biophysical Journal* **83**.3, pp. 1650–1660.

Raub, C. B., A. J. Putnam, B. J. Tromberg and S. C. George (2010). "Predicting bulk mechanical properties of cellularized collagen gels using multiphoton microscopy". In: *Acta biomaterialia* **6**.12, pp. 4657–4665.

Reginster, J. Y. et al. (2005). "Strontium Ranelate Reduces the Risk of Nonvertebral Fractures in Postmenopausal Women with Osteoporosis: Treatment of Peripheral Osteoporosis (TROPOS) Study". In: *The Journal of clinical endocrinology and metabolism* **90**.5, pp. 2816–2822.

Reginster, J.-Y. et al. (2015). "The position of strontium ranelate in today's management of osteoporosis." In: *Osteoporosis international* **26**.6, pp. 1667–71.

Reich, K., C. Gay and J. Frangos (1990). "Effect of flow on prostaglandin E/sub 2/ production and inositol trisphosphate levels in cultured osteoblasts". In: *Sixteenth Annual Northeast Conference on Bioengineering*. IEEE, pp. 152–153.

Reilly, G. C., T. R. Haut, C. E. Yellowley, H. J. Donahue and C. R. Jacobs (2003). "Fluid flow induced PGE2 release by bone cells is reduced by glycocalyx degradation whereas calcium signals are not." In: *Biorheology* **40**.6, pp. 591–603.

Rendenbach, C. et al. (2014). "Effects of Extracellular Phosphate on Gene Expression in Murine Osteoblasts". In: *Calcified Tissue International* **94**.5, pp. 474–483.

Rest, M van der and R Garrone (1991). "Collagen family of proteins." In: *FASEB journal* **5**.13, pp. 2814–23.

Riggs, C., L. Vaughan, G. Evans, L. Lanyon and A. Boyde (1993). "Mechanical implications of collagen fibre orientation in cortical bone of the equine radius". In: *Anatomy and Embryology* **187**.3.

Robin, M., C. Almeida, T. Azaïs, B. Haye, C. Illoul, J. Lesieur, M.-M. Giraud-Guille, N. Nassif and C. Hélary (2016). "Involvement of 3D osteoblast migration and bone apatite during in vitro early osteocytogenesis." In: *Bone* **88**, pp. 146–156.

Robling, A. G., D. B. Burr and C. H. Turner (2001). "Recovery periods restore mechanosensitivity to dynamically loaded bone." In: *The Journal of experimental biology* **204**.Pt 19, pp. 3389–99.

Rosenberg, N., O. Rosenberg and M. Soudry (2012). "Osteoblasts in bone physiology-mini review." In: *Rambam Maimonides medical journal* **3**.2, e0013.

Rubin, J., C. Rubin and C. R. Jacobs (2006). "Molecular pathways mediating mechanical signaling in bone." In: *Gene* **367**, pp. 1–16.

Salek, M. M., P. Sattari and R. J. Martinuzzi (2012). "Analysis of fluid flow and wall shear stress patterns inside partially filled agitated culture well plates." In: *Annals of biomedical engineering* **40**.3, pp. 707–28.

Sbrana, T. and A. Ahluwalia (2012). "Engineering Quasi-Vivo in vitro organ models". In: *New Technologies for Toxicity Testing*. Springer, pp. 138–153.

Scaglione, S, D Wendt, S Miggino, A Papadimitropoulos, M Fato, R Quarto and I Martin (2008). "Effects of fluid flow and calcium phosphate coating on human bone marrow stromal cells cultured in a defined 2D model system." In: *Journal of biomedical materials research. Part A* **86**.2, pp. 411–9.

Schäck, L. M., S. Noack, R. Winkler, G. Wißmann, P. Behrens, M. Wellmann, M. Jagodzinski, C. Krettek and A. Hoffmann (2013). "The Phosphate Source Influences Gene Expression and Quality of Mineralization during In Vitro Osteogenic Differentiation of Human Mesenchymal Stem Cells." In: *PloS one* **8**.6, e65943.

Schiavi, S. C. (2006). "Bone talk." In: *Nature genetics* **38**.11, pp. 1230–1.

Schulze, E, M Witt, M Kasper, C. W. Löwik and R. H. Funk (1999). "Immunohistochemical investigations on the differentiation marker protein E11 in rat calvaria, calvaria cell culture and the osteoblastic cell line ROS 17/2.8." In: *Histochemistry and cell biology* **111**.1, pp. 61–9.

Schumacker, P. T. (2002). "Straining to understand mechanotransduction in the lung." In: *American journal of physiology. Lung cellular and molecular physiology* **282**.5, pp. L881–2.

Scott, J. E. (1995). "Extracellular matrix, supramolecular organisation and shape." In: *Journal of anatomy* **187**, pp. 259–69.

Scully, N. (2015). "Differentiation of osteoblasts to osteocytes in 3D type I collagen gels - a novel tool to study osteocyte responses to mechanical loading". PhD thesis. Cardiff University.

Serpooshan, V., M. Julien, O. Nguyen, H. Wang, A. Li, N. Muja, J. E. Henderson and S. N. Nazhat (2010). "Reduced hydraulic permeability of three-dimensional collagen scaffolds attenuates gel contraction and promotes the growth and differentiation of mesenchymal stem cells". In: *Acta Biomaterialia* **6**.10, pp. 3978–3987.

Seto, J., H. S. Gupta, P. Zaslansky, H. D. Wagner and P. Fratzl (2008). "Tough Lessons From Bone: Extreme Mechanical Anisotropy at the Mesoscale". In: *Advanced Functional Materials* **18**.13, pp. 1905–1911.

Shapiro, F (1988). "Cortical bone repair. The relationship of the lacunar-canalicular system and intercellular gap junctions to the repair process." In: *The Journal of bone and joint surgery. American volume* **70**.7, pp. 1067–81.

— (2008). "Bone development and its relation to fracture repair. The role of mesenchymal osteoblasts and surface osteoblasts." In: *European cells & materials* **15**, pp. 53–76.

Sikavitsas, V. I., J. S. Temenoff and A. G. Mikos (2001). "Biomaterials and bone mechanotransduction". In: *Biomaterials* **22**.19, pp. 2581–2593.

Sikavitsas, V. I., G. N. Bancroft, H. L. Holtorf, J. A. Jansen and A. G. Mikos (2003). "Mineralized matrix deposition by marrow stromal osteoblasts in 3D perfusion culture increases with increasing fluid shear forces." In: *Proceedings of the National Academy of Sciences of the United States of America* **100**.25, pp. 14683–8.

Sikavitsas, V. I., G. N. Bancroft, J. J. Lemoine, M. A. K. Liebschner, M. Dauner and A. G. Mikos (2005). "Flow Perfusion Enhances the Calcified Matrix Deposition of Marrow Stromal Cells in Biodegradable Nonwoven Fiber Mesh Scaffolds". In: *Annals of Biomedical Engineering* **33**.1, pp. 63–70.

Simon, K. A., K. M. Park, B. Mosadegh, A. B. Subramaniam, A. D. Mazzeo, P. M. Ngo and G. M. Whitesides (2014). "Polymer-based mesh as supports for multi-layered 3D cell culture and assays". In: *Biomaterials* **35**.1, pp. 259–268.

Simon, K. A., N. J. Warren, B. Mosadegh, M. R. Mohammady, G. M. Whitesides and S. P. Armes (2015). "Disulfide-Based Diblock Copolymer Worm Gels: A Wholly-Synthetic Thermoreversible 3D Matrix for Sheet-Based Cultures". In: *Biomacromolecules* **16**.12, pp. 3952–3958.

Sittichockechaiwut, A., A. M. Scutt, A. J. Ryan, L. F. Bonewald and G. C. Reilly (2009). "Use of rapidly mineralising osteoblasts and short periods of mechanical loading to accelerate matrix maturation in 3D scaffolds". In: *Bone* **44**.5, pp. 822–829.

Sittichokechaiwut, A, J. H. Edwards, A. M. Scutt and G. C. Reilly (2010). "Short bouts of mechanical loading are as effective as dexamethasone at inducing matrix production by human bone marrow mesenchymal stem cell." In: *European cells & materials* **20**, pp. 45–57.

Song, H. M., R. P. Nacamuli, W. Xia, A. S. Bari, Y.-Y. Shi, T. D. Fang and M. T. Longaker (2005). "High-dose retinoic acid modulates rat calvarial osteoblast biology." In: *Journal of cellular physiology* **202**.1, pp. 255–62.

Spatz, J. M. et al. (2015). "The Wnt Inhibitor Sclerostin Is Up-regulated by Mechanical Unloading in Osteocytes in Vitro." In: *The Journal of biological chemistry* **290**.27, pp. 16744–58.

Spector, J. A., J. A. Greenwald, S. M. Warren, P. J. Bouletreau, F. E. Crisera, B. J. Mehrara and M. T. Longaker (2002). "Co-culture of osteoblasts with immature dural cells causes an increased rate and degree of osteoblast differentiation." In: *Plastic and reconstructive surgery* **109**.2, 631–42; discussion 643–4.

Staines, K. A., M. Prideaux, S. Allen, D. J. Buttle, A. A. Pitsillides and C. Farquharson (2016). "E11/Podoplanin Protein Stabilization Through Inhibition of the Proteasome Promotes Osteocyte Differentiation in Murine in Vitro Models." In: *Journal of cellular physiology* **231**.6, pp. 1392–404.

Stern, A. R., M. M. Stern, M. E. Van Dyke, K. Jähn, M. Prideaux and L. F. Bonewald (2012). "Isolation and culture of primary osteocytes from the long bones of skeletally mature and aged mice." In: *BioTechniques* **52**.6, pp. 361–73.

Stevens, B., Y. Yang, A. Mohandas, B. Stucker and K. T. Nguyen (2008). "A review of materials, fabrication methods, and strategies used to enhance bone regeneration in

engineered bone tissues". In: *Journal of Biomedical Materials Research Part B: Applied Biomaterials* **85B**.2, pp. 573–582.

Su, W.-T., Y.-T. Wang and C.-M. Chou (2014). "Optimal fluid flow enhanced mineralization of MG-63 cells in porous chitosan scaffold". In: *Journal of the Taiwan Institute of Chemical Engineers* **45**.4, pp. 1111–1118.

Suda, T., N. Takahashi, N. Udagawa, E. Jimi, M. T. Gillespie and T. J. Martin (1999). "Modulation of Osteoclast Differentiation and Function by the New Members of the Tumor Necrosis Factor Receptor and Ligand Families". In: *Endocrine Reviews* **20**.3, pp. 345–357.

Sudo, H, H. A. Kodama, Y Amagai, S Yamamoto and S Kasai (1983). "In vitro differentiation and calcification in a new clonal osteogenic cell line derived from newborn mouse calvaria." In: *The Journal of cell biology* **96**.1, pp. 191–8.

Sumanasinghe, R. D., S. H. Bernacki and E. G. Loboa (2006). "Osteogenic Differentiation of Human Mesenchymal Stem Cells in Collagen Matrices: Effect of Uniaxial Cyclic Tensile Strain on Bone Morphogenetic Protein (BMP-2) mRNA Expression". In: *Tissue Engineering* **12**.12, pp. 3459–3465.

Sun, T., S. Jackson, J. W. Haycock and S. MacNeil (2006). "Culture of skin cells in 3D rather than 2D improves their ability to survive exposure to cytotoxic agents". In: *Journal of Biotechnology* **122**.3, pp. 372–381.

Sung, K. E., G. Su, C. Pehlke, S. M. Trier, K. W. Eliceiri, P. J. Keely, A. Friedl and D. J. Beebe (2009). "Control of 3-dimensional collagen matrix polymerization for reproducible human mammary fibroblast cell culture in microfluidic devices." In: *Biomaterials* **30**.27, pp. 4833–41.

Sung, K. E., X. Su, E. Berthier, C. Pehlke, A. Friedl and D. J. Beebe (2013). "Understanding the Impact of 2D and 3D Fibroblast Cultures on In Vitro Breast Cancer Models". In: *PloS one* **8**.10, e76373.

Swartz, M. A. and M. E. Fleury (2007). "Interstitial flow and its effects in soft tissues." In: *Annual review of biomedical engineering* **9**, pp. 229–56.

Tabeling, P. (2010). *Introduction to microfluidics.* Oxford University Press.

Tan, W. and T. A. Desai (2003). "Microfluidic Patterning of Cellular Biopolymer Matrices for Biomimetic 3-D Structures". In: *Biomedical Microdevices* **5**.3, pp. 235–244.

Tanaka, S. M., H. B. Sun, R. K. Roeder, D. B. Burr, C. H. Turner and H. Yokota (2005). "Osteoblast responses one hour after load-induced fluid flow in a three-dimensional porous matrix." In: *Calcified tissue international* **76**.4, pp. 261–71.

Taylor, A. F., M. M. Saunders, D. L. Shingle, J. M. Cimbala, Z Zhou and H. J. Donahue (2007). "Mechanically stimulated osteocytes regulate osteoblastic activity via gap junctions." In: *American journal of physiology. Cell physiology* **292**.1, pp. C545–52.

Tenenbaum, H. C., C. A. G. McCulloch, C. Fair and C. Birek (1989). "The regulatory effect of phosphates on bone metabolism in vitro". In: *Cell and Tissue Research* **257**.3, pp. 555–563.

Toepke, M. W. and D. J. Beebe (2006). "PDMS absorption of small molecules and consequences in microfluidic applications". In: *Lab Chip* **6**.12, pp. 1484–1486.

Tomasek, J. J., G. Gabbiani, B. Hinz, C. Chaponnier and R. A. Brown (2002). "Myofibroblasts and mechano-regulation of connective tissue remodelling." In: *Nature reviews. Molecular cell biology* **3**.5, pp. 349–63.

Torisawa, Y.-s., C. S. Spina, T. Mammoto, A. Mammoto, J. C. Weaver, T. Tat, J. J. Collins and D. E. Ingber (2014). "Bone marrow–on–a–chip replicates hematopoietic niche physiology in vitro". In: *Nature Methods* **11**.6, pp. 663–669.

Toyosawa, S, S Shintani, T Fujiwara, T Ooshima, A Sato, N Ijuhin and T Komori (2001). "Dentin matrix protein 1 is predominantly expressed in chicken and rat osteocytes but not in osteoblasts." In: *Journal of bone and mineral research* **16**.11, pp. 2017–26.

Trappmann, B. et al. (2012). "Extracellular-matrix tethering regulates stem-cell fate". In: *Nature materials* **11**.7, pp. 642–649.

Trietsch, S. J., G. D. Israels, J. Joore, T. Hankemeier and P. Vulto (2013). "Microfluidic titer plate for stratified 3D cell culture". In: *Lab on a Chip* **13**.18, pp. 3548–3554.

Tucker, R. P., P Henningsson, S. L. Franklin, D Chen, Y Ventikos, R. J. Bomphrey and M. S. Thompson (2014). "See-saw rocking: an in vitro model for mechanotransduction research." In: *Journal of the Royal Society, Interface* **11**.97, p. 20140330.

Uchihashi, K., S. Aoki, A. Matsunobu and S. Toda (2013). "Osteoblast migration into type I collagen gel and differentiation to osteocyte-like cells within a self-produced mineralized matrix: a novel system for analyzing differentiation from osteoblast to osteocyte." In: *Bone* **52**.1, pp. 102–10.

Vazquez, M., B. A. J. Evans, D. Riccardi, S. L. Evans, J. R. Ralphs, C. M. Dillingham and D. J. Mason (2014). "A new method to investigate how mechanical loading of osteocytes controls osteoblasts." In: *Frontiers in endocrinology* **5**, p. 208.

Verberckmoes, S. C. et al. (2004). "Effects of strontium on the physicochemical characteristics of hydroxyapatite." In: *Calcified tissue international* **75**.5, pp. 405–15.

Verberckmoes, S. C., M. E. De Broe and P. C. D'Haese (2003). "Dose-dependent effects of strontium on osteoblast function and mineralization". In: *Kidney International* **64**.2, pp. 534–543.

Vezeridis, P. S., C. M. Semeins, Q. Chen and J. Klein-Nulend (2006). "Osteocytes subjected to pulsating fluid flow regulate osteoblast proliferation and differentiation." In: *Biochemical and biophysical research communications* **348**.3, pp. 1082–8.

Vickerman, V., J. Blundo, S. Chung and R. Kamm (2008). "Design, fabrication and implementation of a novel multi-parameter control microfluidic platform for three-dimensional cell culture and real-time imaging." In: *Lab on a chip* **8**, pp. 1468–1477.

Vico, L., P. Collet, A. Guignandon, M.-H. Lafage-Proust, T. Thomas, M. Rehailia and C. Alexandre (2000). "Effects of long-term microgravity exposure on cancellous and cortical weight-bearing bones of cosmonauts". In: *The Lancet* **355**.9215, pp. 1607–1611.

Viguet-Carrin, S, P Garnero and P. D. Delmas (2006). "The role of collagen in bone strength." In: *Osteoporosis international* **17**.3, pp. 319–36.

Voegele, T. J., M Voegele-Kadletz, V Esposito, K Macfelda, U Oberndorfer, V Vecsei and R Schabus (2000). "The effect of different isolation techniques on human osteoblast-like cell growth." In: *Anticancer research* **20**.5B, pp. 3575–81.

Vogel, B., H. Siebert, U. Hofmann and S. Frantz (2015). "Determination of collagen content within picrosirius red stained paraffin-embedded tissue sections using fluorescence microscopy." In: *MethodsX* **2**, pp. 124–34.

Vollrath, M. A., K. Y. Kwan and D. P. Corey (2007). "The micromachinery of mechanotransduction in hair cells." In: *Annual review of neuroscience* **30**, pp. 339–65.

Vos, T., R. M. Barber, B. Bell, A. Bertozzi-Villa, S. Biryukov and E. Al. (2015). "Global, regional, and national age–sex specific all-cause and cause-specific mortality for 240 causes of death, 1990–2013: a systematic analysis for the Global Burden of Disease Study 2013". In: *The Lancet* **385**.9963, pp. 117–171.

Wagner, I. et al. (2013). "A dynamic multi-organ-chip for long-term cultivation and substance testing proven by 3D human liver and skin tissue co-culture". In: *Lab on a Chip* **13**.18, pp. 3538–3547.

Walker, L. M., S. J. Publicover, M. R. Preston, M. A. Said Ahmed and A. J. El Haj (2000). "Calcium-channel activation and matrix protein upregulation in bone cells in response to mechanical strain." In: *Journal of cellular biochemistry* **79**.4, pp. 648–61.

Wang, D, K Christensen, K Chawla, G Xiao, P. H. Krebsbach and R. T. Franceschi (1999). "Isolation and characterization of MC3T3-E1 preosteoblast subclones with distinct in vitro and in vivo differentiation/mineralization potential." In: *Journal of bone and mineral research* **14**.6, pp. 893–903.

Wang, D. M. and J. M. Tarbell (1995). "Modeling interstitial flow in an artery wall allows estimation of wall shear stress on smooth muscle cells". In: *Journal of biomechanical engineering* **117**.3, pp. 358–363.

Wang, J. H.-C., E. S. Grood, J. Florer and R. Wenstrup (2000). "Alignment and proliferation of MC3T3-E1 osteoblasts in microgrooved silicone substrata subjected to cyclic stretching". In: *Journal of Biomechanics* **33**.6, pp. 729–735.

Wang, J. H.-C., F. Jia, T. W. Gilbert and S. L.-Y. Woo (2003). "Cell orientation determines the alignment of cell-produced collagenous matrix". In: *Journal of Biomechanics* **36**.1, pp. 97–102.

Wang, S and J. M. Tarbell (2000). "Effect of fluid flow on smooth muscle cells in a 3-dimensional collagen gel model." In: *Arteriosclerosis, thrombosis, and vascular biology* **20**, pp. 2220–2225.

Wang, Y. et al. (2012). "The predominant role of collagen in the nucleation, growth, structure and orientation of bone apatite." In: *Nature materials* **11**.8, pp. 724–33.

Waters, J. C. (2009). "Accuracy and precision in quantitative fluorescence microscopy". In: *The Journal of Cell Biology* **185**.7, pp. 1135–1148.

Weibel, D. B., W. R. DiLuzio and G. M. Whitesides (2007). "Microfabrication meets microbiology". In: *Nature Reviews Microbiology* **5**.3, pp. 209–218.

Weinbaum, S, S. C. Cowin and Y Zeng (1994). "A model for the excitation of osteocytes by mechanical loading-induced bone fluid shear stresses." In: *Journal of biomechanics* **27**.3, pp. 339–60.

Weiner, S. et al. (1997). "Rotated plywood structure of primary lamellar bone in the rat: Orientations of the collagen fibril arrays". In: *Bone* **20**.6, pp. 509–514.

Weinreb, M., G. Rodan and D. Thompson (1989). "Osteopenia in the immobilized rat hind limb is associated with increased bone resorption and decreased bone formation". In: *Bone* **10**.3, pp. 187–194.

Welldon, K. J., D. M. Findlay, A. Evdokiou, R. T. Ormsby and G. J. Atkins (2013). "Calcium induces pro-anabolic effects on human primary osteoblasts associated with acquisition of mature osteocyte markers." In: *Molecular and cellular endocrinology* **376**.1-2, pp. 85–92.

Wenstrup, R. J., J. B. Florer, E. W. Brunskill, S. M. Bell, I. Chervoneva and D. E. Birk (2004). "Type V collagen controls the initiation of collagen fibril assembly." In: *The Journal of biological chemistry* **279**.51, pp. 53331–7.

Westendorf, J. J., R. A. Kahler and T. M. Schroeder (2004). "Wnt signaling in osteoblasts and bone diseases." In: *Gene* **341**, pp. 19–39.

Whitesides, G. M., E. Ostuni, S. Takayama, X. Jiang and D. E. Ingber (2001). "Soft lithography in biology and biochemistry". In: *Annual review of biomedical engineering* **3**.1, pp. 335–373.

Wilmer, M. J., C. P. Ng, H. L. Lanz, P. Vulto, L. Suter-Dick and R. Masereeuw (2016). "Kidney-on-a-Chip Technology for Drug-Induced Nephrotoxicity Screening". In: *Trends in Biotechnology* **34**.2, pp. 156–170.

Wolff, J (1892). "Das Gesetz der Transformation der Knochen (Berlin A. Hirchwild). Translated as: The Law of Bone Remodeling". In: *Springer-Verlag, Berlin.*

Woo, S. M., J. Rosser, V. Dusevich, I. Kalajzic and L. F. Bonewald (2011). "Cell line IDG-SW3 replicates osteoblast-to-late-osteocyte differentiation in vitro and accelerates bone formation in vivo." In: *Journal of bone and mineral research* **26**.11, pp. 2634–46.

Wornham, D. P., M. O. Hajjawi, I. R. Orriss and T. R. Arnett (2014). "Strontium potently inhibits mineralisation in bone-forming primary rat osteoblast cultures and reduces numbers of osteoclasts in mouse marrow cultures." In: *Osteoporosis international* **25**.10, pp. 2477–84.

Xia, Y. and G. M. Whitesides (1998). "Soft lithography". In: *Annual review of materials science* **28**.1, pp. 153–184.

Xiao, G., D. Wang, M. D. Benson, G. Karsenty and R. T. Franceschi (1998). "Role of the alpha 2-Integrin in Osteoblast-specific Gene Expression and Activation of the Osf2 Transcription Factor". In: *Journal of Biological Chemistry* **273**.49, pp. 32988–32994.

Xiao, G., R. Gopalakrishnan, D. Jiang, E. Reith, M. D. Benson and R. T. Franceschi (2002). "Bone Morphogenetic Proteins, Extracellular Matrix, and Mitogen-Activated

Protein Kinase Signaling Pathways Are Required for Osteoblast-Specific Gene Expression and Differentiation in MC3T3-E1 Cells". In: *Journal of Bone and Mineral Research* **17**.1, pp. 101–110.

Xing, J., Y. Li, M. Lin, J. Wang, J. Wu, Y. Ma, Y. Wang, L. Yang and Y. Luo (2014). "Surface chemistry modulates osteoblasts sensitivity to low fluid shear stress." In: *Journal of biomedical materials research. Part A* **102**.11, pp. 4151–60.

Xu, F., J. Wu, S. Wang, N. G. Durmus, U. A. Gurkan and U. Demirci (2011). "Microengineering methods for cell-based microarrays and high-throughput drug-screening applications". In: *Biofabrication* **3**.3, p. 34101.

Xu, J., Z. Li, Y. Hou and W. Fang (2015). "Potential mechanisms underlying the Runx2 induced osteogenesis of bone marrow mesenchymal stem cells." In: *American journal of translational research* **7**.12, pp. 2527–35.

Yamada, K. M. and E. Cukierman (2007). "Modeling Tissue Morphogenesis and Cancer in 3D". In: *Cell* **130**.4, pp. 601–610.

Yang, F., D. Yang, J. Tu, Q. Zheng, L. Cai and L. Wang (2011). "Strontium Enhances Osteogenic Differentiation of Mesenchymal Stem Cells and In Vivo Bone Formation by Activating Wnt/Catenin Signaling". In: *STEM CELLS* **29**.6, pp. 981–991.

Yang, J.-Y., Y.-C. Ting, J.-Y. Lai, H.-L. Liu, H.-W. Fang and W.-B. Tsai (2009). "Quantitative analysis of osteoblast-like cells (MG63) morphology on nanogrooved substrata with various groove and ridge dimensions." In: *Journal of biomedical materials research. Part A* **90**.3, pp. 629–40.

Yellowley, C. E., Z Li, Z Zhou, C. R. Jacobs and H. J. Donahue (2000). "Functional gap junctions between osteocytic and osteoblastic cells." In: *Journal of bone and mineral research* **15**.2, pp. 209–17.

You, J, C. E. Yellowley, H. J. Donahue, Y Zhang, Q Chen and C. R. Jacobs (2000). "Substrate deformation levels associated with routine physical activity are less stimulatory to bone cells relative to loading-induced oscillatory fluid flow." In: *Journal of biomechanical engineering* **122**.4, pp. 387–93.

You, J, G. C. Reilly, X Zhen, C. E. Yellowley, Q Chen, H. J. Donahue and C. R. Jacobs (2001a). "Osteopontin gene regulation by oscillatory fluid flow via intracellular calcium mobilization and activation of mitogen-activated protein kinase in MC3T3-E1 osteoblasts." In: *The Journal of biological chemistry* **276**.16, pp. 13365–71.

You, L.-D., S. Weinbaum, S. C. Cowin and M. B. Schaffler (2004). "Ultrastructure of the osteocyte process and its pericellular matrix." In: *The anatomical record. Part A, Discoveries in molecular, cellular, and evolutionary biology* **278**.2, pp. 505–13.

You, L., S. C. Cowin, M. B. Schaffler and S. Weinbaum (2001b). "A model for strain amplification in the actin cytoskeleton of osteocytes due to fluid drag on pericellular matrix". In: *Journal of Biomechanics* **34**.11, pp. 1375–1386.

Young, M. F. (2003). "Bone matrix proteins: their function, regulation, and relationship to osteoporosis." In: *Osteoporosis international* **14**.Suppl 3, S35–42.

Young, S. R. L., J. M. Hum, E. Rodenberg, C. H. Turner and F. M. Pavalko (2011). "Non-overlapping functions for Pyk2 and FAK in osteoblasts during fluid shear stress-induced mechanotransduction." In: *PloS one* **6**.1, e16026.

Yu, W., H. Qu, G. Hu, Q. Zhang, K. Song, H. Guan, T. Liu and J. Qin (2014). "A microfluidic-based multi-shear device for investigating the effects of low fluid-induced stresses on osteoblasts." In: *PloS one* **9**.2, e89966.

Yuen, P. K. and V. N. Goral (2010). "Low-cost rapid prototyping of flexible microfluidic devices using a desktop digital craft cutter." In: *Lab on a chip* **10**.3, pp. 384–7.

Zahn, J. D. (2009). *Methods in bioengineering: biomicrofabrication and biomicrofluidics.* Artech House.

Zanoni, M. et al. (2016). "3D tumor spheroid models for in vitro therapeutic screening: a systematic approach to enhance the biological relevance of data obtained". In: *Scientific Reports* **6**, p. 19103.

Zhang, K. et al. (2006). "E11/gp38 selective expression in osteocytes: regulation by mechanical strain and role in dendrite elongation." In: *Molecular and cellular biology* **26**.12, pp. 4539–52.

Zhao, Y., R. Yao, L. Ouyang, H. Ding, T. Zhang, K. Zhang, S. Cheng and W. Sun (2014). "Three-dimensional printing of Hela cells for cervical tumor model in vitro". In: *Biofabrication* **6**.3, p. 35001.

Zheng, W., Z. Wang, W. Zhang and X. Jiang (2010). "A simple PDMS-based microfluidic channel design that removes bubbles for long-term on-chip culture of mammalian cells." In: *Lab on a chip* **10**.21, pp. 2906–10.

Zhou, X., D. Liu, L. You and L. Wang (2010). "Quantifying fluid shear stress in a rocking culture dish." In: *Journal of biomechanics* **43**.8, pp. 1598–602.

Zhu, B., Q. Lu, J. Yin, J. Hu and Z. Wang (2005). "Alignment of osteoblast-like cells and cell-produced collagen matrix induced by nanogrooves." In: *Tissue engineering* **11**.5-6, pp. 825–34.

Zhu, L.-L., S. Zaidi, Y. Peng, H. Zhou, B. S. Moonga, A. Blesius, I. Dupin-Roger, M. Zaidi and L. Sun (2007). "Induction of a program gene expression during osteoblast differentiation with strontium ranelate". In: *Biochemical and Biophysical Research Communications* **355**.2, pp. 307–311.

Appendix

Publications

Castro APG, Laity P, Shariatzadeh M, **Wittkowske C**, Holland C, Lacroix D (2016) Combined numerical and experimental biomechanical characterization of soft collagen hydrogel substrate. Journal of Materials Science: Materials in Medicine, 27(4).

Wittkowske C, Reilly G, Lacroix D, Perrault CM. In vitro bone cell models: Impact of fluid shear stress on bone formation. Frontiers in Bioengineering and Biotechnology. (*under review*)

Oral presentations

Advances in Cell and Tissue Culture: 'Modelling Flow Behaviour in a Cell Culture Chamber', June 2015, Pisa, Italy.

University of Sheffield Engineering Symposium (USES), 'Stackable organ-on-a-chip device with cell-laden collagen layers', June 2014, Sheffield, UK.

Poster presentations

European Society of Biomechanics: 'Investigation of long term responses of osteoblasts and osteocytes to low fluid shear stress', July 2016, Lyon, France.

17th BiTEG meeting: 'Long-term effects of low shear stress on osteoblast behaviour', December 2015, University of York, UK.

CellMech Congress: 'Traction Forces exerted by Osteoblasts and their role in the Alignment of Collagen Fibres during Bone Formation', May 2015, Barcelona, Spain.

EMBL Conference Series Microfluidics 2014: 'Stackable organ-on-a-chip device with cell-laden collagen layers', July 2014, Frankfurt, Germany.

Horizon in Human Cells: 'Stackable organ-on-a-chip device with cell-laden collagen layers', May 2014, Royal College of Surgeons, Edinburgh, UK.

Awards

Winning team to solve a complex Multi Scale Modelling problem in the MultiSim Modelathon, September 2015, University of Sheffield.

1st place prize for 2nd year PhD departmental poster presentation, May 2015, University of Sheffield.

Two travel grants awarded from University of Sheffield Learned Society Fund (£850 in 2014 and £230 in 2016)